Peristaltic flows in a tube and endoscope

By

Noreen Sher Akbar

Department of Mathematics
Quaid-i-Azam University
Islamabad, Pakistan
2012

Peristaltic flows in a tube and endoscope

By

Noreen Sher Akbar

Supervised By

Dr. Sohail Nadeem

Department of Mathematics
Quaid-i-Azam University
Islamabad, Pakistan
2012

Peristaltic flows in a tube and endoscope

By

Noreen Sher Akbar

A Dissertation Submitted in the Partial Fulfillment of the requirements for the degree of

DOCTOR OF PHILOSOPHY

IN

MATHEMATICS

Supervised By

Dr. Sohail Nadeem

Department of Mathematics
Quaid-i-Azam University
Islamabad, Pakistan

2012

Peristaltic flows in a tube and endoscope

By

Noreen Sher Akbar

CERTIFICATE

A DISSERTATION SUBMITTED IN THE PARTIAL FULFILLMENT OF THE REQUIREMENTS FOR THE DEGREE OF THE DOCTOR OF PHILOSOPHY

We accept this dissertation as conforming to the required standard

1. _____
Prof. Dr. Muhammad Ayub
(Chairman)

2. _____
Dr. Sohail Nadeem
(Supervisor)

3. _____
Prof. Dr. Muhammad Akram Javaid
(External Examiner)
Ex-Vice Chancellor
University of Eng. Taxila

4. _____
Prof. Dr. Nawazish Ali Shah
(External Examiner)
University of Eng. and Tech. Lahore

Department of Mathematics
Quaid-i-Azam University
Islamabad, Pakistan
2012

Acknowledgement

I sincerely thanks Allah the the Most Gracious, Most Merciful for enabling me to complete my P h.D successfully and situate so many good people in my way specially my parents and my supervisor Dr. Sohail Nadeem. I think my parents and my supervisor are most precious gift of Allah for me. I also pay my tribute to our beloved Holy Prophet Hazrat Muhammad (PBUH) whose life is a guideline for whole humanity.

I would like to express my sincere gratitude to my great, superb, worthy supervisor Dr. Sohail Nadeem for the continuous endless support for my Ph.D thesis and research, for his patience, motivation, enthusiasm, and immense knowledge. His guidance helped me in all the time of research and writing of this thesis. I could not even imagine having a better supervisor and advisor for my Ph.D thesis except Dr. Sohail Nadeem. He really proved that teachers are like the parents for the students. I think without Dr. Sohail Nadeem help I cannot move a single step forward in my research. No supervisor could be like Dr. Sohail Nadeem. I think there is no word which can really explore the honor of His supervision.

My thanks also goes to Prof. Dr. Tasawar Hayat, Dr. Malik Muhammad Yousaf and Prof. Dr. Muhammad Ayub.

I sincerely acknowledge my fellows , Iffat, Farzana, Ehnber, Tayyab, Rizwan, Rashid, Sajjad, Afzal, Irfan and Salman for all the funs we have in the last four years.

Last but not the least, I would like to thank my family my parents , Javed Bahi, my sisters, brothers and bahbi, for supporting me spiritually throughout my life.

Contents

Chapter 0

Introduction

Peristalsis is a mechanism to pump a fluid by means of a moving contraction on the tube walls. Peristaltic flow has paramount importance in physiology. Occurrence of such flows are quite prevalent in nature. Particularly, these flows are encountered in smooth muscle contraction. Peristalsis occur in swallowing food through the esophagus, urine transport from kidney to bladder through the ureter, transport of the spermatozoa in the ducts afferents of the male reproductive tract, movement of the ovum in the fallopian tube, movement of the chyme in the gastrointestinal tract, the transport of lymph in the lymphatic vessels and the vasomotion in small blood vessels such as arterioles, veins and capillaries. Flows due to peristalsis has wide range of applications in industry and engineering science. Peristaltic pumps are relatively inexpensive to manufacture and commercially used in industries such as printing, chemical, and food processing. They also have a variety of uses in the medical field. Since there is very little damage caused by the mechanical action of the roller on the fluid, a peristaltic pump is ideal for pumping such fluids as blood and is used for that purpose in blood filtration devices.

Shapiro [1] gave the theoretical idea of peristaltic mechanism which was later on tested experimentally by Latham [2]. After the work of Latham [2] , peristalsis mechanism has become an interesting and important topic of research for scientist and engineers. Peristaltic motion of a viscous fluid through a pipe and a channel was investigated by Burns and Parkes [3] by considering sinusoidal variation at the walls. Barton and Raynor [4] studied peristaltic flow in tubes using long wave approximation. Barton and Raynor also analyzed the case for low Reynolds number. Jaffrin and Shapiro [5] provided an elaborate review of the earlier literature

regarding peristalsis. Elshehawey et al. [6] discussed the problem of peristaltic transport of an incompressible viscous fluid in an asymmetric channel through a porous medium. Kothandapani and Srinivas [7] have discussed the peristaltic flow of a Jeffrey fluid in an asymmetric channel in the presence of a transverse magnetic field. According to them, Jeffrey fluid is relatively simple linear model using time derivatives instead of convective derivatives. They noted that the size of trapped bolus in Jeffrey fluid is much smaller than the Newtonian fluid. Nadeem and Safia [8] have considered the peristaltic transport of a hyperbolic tangent fluid model in an asymmetric channel. An unsteady peristaltic transport phenomena of non-Newtonian fluid have been studied by Ikbal et.al [9]. Johnson-Segalman fluid have been studied by Elshahed and Haroun [10]. Haroun [11] has discussed the effect of Deborah number and phase difference on peristaltic transport of a third order fluid in an asymmetric channel. A mathematical description of peristaltic hydromagnetic flow of Johnson-Segalmanin fluid have been investigated by Hayat and Ali [12]. Seshadri et.al. [13] studied the peristaltic pumping in non-uniform distensible tubes with different wave forms. Nadeem and Akbar [14] have studied the peristaltic motion of a Herschel Bulkly fluid in a non-uniform inclined tube. Peristaltic transport of a Herschel-Bulkley fluid in an inclined tube have been studied by Vajravelu et al. [15] .

The study of heat transfer in connection with peristaltic motion has industrial and biological applications such as sanitary fluid transport, blood pumps in heart lungs machine and transport of corrosive fluids where the contact of the fluid with machinery parts are prohibited. Effect of heat transfer on the peristaltic flow of an electrically conducting fluid in a porous space have been investigated by Hayat et al [16]. The effects of the elasticity of the flexible walls on the peristaltic transport of viscous fluid with heat transfer in a two dimensional uniform channel have been analyzed by Radhakrishnamacharya and Srinivasulu [17] . Vajravelu et. al.[18] have discussed the interaction of peristalsis with heat transfer for the flow of a viscous fluid in a vertical porous annular region between two concentric tubes. They concluded that for the large values of the amplitude ratio, the effects of pressure rise on the flow rate are negligible. Mekheimer and Abd-Elmaboud [19] have discussed the influence of heat transfer and magnetic field on peristaltic transport of a Newtonian fluid on a vertical annulus and concluded that the heat transfer analysis may be used to obtain information about the properties of the tissues. Bio heat transfer phenomena is common in many biological processes as well as in some biomedical

applications such as in hypothermia treatment and radio frequency ablation [20]. Srinivas and Gayathri [21] studied peristaltic transport of a Newtonian fluid in a vertical asymmetric channel with heat transfer and porous medium. Kothandapani and Srinivas [22] analyzed the influence of wall properties in the MHD peristaltic transport with heat transfer and porous medium. Since most of the biochemical reactions in human body take place in very narrow temperature range and the reaction rate is largely dependent on the local temperature, the heat transfer plays a major role in many processes in living systems.

In the studies mentioned above, fluid viscosity is assumed to be constant. But this assumption is not true always. In many thermal transport processes, the temperature distribution within the flow field is never uniform, i.e, the fluid viscosity may be change noticeably if a large temperature differences exists in the system. Therefore, it is highly desirable to include the temperature dependent viscosity in the momentum and thermal transport processes. The peristaltic transport of MHD fluid with variable viscosity was investigated by Ali et al. [23]. Nadeem and Akbar [24] have examined the effects of heat transfer on the peristaltic transport of MHD Newtonian fluid with variable viscosity and found the solution by Adomian decomposition method. Hakeem et al. [25] have investigated the effects of hydromagnetic flow of fluid with variable viscosity in a uniform tube with peristalsis. Recently Nadeem et al. [26] have examined the variable viscosity effects on the peristaltic flow of a MHD Newtonian fluid.

The study of heat and mass transfer is also important because of its large number of applications in geothermal and geophysical engineering. Such applications are extraction of geothermal energy, the migration of moisture in fibrous insulation, under ground disposal of nuclear waste and the spreading of chemical pollutants in saturated soil. Only a few attempts have been made to study the combined effects of heat and mass transfer in peristaltic literature. Eldabe et al. [27] considered mixed convective heat and mass transfer in a non-Newtonian fluid at a peristaltic surface with temperature-dependent viscosity. The influence of heat and mass transfer on MHD peristaltic flow through a porous space with compliant walls was taken into account by Srinivas and Kothandapani [28] . Nadeem et al. [29] studied the influence of heat and mass transfer on peristaltic flow of a third order fluid in a diverging tube. Influence of radially varying MHD on the peristaltic flow in an annulus with heat and mass transfer was investigated by the Nadeem and Akbar [30]. Some more important investigations related to the

thesis work are cited in Refs. [31 – 42].

Motivated by the above analysis the peristaltic flows of non-Newtonian fluids have been discussed, the purpose of the present thesis is to investigate the peristaltic flows of some non-Newtonian fluids in tubes and endoscope. Thesis consists of eleven chapters including chapter zero consists literature survey and the other ten chapters are developed as follow:

In chapter one, we discuss the peristaltic flow of a Walter's B fluid in a uniform inclined tube. The governing equations of Walter's B fluid in cylindrical coordinates are first obtained. The highly nonlinear partial differential equations are simplified with the help of transformation and nondimensional variables. Their analytical solutions are calculated by using regular perturbation method. The content of this chapter are published in **Journal of Biorheology, 24(2010)22 – 28**.

Peristaltic flow of Williamson fluid model in an endoscope have been discussed in chapter two. The governing equations of Williamson fluid model in cylindrical coordinates are given for a two dimensional flow. The solutions of the reduced nonlinear equations are calculated with the help of (i) perturbation method (ii) homotopy analysis method and (iii) numerically by the shooting method. This chapter is published in **Journal of Mechanics in Medicine and Biology**. **4(2011)941 – 957**.

Chapter three is devoted to the study of peristaltic flow of Sisko fluid in a uniform inclined tube. In this chapter, we analyze an incompressible Sisko fluid through an axisymmetric uniform inclined tube with a sinusoidal wave propagating down its walls. The present analysis of non-Newtonian fluid is investigated under the considerations of long wavelength and low Reynolds number approximation. The analytic solutions are obtained by using (i) regular perturbation method and (ii) homotopy analysis method (HAM). The content of this chapter is published in **Acta Mechanica Sinica. 26(2010)675 – 683**.

Endoscopic effects on the peristaltic flow of a nanofluid has been examined in chapter four. This chapter deals with the peristaltic flow of a nanofluid in an endoscope. The flow is investigated in a wave frame of reference moving with velocity of the wave. Analytical solutions have been calculated using homotopy perturbation method (HPM) for temperature and nanoparticle equation while exact solutions are obtain for velocity and pressure gradient. The content of this chapter is published in **Communications in Theoretical Physics. 56(2011)761 – 768**.

In chapter 5, we analyze influence of heat transfer on a peristaltic flow of Johnson Segalman fluid in a non uniform tube. The governing equations of Johnson Segalman are simplified using the long wavelength and low Reynolds number assumptions. In the wave frame of reference, an analytical solutions are computed with the help of two techniques namely (i) perturbation technique, (ii) hAM technique. The work of this chapter is published in **International Communications in Heat and Mass Transfer. 36(2009)1050 − 1059.**

Chapter 6 discussed the peristaltic transport of a tangent hyperbolic fluid in an endoscope. The modelling of hyperbolic tangent fluid model for two dimensional flow in cylindrical coordinates are presented. Using the assumption of long wavelength and low Reynold number, the governing equations of hyperbolic tangent fluid for an endoscope have been solved using regular perturbation method and shooting method. The contents of this chapter is published in **Journal of Aerospace Engineering. 24 (2011) 309**.

In chapter 7, combined effects of heat and chemical reactions on the peristaltic flow of Carreau fluid model in a diverging tube. Analysis of the chapter have been done under the consideration of long wavelength in the presence of heat and mass transfer. The flow is investigated in a wave frame of reference moving with velocity of the wave. Two types of analytical solutions have been evaluated (i) Perturbation method (ii) Homotopy analysis method for velocity, the temperature and concentration field. The work of this chapter is accepted for publication in **International Journal of Numerical Methods in fluid 2011.**

Chapter 8 described the analytical and numerical analysis of Vogel's model of viscosity on the peristaltic flow of Jeffrey fluid. We have analyzed the effects of temperature dependent viscosity on the peristaltic flow of Jeffrey fluid between two coaxial horizontal tubes. The governing problem is simplified using longwave length and low Reynolds number approximations. Regular perturbation in terms of small viscosity parameter is used to get the expressions for the temperature and velocity for Vogel's models of viscosity. The numerical solution of the problem has also been computed by shooting methodd. The content of this chapter is accepted for publication in **Journal of Aerospace Engineering 2011.**

Characteristics of heating scheme and mass transfer on the peristaltic flow for an Eyring-Powell fluid in an endoscope has been given in chapter nine. The governing equations of proposed model are first modeled and then solved analytically and numerically. The content

of this chapter is published in **International Journal of Heat and Mass Transfer 2011. 55(2012)375 – 383**.

Chapter ten is developed to study the simulation of heat transfer on the peristaltic flow of a Jeffrey-six constant fluid in a diverging tube. The modeling of proposed fluid model is given and regular perturbation method is invoked to find an analytical solution for the velocity and temperature field. This chapter has been published in **Communication in Heat and Mass transfer. 38(2011)154 – 159**.

Nomenclature

$\mathbf{V}$	Velocity	$\bar{R}$	Space coordinate
$\mathbf{S}$	Shear stress	$\bar{Z}$	Space coordinate
ρ	Density of the fluid	g	Gravitational force
$\boldsymbol{\tau}$	Extra stress tensor	α	Angle of Inclination
μ	Viscosity	$\bar{U}$	Velocity in radial direction
t_1	Transpose	$\bar{W}$	Velocity in axial direction
a	Radius of tube	$\bar{u}$	Velocity in radial direction
b	Wave of amplitude	$\bar{w}$	Velocity in axial direction
c	Wave speed	δ	Wave length
λ	Wave length	α_1	Walters B fluid parameter
t	Time	h	Height of the tube wall
Re	Reynold number	P	Pressure
ϕ	amplitude ratio	ψ	stream function
e	Rate of strain tensor	ΔP	Pressure rise
$\mathbf{f}$	Body force	F	Frictional force
μ_∞	Infinite shear rate viscosity	Q	Flow rate
μ_0	Zero shear rate viscosity	Γ	Time constant
a_1	radius of inner tube	Π	Second invariant strain tensor
a_2	radius of outer tube	ε	Radius ratio
r_2	Height of endoscope	W_e	Weissenberg number
B_r	Local concentration Grashof	$F^{(0)}$	Frictional force for inner tube
$F^{(i)}$	Frictional force for outer tube	q	Embedding parameter
h_w	Auxiliary parameter	n	Power Law index
b^*	Sisko fluid parameter	Pr	Prandtl number
k	thermal conductivity,	N_b	Brownian motion parameter
K_T	thermal-diffusion ratio,	N_t	Themophoresis parameter
B_r	Brinkmann number	$\bar{C}$	Concentration in dimensional form
σ	Concentration in nondimensional form	$\bar{T}$	Temperature in dimensional form

θ	Temperature in nondimensional form	E_c	Eckert number
μ, η	Viscosities	S_r	Soret number
λ_1	Ratio of relaxation to retardation time	λ_2	Retardation time
A, B	Constants of Vogels models	β	heat source parameter
T_m	Temperature of the medium,	Γ_1	Vogels models parameter
u	Velocity component in r-direction,	μ_0	Reference viscosity
S_c	Schmidt number	ρ_p	Density of particle
K_T	Thermal diffusion ratio	N, M	Eyring Powell fluid parameter
$\hat{Q}$	Heat flux	D_T	Thermophoretic diffusion coefficient
τ_1	Ratio between the effective heat capacity of the nano particle and heat capacity of fluid	ν	Kinematic Viscosity
β_1, c_1	Material constant of Eyring Powell fluid	c_p	Specific heat
w	Velocity component in z-direction,	a_3	Slip parameter
$\bar{D}$	Symmetric part of the velocity gradient	e_1	Specific internal energy
$\bar{W}_1$	Axisymmetric part of the velocity gradient	r_3	Radient heating
D_B	Brownian diffusion coefficient	k	Thermal conductivity
a_0	Radius of inlet	K	Constant depend on tube length
g, i	Material constant of Jeffrey six constant fluid model	G_r	Grashof number

Chapter 1

Peristaltic flow of Walter's B fluid in a uniform inclined tube

1.1 Introduction

In this chapter, we have investigated the peristaltic flow of a Walter's B fluid in a uniform inclined tube. The governing equations of Walter's B fluid in cylindrical coordinates have been modeled. The highly nonlinear partial differential equations are simplified with the help of transformation and nondimensional variables. The analytical solutions have been calculated by using regular perturbation method by taking δ as perturbation parameter. The expressions for pressure rise and friction forces have been calculated using numerical integration. The graphical results are presented to discuss the various nondimensional physical quantities of Walter's B fluid parameter α_1, amplitude ratio ϕ, angle of inclination α and wave length δ.

1.2 Mathematical Model

For an incompressible fluid the balance of mass and momentum are given by

$$\operatorname{div} \mathbf{V} = 0, \tag{1.1}$$

$$\rho \frac{d\mathbf{V}}{dt} = \operatorname{div} \mathbf{S} + \rho \mathbf{f}, \tag{1.2}$$

where ρ is the density, $\mathbf{V}$ is the velocity vector, $\mathbf{S}$ is the Cauchy stress tensor, $\mathbf{f}$ represents the specific body force and d/dt represents the material time derivative. The constitutive equation for Walter's B' fluid is given by [32]

$$\begin{aligned}
\mathbf{S} &= -\bar{P}\mathbf{I} + \boldsymbol{\tau}, && (1.3)\\
\boldsymbol{\tau} &= 2\mu\mathbf{e} - 2k_0\frac{\delta_1\mathbf{e}}{\delta_1 t}, && (1.4)\\
\mathbf{e} &= \boldsymbol{\nabla}\mathbf{V} + (\boldsymbol{\nabla}\mathbf{V})^T, && (1.5)\\
\frac{\delta_1\mathbf{e}}{\delta_1 t} &= \frac{\partial\mathbf{e}}{\partial t} + \mathbf{V}.\nabla\mathbf{e} - \mathbf{e}\boldsymbol{\nabla}\mathbf{V} - (\boldsymbol{\nabla}\mathbf{V})^T\mathbf{e}, && (1.6)
\end{aligned}$$

in which $-\bar{P}\mathbf{I}$ is the spherical part of the stress due to constraint of incompressibility, $\boldsymbol{\tau}$ is the extra stress tensor, μ is the coefficient of viscosity, $\mathbf{e}$ is the rate of strain tensor T denotes the transpose and $\delta_1/\delta_1 t$ denotes the convected differentiation of a tensor quantity in relation to the material motion.

1.3 Problem Formulation

We have considered an incompressible Walter's B fluid in a uniform inclined tube. The flow is produced due to a sinusoidal wave trains propagating with constant speed c along the walls of the tube and the geometry of the wall surface is defined in Fig. $1\,(a)$.

$$h{=}a{+}b\sin\frac{2\pi}{\lambda}\left(\bar{Z} - c\bar{t}\right), \qquad (1.7)$$

where a is the radius of the tube at inlet, b is the wave amplitude, λ is the wavelength, c is the wave speed and $\bar{t}$ is the time. We are considering the cylindrical coordinate system $(\bar{R}, \bar{Z})$, in which $\bar{Z} - axis$ lies along the centerline of the tube and $\bar{R}$ is transverse to it.

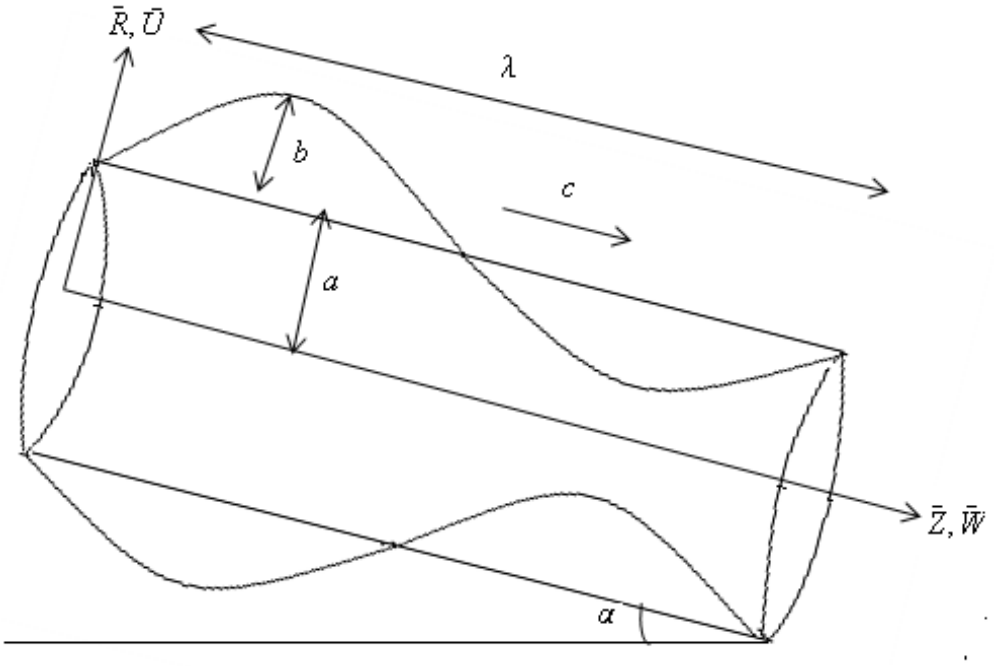

Fig. 1 (a). Geometry of the problem.

The governing equations in the fixed frame for an incompressible flow are given as

$$\frac{\partial \bar{U}}{\partial \bar{R}} + \frac{\bar{U}}{\bar{R}} + \frac{\partial \bar{W}}{\partial \bar{Z}} = 0, \tag{1.8}$$

$$\rho\left(\frac{\partial}{\partial \bar{t}} + \bar{U}\frac{\partial}{\partial \bar{R}} + \bar{W}\frac{\partial}{\partial \bar{Z}}\right)\bar{U} = -\frac{\partial \bar{P}}{\partial \bar{R}} + \frac{1}{\bar{R}}\frac{\partial}{\partial \bar{R}}\left(\bar{R}\bar{\boldsymbol{\tau}}_{\bar{R}\bar{R}}\right) + \frac{\partial}{\partial \bar{Z}}\left(\bar{\boldsymbol{\tau}}_{\bar{R}\bar{Z}}\right) - \frac{\bar{\boldsymbol{\tau}}_{\bar{\theta}\bar{\theta}}}{\bar{R}} + \rho g \sin\alpha, \tag{1.9}$$

$$\rho\left(\frac{\partial}{\partial \bar{t}} + \bar{U}\frac{\partial}{\partial \bar{R}} + \bar{W}\frac{\partial}{\partial \bar{Z}}\right)\bar{W} = -\frac{\partial \bar{P}}{\partial \bar{Z}} + \frac{1}{\bar{R}}\frac{\partial}{\partial \bar{R}}\left(\bar{R}\bar{\boldsymbol{\tau}}_{\bar{R}\bar{Z}}\right) + \frac{\partial}{\partial \bar{Z}}\left(\bar{\boldsymbol{\tau}}_{\bar{Z}\bar{Z}}\right) + \rho g \cos\alpha, \tag{1.10}$$

where $\bar{P}$ is the pressure, $\bar{U}$, $\bar{W}$ are the respective velocity components in the radial and axial directions in the fixed frame respectively, g is the constant of gravity and α represent the inclination angle. In the fixed coordinates $\left(\bar{R}, \bar{Z}\right)$, the flow is unsteady, it becomes steady in a wave frame $(\bar{r}, \bar{z})$ moving with the same speed as the wave moves in the $\bar{Z}-$direction. The transformations between the two frames are

$$\bar{r} = \bar{R}, \quad \bar{z} = \bar{Z} - c\bar{t}, \tag{1.11}$$

$$\bar{u} = \bar{U}, \quad \bar{w} = \bar{W} - c, \tag{1.12}$$

here $\bar{u}$ and $\bar{w}$ are the velocities in the wave frame. The corresponding boundary conditions are

$$\frac{\partial \bar{w}}{\partial \bar{r}} = 0, \qquad \bar{u} = 0 \qquad \text{at} \quad \bar{r} = 0, \tag{1.13a}$$

$$\bar{w} = -c, \quad \bar{u} = -c\frac{d\bar{h}}{d\bar{z}} \quad at \quad \bar{r} = \bar{h} = a + b\sin\frac{2\pi}{\lambda}(\bar{z}). \tag{1.13b}$$

We introduce the non-dimensional variables as

$$\begin{aligned} R &= \frac{\bar{R}}{a}, \quad r = \frac{\bar{r}}{a}, \quad Z = \frac{\bar{Z}}{\lambda}, \quad z = \frac{\bar{z}}{\lambda}, \quad W = \frac{\bar{W}}{c}, \quad w = \frac{\bar{w}}{c}, \ \tau = \frac{a\boldsymbol{\tau}}{c\mu} \\ U &= \frac{\lambda\bar{U}}{ac}, \quad u = \frac{\lambda\bar{u}}{ac}, \quad P = \frac{a^2\bar{P}}{c\lambda\mu}, \quad t = \frac{c\bar{t}}{\lambda}, \quad \delta = \frac{a}{\lambda}, \mathrm{Re} = \frac{\rho c a}{\mu}, \\ h &= \frac{\bar{h}}{a} = 1 + \phi\sin 2\pi z, \quad \alpha_1 = \frac{k_0 c}{\mu a}, \ E = \frac{\mu c}{\rho g a^2}. \end{aligned} \tag{1.14}$$

Making use of Eqs. (1.11), (1.12) and (1.14), Eqs. (1.8) to (1.10) along with boundary conditions (1.13a) and (1.13b) take the form

$$\frac{\partial u}{\partial r} + \frac{u}{r} + \frac{\partial w}{\partial z} = 0, \tag{1.15}$$

$$\mathrm{Re}\,\delta^3\left(u\frac{\partial}{\partial r} + w\frac{\partial}{\partial z}\right)u = -\frac{\partial P}{\partial r} - \frac{\delta}{r}\frac{\partial}{\partial r}(r\tau_{rr}) - \delta^2\frac{\partial}{\partial z}(\tau_{rz}) - \frac{\delta\tau_{\theta\theta}}{r} + \delta\frac{\cos\alpha}{E}, \tag{1.16}$$

$$\mathrm{Re}\,\delta\left(u\frac{\partial}{\partial r} + w\frac{\partial}{\partial z}\right)w = -\frac{\partial P}{\partial z} - \frac{1}{r}\frac{\partial}{\partial r}(r\tau_{rz}) - \delta\frac{\partial}{\partial z}(\tau_{zz}) + \frac{\sin\alpha}{E}, \tag{1.17}$$

$$\frac{\partial w}{\partial r} = 0, \quad u = 0 \ \text{ at } \quad r = 0, \tag{1.17a}$$

$$w = -1, \ u = -\frac{dh}{dz}, \ \text{at} \quad r = h = 1 + \phi\sin 2\pi z, \tag{1.17b}$$

where

$$
\begin{aligned}
\tau_{rr} &= 2\delta\frac{\partial u}{\partial r} - 2\alpha_1\left[\delta^2 u\frac{\partial^2 u}{\partial r^2} + \delta^2 w\frac{\partial^2 u}{\partial r\partial z} - 2\delta^2\left(\frac{\partial u}{\partial r}\right)^2 - \frac{\partial w}{\partial r}\left(\frac{\partial u}{\partial z}\delta^2 + \frac{\partial w}{\partial r}\right)\right],\\
\tau_{rz} &= \left(\frac{\partial u}{\partial z}\delta^2 + \frac{\partial w}{\partial r}\right) - \alpha_1\left[\delta^3 u\frac{\partial^2 u}{\partial r^2} + \delta u\frac{\partial^2 w}{\partial r^2} + w\delta\frac{\partial^2 w}{\partial r\partial z} + w\frac{\partial^2 u}{\partial z^2}\delta^3 -\right.\\
&\quad \left. 2\frac{\partial u}{\partial r}\frac{\partial u}{\partial z}\delta^3 - \delta\left(\frac{\partial u}{\partial z}\delta^2 + \frac{\partial w}{\partial r}\right)\left(\frac{\partial u}{\partial r} + \frac{\partial w}{\partial z}\right) - \frac{\partial w}{\partial r}\frac{\partial w}{\partial z}\delta\right],\\
\tau_{zz} &= 2\delta\frac{\partial w}{\partial z} - 2\alpha_1\left[\delta^2 u\frac{\partial^2 w}{\partial r\partial z} + \delta^2 w\frac{\partial^2 w}{\partial z^2} - \frac{\partial u}{\partial z}\delta^2\left(\frac{\partial u}{\partial z}\delta^2 + \frac{\partial w}{\partial r}\right) + 2\delta^2\left(\frac{\partial w}{\partial z}\right)^2\right],\\
\tau_{\theta\theta} &= 2\frac{u}{r}\delta - 2\alpha_1\delta^2\left[u\frac{\partial u}{\partial z} - \frac{3u^2}{r^2}\right].
\end{aligned}
$$

In above equations δ, Re and α_1 represent the wave number, Reynolds number and Walter's B fluid parameter respectively. Elimination of pressure gradient from Eqs. (1.16) and (1.17), we obtain

$$
\frac{\partial}{\partial r}\begin{bmatrix} -\operatorname{Re}\delta\left(u\frac{\partial}{\partial r} + w\frac{\partial}{\partial z}\right)w + \\ \frac{1}{r}\frac{\partial}{\partial r}\left(r\boldsymbol{\tau}_{rz}\right) + \delta\frac{\partial}{\partial z}\left(\boldsymbol{\tau}_{zz}\right) + \frac{\delta\cos\alpha}{E}\end{bmatrix} = \frac{\partial}{\partial z}\begin{bmatrix} -\operatorname{Re}\delta^3\left(u\frac{\partial}{\partial r} + w\frac{\partial}{\partial z}\right)u + \\ \frac{\delta}{r}\frac{\partial}{\partial r}\left(r\boldsymbol{\tau}_{rr}\right) + \delta^2\frac{\partial}{\partial z}\left(\boldsymbol{\tau}_{rz}\right) - \delta\frac{\boldsymbol{\tau}_{\boldsymbol{\theta\theta}}}{r} + \frac{\sin\alpha}{E}\end{bmatrix}. \tag{1.18}
$$

Corresponding boundary conditions in dimensionless form are

$$
u = 0, \quad \frac{\partial w}{\partial r} = 0, \qquad \text{at} \qquad r = 0, \tag{1.19}
$$

$$
u = -\frac{dh}{dz}, \; w = -1, at \;\; r = h = 1 + \phi\sin 2\pi z. \tag{1.20}
$$

1.4 Solution of the Problem

Since Eq. (1.18) is highly non-linear equation so its exact solution may be not possible. Therefore we are interested to calculate the solution with the help of perturbation method. For perturbation solution we expand u, w and P by taking δ as perturbation parameter

$$w = w_0 + \delta w_1 + O(\delta^2), \tag{1.21a}$$

$$u = u_0 + \delta u_1 + O(\delta^2), \tag{1.21b}$$

$$P = P_0 + \delta P_1 + O(\delta^2). \tag{1.21c}$$

Substituting Eqs. (1.21a) to (1.21c) in Eqs. (1.16) to (1.20), we get zeroth order and first order system of equation then find the solutions of all systems we arrive at the final solutions which are defined as

$$w(r,z) = -1 + \left(\frac{r^2-h^2}{4}\right)\left(\frac{\partial P}{\partial z} - \frac{\sin\alpha}{E}\right) + \delta\left(B_{18}\left(r^6-h^6\right) + B_{19}\left(r^4-h^4\right) + B_{20}\left(r^2-h^2\right)\right), \tag{1.22}$$

$$u(r,z) = B_5 r + \delta\left(B_{21}r^7 + B_{22}r^5 + B_{23}r^4 + B_{24}r^3 + B_{25}r\right), \tag{1.23}$$

$$\frac{dP}{dz} = \frac{-8E\left(2F_1+h^2\right) + h^4\sin\alpha}{Eh^4} + \delta\left(\frac{B_{21}}{h^4}\right). \tag{1.24}$$

The corresponding stream function can be calculated as

$$u = -\frac{1}{r}\frac{\partial\Psi}{\partial z} \quad \text{and} \quad w = \frac{1}{r}\frac{\partial\Psi}{\partial r}. \tag{1.25}$$

The pressure rise ΔP and friction force F can be calculated with the help of following relations

$$\Delta P = \int_0^1 \frac{dP}{dz}dz, \tag{1.26}$$

$$F = \int_0^1 h^2\left(-\frac{dP}{dz}\right)dz, \tag{1.27}$$

where $\frac{dP}{dz}$ is defined in Eq. (1.24). The constants appears in above differential equations are defined as

$$
\begin{aligned}
B_1 &= \frac{1}{2}\left(\frac{\partial P_0}{\partial z} - \frac{\sin\alpha}{E}\right), \quad B_2 = B_1^2\lambda_1, \quad B_3 = -B_1 hh' - \frac{B_1^2 h^3 h'}{2} + \frac{b_1 h^2}{4} + \frac{b_1 B_1 h^4}{4}, \\
B_4 &= \frac{B_1^2 hh'}{4} - \frac{b_1}{4} - b_1 B_1 h^2, \quad b_1 = \left(\frac{dP_0}{dz}\right)', \quad b_2 = \frac{b_1 B_1 h^4}{2}, \; b_3 = \left(\frac{dP_1}{dz}\right)', \\
B_5 &= -\frac{B_1 hh'}{2}, \quad B_6 = B_5 B_1, \quad a_7 = \mathrm{Re}\, B_2, \quad B_8 = \frac{3B_2'}{2} + \mathrm{Re}\, B_6 + \mathrm{Re}\, B_4, \quad B_9 = \mathrm{Re}\, B_3, \\
B_{10} &= \alpha_1 B_5 B_1, \quad B_{11} = \frac{\alpha_1 B_1 B_1'}{2}, \quad B_{12} = -\frac{\alpha_1 B_1 B_1' h^2}{2}, \quad B_{13} = \frac{\alpha_1 B_1 B_1'}{2}, \\
B_{14} &= -\frac{\alpha_1 B_1 B_1' h^2}{2} + \alpha B_5 B_1 - \alpha B_1^2 hh', \quad a_{15} = \frac{\alpha_1 B_1 hh'}{2}\left(\frac{\partial P_0}{\partial z} - \frac{\sin\alpha}{E}\right), \\
B_{16} &= \frac{B_8}{4} + B_{11} - B_{13}, \quad B_{17} = \frac{B_9}{2} + B_{10} + B_{12} - B_{14} - B_{15}, \quad B_{18} = \frac{B_7}{36}, \\
B_{19} &= \frac{B_{16}}{4}, \quad B_{20} = \frac{B_{17}}{2}, \quad B_{21} = B_{18}\left(-6h^8\right) + B_{19}\left(\frac{-16h^6}{3}\right) + B_{20}\left(-4h^4\right).
\end{aligned}
$$

The non-dimensional expressions for the five considered wave forms are given [13] by the following equations:

1. Sinusoidal wave:

$$h(z) = 1 + \phi \sin(2\pi z)$$

2. Triangular wave:

$$h(z) = 1 + \phi\left\{\frac{8}{\pi^3}\sum_{n=1}^{\infty}\frac{(-1)^{n+1}}{(2n-1)}\sin\left(2\pi(2n-1)z\right)\right\}$$

3. Square wave:

$$h(z) = 1 + \phi\left\{\frac{4}{\pi}\sum_{n=1}^{\infty}\frac{(-1)^{n+1}}{(2n-1)}\cos\left(2\pi(2n-1)z\right)\right\}$$

4. Trapezoidal wave:

$$h(z) = 1 + \phi\left\{\frac{32}{\pi^2}\sum_{n=1}^{\infty}\frac{\sin\frac{\pi}{8}(2n-1)}{(2n-1)^2}\sin\left(2\pi(2n-1)z\right)\right\}$$

5. Multi sinusoidal wave:

$$h(z) = 1 + \phi\sin(2m\pi z)$$

1.5 Graphical Discussion

In this section the pressure rise, frictional forces, axial pressure gradient and stream lines are discussed and shown graphically (see Figs. 1.1 to 1.10). The pressure rise is calculated numerically by using Mathematica. Figs. 1.1 to 1.4 show the pressure rise ΔP against volume flow rate Q for different values of angle of inclination α, amplitude ratio ϕ, wave length δ and Walter's B fluid parameter α_1. These figures indicate that the relation between pressure rise and volume flow rate are inversely proportional to each other. Fig. 1.1 shows that with the increase in α pressure rise increases. Peristaltic pumping occurs in the region $-1 \leq Q \leq 0.5$ for various values of ϕ and α_1 (see Figs.1.2 and 1.4) and $-1 \leq Q \leq -0.4$ for Fig. 1.3, other wise augmented pumping occurs. Further, the pressure rise increases with an increase in ϕ and δ while decreases with increase in α. Figs. 1.5 to 1.8 describe the variation of frictional forces. It is seen that frictional forces have opposite behavior as compared to the pressure rise. Figs. 1.9 (a) to 1.9 (e) are prepared to see the behavior of pressure gradient for different wave shapes. It is observed that for $z\epsilon\,[0, 0.5]$ and $[1.1, 1.5]$, the pressure gradient is small, while the pressure gradient is large in the interval $z\epsilon\,[0.51, 1]$. Moreover, it is seen that pressure gradient increases with increase in ϕ. The effects of different parameters on streamlines for the trapping phenomenon for five different wave forms can be seen through Figs. 1.10 $(a$ to $c)$. It is observed

that the size of trapping bolus in triangular wave is smaller as compared to other waves.

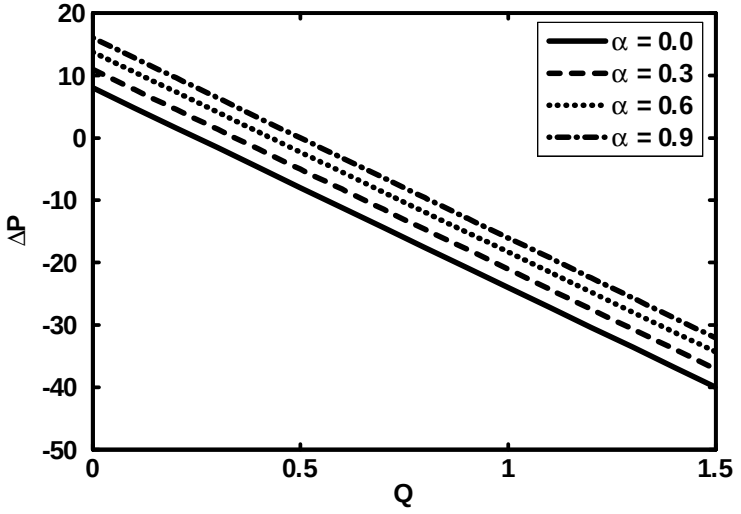

Fig.1.1. Pressure rise versus flow rate for $\alpha_1 = 0.05$, $\phi = 0.01$, $\delta = 0.4$, Re $= 6$, $E = 0.1$.

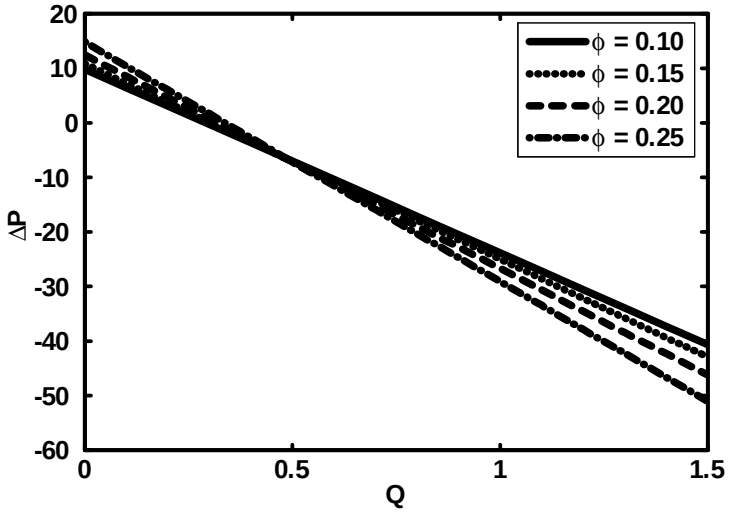

Fig.1.2. Pressure rise versus flow rate for for $\alpha_1 = 0.05$, $\alpha = 0.4$, $\delta = 0.1$, Re $= 8$, $E = 0.1$.

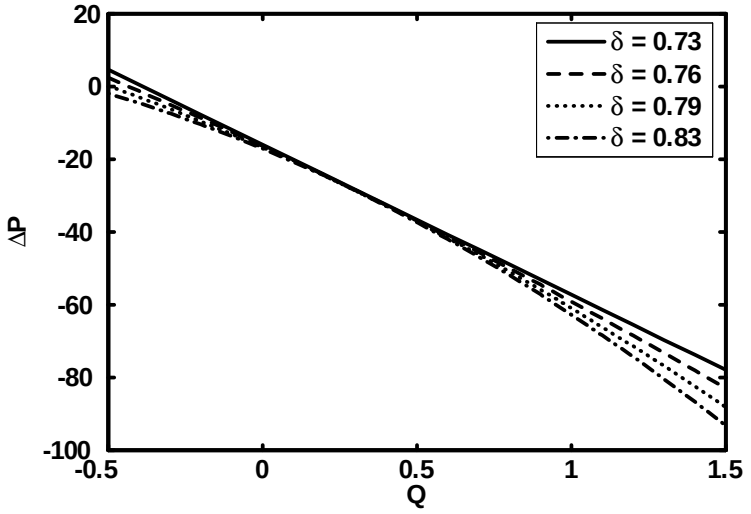

Fig.1.3. Pressure rise versus flow rate for $\alpha = 0.05$, $\alpha_1 = 0.4$, $\phi = 0.1$, Re $= 5$, $E = 0.1$.

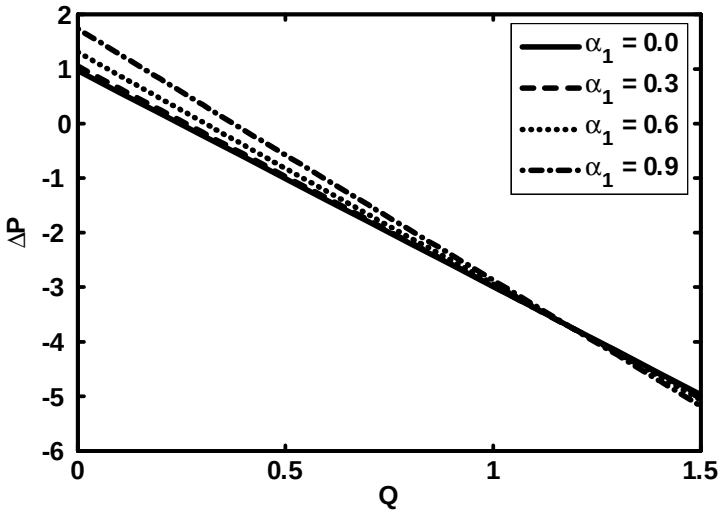

Fig.1.4. Pressure rise versus flow rate for $\alpha = 0.05$, $\delta = 0.4$, $\phi = 0.1$, Re $= 6$, $E = 0.1$.

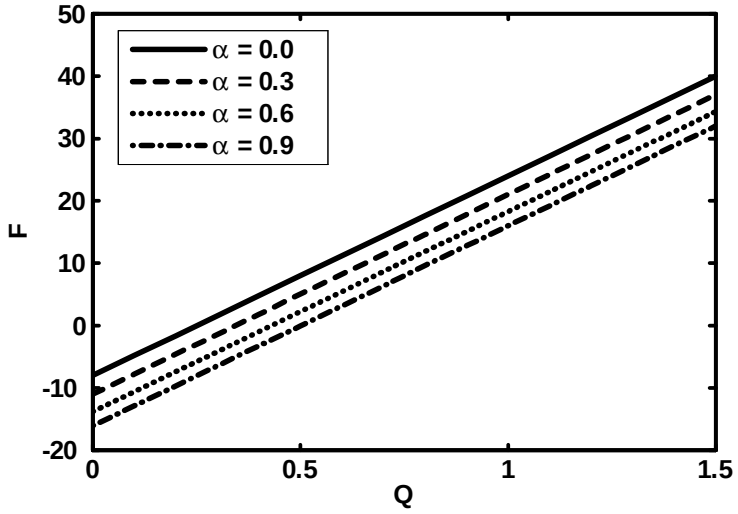

Fig.1.5. Frictional forces versus flow rate for $\alpha_1 = 0.05$, $\phi = 0.01$, $\delta = 0.4$, Re $= 6$, $E = 0.1$.

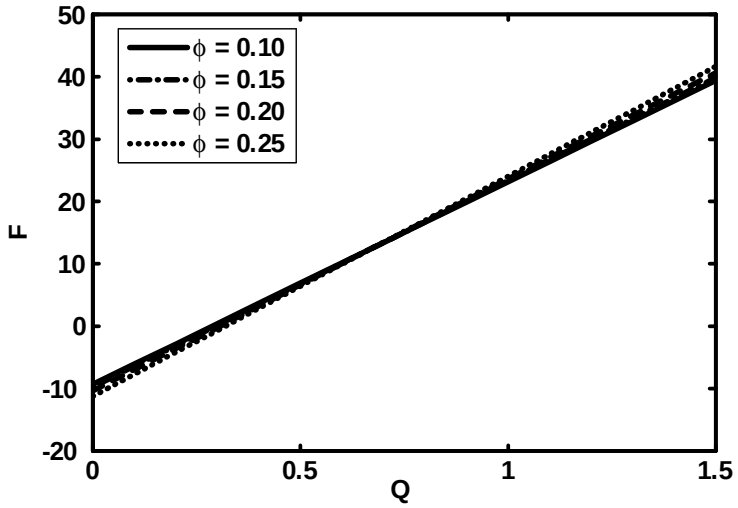

Fig.1.6. Frictional force versus flow rate for $\alpha_1 = 0.05$, $\alpha = 0.4$, $\delta = 0.1$, Re $= 8$, $E = 0.1$.

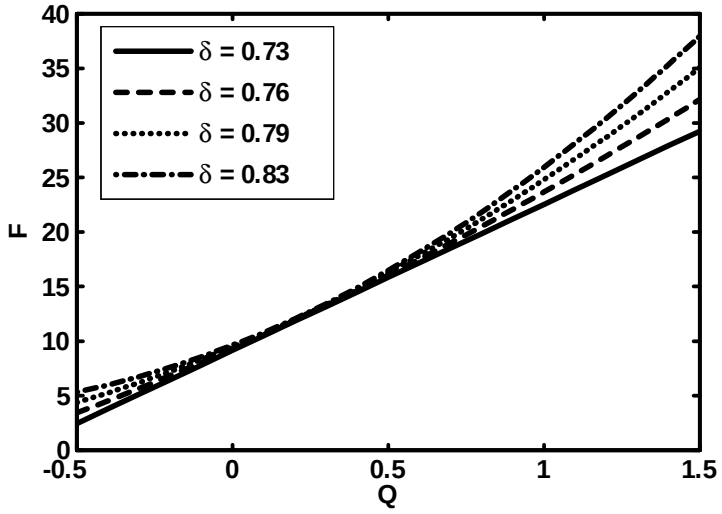

Fig.1.7. Frictional force versus flow rate for $\alpha_1 = 0.05$, $\alpha = 0.4$, $\phi = 0.1$, Re $= 5$, $E = 0.1$.

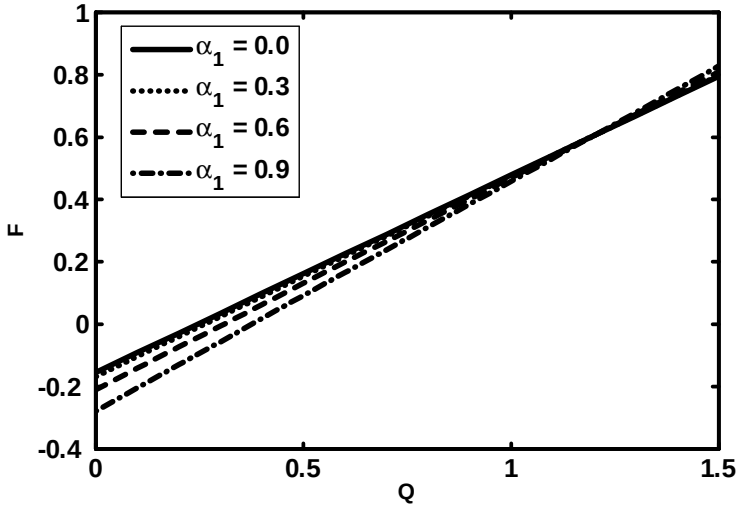

Fig.1.8. Frictional force versus flow rate for $\alpha = 0.05$, $\delta = 0.4$, $\phi = 0.1$, Re $= 6$, $E = 0.1$.

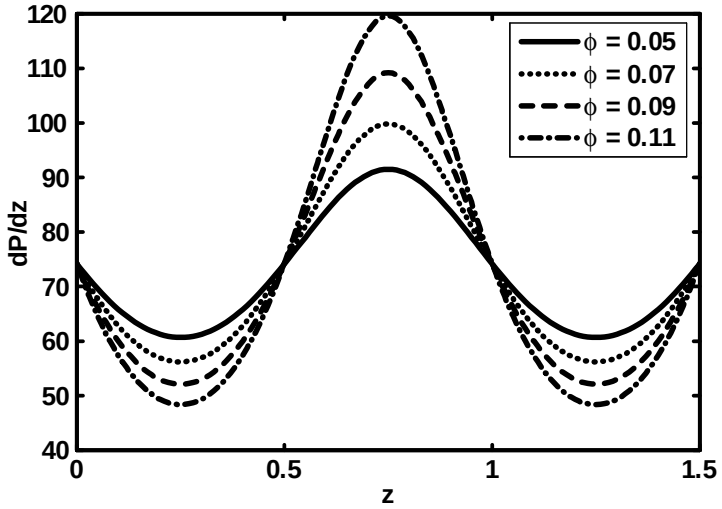

Fig.1.9 (a). Pressure gradient versus (Sinusoidal waves) z for $\alpha = 0.1$, $\alpha_1 = 0.4$, Re $= 8$, $\delta = 0.2$, $E = 0.1$, $Q = -1$.

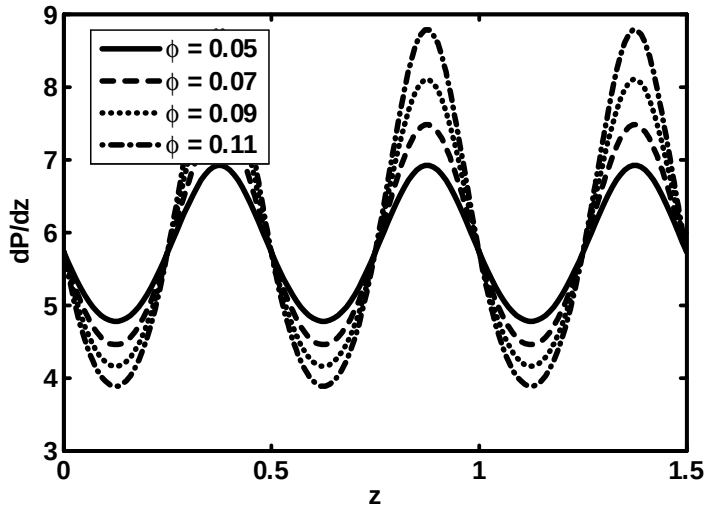

Fig.1.9 (b). Pressure gradient versus (Multisinusoidal waves) z for $\alpha = 0.1$, $\alpha_1 = 0.4$, Re $= 8$, $\delta = 0.2$, $E = 0.1$, $Q = -1$.

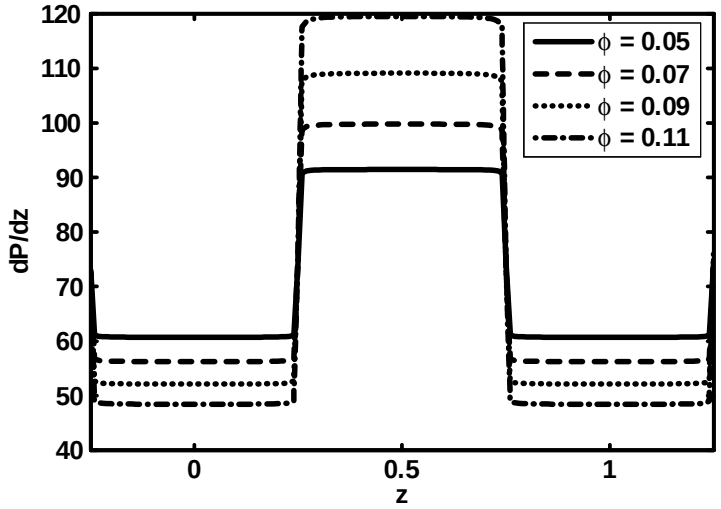

Fig.1.9 (c). Pressure gradient versus (Square waves) z for $\alpha = 0.1$, $\alpha_1 = 0.4$, Re $= 8$, $\delta = 0.2$, $E = 0.1$, $Q = -1$.

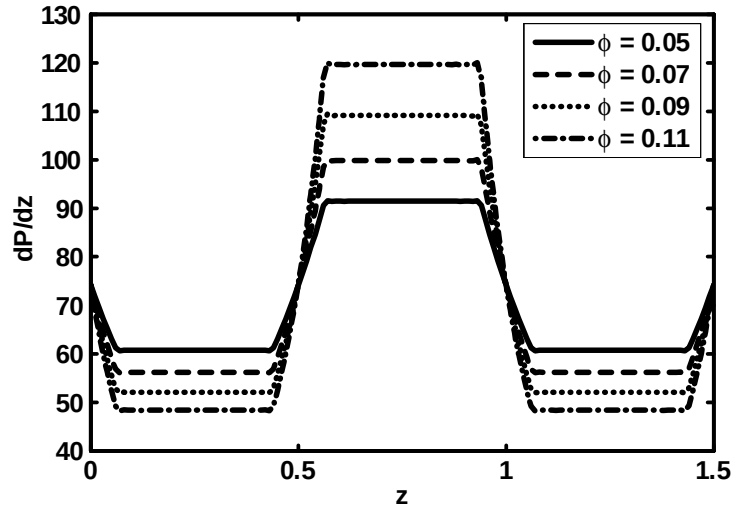

Fig.1.9 (d). Pressure gradient versus (Trapezoidal waves) z for $\alpha = 0.1$, $\alpha_1 = 0.4$, Re $= 8$, $\delta = 0.2$, $E = 0.1$, $Q = -1$.

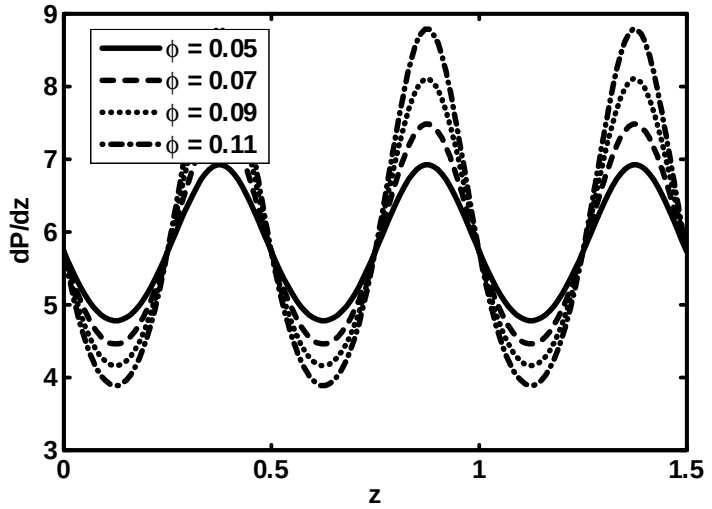

Fig.1.9 (e). Pressure gradient versus (Triangular waves) z for $\alpha = 0.1$, $\alpha_1 = 0.4$, Re $= 8$, $\delta = 0.2$, $E = 0.1$, $Q = -1$.

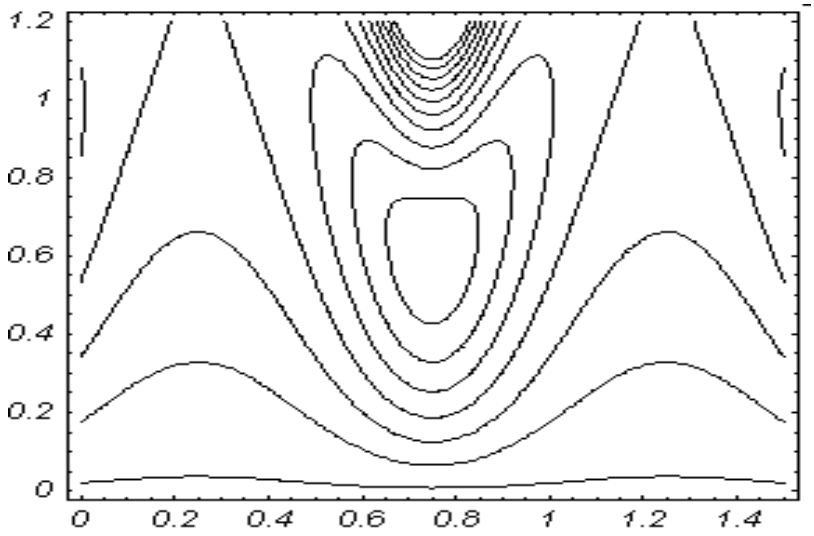

Fig. (1.10) (a) . Streamlines for Sinusoidal wave when $\alpha_1 = 0.05$, $\phi = 0.4$, Re $= 7$, $E = 0.1$, $\delta = 0.1$, $\alpha = 0.3$, $Q = -1$.

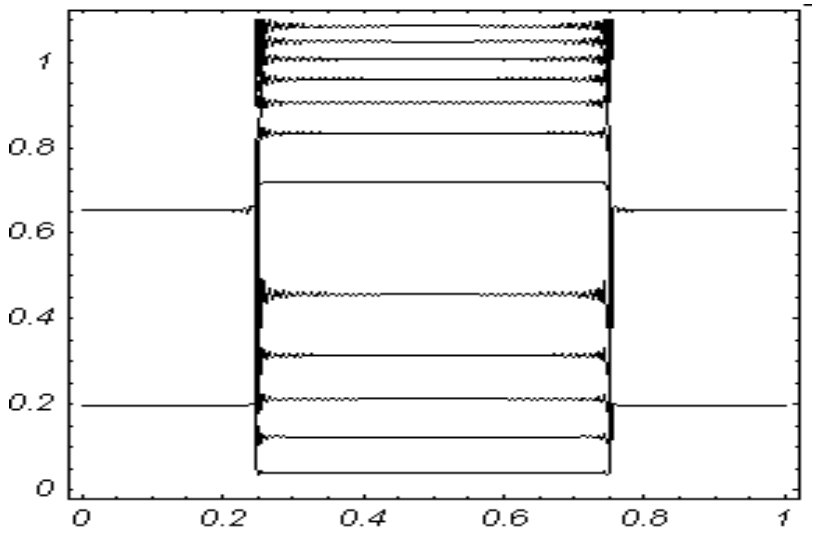

Fig. (1.10) (b) . Streamlines for square wave when $\alpha_1 = 0.05$, $\phi = 0.4$, Re $= 7$, $E = 0.1$, $\delta = 0.1$, $\alpha = 0.3$, $Q = -1$.

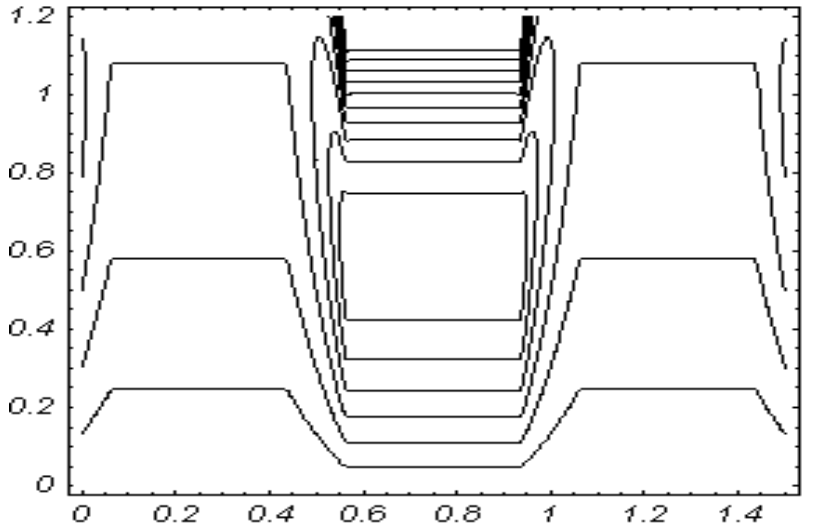

Fig. (1.10) (c) . Streamlines for trapezoidal wave when $\alpha_1 = 0.05$, $\phi = 0.4$, Re $= 7$, $E = 0.1$, $\Theta = 1.5$, $\delta = 0.1$, $\alpha = 0.3$, $Q = -1$.

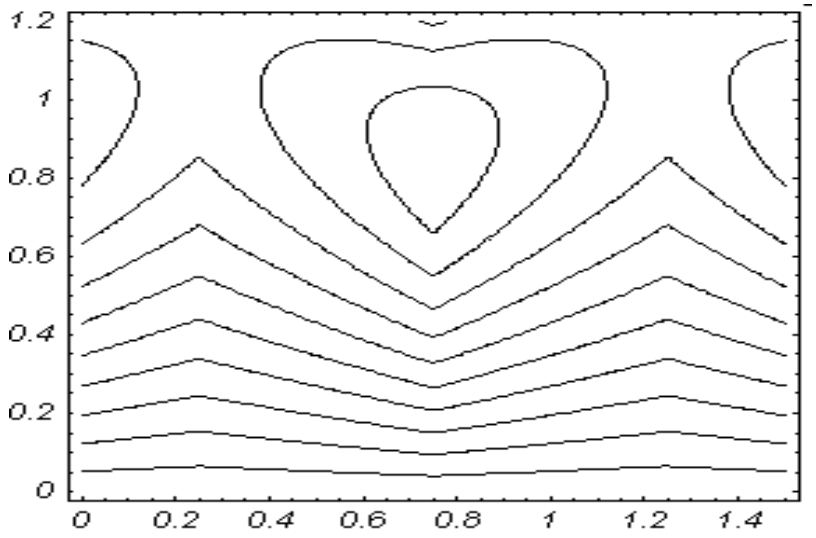

Fig. (1.10) (d) . Streamlines for triangular wave when
$\alpha_1 = 0.05$, $\phi = 0.4$, Re $= 7$, $E = 0.1$, $\delta = 0.1$, $\alpha = 0.3$, $Q = -1$.

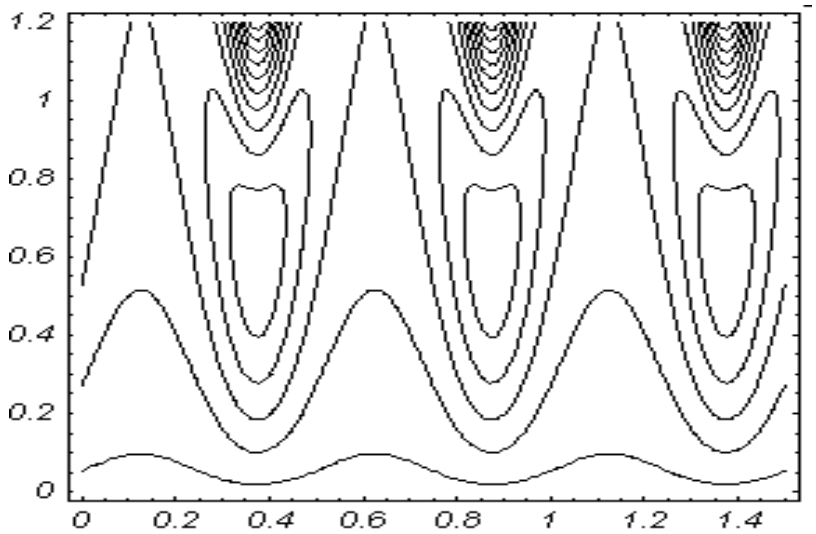

Fig. (1.10) (e) . Streamlines for multisinusoidal wave when
$\alpha_1 = 0.05$, $\phi = 0.4$, Re $= 7$, $E = 0.1$, $\delta = 0.1$, $\alpha = 0.3$, $Q = -1$.

1.6 Conclusion

This chapter concerns with the peristaltic flow of Walter,s B fluid in a uniform inclined tube. The governing two dimensional equations have been modeled and then simplified using long wave length and low Reynold's number approximation. The main points can be summarized as:

1. It is observed that the relation between pressure rise and volume flow rate are inversely proportional to each other.

2. In the peristaltic pumping region the pressure rise increases with the increase in angle of inclination α, amplitude ratio ϕ, wave length δ and decreases with an increase in Walter's B fluid parameter α_1.

3. It is seen that frictional forces have opposite behavior as compared to the pressure rise.

4. It is seen that pressure gradient increases with increase in ϕ.

5. It is observed that the size of trapping bolus in triangular wave is smaller as compared to the trapezoidal and sinusoidal waves.

6. If Walter's B fluid parameter $\alpha = 0$, the solution of Newtonian fluid can be recovered as a special case of our problem.

Chapter 2

Peristaltic flow of Williamson fluid model in an endoscope

2.1 Introduction

In this chapter, we have presented the peristaltic flow of an incompressible Williamson fluid model in an endoscope. The governing equations of Williamson fluid model in cylindrical coordinates are modelled for two dimensional flow. The highly nonlinear equations of Williamson fluid model are simplify using the assumptions of longwave length and low Reynolds number. The solutions of the reduced nonlinear equations are calculated with the help of (i) Perturbation method (ii) Homotopy analysis method and (iii) Shooting method. An excellent agreement between all the solutions are also presented. Also the expressions for pressure rise and velocity for various physical parameter are discussed through graphs.

2.2 Mathematical Model

For an incompressible fluid the balance of mass and momentum are defined in Eqs. (1.1) and (1.2). The constitutive equation for Williamson fluid is given by [34]

$$\mathbf{S} = -P\mathbf{I} + \boldsymbol{\tau} \tag{2.1}$$

$$\boldsymbol{\tau} = -\left[\mu_\infty + (\mu_0 + \mu_\infty)\left(1 - \Gamma\bar{\dot{\gamma}}\right)^{-1}\right]\bar{\dot{\gamma}}, \tag{2.2}$$

in which $\boldsymbol{\tau}$ is the extra stress tensor for Williamson fluid, μ_∞ is the infinite shear rate viscosity, μ_0 is the zero shear rate viscosity, Γ is the time constant, and $\bar{\dot{\gamma}}$ is defined as

$$\bar{\dot{\gamma}} = \sqrt{\frac{1}{2}\sum_i \sum_j \bar{\dot{\gamma}}_{ij}\bar{\dot{\gamma}}_{ji}} = \sqrt{\frac{1}{2}\Pi}. \tag{2.3}$$

Here Π is the second invariant strain tensor. We consider the constitutive Eq. (2.2), the case for which $\mu_\infty = 0$ and $\Gamma\dot{\gamma} < 1$. The component of extra stress tensor therefore, can be written as

$$\boldsymbol{\tau} = -\mu_0\left[(1 - \Gamma\bar{\dot{\gamma}})^{-1}\right]\bar{\dot{\gamma}} = -\mu_0\left[(1 + \Gamma\bar{\dot{\gamma}})\right]\bar{\dot{\gamma}}. \tag{2.4}$$

2.3 Mathematical Formulation

Let us consider the peristaltic transport of an incompressible Williamson fluid in a an endoscope. The flow is generated by sinusoidal wave trains propagating with constant speed c along the walls. The geometry of the wall surface is defined as and shown through the Fig. 2.

$$\bar{R}_1 = a_1, \tag{2.5}$$

$$\bar{R}_2 = a_2 + b\sin\frac{2\pi}{\lambda}\left(\bar{Z} - c\bar{t}\right), \tag{2.6}$$

where a_1 is the radius of the inner tube, a_2 is the radius of the outer tube at inlet, b is the wave amplitude, λ is the wavelength, c the wave speed and $\bar{t}$ the time.

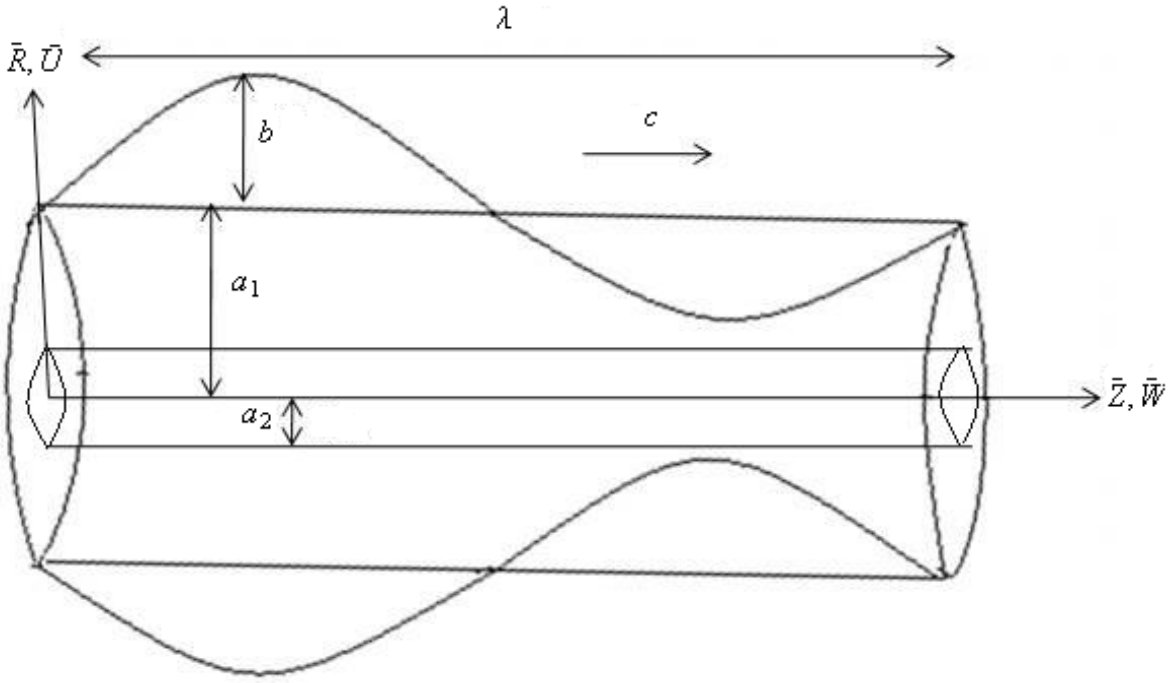

Fig. 2.. Geometry of the problem.

Making use of Eq. (2.4) , Eqs. (1.1) and (1.2) in component form take the form

$$\frac{\partial \bar{U}}{\partial \bar{R}} + \frac{\bar{U}}{\bar{R}} + \frac{\partial \bar{W}}{\partial \bar{Z}} = 0, \tag{2.7}$$

$$\rho\left(\frac{\partial}{\partial \bar{t}} + \bar{U}\frac{\partial}{\partial \bar{R}} + \bar{W}\frac{\partial}{\partial \bar{Z}}\right)\bar{U} = -\frac{\partial \bar{P}}{\partial \bar{R}} - \frac{1}{\bar{R}}\frac{\partial}{\partial \bar{R}}\left(\bar{R}\boldsymbol{\tau}_{\bar{R}\bar{R}}\right) - \frac{\partial}{\partial \bar{Z}}\left(\boldsymbol{\tau}_{\bar{R}\bar{Z}}\right), \tag{2.8}$$

$$\rho\left(\frac{\partial}{\partial \bar{t}} + \bar{U}\frac{\partial}{\partial \bar{R}} + \bar{W}\frac{\partial}{\partial \bar{Z}}\right)\bar{W} = -\frac{\partial \bar{P}}{\partial \bar{Z}} - \frac{1}{\bar{R}}\frac{\partial}{\partial \bar{R}}\left(\bar{R}\boldsymbol{\tau}_{\bar{R}\bar{Z}}\right) - \frac{\partial}{\partial \bar{Z}}\left(\boldsymbol{\tau}_{\bar{Z}\bar{Z}}\right), \tag{2.9}$$

where $\bar{U}$, $\bar{W}$ are the respective velocity components in the radial and axial directions in the fixed frame respectively.

In the fixed coordinates $\left(\bar{R}, \bar{Z}\right)$, the flow between the two tubes is unsteady. It becomes steady in a wave frame $(\bar{r}, \bar{z})$ moving with the same speed as the wave moves in the $\bar{Z}-$direction. The transformations between the two frames are

$$\begin{aligned} \bar{r} &= \bar{R}, \quad \bar{z} = \bar{Z} - c\bar{t}, \\ \bar{u} &= \bar{U}, \quad \bar{w} = \bar{W} - c, \end{aligned} \tag{2.10}$$

where $\bar{u}$ and $\bar{w}$ are the velocities in the wave frame.

The appropriate boundary conditions in the wave frame are of the following form

$$\bar{w} = -c, \quad \bar{u} = 0 \quad \text{at } \bar{r} = \bar{r}_1, \tag{2.11}$$

$$\bar{w} = -c, \quad \text{at } \bar{r} = \bar{r}_2 + b \sin \frac{2\pi}{\lambda} \bar{z}. \tag{2.12}$$

We introduce the non-dimensional variables

$$\begin{aligned} R &= \frac{\bar{R}}{a}, \quad r = \frac{\bar{r}}{a_2}, \quad Z = \frac{\bar{Z}}{\lambda}, \quad z = \frac{\bar{z}}{\lambda}, \quad W = \frac{\bar{W}}{c}, \quad w = \frac{\bar{w}}{c}, \; \dot{\gamma} = \frac{a_2}{c} \overline{\dot{\gamma}}, \\ U &= \frac{\lambda \bar{U}}{a_2 c}, \quad u = \frac{\lambda \bar{u}}{a_2 c}, \quad P = \frac{a_2^2 \bar{P}}{c \lambda \mu_0}, \; t = \frac{c\bar{t}}{\lambda}, \quad \delta = \frac{a_2}{\lambda}, \; \mathrm{Re} = \frac{\rho c a_2}{\mu_0}, \\ \tau &= \frac{a_2 \boldsymbol{\tau}}{c \mu_0}, \; r_1 = \frac{\bar{r}_1}{a_2} = \epsilon, \; r_2 = \frac{\bar{r}_2}{a_2} = 1 + \phi \sin(2\pi z). \end{aligned} \tag{2.13}$$

Making use of Eqs. (2.10) and (2.13) , Eqs. (2.7) to (2.9) along with boundary conditions (2.11) and (2.12) take the form

$$\frac{\partial u}{\partial r} + \frac{u}{r} + \frac{\partial w}{\partial z} = 0, \tag{2.14}$$

$$\mathrm{Re}\, \delta^3 \left(u \frac{\partial}{\partial r} + w \frac{\partial}{\partial z} \right) u = -\frac{\partial P}{\partial r} - \frac{\delta}{r} \frac{\partial}{\partial r} (r \tau_{rr}) - \delta^2 \frac{\partial}{\partial z} (\tau_{rz}), \tag{2.15}$$

$$\mathrm{Re}\, \delta \left(u \frac{\partial}{\partial r} + w \frac{\partial}{\partial z} \right) w = -\frac{\partial P}{\partial z} - \frac{1}{r} \frac{\partial}{\partial r} (r \tau_{rz}) - \delta \frac{\partial}{\partial z} (\tau_{zz}), \tag{2.16}$$

$$w = -1, \quad \text{at } r = r_1 = \varepsilon, \tag{2.17a}$$

$$w = -1, \quad \text{at } r = r_2 = 1 + \phi \sin(2\pi z), \tag{2.17b}$$

where

$$\begin{aligned}
\tau_{rr} &= -2\delta\left[1+We\dot{\gamma}\right]\frac{\partial u}{\partial r},\\
\tau_{rz} &= -\left[1+We\dot{\gamma}\right]\left(\frac{\partial u}{\partial z}\delta^2+\frac{\partial w}{\partial r}\right),\\
\tau_{zz} &= -2\delta\left[1+We\dot{\gamma}\right]\delta\frac{\partial w}{\partial z},\\
\dot{\gamma} &= \left[2\delta^2\left(\frac{\partial u}{\partial r}\right)^2+\left(\frac{\partial u}{\partial z}\delta^2-\frac{\partial w}{\partial r}\right)^2+2\delta^2\left(\frac{\partial w}{\partial z}\right)^2\right]^{1/2},
\end{aligned}$$

in which δ, Re, We represent the wave, Reynolds and Weissenberg numbers, respectively. Under the assumptions of long wavelength $\delta << 1$ and low Reynolds number, neglecting the terms of order δ and higher, Eqs. (2.15) and (2.16) take the form

$$\frac{\partial P}{\partial r} = 0, \tag{2.18}$$

$$\frac{\partial P}{\partial z} = \frac{1}{r}\frac{\partial}{\partial r}\left[r\left(1+We\frac{\partial w}{\partial r}\right)\frac{\partial w}{\partial r}\right], \tag{2.19}$$

$$w = -1, \quad \text{at } r = r_1 = \varepsilon, \tag{2.20a}$$

$$w = -1, \quad \text{at } r = r_2 = 1+\phi\sin\left(2\pi z\right). \tag{2.20b}$$

2.4 Solution of the Problem

2.4.1 Perturbation Solution

To get the solution of Eq. (2.19), we employ the regular perturbation to find the solution.

For perturbation solution, we expand w, F and P as

$$w = w_0 + We w_1 + O(We^2), \tag{2.21a}$$

$$F_1 = F_{10} + We F_{11} + O(We^2), \tag{2.21b}$$

$$P = P_0 + We P_1 + O(We^2). \tag{2.21c}$$

The perturbation results for small parameter We, satisfying the conditions $(2.20a)$ and $(2.20b)$,

for velocity and pressure gradient can be directly written as

$$\begin{aligned} w &= -1 + \left(\frac{r^2}{4} + a_{11}\ln r + a_{12}\right)\frac{dP}{dz} \\ &\quad + We\left(-\left(\frac{r^3}{12} - \frac{a_{11}}{r} + a_{11}r\right)\left(\frac{dP_0}{dz}\right)^2 + a_{13}\ln r + a_{15})\right), \end{aligned} \tag{2.22}$$

$$\frac{dP}{dz} = \frac{2F_1 + \left(r_2^2 - r_1^2\right)}{a_{16}} + We\left(\frac{-a_{17}}{a_{16}}\right), \tag{2.23}$$

where

$$\begin{aligned} a_{11} &= -\frac{1}{4}\left(\frac{r_1^2 - r_2^2}{\ln r_1 - \ln r_2}\right), \quad a_{12} = -\left(\frac{r_1^2}{4} + a_{11}\ln r_1\right), \\ a_{13} &= +\frac{1}{\ln r_1 - \ln r_2}\left(\frac{r_1^3 - r_2^3}{12} - \left(\frac{1}{r_1} - \frac{1}{r_2}\right)a_{11}^2 + 2a_{11}(r_1 - r_2)\right)\left(\frac{dP_0}{dz}\right)^2, \\ a_{14} &= -\left(\frac{r_1^3}{12} - \frac{a_{11}^2}{r_1} + 2a_{11}r_1\right)\left(\frac{dP_0}{dz}\right)^2, \quad a_{15} = a_{14} - a_{13}\ln r_1, \\ a_{16} &= \left(\frac{r_2^4 - r_1^4}{8} + a_{11}\left(r_2^2\ln r_2 - r_1^2\ln r_1\right) - a_{11}\frac{\left(r_2^2 - r_1^2\right)}{2} + a_{12}\left(r_2^2 - r_1^2\right)\right), \\ a_{17} &= -\left(\frac{r_2^5 - r_1^5}{30} - 2a_{11}^2\left(r_2 - r_1\right) + 4a_{11}\frac{r_2^3 - r_1^3}{3}\right)\left(\frac{dP_0}{dz}\right)^2 \\ &\quad + a_{13}\left(r_2^2\ln r_2 - r_1^2\ln r_1 - \frac{\left(r_2^2 - r_1^2\right)}{2}\right) + a_{15}\left(r_2^2 - r_1^2\right). \end{aligned}$$

The pressure rise ΔP and friction forces F on inner and outer tubes $F^{(0)}$, $F^{(i)}$, are given by

$$\Delta P = \int_0^1 \frac{dP}{dz}dz, \tag{2.24}$$

$$F^{(0)} = \int_0^1 r_1^2\left(-\frac{dP}{dz}\right)dz, \tag{2.25}$$

$$F^{(i)} = \int_0^1 r_2^2\left(-\frac{dP}{dz}\right)dz, \tag{2.26}$$

where $\frac{dP}{dz}$ is defined in Eqs. (2.23).

2.4.2 HAM Solution

In this section, we have found the HAM solutions of Eqs. (2.18) and (2.19). For that we choose [40]

$$w_0 = -1 + \left(\frac{r^2}{4} + a_{11}\ln r + a_{12}\right)\frac{dP}{dz}. \tag{2.27}$$

as the initial guess. Further, the auxiliary linear operator for the problem is taken as

$$\mathcal{L}_{wr}(w) = \frac{1}{r}\frac{\partial}{\partial r}\left(r\frac{\partial w_0}{\partial r}\right). \tag{2.28}$$

From Eqs. (2.18) and (2.19) we can define the following zeroth-order deformation problems

$$(1-q)\mathcal{L}_{wr}[\ \bar{w}\,(r,q) - \ w_0(r)] = q\hbar_w N_{wr}[\bar{w}\,(r,q)], \tag{2.29}$$

$$\bar{w}\,(r,q) \ = \ -1,\ at\ r = r_1, \tag{2.30}$$

$$\bar{w}\,(r,q) \ = \ -1,\ at\ r = r_2. \tag{2.31}$$

In Eqs. (2.30) and (2.31), $\hbar_w$ denote the non-zero auxiliary parameter, $q\epsilon[0,1]$ is the embedding parameter and

$$N_{wr}[w(r,q)] = \frac{\partial^2 w}{\partial r^2} + \frac{1}{r}\frac{\partial w}{\partial r} + \frac{We}{r}\left(\frac{\partial w}{\partial r}\right)^2 + 2We\frac{\partial^2 w}{\partial r^2}\frac{\partial w}{\partial r} - \frac{dP}{dz}. \tag{2.32}$$

Obviously

$$\hat{w}\,(r,0) = w_0, \quad \hat{w}\,(r,1) = w\,(r)\,, \tag{2.33}$$

when q varies from 0 to 1, then $\hat{w}\,(r,q)$ varies from initial guess to the solution $w\,(r)$. Expanding $\hat{w}\,(r,q)$ in Taylor's with respect to an embedding parameter q, we have

$$\hat{w}\,(r,q) = w_0\,(r) + \sum_{n=1}^{\infty} w_m(r)q^m, \tag{2.34}$$

$$w_m = \frac{1}{m!}\left.\frac{\partial^m \bar{w}\,(r,q)}{\partial q^m}\right|_{q=0}. \tag{2.35}$$

Differentiating the zeroth order deformation m-times with respect to q and then dividing by $m!$ and finally setting $q = 0$, we get the following mth order deformation problem

$$\mathcal{L}_w[w_m(r) - \chi_m w_{m-1}(r)] = \hbar_w R_{wr}(r), \tag{2.36}$$

where

$$\begin{aligned} R_{wr} &= w''_{m-1} + \frac{1}{r} w'_{m-1} + \frac{We}{r} \sum_{i=0}^{m-1} w'_{m-1} w'_{m-1-i} \\ &\quad + 2We \sum_{i=0}^{m-1} w'_{m-1} w''_{m-1-i} - \frac{dP}{dz}(1 - \chi_m) \end{aligned} \tag{2.37}$$

$$\chi_m = \begin{cases} 0, & m \leq 1, \\ 1, & m > 1. \end{cases} \tag{2.38}$$

The solution of the above equation with the help of Mathematica can be calculated and is presented as

$$w_m(r) = \lim_{M\to\infty} \left[\sum_{m=0}^{M} a^0_{m,0} + \sum_{n=1}^{2M+1} \left(\sum_{m=n-1}^{2M} \sum_{k=1}^{2m+1-n} a^k_{m,n} r^n \ln r \right) \right] + \lim_{M\to\infty} \left[\sum_{n=1}^{2M+1} \left(\sum_{m=n-1}^{2M} \sum_{k=0}^{2m+1-n} a^k_{m,n} r^{n+2} \right) \right],$$

where $a^0_{m,0}$ and $a^k_{m,n}$ are constants.

2.4.3 Numerical Solution

The present problem consisting of Eqs. (2.18) and (2.19) and solved numerically by employing shooting method. The numerical results are compared with the perturbation and HAM results and get a very good agreement between the three solutions. The comparison is made for small values of Weissenberg number.

2.5 Graphical Results and Discussion

In this section we have presented the solution of the Williamson fluid model graphically. The expression for pressure rise ΔP is calculated numerically using mathematics software. The effects of various parameters on the pressure rise ΔP are shown in Figs. 2.3 to 2.5 for various

values of Weissenberg number We, amplitude ratio ϕ and radius ratio ε. It is observed from Figs. 2.3 to 2.5 that pressure rise increases with the increase in We while the pressure rise decreases with increase in ε and ϕ. Peristaltic pumping region is $(-2 \leq Q \leq -1.3)$ for Fig. 2.3 and $(-2 \leq Q \leq 0)$ for Figs. 2.4 and 2.4, otherwise there is augmented pumping. Figs. 2.6 to 2.11 represent the behavior of frictional forces. It is depicted that frictional forces have an opposite behavior as compared to the pressure rise. The pressure gradient for different values of We, ϕ, ε and Q against z is plotted in Figs. 2.12 to 2.15. It is shown through the figures that in the region $z\epsilon\,[0, 0.5]$ and $z\epsilon\,[1, 1.5]$, the pressure gradient is small, while pressure gradient is large in the region $z\epsilon\,[0.6, 0.9]$, further it is seen that with increase in We and Q pressure gradient decreases while pressure gradient increases with increase in ϕ and ε.

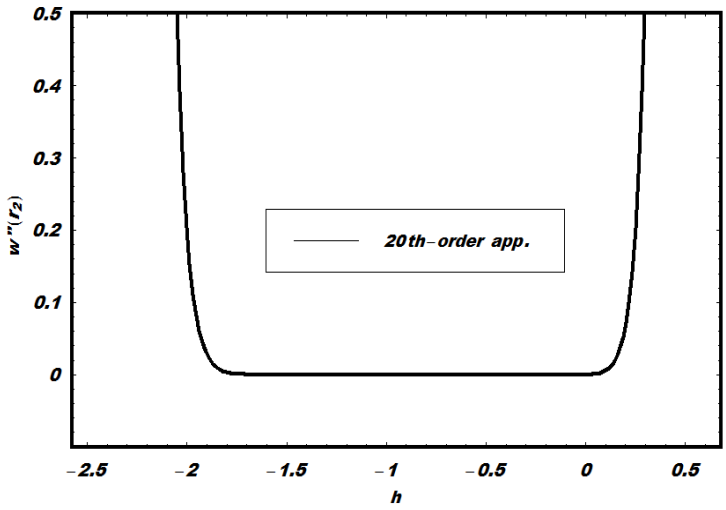

Fig.2.1. h-curve for velocity profile for $\varepsilon = 0.1$, $We = 0.1$, $z = 0.1$, $\phi = 0.3$.

r	Numerical sol	Perturbation sol	Error	HAM sol	Error
0.1	-1.00000	-1.00000	0.00000	-1.00000	0.00000
0.2	-1.02651	-1.02672	0.00020	-1.02708	0.00055
0.3	-1.04062	-1.03992	0.00067	-1.04021	0.00040
0.4	-1.04692	-1.04669	0.00021	-1.04686	0.00210
0.5	-1.04929	-1.04927	0.00010	-1.04931	0.00005
0.6	-1.04867	-1.04864	0.00016	-1.04857	0.00009
0.7	-1.04505	-1.04534	0.00027	-1.04519	0.00013
0.8	-1.03949	-1.03967	0.00116	-1.03947	0.00116
0.9	-1.03194	-1.03184	0.00069	-1.03163	0.00001
1.0	-1.02137	-1.02199	0.00060	-1.02182	0.00044
1.1	-1.01000	-1.01023	0.00027	-1.01013	0.00012
1.2	-1.00000	-1.00000	0.00000	-1.00000	0.00000

Table. 2.1. Comparison of three methods for different values of $\varepsilon = 0.1$, $We = 0.1$, $z = 0.1$, $\phi = 0.3$.

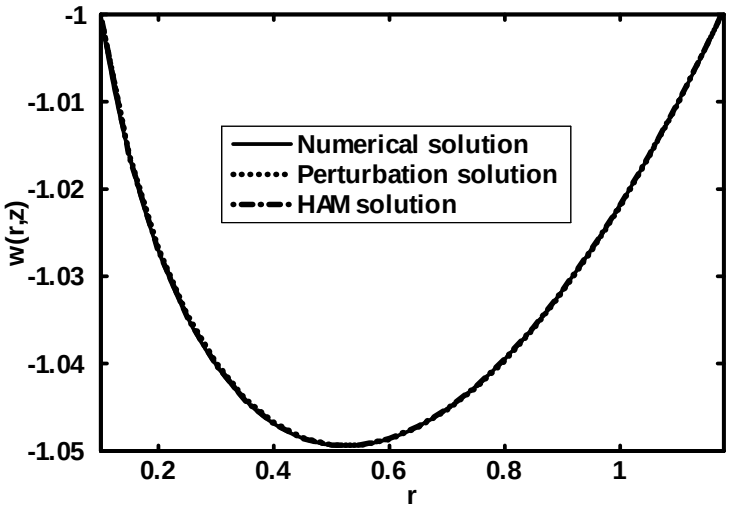

Fig. 2.2. Comparison of velocity field for $\varepsilon = 0.1$, $We = 0.1$, $z = 0.1$, $\phi = 0.3$.

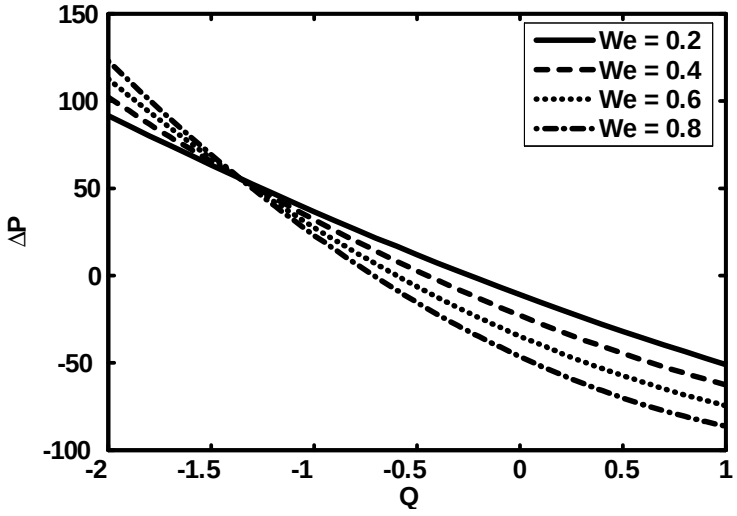

Fig.2.3. Pressure rise versus flow rate for $\varepsilon = 0.2$, $\phi = 0.2$.

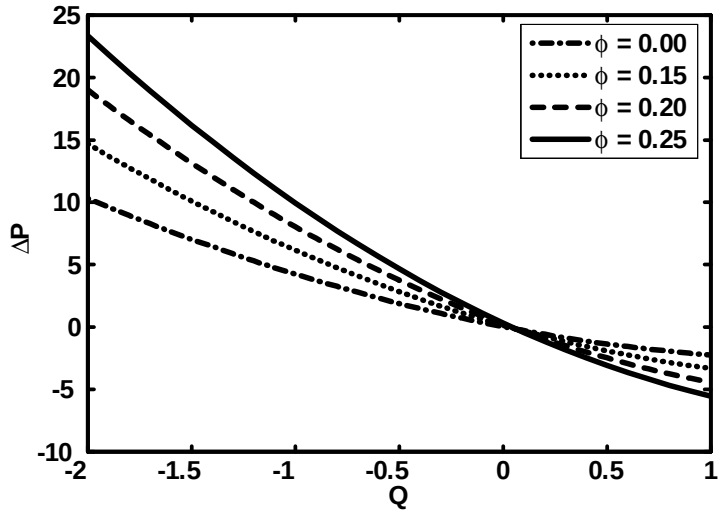

Fig.2.4. Pressure rise versus flow rate for $\varepsilon = 0.1$, $We = 0.01$.

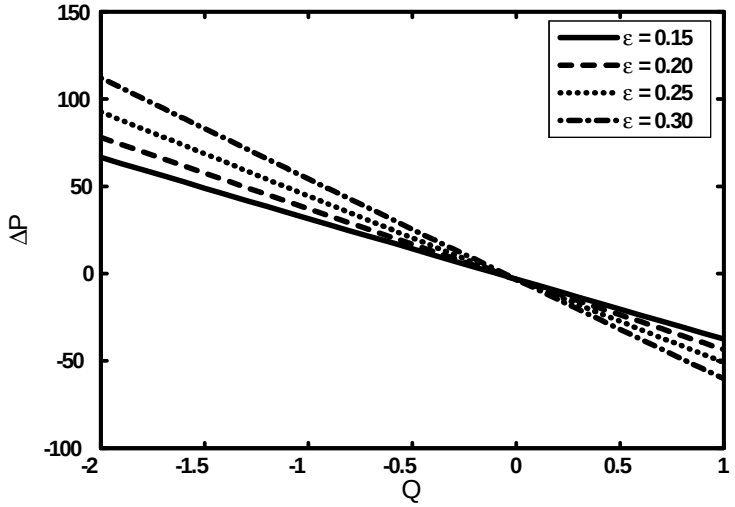

Fig.2.5. Pressure rise versus flow rate for $We = 0.01$, $\phi = 0.1$.

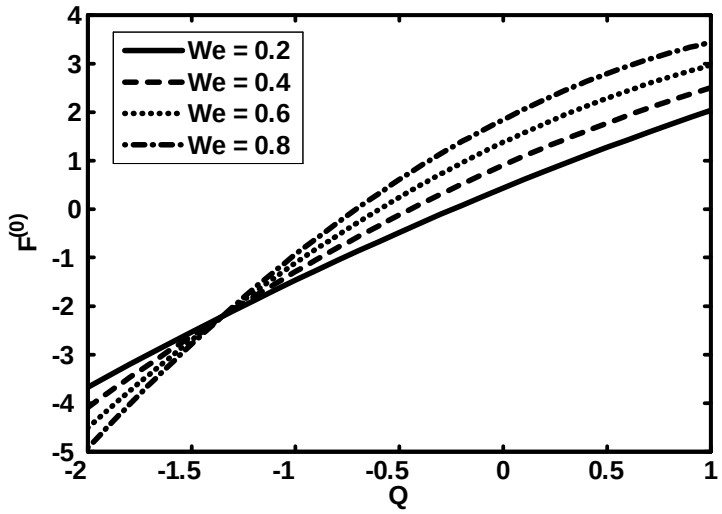

Fig.2.6. Frictional force versus flow (for inner tube) rate for $\varepsilon = 0.2$, $\phi = 0.2$.

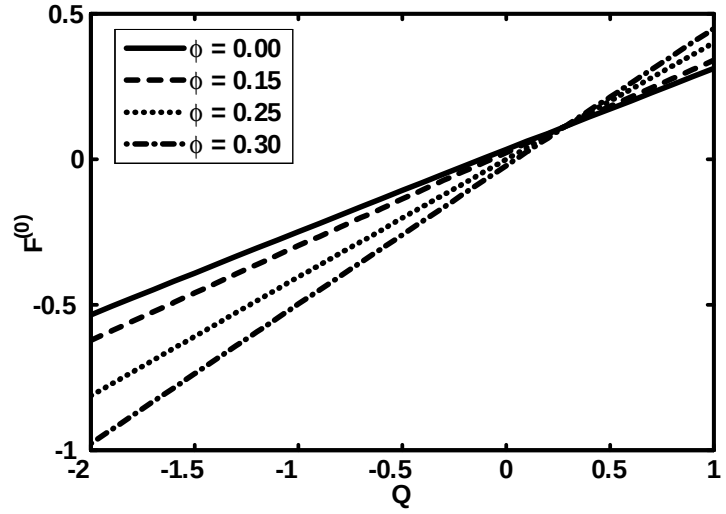

Fig.2.7. Frictional force versus flow (for inner tube) rate for $\varepsilon = 0.1$, $We = 0.01$.

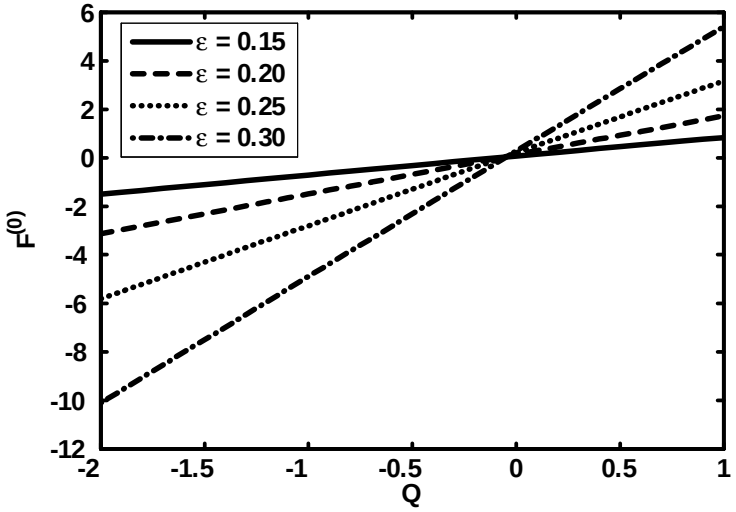

Fig.2.8. Frictional force versus flow (for inner tube) rate for $\phi = 0.1$, $We = 0.01$.

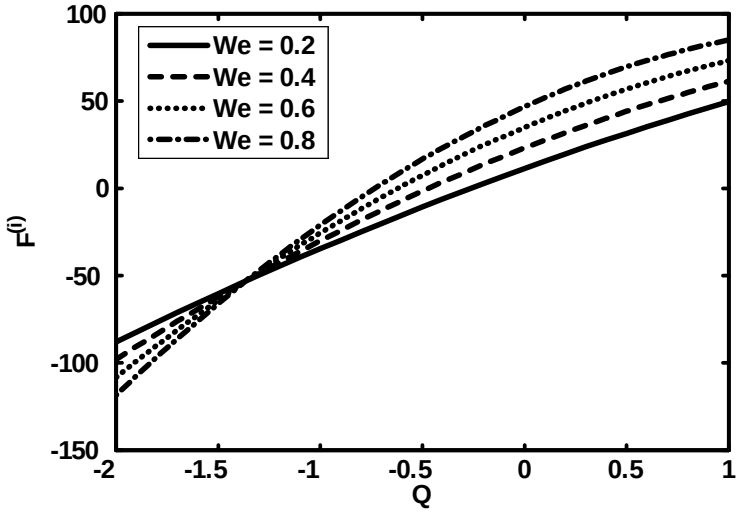

Fig.2.9. Frictional force versus flow (for outer tube) rate for $\varepsilon = 0.2$, $\phi = 0.1$.

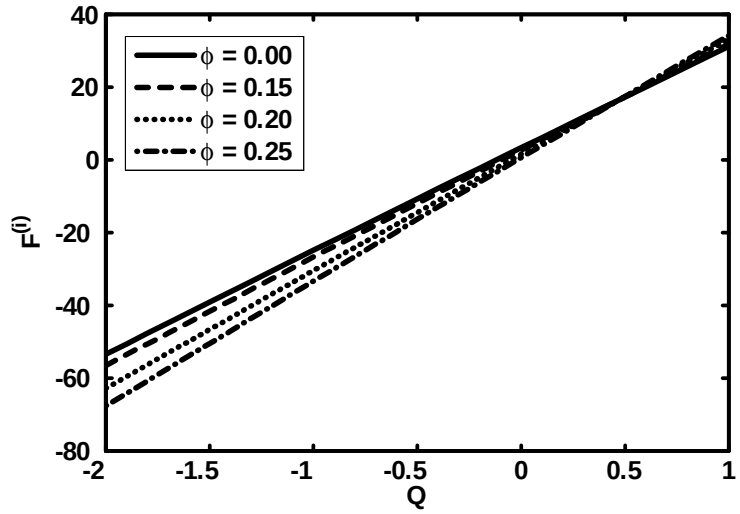

Fig.2.10. Frictional force versus flow (for outer tube) rate for $We = 0.01$, $\varepsilon = 0.1$.

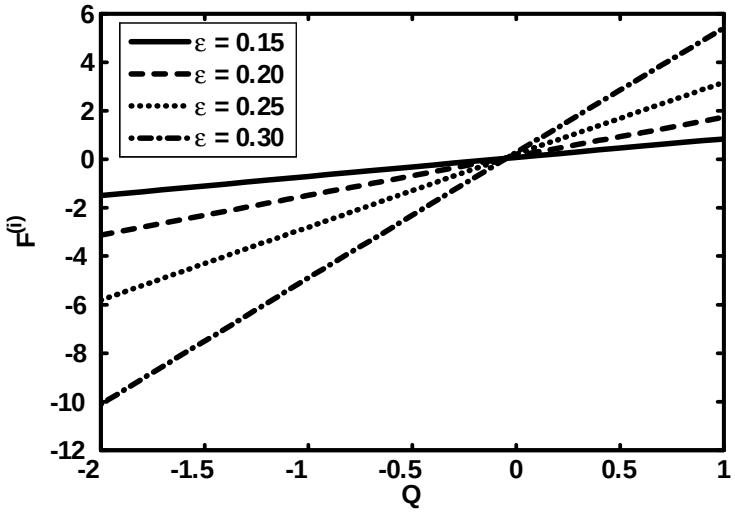

Fig.2.11. Frictional force versus flow (for outer tube) rate for $We = 0.01$, $\phi = 0.1$.

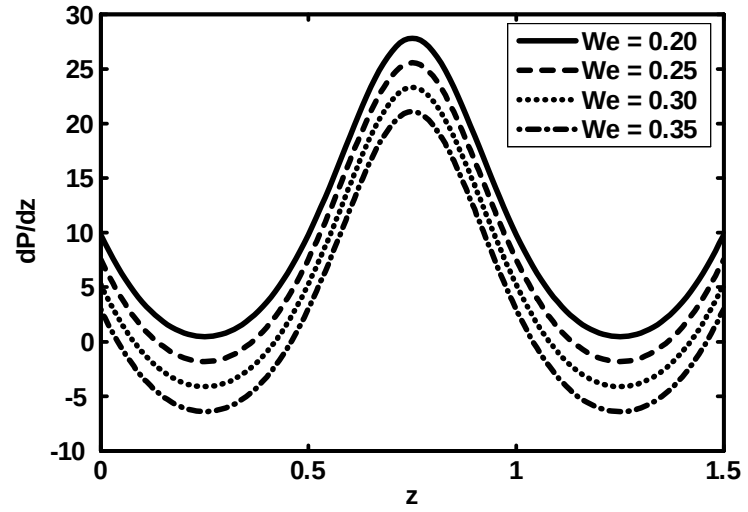

Fig.2.12. Pressure gradient versus z for $\varepsilon = 0.2$, $Q = -0.5$, $\phi = 0.1$.

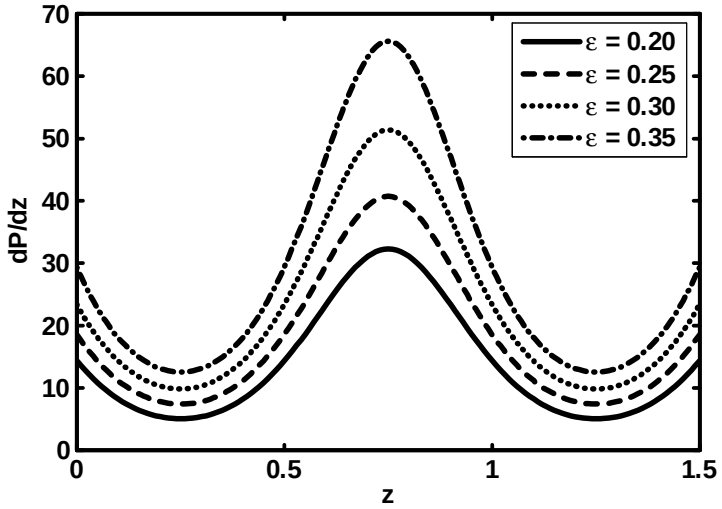

Fig.2.13. Pressure gradient versus z for $We = 0.1$, $Q = -0.5$, $\phi = 0.1$.

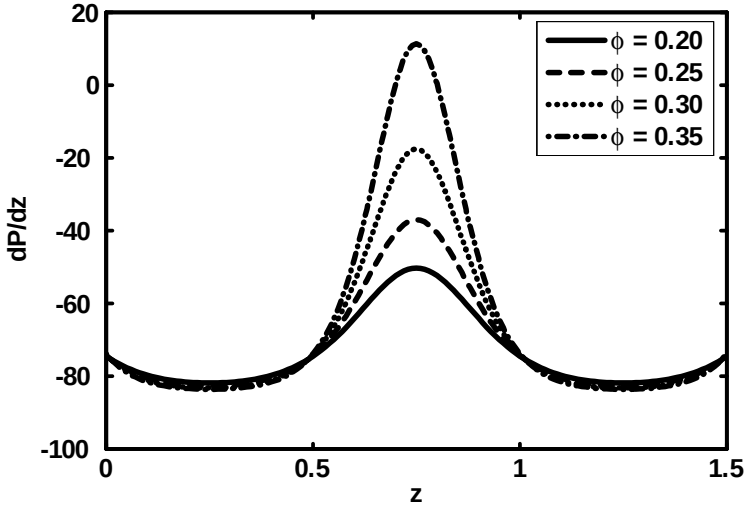

Fig.2.14. Pressure gradient versus z for $We = 0.1$, $Q = -0.5$, $\varepsilon = 0.01$.

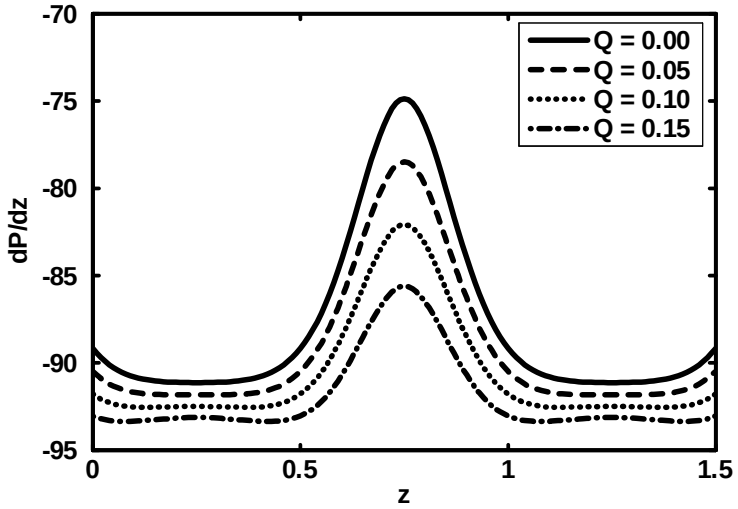

Fig.2.15. Pressure gradient versus z for $We = 0.1$, $\phi = 0.25$, $\varepsilon = 0.01$.

2.6 Conclusion

This chapter presents the analytical and numerical treatment of peristaltic flow of Williamson fluid model in an endoscope. The governing two dimensional equations are modeled in cylindrical coordinates system and simplified using long wave length approximation. The analytical and numerical solutions of simplified equations are calculated. The results are discussed pictorially through graphs. The main points can be discussed as follows

1. It is analyzed that analytical and numerical solutions are same upto four decimal place.

2. It is observed that in the peristaltic pumping region, pressure rise increases with the increase in Weissenberg number We while the pressure rise decreases with increase in amplitude ratio ϕ and radius ratio ε.

3. It is seen that frictional forces have opposite behavior as compared to the pressure rise.

4. It is depicted that with increase in We and Q pressure gradient decreases while pressure gradient increases with increase in ϕ and ε.

Chapter 3

Peristaltic flow of Sisko fluid in a uniform inclined tube

3.1 Introduction

In the present chapter, we have analyzed an incompressible Sisko fluid through an axisymmetric uniform inclined tube with a sinusoidal wave propagating down its walls. The present analysis of non-Newtonian fluid is investigated under the considerations of long wavelength and low Reynolds number approximation. The analytic solution is obtained using (i) regular perturbation method and (ii) Homotopy analysis method (HAM). The comparison of both the solutions are presented graphically. The results for the pressure rise, frictional forces

and pressure gradient have been calculated numerically and the results are studied for various values of the physical parameters of interest, such as α (angle of inclination) , b^* (Sisko fluid parameter) , ϕ (amplitude ratio) and n (power law index). Trapping phenomena is discussed at the end of the article.

3.2 Physical Model and Fundamental Equations

For an incompressible fluid the balance of mass and momentum in the presence of body forces are given by

$$\begin{aligned} \operatorname{div} \mathbf{V} &= 0, && (3.1)\\ \rho \frac{d\mathbf{V}}{dt} &= \operatorname{div} \mathbf{S} + \rho f, && (3.2) \end{aligned}$$

$$\mathbf{S} = -P\mathbf{I} + \boldsymbol{\tau}, \tag{3.3}$$

where $\mathbf{S}$ is the Cauchy stress tensor for Sisko fluid model and $\boldsymbol{\tau}$ is the extra stress tensor for Sisko fluid which is defined as [33]

$$\boldsymbol{\tau} = \left[a_* + b_5 \left(\sqrt{\bar{\Pi}} \right)^{n-1} \right] \mathbf{A}_1, \tag{3.3a}$$

$$\mathbf{A}_1 = \mathbf{L} + \mathbf{L}^{\mathbf{T}}, \quad \mathbf{L} = \operatorname{grad} \mathbf{V}, \quad \bar{\Pi} = \frac{1}{2} tr \left(\mathbf{A}_1^2 \right). \tag{3.3b}$$

3.3 Mathematical Formulation

Let us consider the peristaltic transport of an incompressible Sisko fluid in a uniform inclined tube. The flow is generated by sinusoidal wave trains propagating with constant speed c along the walls of the tube. The geometry of the wall surface is defined in chapter one

$$\bar{h} = a + b \sin \frac{2\pi}{\lambda} \left(\bar{Z} - c\bar{t} \right). \tag{3.4}$$

The governing equations for Sisko fluid in the fixed frame of reference in component form are given as

$$\frac{\partial \bar{U}}{\partial \bar{R}} + \frac{\bar{U}}{\bar{R}} + \frac{\partial \bar{W}}{\partial \bar{Z}} = 0, \tag{3.5}$$

$$\rho \left(\frac{\partial}{\partial \bar{t}} + \bar{U} \frac{\partial}{\partial \bar{R}} + \bar{W} \frac{\partial}{\partial \bar{Z}} \right) \bar{U} = -\frac{\partial \bar{P}}{\partial \bar{R}} + \frac{1}{\bar{R}} \frac{\partial}{\partial \bar{R}} \left(\bar{R} \boldsymbol{\tau}_{\bar{R}\bar{R}} \right) + \frac{\partial}{\partial \bar{Z}} \left(\boldsymbol{\tau}_{\bar{R}\bar{Z}} \right) - \frac{\boldsymbol{\tau}_{\bar{\theta}\bar{\theta}}}{\bar{R}} + \rho g \cos \alpha, \tag{3.6}$$

$$\rho \left(\frac{\partial}{\partial \bar{t}} + \bar{U} \frac{\partial}{\partial \bar{R}} + \bar{W} \frac{\partial}{\partial \bar{Z}} \right) \bar{W} = -\frac{\partial \bar{P}}{\partial \bar{Z}} + \frac{1}{\bar{R}} \frac{\partial}{\partial \bar{R}} \left(\bar{R} \boldsymbol{\tau}_{\bar{R}\bar{Z}} \right) + \frac{\partial}{\partial \bar{Z}} \left(\boldsymbol{\tau}_{\bar{Z}\bar{Z}} \right) + \rho g \sin \alpha. \tag{3.7}$$

In the fixed coordinates $\left(\bar{R}, \bar{Z}\right)$, the flow is unsteady, it becomes steady in a wave frame $(\bar{r}, \bar{z})$ moving with the same speed as the wave moves in the $\bar{Z}-$direction. The transformations between the two frames are defined in Eqs. (1.11) and (1.12). The corresponding boundary conditions are defined in Eqs. (1.13) and (1.14).

Making use of Eqs. (1.11), (1.12) and (1.15), Eq. (3.5) to Eq. (3.7) take the form

$$\frac{\partial u}{\partial r} + \frac{u}{r} + \frac{\partial w}{\partial z} = 0, \tag{3.8}$$

$$\mathrm{Re}\,\delta^3 \left(u\frac{\partial}{\partial r} + w\frac{\partial}{\partial z} \right) u = -\frac{\partial P}{\partial r} + \frac{\delta}{r}\frac{\partial}{\partial r}\left(r\tau_{rr}\right) + \delta^2 \frac{\partial}{\partial z}\left(\tau_{rz}\right) - \delta\frac{\tau_{\boldsymbol{\theta\theta}}}{r} + \frac{\delta\cos\alpha}{E}, \tag{3.9}$$

$$\mathrm{Re}\,\delta \left(u\frac{\partial}{\partial r} + w\frac{\partial}{\partial z} \right) w = -\frac{\partial P}{\partial z} + \frac{1}{r}\frac{\partial}{\partial r}\left(r\tau_{rz}\right) + \delta\frac{\partial}{\partial z}\left(\tau_{zz}\right) + \frac{\sin\alpha}{E}, \tag{3.10}$$

where

$$\begin{aligned}
\tau_{rr} &= 2\left[1 + b^*\left(\frac{\partial w}{\partial r}\right)^{n-1}\right]\frac{\partial u}{\partial r}, \\
\tau_{rz} &= \left[1 + b^*\left(\frac{\partial w}{\partial r}\right)^{n-1}\right]\left(\frac{\partial u}{\partial z}\delta^2 + \frac{\partial w}{\partial r}\right), \\
\tau_{zz} &= 2\delta\left[1 + b^*\left(\frac{\partial w}{\partial r}\right)^{n-1}\right]\frac{\partial w}{\partial z},
\end{aligned}$$

in which $\delta = a/\lambda$, $\mathrm{Re} = \rho ca/\mu$ and $b^* = b_5/a_*\,(a/c)^{n-1}$ represent the wave number, Reynolds number and Sisko fluid parameter respectively. Under the assumptions of long wavelength $\delta << 1$ and low Reynolds number, neglecting the terms of order δ and higher, Eqs. (3.9) and (3.10) take the form

$$\frac{\partial P}{\partial r} = 0, \tag{3.11}$$

$$\frac{\partial P}{\partial z} = \frac{1}{r}\frac{\partial}{\partial r}\left(r\left(\left[1 + b^*\left(\frac{\partial w}{\partial r}\right)^{n-1}\right]\frac{\partial w}{\partial r}\right)\right) + \frac{\sin\alpha}{E}, \tag{3.12}$$

$$\frac{\partial w}{\partial r} = 0, \quad \text{at} \quad r = 0, \tag{3.13a}$$

$$w = -1, \ \text{at} \quad r = h = 1 + \phi\sin 2\pi z. \tag{3.13b}$$

3.4 Solution of the problem

3.4.1 Perturbation Solution

Since, Eq. (3.17) is non linear equation, its exact solution may be not possible, therefore, we employ the regular perturbation to find the solution.

For perturbation solution, we expand w, F and P as

$$w = w_0 + b^* w_1 + O(b^{*2}), \tag{3.14}$$

$$F_1 = F_{10} + b^* F_{11} + O(b^{*2}), \tag{3.15}$$

$$P = P_0 + b^* P_1 + O(b^{*2}). \tag{3.16}$$

Substituting Eqs. (3.14) to (3.16) in Eqs. (3.11) to (3.13) and then find the solutions of all the systems we arrive at the final solutions which are defined as follow

$$w = -1 + \left(\frac{r^2 - h^2}{4}\right)\left(\frac{\partial P}{\partial z} - \frac{\sin\alpha}{E}\right) + b^*\left(-\frac{a_1^*}{n+1}\left(r^{n+1} - h^{n+1}\right)\right), \tag{3.17}$$

$$\frac{dP}{dz} = \frac{-8E\left(2F_1 + h^2\right) + h^4 \sin\alpha}{Eh^4} + b^*\left(\frac{16 a_1^{*n} h^{n+3}}{h^4}\right), \tag{3.18}$$

where

$$a_1^* = \left(\frac{dP_0}{dz} - \frac{\sin\alpha}{E}\right)\frac{1}{2}.$$

The pressure rise ΔP and friction force F are defined as follow

$$\Delta P = \int_0^1 \frac{dP}{dz} dz, \tag{3.19}$$

$$F = \int_0^1 h^2 \left(-\frac{dP}{dz}\right) dz, \tag{3.20}$$

where $\frac{dP}{dz}$ is defined in Eqs. (3.18).

3.4.2 HAM Solution

In this section, we have found the HAM solution of Eqs. (3.16) to (3.18). For that we choose

$$w_0 = -1 + \left(\frac{r^2 - h^2}{4}\right)\left(\frac{\partial P}{\partial z} - \frac{\sin\alpha}{E}\right), \tag{3.21}$$

as the initial guess. Further, the auxiliary linear operator for the problem is taken as

$$\mathcal{L}_{wr}(w) = \frac{1}{r}\frac{\partial}{\partial r}\left(r\frac{\partial w_0}{\partial r}\right), \tag{3.22}$$

we can define the following zeroth-order deformation problems

$$(1-q)\mathcal{L}_{wr}[\ \bar{w}\,(r,q) - \ w_0(r)] = q\hbar_w N_{wr}[\bar{w}\,(r,q)], \tag{3.23}$$

$$\frac{\partial \bar{w}\,(r,q)}{\partial r} = 0,\ at\ r = 0, \tag{3.24}$$

$$\bar{w}\,(r,q) = -1,\ at\ r = h. \tag{3.25}$$

In Eqs. (3.23) to (3.25), $\hbar_w$ denote the non-zero auxiliary parameter, $q\epsilon[0,1]$ is the embedding parameter and

$$N_{wr}[\bar{w}(r,q)] = \frac{\partial^2 w}{\partial r^2} + \frac{1}{r}\frac{\partial w}{\partial r} + b^* n\frac{\partial^2 w}{\partial r^2}\left(\frac{\partial w}{\partial r}\right)^{n-1} + \frac{b^*}{r}\left(\frac{\partial w}{\partial r}\right)^n - \frac{dP}{dz}. \tag{3.26}$$

Obviously

$$\frac{\partial \hat{w}\,(r,0)}{\partial r} = w_0, \quad \hat{w}\,(r,1) = w\,(r)\,, \tag{3.27}$$

when q varies from 0 to 1, then $\hat{w}\,(r,q)$ varies from initial guess to the solution $w\,(r)$. Expanding $\hat{w}\,(r,q)$ in Taylor's with respect to an embedding parameter q, we have

$$\hat{w}\,(r,q) = w_0\,(r) + \sum_{n=1}^{\infty} w_m(r)q^m, \tag{3.28}$$

$$w_m = \frac{1}{m!}\left.\frac{\partial^m \bar{w}\,(r,q)}{\partial q^m}\right|_{q=0}. \tag{3.29}$$

Differentiating the zeroth order deformation m-times with respect to q and then dividing by $m!$ and finally setting $q = 0$, we get the following mth order deformation problem

$$\mathcal{L}_w[w_m(r) - \chi_m w_{m-1}(r)] = \hbar_w R_{wr}(r), \tag{3.30}$$

where

$$\begin{aligned} R_{wr} &= w''_{m-1} + \frac{1}{r} w'_{m-1} + \frac{b^*}{r} \left(w'_{m-1}\right)^n + b^* n \sum_{i=0}^{m-1} w'_{m-1} w''_{m-1-i} \\ &\quad - \frac{dP}{dz} \left(1 - \chi_m\right), \end{aligned} \tag{3.31}$$

$$\chi_m = \begin{cases} 0, & m \leq 1, \\ 1, & m > 1. \end{cases} \tag{3.32}$$

The solution of the above equation with the help of Mathematica can be calculated and presented as follows

$$w_m(r) = \lim_{M \to \infty} \left[\sum_{m=0}^{M} a^0_{m,0} + \sum_{n=1}^{2M+1} \left(\sum_{m=n-1}^{2M} \sum_{k=0}^{2m+1-n} a^k_{m,n} r^{2n+2} \right) \right], \tag{3.33}$$

where $a^0_{m,0}$ and $a^k_{m,n}$ are constants.

3.5 Graphical Results and Discussion

In this section we have presented the solution of the Sisko fluid model graphically. Figs. $3.1\,(a)$, $3.2\,(a)$ and $3.3\,(a)$ show the h-curve for velocity profile. Figs. $3.1\,(b,c)$, $3.2\,(b,c)$, $3.3\,(b,c)$ show the comparison of velocity field. The expression for pressure rise ΔP frictional forces F, pressure gradient dP/dz is calculated numerically using mathematics software. The effects of various parameters on the pressure rise ΔP are shown in Figs. 3.4 to 3.6 for various values of angle of inclination α, Weissenberg number We, amplitudes ratio ϕ, different wave forms and for different fluids. It is observed from Figs. 3.4 to 3.6 that pressure rise increases with the increase in α, We and ϕ. Moreover, the peristaltic pumping occurs in the region $0 \leq Q \leq 0.3$ for Figs. 3.4 and $0 \leq Q \leq 0.5$ for Figs. 3.5 and 3.6, other wise augmented pumping occurs. Fig.

3.7 shows the effects of five different wave form on pressure rise. It is analyzed that the square wave has best peristaltic pumping characteristics, while triangular waves has worst pumping characteristics. The peristaltic pumping occurs in the region $(0 \leq Q \leq 0.5)$ for Fig. 3.7, otherwise augmented pumping occurs. Fig. 3.8 shows the effects of pressure rise for different fluids. From figures it is seen that Newtonian fluid has best peristaltic pumping characteristics. The variations of frictional forces are plotted in Figs. 3.9 to 3.13. It can be seen that frictional forces have opposite behavior as compared to the pressure rise. Figs. 3.14 (a) to 3.14 (e) are prepared to see the behavior of pressure gradient for different wave shapes. It is observed from the figures that for $z\epsilon\,[0, 0.5]$ and $[1.1, 1.5]$ the pressure gradient is small and large pressure gradient occurs for $z\epsilon\,[0.51, 1]$. Moreover it is seen that with increase in ϕ pressure gradient increases. The effects of different parameters on streamlines for the trapping phenomenon for four different wave forms can be seen through Fig. 3.15. It is depicted that the size of trapping bolus in triangular wave is smaller as compared to the trapezoidal and sinusoidal waves.

Case. 1 ($n = 0$ Shear Thinning Fluid)

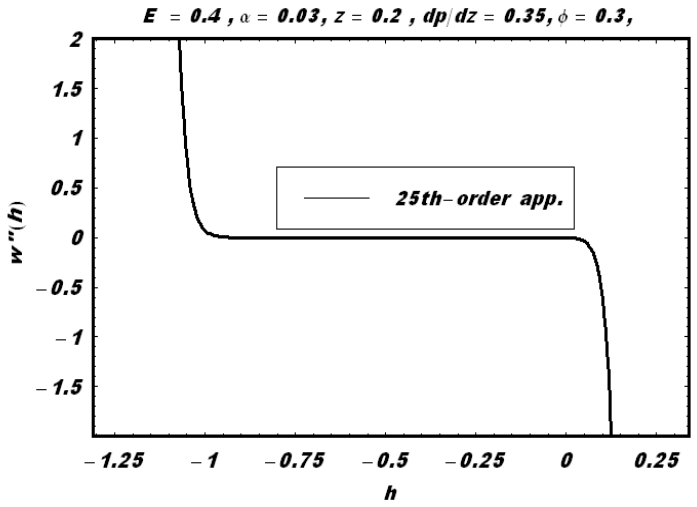

Fig.3.1 (a). h-curve for velocity profile.

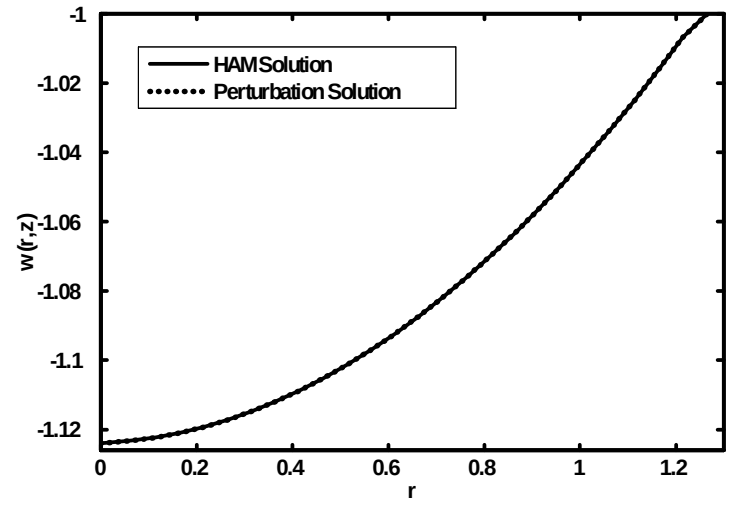

Fig.3.1 (b). Comparison of velocity field for $E = 0.4$, $z = 0.2$, $\phi = 0.3$.

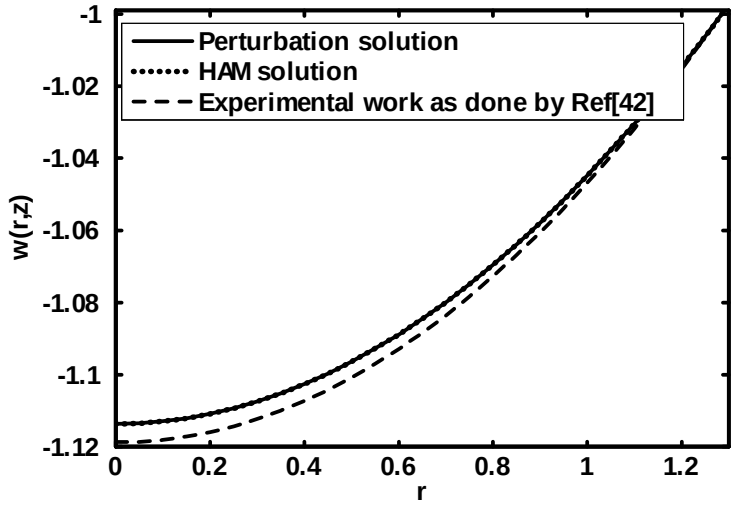

Fig.3.1 (c). Comparison of velocity field for $E = 0.5$, $z = 0.2$, $\phi = 0.3$, $b^* = 0.01$, $\alpha = 0.03$, $n = 1$, $L = 4$, $R = 1.25$.

Case. 2 ($n = 1$ Newtonian Fluid)

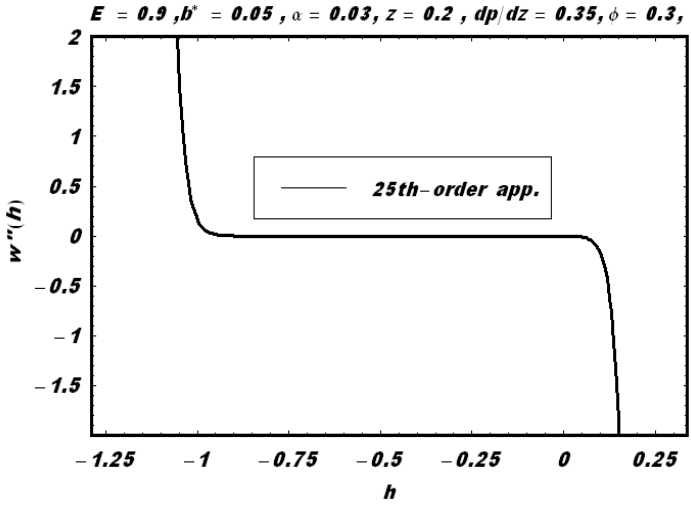

Fig.3.2 (a). h-curve for velocity profile

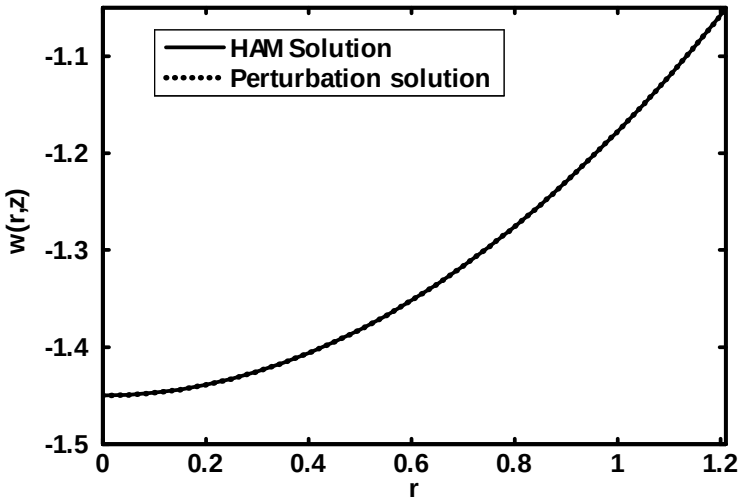

Fig.3.2 (b). Comparison of velocity field for $E = 0.5$, $z = 0.2$, $\phi = 0.3$, $b^* = 0.01$, $\alpha = 0.03$, $n = 1$.

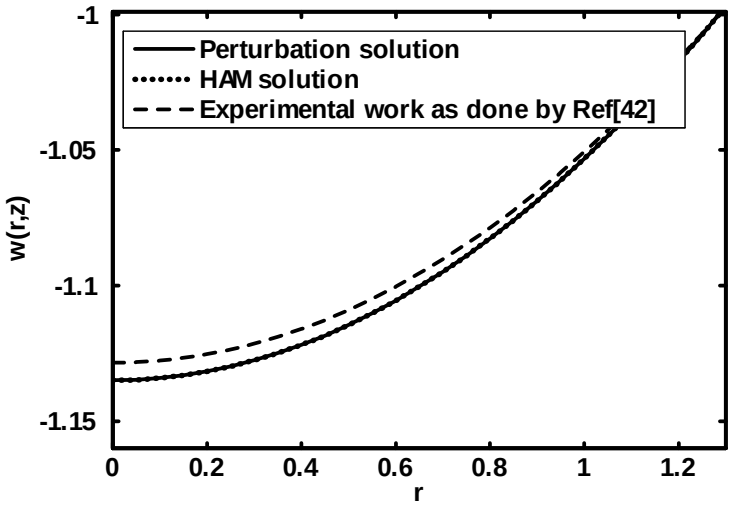

Fig.3.2 (c). Comparison of velocity field for $E = 0.5$, $z = 0.2$, $\phi = 0.3$, $b^* = 0.01$, $\alpha = 0.03$, $n = 1, L = 4$, $R = 1.25$.

Case. 3 ($n = 3$ Shear Thickening Fluid)

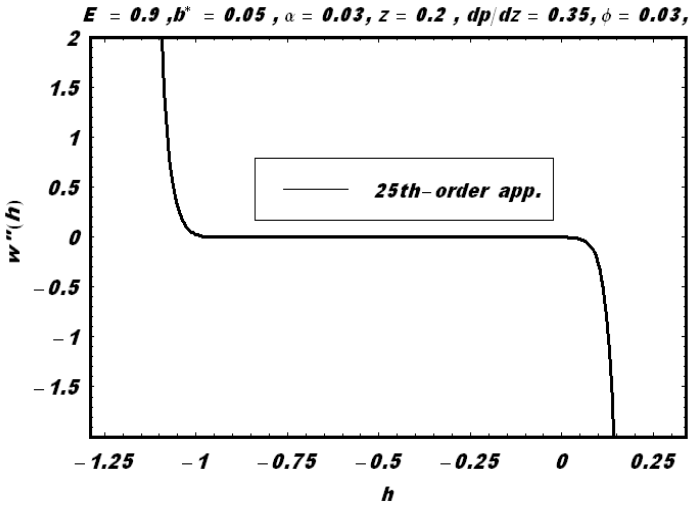

Fig.3.3 (a). h-curve for velocity profile.

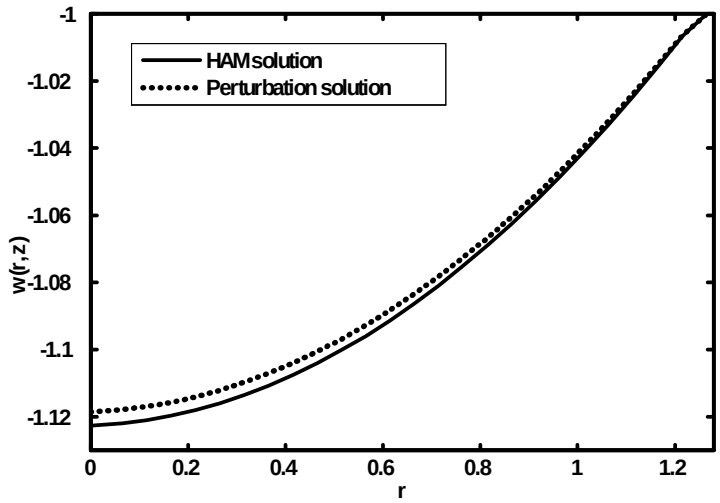

Fig.3.3 (b). Comparison of velocity field for $E = 0.5$, $z = 0.2$, $\phi = 0.3$, $b^* = 0.01$, $\alpha = 0.03$, $n = 2$.

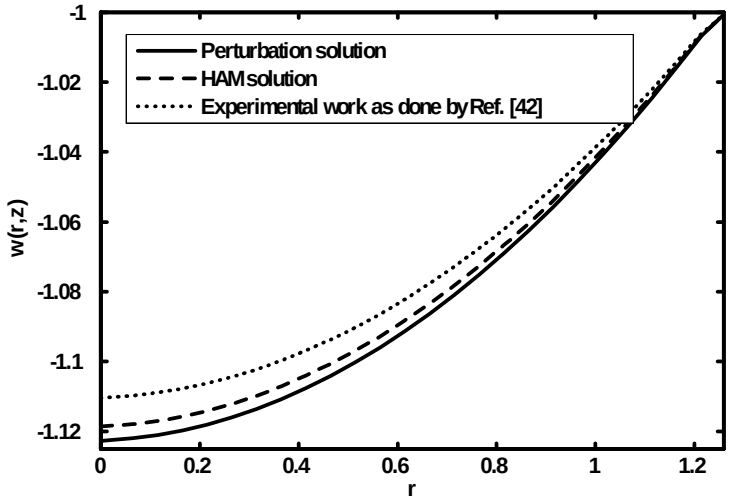

Fig.3.3 (c). Comparison of velocity field for $E = 0.5$, $z = 0.2$, $\phi = 0.3$, $b^* = 0.01$, $\alpha = 0.03$, $n = 2$.

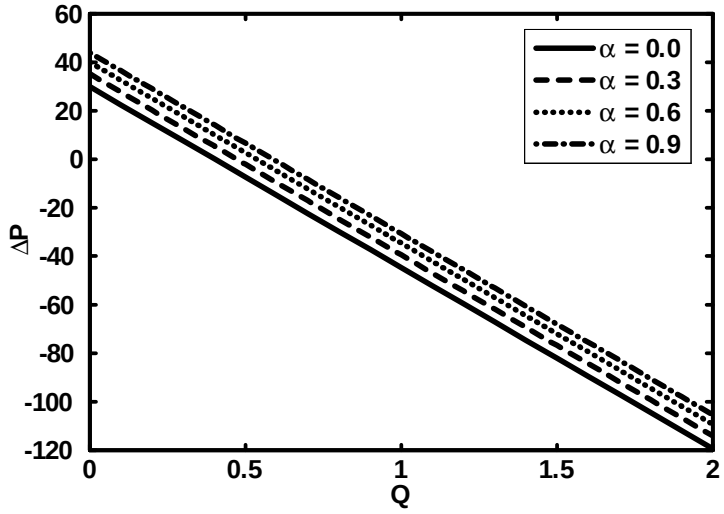

Fig.3.4. Pressure rise versus flow rate for $b^* = 0.1$, $E = 0.1$, $n = 2$, $\phi = 0.4$.

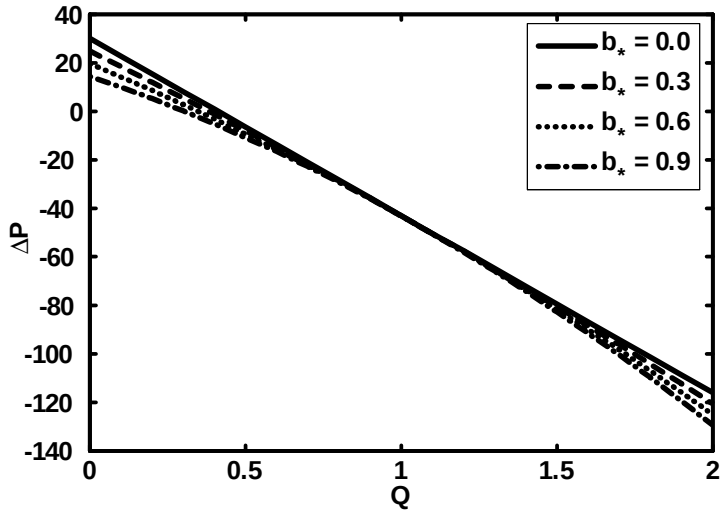

Fig.3.5. Pressure rise versus flow rate for $n = 2$, $E = 0.1$, $\alpha = 0.1$, $\phi = 0.4$.

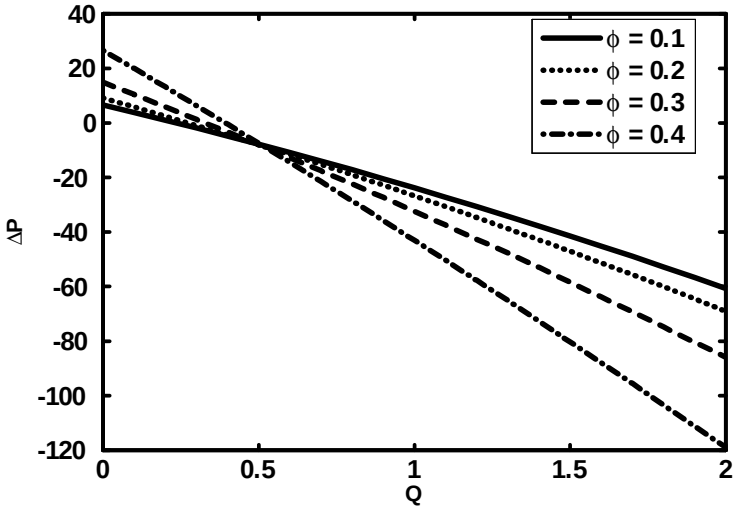

Fig.3.6. Pressure rise versus flow rate for $n = 2$, $E = 0.1$, $\alpha = 0.1$, $b^* = 0.4$.

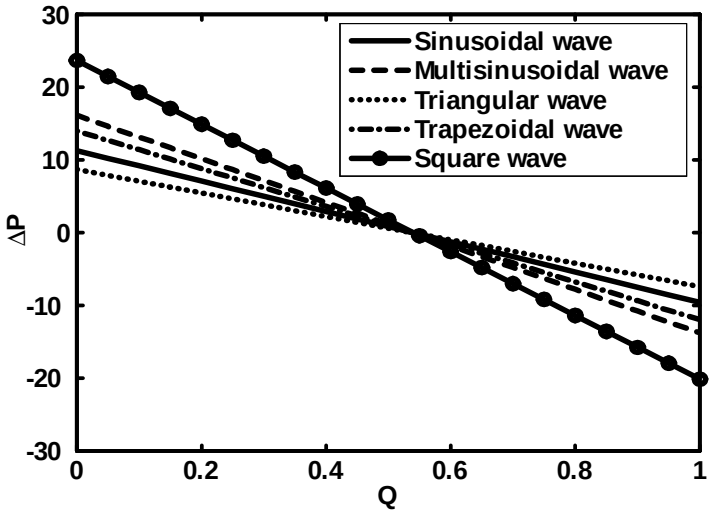

Fig.3.7. Pressure rise versus flow rate for $b^* = 0.1$, $E = 0.1$, $n = 2$, $\phi = 0.4$, $\alpha = 0.2$.

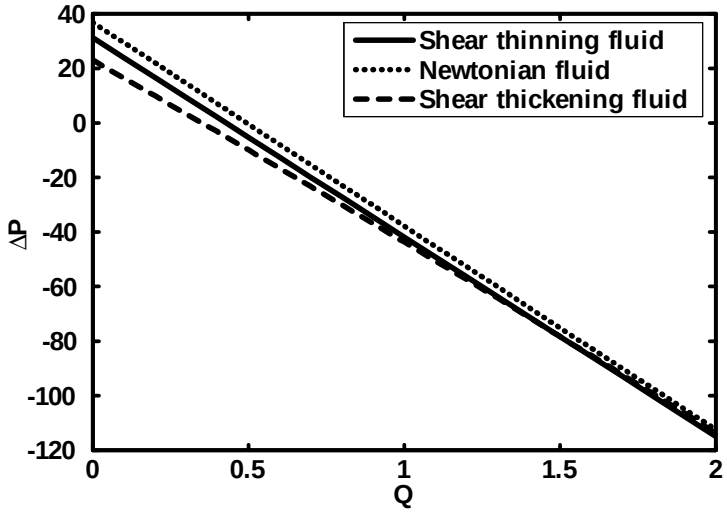

Fig.3.8. Pressure rise versus flow rate for $b^* = 0.1$, $E = 0.1$, $\alpha = 0.4$, $\phi = 0.4$.

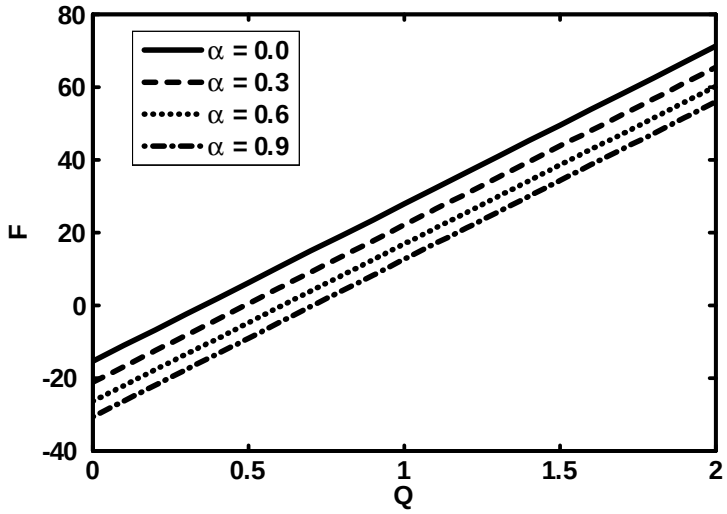

Fig.3.9. Frictional force versus flow rate for $b^* = 0.1$, $E = 0.1$, $n = 2$, $\phi = 0.4$.

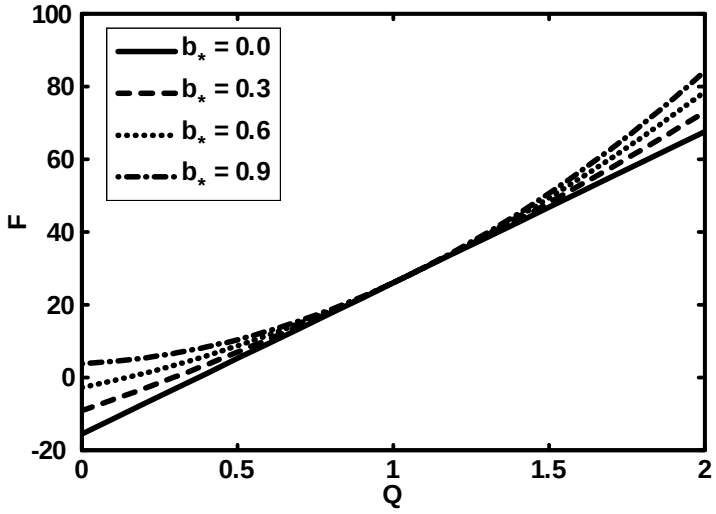

Fig.3.10. Frictional force versus flow rate for $n = 2$, $E = 0.1$, $\alpha = 0.1$, $\phi = 0.4$.

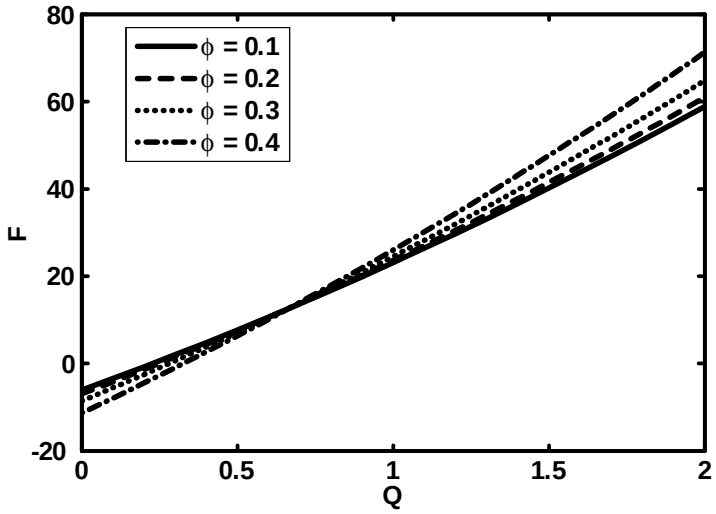

Fig.3.11. Frictional force versus flow rate for $n = 2$, $E = 0.1$, $\alpha = 0.1$, $b^* = 0.4$.

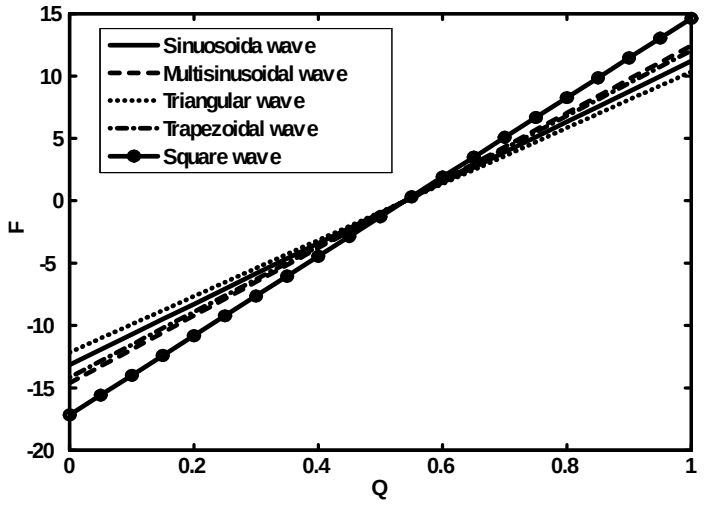

Fig.3.12. Frictional force versus flow rate for $b^* = 0.1$, $E = 0.1$, $n = 2$, $\phi = 0.4$, $\alpha = 0.2$.

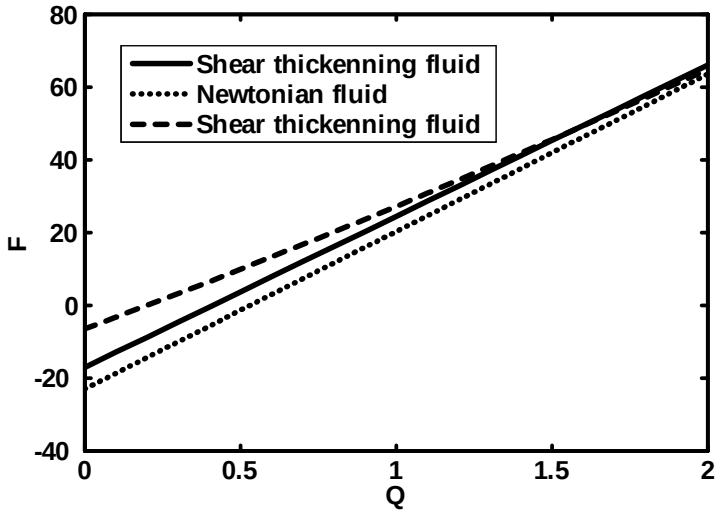

Fig.3.13. Frictional force versus flow rate for $b^* = 0.1$, $E = 0.1$, $\alpha = 0.4$, $\phi = 0.4$.

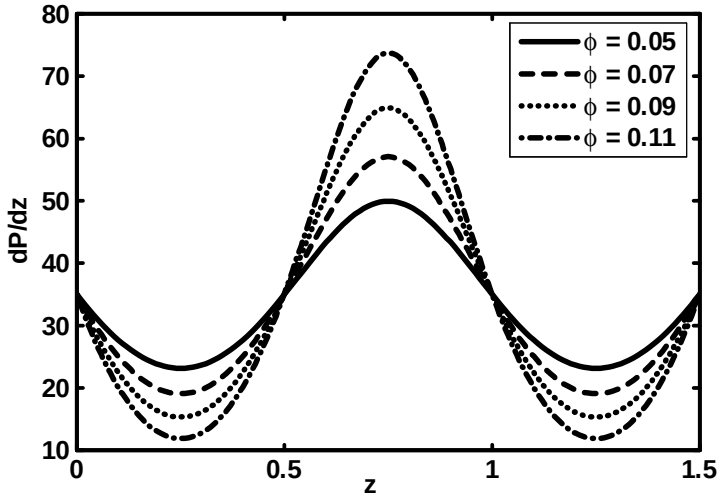

Fig.3.14 (a). Pressure gradient versus z for sinusoidal wave, for $n = 2$, $E = 0.1$, $\alpha = 0.4$, $b^* = 0.1.$, $Q = -1.5$.

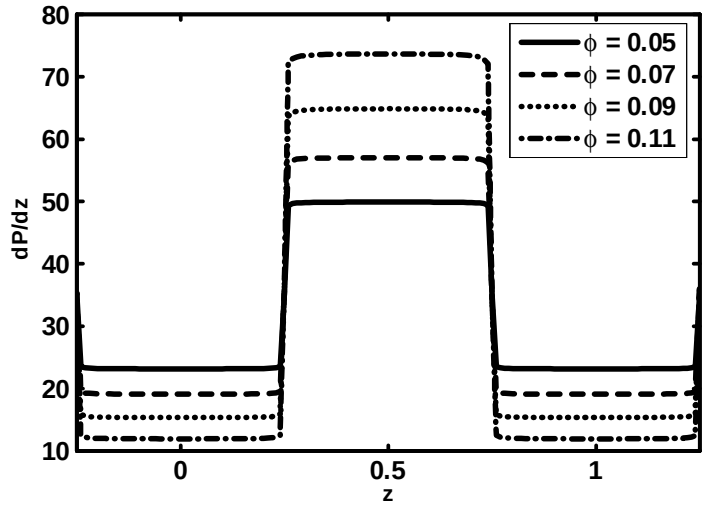

Fig.3.14 (b). Pressure gradient versus z for square wave, for $n = 2$, $E = 0.1$, $\alpha = 0.4$, $b^* = 0.1.$, $Q = -1.5$.

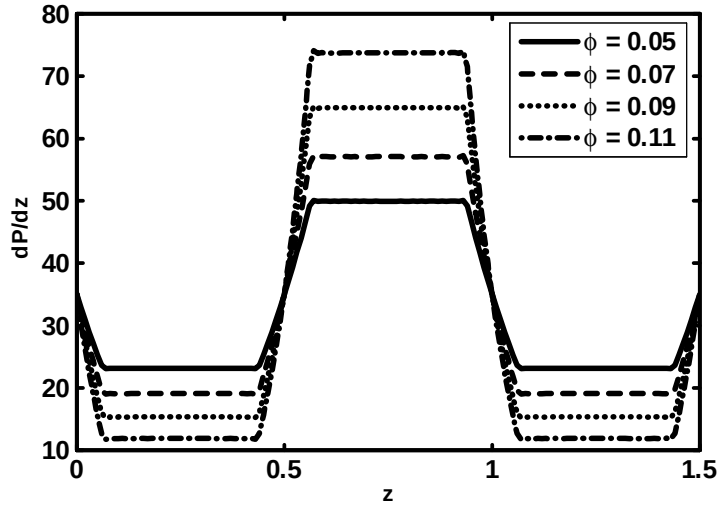

Fig.3.14 (c). Pressure gradient versus z for Trapezoidal wave, for $n = 2$, $E = 0.1$, $\alpha = 0.4$, $b^* = 0.1.$, $Q = -1.5$.

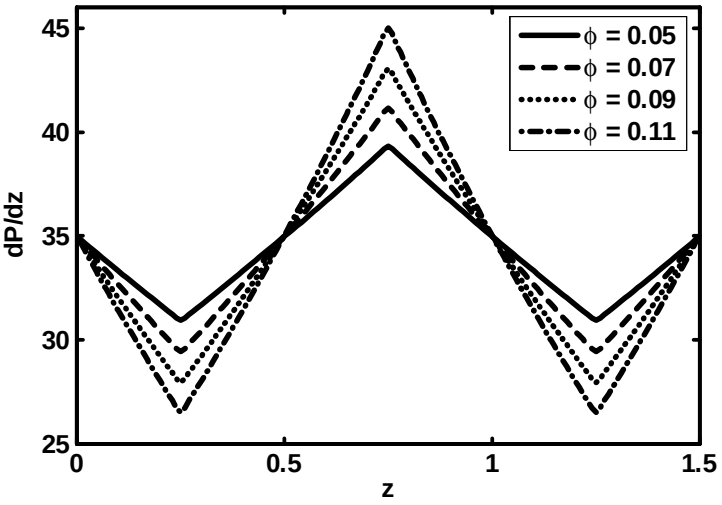

Fig.3.14 (d). Pressure gradient versus z for triangular wave, for $n = 2$, $E = 0.1$, $\alpha = 0.4$, $b^* = 0.1.$, $Q = -1.5$.

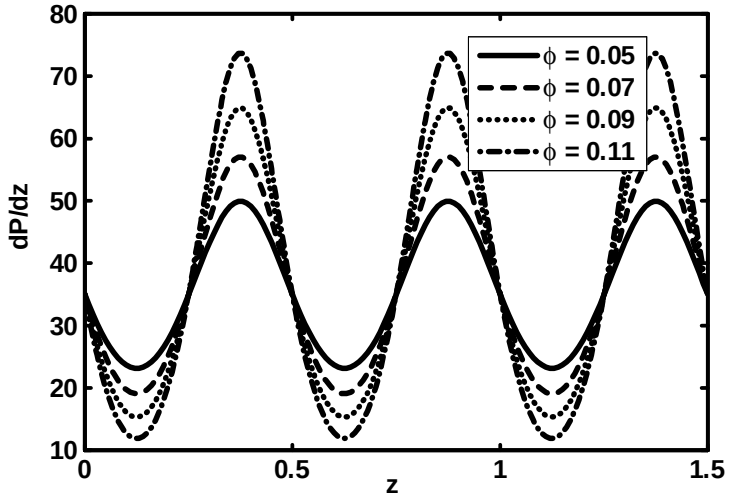

Fig.3.14 (e). Pressure gradient versus z for multisinusoidal wave for $n = 2$, $E = 0.1$, $\alpha = 0.4$, $b^* = 0.1.$, $Q = -1.5$.

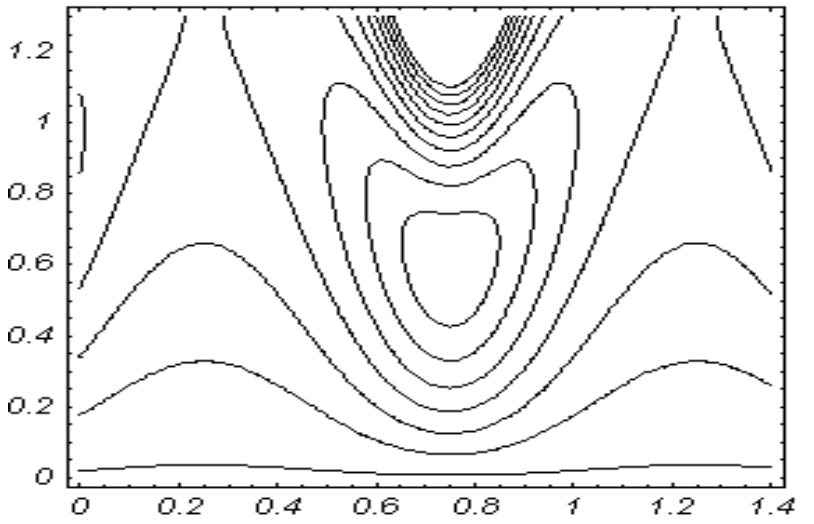

Fig. 3.15 (a) . Streamlines for sinusoidal wave when $\alpha = 0.4$, $b^* = 0.1$, $\phi = 0.4$, $E = 0.1$, $Q = 2.5$.

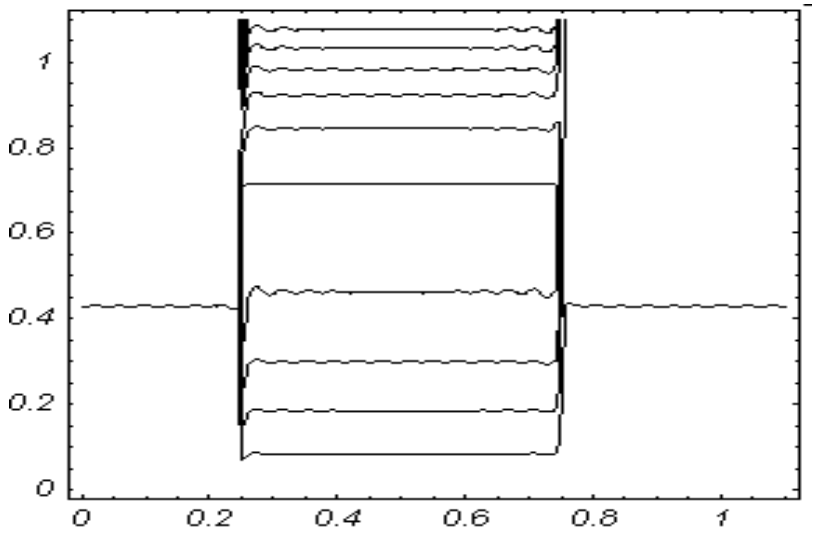

Fig. 3.15 (b) . Streamlines for square wave when $\alpha = 0.4$, $b^* = 0.1$, $\phi = 0.4$, $E = 0.1$, $Q = 2.5$.

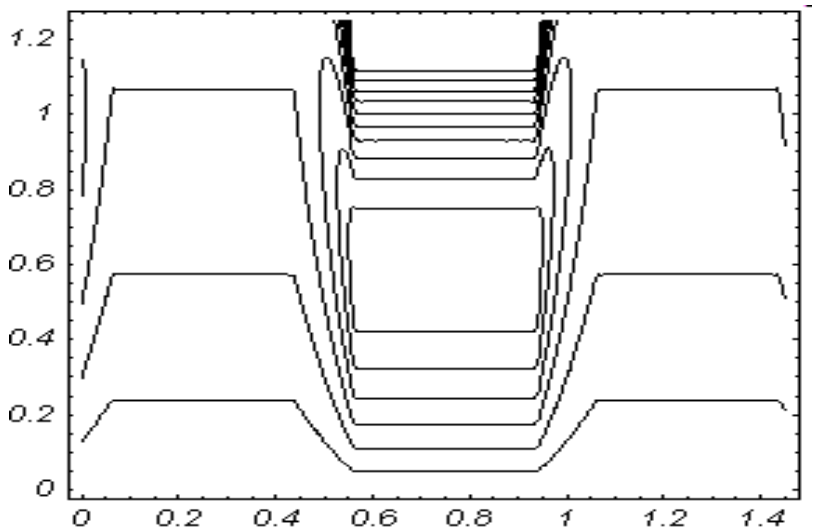

Fig. 3.15 (c) . Streamlines for trapezoidal wave when $\alpha = 0.4$, $b^* = 0.1$, $\phi = 0.4$, $E = 0.1$, $Q = 2.5$.

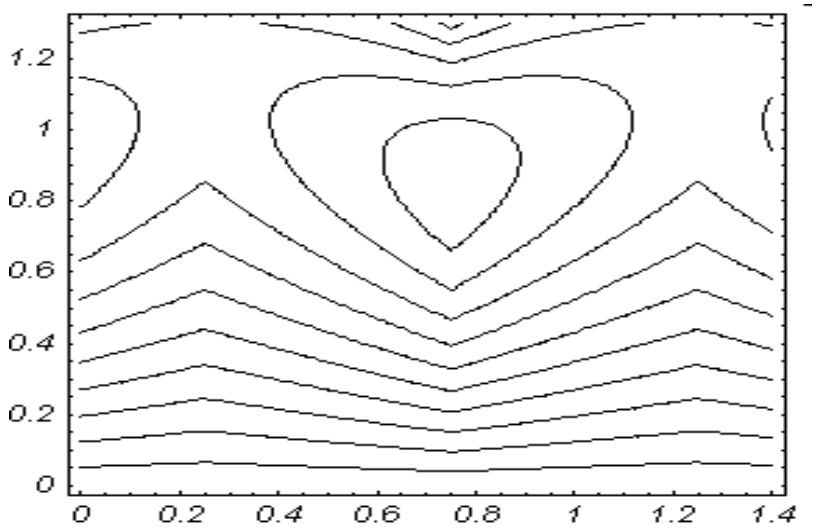

Fig. 3.15 (d) . Streamlines for triangular wave when $\alpha = 0.4$, $b^* = 0.1$, $\phi = 0.4$, $E = 0.1$, $Q = 2.5$.

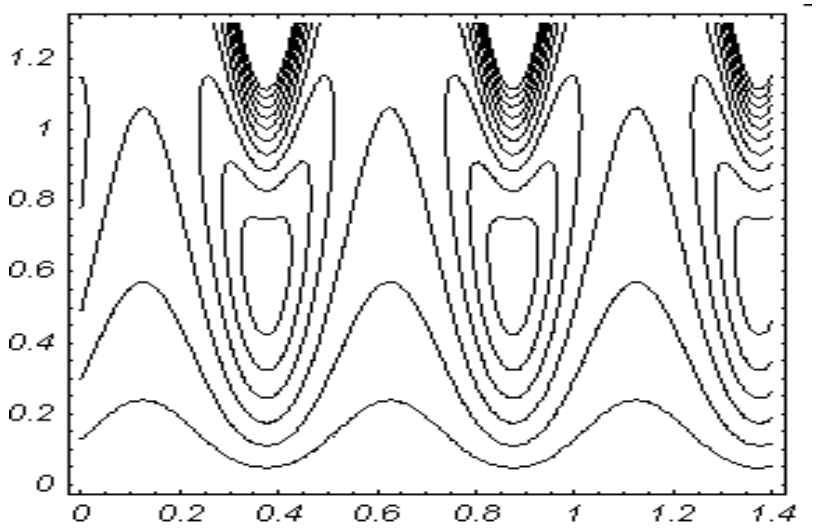

Fig. 3.15 (e) . Streamlines for multisinusoidal wave when $\alpha = 0.4$, $b^* = 0.1$, $\phi = 0.4$, $E = 0.1$, $Q = 2.5$.

3.6 Conclusion

The perturbation and HAM solutions of Eqs. (3.10) to (3.12) have been computed for velocity profile. The expressions for pressure rise and pressure gradient have been discussed for five wave shapes. The following observations have been found.

1. The pressure rise increases with the increase in α, b^* and ϕ.

2. It is observed that frictional forces have an opposite behavior as compared to the pressure rise

3. The pressure rise for square wave gives larger pumping among the five wave shapes and trapezoidal wave has the lowest pumping characteristics

4. The size of trapped bolus in triangular wave is smaller as compared to trapezoidal and sinusoidal wave

5. The pressure gradient increases with increase in ϕ for all five wave shapes.

Chapter 4

Endoscopic effects on the peristaltic flow of a nanofluid

4.1 Introduction

This chapter deals with the peristaltic flow of a nanofluid in an endoscope. The flow is investigated in a wave frame of reference moving with velocity of the wave c. Analytical solutions have been calculated using Homotopy Perturbation Method (HPM) for temperature and nanoparticle equation while exact solutions have been calculated for velocity and pressure gradient. Numerical integration have been used to obtain the graphical results for pressure rise and frictional forces. The effects of various emerging parameters are investigated for five different peristaltic waves. Streamlines have been plotted at the end of the chapter.

4.2 Mathematical Formulation

Let us consider the peristaltic flow of an incompressible nanofluid in an endoscope. The flow is generated by sinusoidal wave trains propagating with constant speed c along the walls of the tube. Heat transfer along with nanoparticle phenomena has been taken into account. The inner tube is rigid and maintained at temperature $\bar{T}_0$ while the outer tube has a sinusoidal wave traveling down its walls and maintained at temperature $\bar{T}_1$. The geometry of the wall surfaces is defined in Eqs. (2.7) and (2.8) .

With the help of transformations (2.12) , the governing equations along with nanoparticles [36] take the following form

$$\frac{1}{\bar{r}}\frac{\partial\left(\bar{r}\bar{u}\right)}{\partial\bar{r}}+\frac{\partial\bar{w}}{\partial\bar{z}}=0, \tag{4.1}$$

$$\rho\left[\bar{u}\frac{\partial\bar{u}}{\partial\bar{r}}+\bar{w}\frac{\partial\bar{u}}{\partial\bar{r}}\right]=-\frac{\partial\bar{P}}{\partial\bar{r}}+\mu\left[\frac{\partial^2\bar{u}}{\partial\bar{r}^2}+\frac{1}{\bar{r}}\frac{\partial\bar{u}}{\partial\bar{r}}+\frac{\partial^2\bar{u}}{\partial\bar{z}^2}-\frac{\bar{u}}{\bar{r}^2}\right], \tag{4.2}$$

$$\rho\left[\bar{u}\frac{\partial\bar{w}}{\partial\bar{r}}+\bar{w}\frac{\partial\bar{w}}{\partial\bar{z}}\right]=-\frac{\partial\bar{P}}{\partial\bar{z}}+\mu\left[\frac{\partial^2\bar{w}}{\partial\bar{r}^2}+\frac{1}{\bar{r}}\frac{\partial\bar{w}}{\partial\bar{r}}+\frac{\partial^2\bar{w}}{\partial\bar{z}^2}\right]+\rho g\alpha\left(\bar{T}-\bar{T}_0\right)+\rho g\alpha\left(\bar{C}-\bar{C}_0\right), \tag{4.3}$$

$$\begin{aligned}\rho c_p\left(\bar{u}\frac{\partial\bar{T}}{\partial\bar{r}}+\bar{w}\frac{\partial\bar{T}}{\partial\bar{z}}\right) &= \alpha_2\left(\frac{\partial^2\bar{T}}{\partial\bar{r}^2}+\frac{1}{\bar{r}}\frac{\partial\bar{T}}{\partial\bar{r}}+\frac{\partial^2\bar{T}}{\partial\bar{z}^2}\right)+\tau_1\left\{D_B\left(\frac{\partial\bar{C}}{\partial\bar{r}}\frac{\partial\bar{T}}{\partial\bar{r}}+\frac{\partial\bar{C}}{\partial\bar{z}}\frac{\partial\bar{T}}{\partial\bar{z}}\right)\right.\\ &\left.+\frac{D_T}{\bar{T}_0}\left[\left(\frac{\partial\bar{T}}{\partial\bar{r}}\right)^2+\left(\frac{\partial\bar{T}}{\partial\bar{z}}\right)^2\right]\right\},\end{aligned} \tag{4.4}$$

$$\left(\bar{u}\frac{\partial\bar{C}}{\partial\bar{r}}+\bar{w}\frac{\partial\bar{C}}{\partial\bar{z}}\right)=D_B\left(\frac{\partial^2\bar{C}}{\partial\bar{r}^2}+\frac{1}{\bar{r}}\frac{\partial\bar{C}}{\partial\bar{r}}+\frac{\partial^2\bar{C}}{\partial\bar{z}^2}\right)+\frac{D_{\bar{T}}}{\bar{T}_0}\left(\frac{\partial^2\bar{T}}{\partial\bar{r}^2}+\frac{1}{\bar{r}}\frac{\partial\bar{T}}{\partial\bar{r}}+\frac{\partial^2\bar{T}}{\partial\bar{z}^2}\right), \tag{4.5}$$

where $\bar{C}$ is the nanoparticle phenomena, the ambient values of $\bar{T}$ and $\bar{C}$ as $\bar{r}$ approaches to $\bar{h}$ is denoted by $\bar{T}_0$ and $\bar{C}_0$, D_B is the Brownian diffusion coefficient, $D_{\bar{T}}$ is the thermophoretic diffusion coefficient, and $\tau_1=\left(\rho c_1\right)_p/\left(\rho c_1\right)_f$ is the ratio between the effective heat capacity of the nano particle material and heat capacity of the fluid when ρ being the density, c is the volumetric volume expansion coefficient and ρ_p is the density of the particle.

The corresponding boundary conditions in the wave frame are

$$\bar{w}=-c,\ \bar{T}=\bar{T}_0,\ \bar{C}=\bar{C}_0,\text{ at }\bar{r}=\bar{r}_1, \tag{4.6}$$

$$\bar{w}=-c,\ \bar{T}=\bar{T}_1,\ \bar{C}=\bar{C}_1\ at\ \bar{r}=\bar{r}_2=a_2+b\sin\frac{2\pi}{\lambda}\left(\bar{z}\right). \tag{4.7}$$

We introduce the non-dimensional variables

$$\begin{aligned}
R &= \frac{\bar{R}}{a_2},\ r=\frac{\bar{r}}{a_2},\ Z=\frac{\bar{Z}}{\lambda},\ z=\frac{\bar{z}}{\lambda},\ W=\frac{\bar{W}}{c},\ w=\frac{\bar{w}}{c}, U=\frac{\lambda\bar{U}}{a_2 c},\ u=\frac{\lambda\bar{u}}{a_2 c},\\
P &= \frac{a_2^2\bar{P}}{c\lambda\mu},\ \theta=\frac{\left(\bar{T}-\bar{T}_1\right)}{\left(\bar{T}_0-\bar{T}_1\right)},\ t=\frac{c\bar{t}}{\lambda},\ \delta=\frac{a_2}{\lambda},\ \mathrm{Re}=\frac{\rho c a_2}{\mu},\ \sigma=\frac{\left(\bar{C}-\bar{C}_1\right)}{\left(\bar{C}_0-\bar{C}_1\right)},\\
r_2 &= \frac{\bar{r}_2}{a_2}=1+\phi\sin\left(2\pi z\right),\ \alpha_2=\frac{k}{(\rho c)_f},\ N_b=\frac{(\rho c)_p D_B\left(\bar{C}_0-\bar{C}_1\right)}{(\rho c)_f},\\
N_t &= \frac{(\rho c)_p D_{\bar{T}}\left(\bar{C}_0-\bar{C}_1\right)}{(\rho c)_f \alpha_2},\ P_r=\frac{\nu}{\alpha_2},\ G_r=\frac{g\alpha_2 a_2^3\left(\bar{T}_0-\bar{T}_1\right)}{\nu^2},\\
B_r &= \frac{g\alpha_2 a_2^3\left(\bar{C}_0-\bar{C}_1\right)}{\nu^2}.
\end{aligned} \tag{4.8}$$

in which P_r, N_b , N_t, G_r and B_r are the Prandtl number, the Brownian motion parameter , the thermophoresis parameter, local temperature Grashof number, nanoparticle Grashof number.

With the help of Eq. (4.8), Eqs. (4.1) to (4.7) under the assumptions of long wavelength and low Reynolds number approximation take the form

$$\frac{\partial u}{\partial r}+\frac{u}{r}+\frac{\partial w}{\partial z}=0, \tag{4.9}$$

$$\frac{\partial P}{\partial r}=0, \tag{4.10}$$

$$\frac{\partial P}{\partial z}=\frac{1}{r}\frac{\partial}{\partial r}\left(r\frac{\partial w}{\partial r}\right)+G_r\theta+B_r\sigma, \tag{4.11}$$

$$\frac{1}{r}\frac{\partial}{\partial r}\left(r\frac{\partial\theta}{\partial r}\right)+N_b\frac{\partial\sigma}{\partial r}\frac{\partial\theta}{\partial r}+N_t\left(\frac{\partial\theta}{\partial r}\right)^2=0, \tag{4.12}$$

$$\left(\frac{1}{r}\frac{\partial}{\partial r}\left(r\frac{\partial\sigma}{\partial r}\right)\right)+\frac{N_t}{N_b}\left(\frac{1}{r}\frac{\partial}{\partial r}\left(r\frac{\partial\theta}{\partial r}\right)\right)=0. \tag{4.13}$$

The corresponding boundary conditions are

$$w = -1,\ \text{at } r=r_1=\varepsilon, \qquad w=-1,\ \ \text{at } r=r_2=1+\phi\sin\left(2\pi z\right), \tag{4.14a}$$

$$\theta = 1, \qquad \text{at } \ r=r_1, \quad \theta=0, \qquad \text{at } \ r=r_2, \tag{4.14b}$$

$$\sigma = 1, \qquad \text{at } \ r=r_1, \quad \sigma=0, \qquad \text{at } \ r=r_2. \tag{4.14c}$$

4.3 Solution of the Problem

4.3.1 Homotopy Perturbation Solution

The homotopy perturbation method for Eqs. (4.12) and (4.13) can be defined as [38, 39]

$$H\left(q,\theta\right)=\left(1-q\right)\left[L\left(\theta\right)-L\left(\theta_{10}\right)\right]+q\left[L\left(\theta\right)+N_b\frac{\partial\sigma}{\partial r}\frac{\partial\theta}{\partial r}+N_t\left(\frac{\partial\theta}{\partial r}\right)^2\right], \tag{4.15}$$

$$H\left(q,\sigma\right)=\left(1-q\right)\left[L\left(\sigma\right)-L\left(\sigma_{10}\right)\right]+q\left[L\left(\sigma\right)+\frac{N_t}{N_b}\left(\frac{1}{r}\frac{\partial}{\partial r}\left(r\frac{\partial\theta}{\partial r}\right)\right)\right], \tag{4.16}$$

or

$$H\left(q,\theta\right)=L\left(\theta\right)-L\left(\theta_{10}\right)+qL\left(\theta_{10}\right)+q\left[N_b\frac{\partial\sigma}{\partial r}\frac{\partial\theta}{\partial r}+N_t\left(\frac{\partial\theta}{\partial r}\right)^2\right], \tag{4.17}$$

$$H\left(q,\sigma\right)=L\left(\sigma\right)-L\left(\sigma_{10}\right)+qL\left(\sigma_{10}\right)+q\left[\frac{N_t}{N_b}\left(\frac{1}{r}\frac{\partial}{\partial r}\left(r\frac{\partial\theta}{\partial r}\right)\right)\right]. \tag{4.18}$$

According to method, $L=\frac{1}{r}\frac{\partial}{\partial r}\left(r\frac{\partial}{\partial r}\right)$ as the linear operator, therefore we can choose the initial guesses as

$$\theta_{10}\left(r,z\right)=\left(\frac{\ln r-\ln r_2}{\ln r_1-\ln r_2}\right),\quad \sigma_{10}\left(r,z\right)=\left(\frac{\ln r-\ln r_2}{\ln r_1-\ln r_2}\right). \tag{4.19}$$

Let us define

$$\theta\left(r,q\right)=\theta_0+q\theta_1+q^2\theta_2+.....,\tag{4.20}$$

$$\sigma\left(r,q\right)=\sigma_0+q\sigma_1+q^2\sigma_2+....\tag{4.21}$$

Adopting the same procedure as done by [38, 39], the solution for temperature and nanoparticle phenomena can be written as for $q=1$

$$\begin{aligned}\theta\left(r,z\right) &= \frac{1}{A_1}((A_2(\log r-\log r_1)(2\log r-A_4)-6(N_b+N_t)(\log r-\log r_1)\\ &\quad (\log r-\log r_2)+12A_4^2)(\log r-\log r_2))),\end{aligned} \tag{4.22}$$

$$\sigma\left(r,z\right)=\frac{1}{A_4A_5}(A_5(\log r-\log r_2)+A_3A_4(\log r-\log r_1)(\log r-\log r_2)(2\log r-A_4). \tag{4.23}$$

Substituting Eqs. (4.22) and (4.23) into Eq. (4.11), the exact solution for velocity and pressure gradient can be directly written as

$$\begin{aligned} w\,(r,z) \;=\; & -\frac{1}{96A_4^3N_b}(r^2(-A_{10}+A_{19}+3A_{17}(N_b+N_t)-(A_9+6A_8(N_b+N_t))\log r \\ & +6A_7(N_b+N_t)\log r^2-2A_6\log r^3-24\frac{dP}{dz}N_b\left(\log r_1^3-\log r_2^3\right)+\log r_1\log r_2 \\ & (A_{14}+A_{20}-2(A_{15}B_r-A_{16}G_rN_b+36\frac{dP}{dz}N_b)\log r_2+\log r_1^2(A_{18}-A_{11}B_r \\ & -2(A_{12}-N_b(A_{13}+36\frac{dP}{dz}))\log r_2)))+(A_{21}+A_{22}\frac{dP}{dz})\log r+(A_{23} \\ & +A_{24}\frac{dP}{dz}). \end{aligned} \tag{4.24}$$

$$\frac{dP}{dz}=\frac{F_1-A_{25}}{A_{26}}. \tag{4.25}$$

Flow rate in dimensionless form can be define as $[1-5]$.

$$F_1=2Q-\frac{\phi^2}{2}-1.$$

The pressure rise ΔP and friction force F on inner and outer tubes $F^{(0)}$, $F^{(i)}$, are given by

$$\Delta P=\int_0^1\frac{dP}{dz}dz, \tag{4.26}$$

$$F^{(0)}=\int_0^1 r_1^2\left(-\frac{dP}{dz}\right)dz, \tag{4.27}$$

$$F^{(i)}=\int_0^1 r_2^2\left(-\frac{dP}{dz}\right)dz, \tag{4.28}$$

where $\frac{dP}{dz}$ is defined in Eq. (4.25).

For analysis, we have considered five wave forms namely sinusoidal, multi-sinusoidal, triangular, square and trapezoidal. The non-dimensional expressions for these wave forms are given by

1. Sinusoidal wave:

$$r_2(z) = 1 + \phi \sin(2\pi z)$$

2. Triangular wave:

$$r_2(z) = 1 + \phi \left\{ \frac{8}{\pi^3} \sum_{n=1}^{\infty} \frac{(-1)^{n+1}}{(2n-1)} \sin(2\pi (2n-1) z) \right\}$$

3. Square wave:

$$r_2(z) = 1 + \phi \left\{ \frac{4}{\pi} \sum_{n=1}^{\infty} \frac{(-1)^{n+1}}{(2n-1)} \cos(2\pi (2n-1) z) \right\}$$

4. Trapezoidal wave:

$$r_2(z) = 1 + \phi \left\{ \frac{32}{\pi^2} \sum_{n=1}^{\infty} \frac{\sin\frac{\pi}{8}(2n-1)}{(2n-1)^2} \sin(2\pi (2n-1) z) \right\}$$

5. Multi sinusoidal wave:

$$r_2(z) = 1 + \phi \sin(2m\pi z).$$

4.4 Numerical Results and Discussion

In this section we have presented the solution for the peristaltic flow of a nanofluid in an endoscope graphically. The expression for pressure rise ΔP is calculated numerically using mathematics software. The effects of various parameters on the pressure rise ΔP against volume flow rate Q are shown in Figs. 4.1 to 4.3 for various values of amplitude ratio ϕ, thermophoresis parameter N_t and radius ratio λ. It is observed that the pressure rise and volume flow rate give opposite results. It is analyzed from Figs. 4.1 to 4.3 that pressure rise increases with the increase in amplitude ratio ϕ and thermophoresis parameter N_t, while the pressure rise decreases with the increase in radius ratio ϵ. Peristaltic pumping region is $(-1 \leq Q \leq 0.3)$, where as augmented pumping region is $(0.31 \leq Q \leq 2)$ for Figs. 4.1 and 4.2, peristaltic pumping region is $(-1 \leq Q \leq 0.2)$ and augmented pumping region is $(0.21 \leq Q \leq 2)$ for Fig. 4.3. Figs. 4.4 to 4.9 represents the behavior of frictional forces for inner and outer tubes. It is depicted that frictional forces have an opposite behavior as compared to the pressure

rise. Effects of temperature profile have been shown through Figs. 4.10 and 4.11. It is seen that with the increase in the Brownian motion parameter N_b and the thermophoresis parameter N_t temperature profile increases in the region $0.1 \leq r \leq 0.4$, decreases in the region $0.41 \leq r \leq 1$ for Fig. 4.10, and increases in the whole region $0.1 \leq r \leq 1$ for Fig. 4.11. It can also be analyzed through figures that Brownian motion parameter N_b and the thermophoresis parameter N_t have qualitatively similar effects on temperature profile. Maximum temperature profile occurs at $r = 0.7$ while minimum temperature profile occurs at $r = 0.2$. The nanoparticle phenomena σ for different values of the Brownian motion parameter N_b and the thermophoresis parameter N_t are shown in Figs. 4.12 and 4.13. We observed that the nanoparticle phenomena decrease with an increase in Brownian motion parameter N_b and thermophoresis parameter N_t in the region $0.1 \leq r \leq 0.3$ and increases in the region $0.31 \leq r \leq 1$. Brownian motion parameter N_b and thermophoresis parameter N_t have similar effects on nanoparticle phenomena. Maximum nanoparticle phenomena is at $r = 0.7$ and minimum nanoparticle phenomena is at $r = 0.2$. Figs. 4.10 and 4.13 show that temperature profile and nanoparticle phenomena have qualitatively opposite behaviour for every parameter. Figs. 4.14 (a to e) are prepared to see the behavior of pressure gradient for different wave shapes. It is observed from the figures that for $z\epsilon\,[0, 0.5]$ and $[1.1, 1.5]$, the pressure gradient is small and large pressure gradient occurs for $z\epsilon\,[0.51, 1]$, moreover, it is seen that with increase in ϕ pressure gradient increases and maximum change in pressure is at $r = 0.3$. Figs. 4.15 (a to e) show the streamlines for different wave forms. It is observed that the size of the trapped bolus in triangular wave is small as compared to the

other waves.

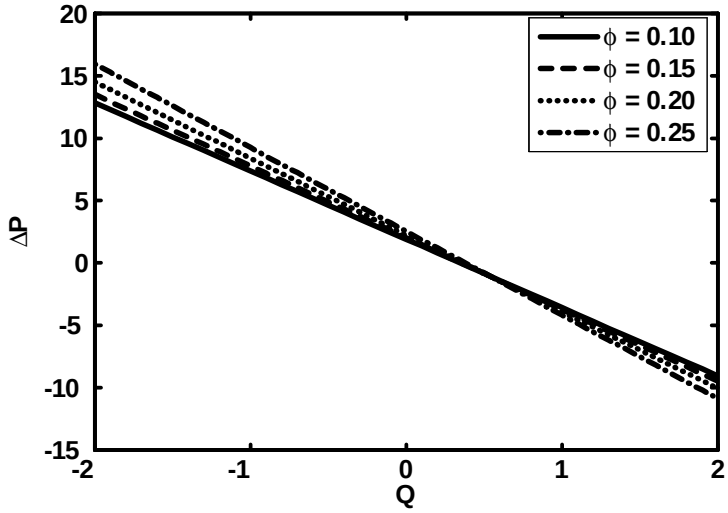

Fig.4.1. Pressure rise versus for $r_1 = 0.05$, $\epsilon = 0.05$, $G_r = 0.3$, $B_r = 0.2$, $N_t = 0.8$, $N_b = 0.3$.

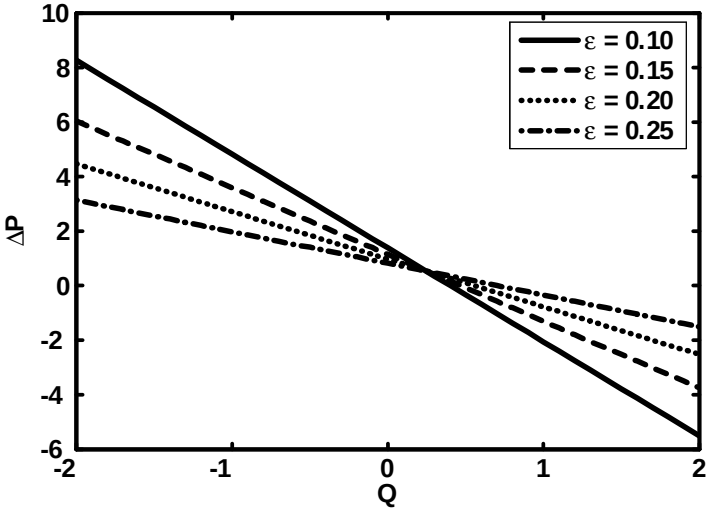

Fig.4.2. Pressure rise versus flow rate for $r_1 = 0.05$, $\phi = 0.01$, $G_r = 3$, $B_r = 0.2$, $N_b = 10$.

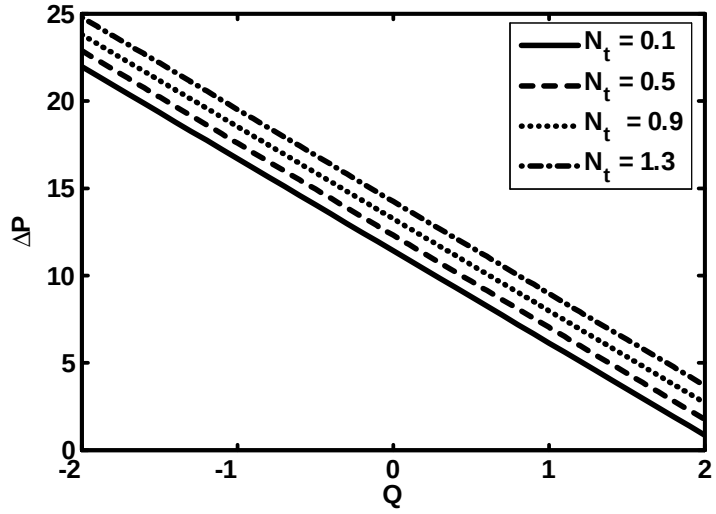

Figs.4.3. Pressure rise versus flow rate for $r_1 = 0.05$, $\phi = 0.05$, $G_r = 0.3$, $B_r = 0.2$, $N_t = 0.8$, $N_b = 0.3$.

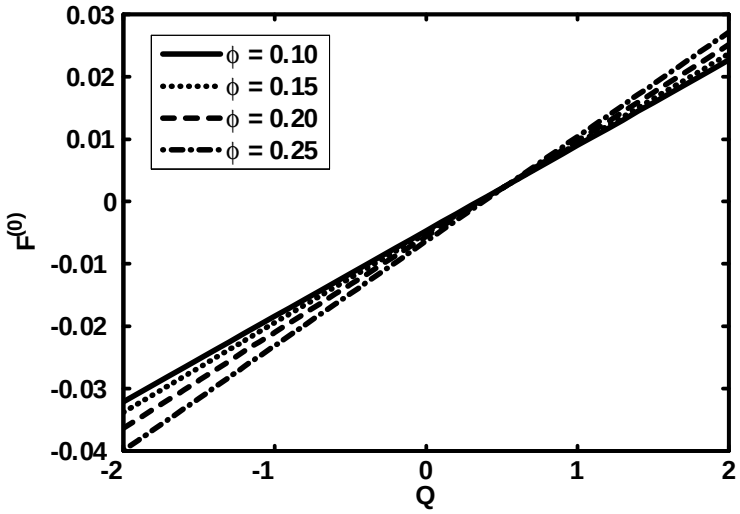

Figs.4.4. Frictional force for inner tube versus flow rate for $r_1 = 0.05$, $\epsilon = 0.05$, $G_r = 0.3$, $B_r = 0.2$, $N_t = 0.8$, $N_b = 0.3$.

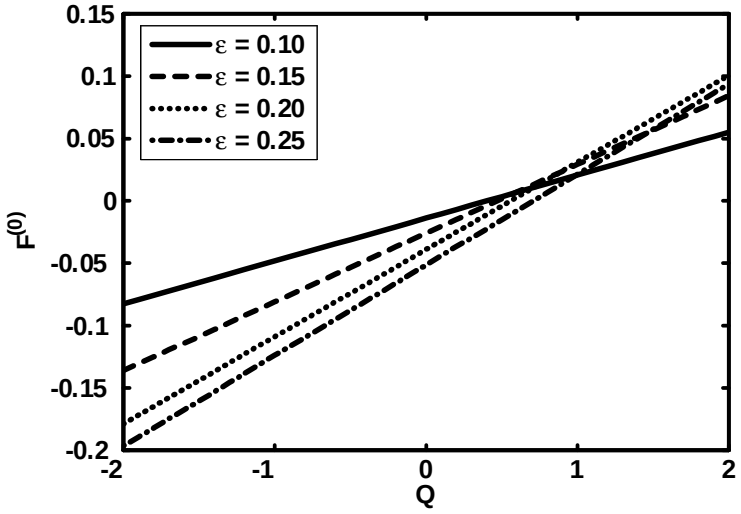

Fig.4.5. Frictional force for inner tube versus flow rate for $r_1 = 0.05$, $\phi = 0.01$, $G_r = 3$, $B_r = 0.2$, $N_b = 10$.

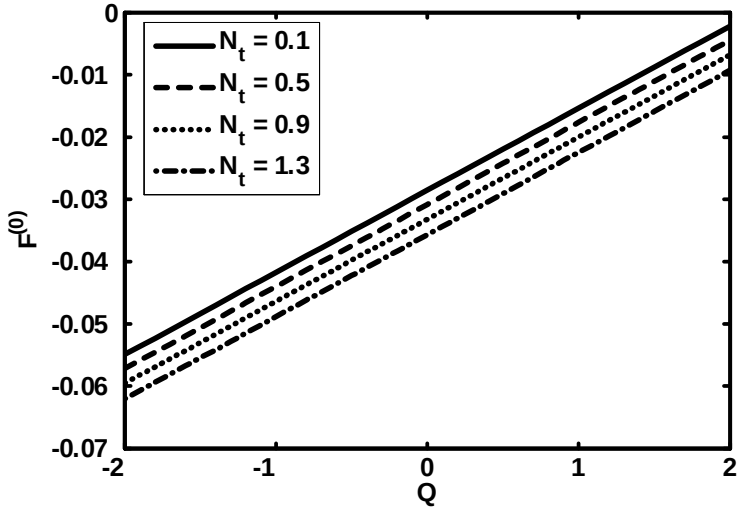

Figs.4.6. Frictional force for inner tube versus flow rate for $r_1 = 0.05$, $\phi = 0.05$, $G_r = 0.3$, $B_r = 0.2$, $N_t = 0.8$, $N_b = 0.3$.

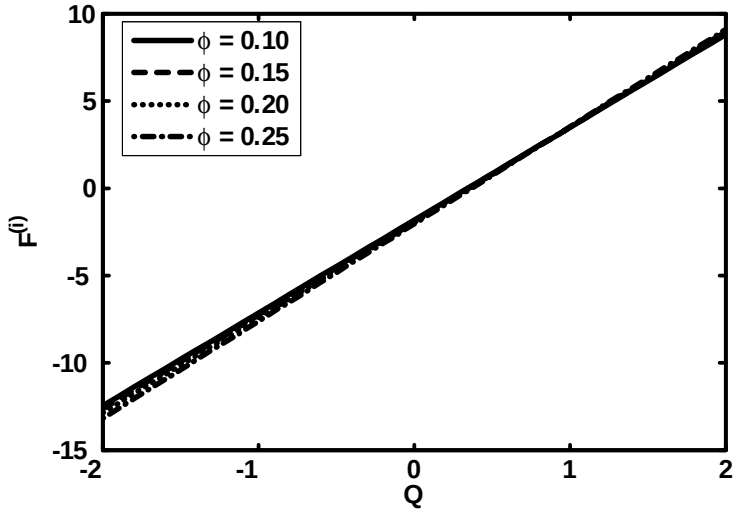

Fig.4.7. Frictional force for outer tube versus flow rate for $r_1 = 0.05$, $\epsilon = 0.05$, $G_r = 0.3$, $B_r = 0.2$, $N_t = 0.8$, $N_b = 0.3$.

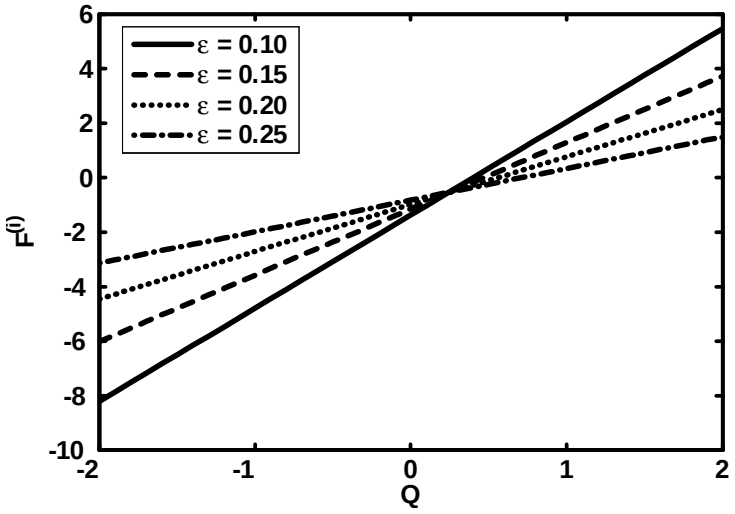

Figs.4.8. Frictional force for outer tube versus flow rate for $r_1 = 0.05$, $\phi = 0.01$, $G_r = 3$, $B_r = 0.2$, $N_b = 10$.

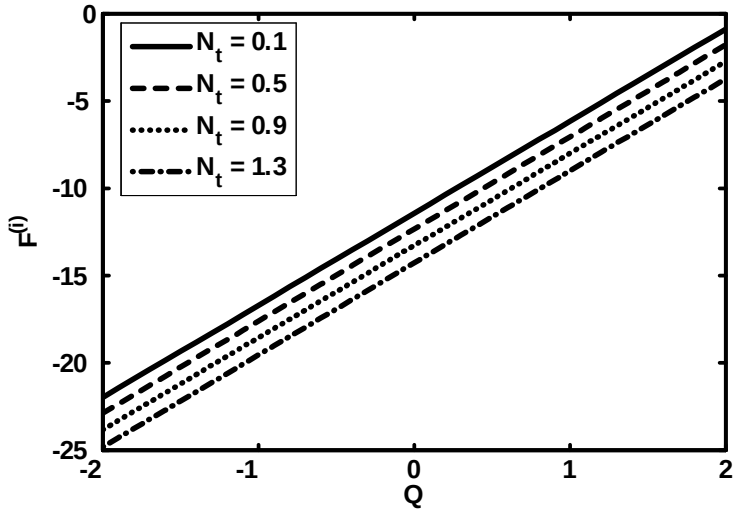

Fig.4.9. Frictional force for outer tube versus flow rate for $r_1 = 0.05$, $\phi = 0.05$, $G_r = 0.3$, $B_r = 0.2$, $N_t = 0.8$, $N_b = 0.3$.

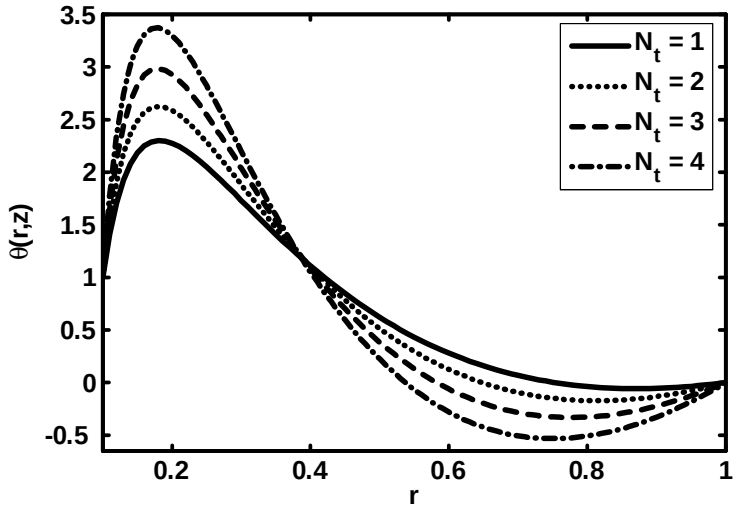

Figs.4.10 Temperature profile for $N_b = 8$, $r_{_1} = 0.1$, $\phi = 0.2$, $z = 0.5$.

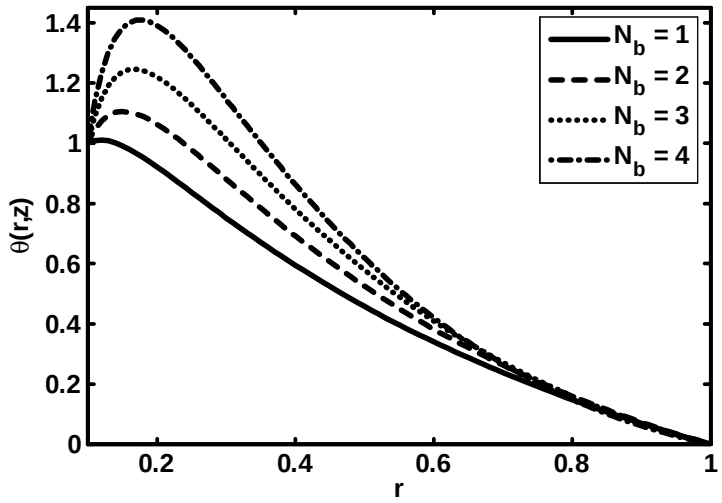

Figs.4.11 Temperature profile for $N_t = 0.5$, $r_1 = 0.1$, $\phi = 0.2$, $z = 0.5$.

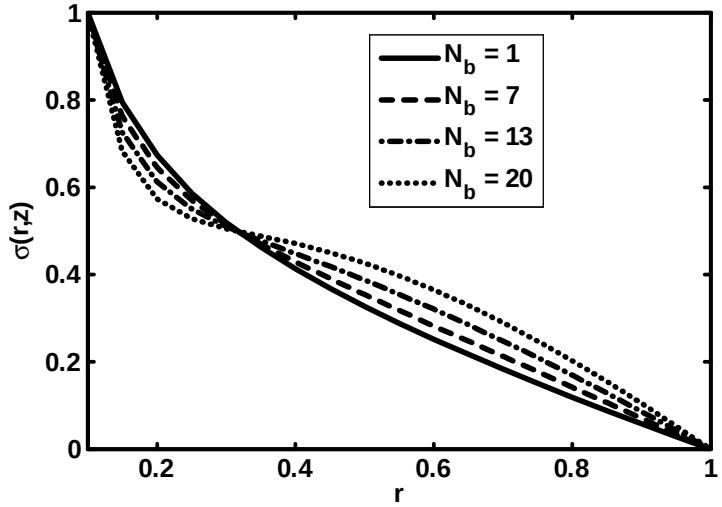

Fig.4.12. Concentration profile for $N_t = 8$, $r_1 = 0.1$, $\phi = 0.2$, $z = 0.5$.

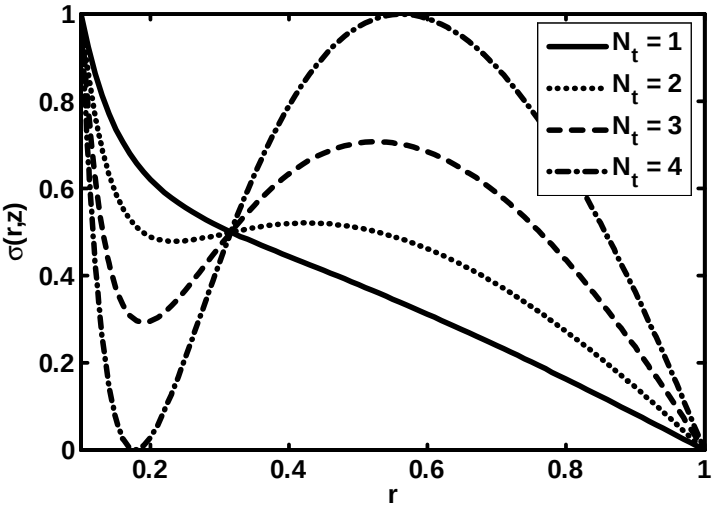

Figs.4.13. Concentration profile for $N_b = 8$, $r_1 = 0.1$, $\phi = 0.2$, $z = 0.5$.

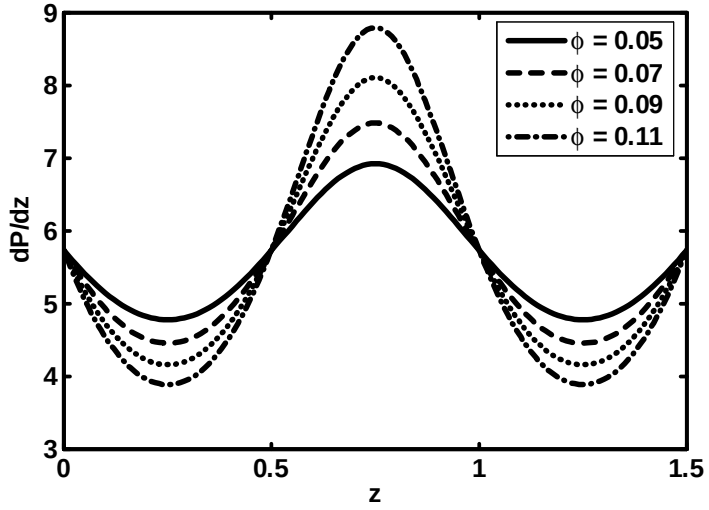

Fig.4.14 (a). Pressure gradient versus z for (Sinusoidal wave) for $r_1 = 0.05$, $\epsilon = 0.05$, $Q = -2$, $N_t = 0.3$, $G_r = 0.3$, $B_r = 0.2$, $N_b = 0.3$.

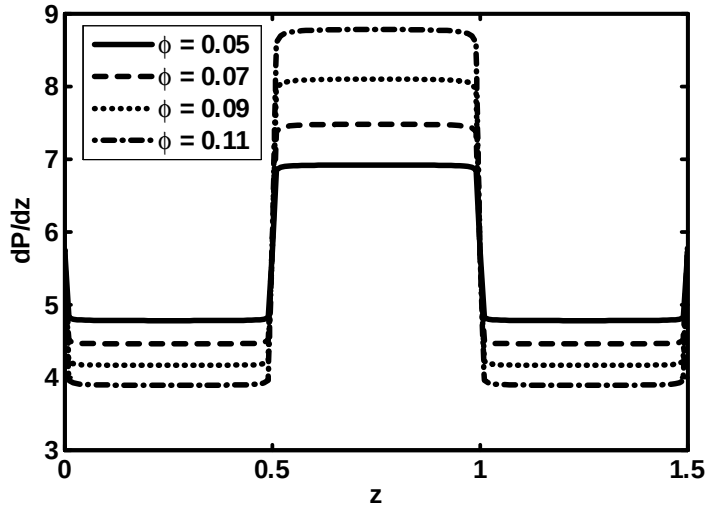

Fig.4.14 (b). Pressure gradient versus z for (Square wave) for $r_1 = 0.05$, $\epsilon = 0.05$, $Q = -2$, $N_t = 0.3$, $G_r = 0.3$, $B_r = 0.2$, $N_b = 0.3$.

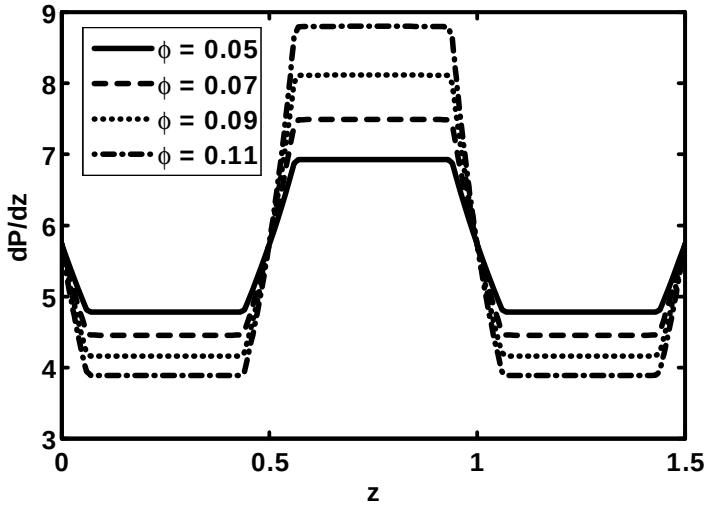

Fig.4.14 (c). Pressure gradient versus z for (Trapezoidal wave) for $r_1 = 0.05$, $\epsilon = 0.05$, $Q = -2$, $N_t = 0.3$, $G_r = 0.3$, $B_r = 0.2$, $N_b = 0.3$.

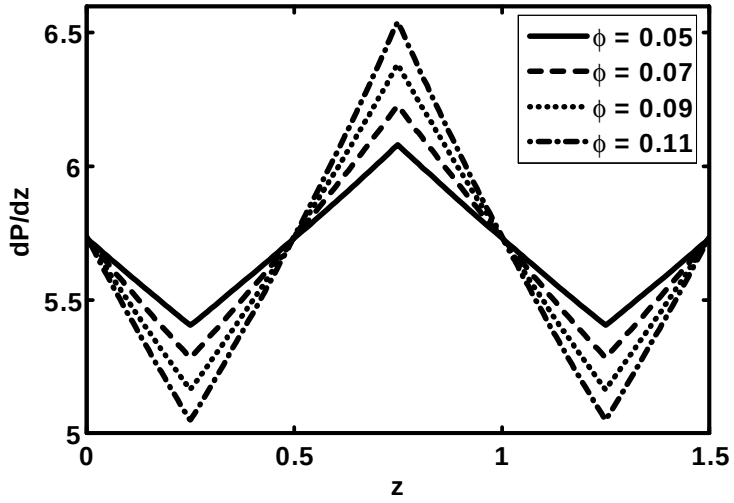

Fig.4.14 (d). Pressure gradient versus z for (Triangular wave) for $r_1 = 0.05$, $\epsilon = 0.05$, $Q = -2$, $N_t = 0.3$, $G_r = 0.3$, $B_r = 0.2$, $N_b = 0.3$.

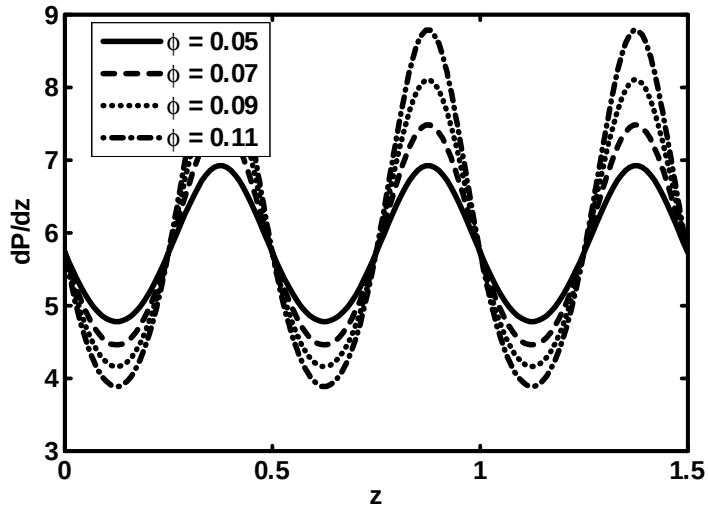

Fig.4.14 (e). Pressure gradient versus z for (Multisinusoidal wave) for $r_1 = 0.05$, $\epsilon = 0.05$, $Q = -2$, $N_t = 0.3$, $G_r = 0.3$, $B_r = 0.2$, $N_b = 0.3$.

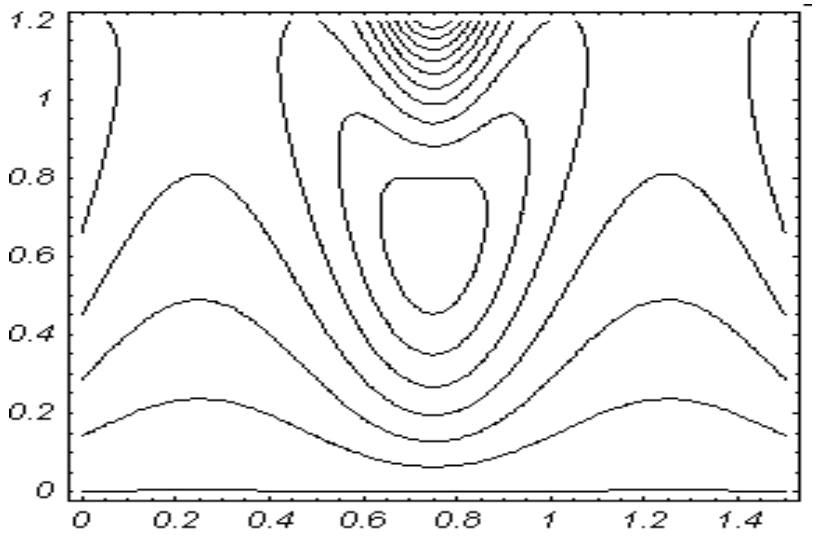

Figs.4.15 (a). Streamlines for sinusoidal wave when $r_1 = 0.1$, $\epsilon = 0.1$, $Q = -2$, $N_t = 0.3$, $G_r = 0.3$, $B_r = 0.2$, $N_b = 0.3$.

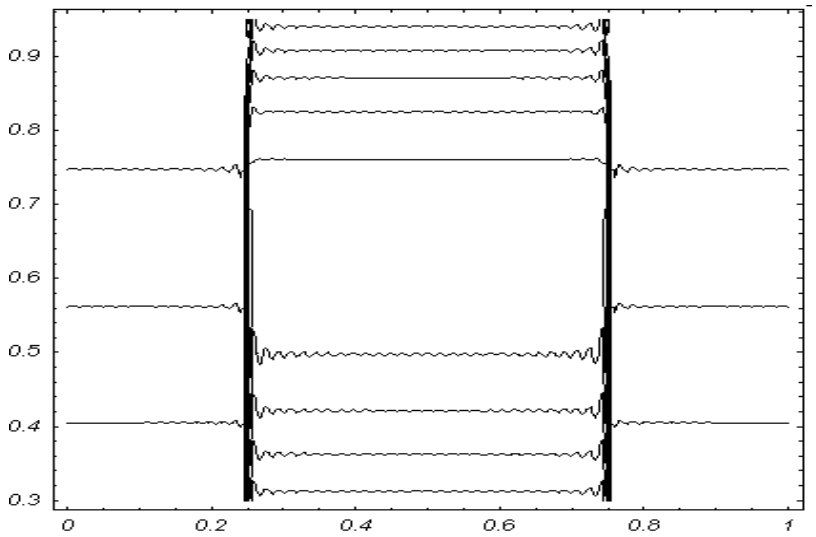

Figs.4.15 (b). Streamlines for square wave when $r_1 = 0.1$, $\epsilon = 0.1$, $Q = -2$, $N_t = 0.3$, $G_r = 0.3$, $B_r = 0.2$, $N_b = 0.3$.

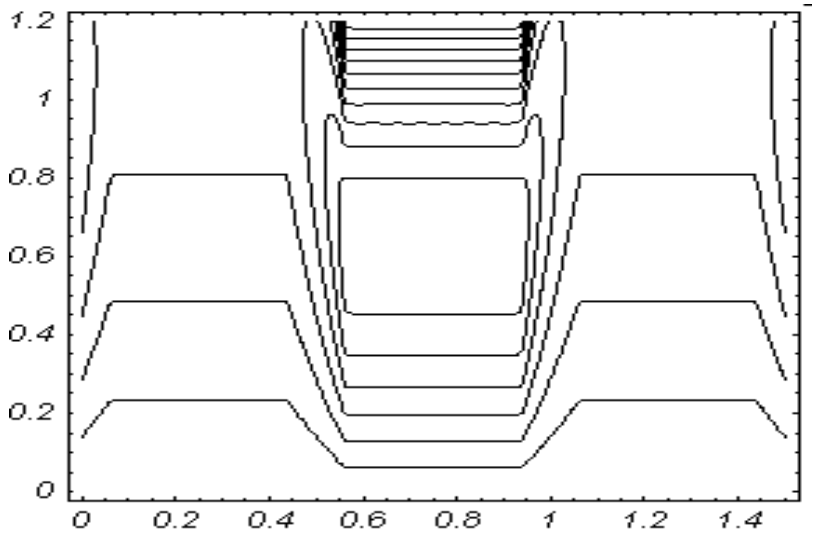

Figs.4.15 (c). Streamlines for trapezoidal wave when $r_1 = 0.1$, $\epsilon = 0.1$, $Q = -2$, $N_t = 0.3$, $G_r = 0.3$, $B_r = 0.2$, $N_b = 0.3$.

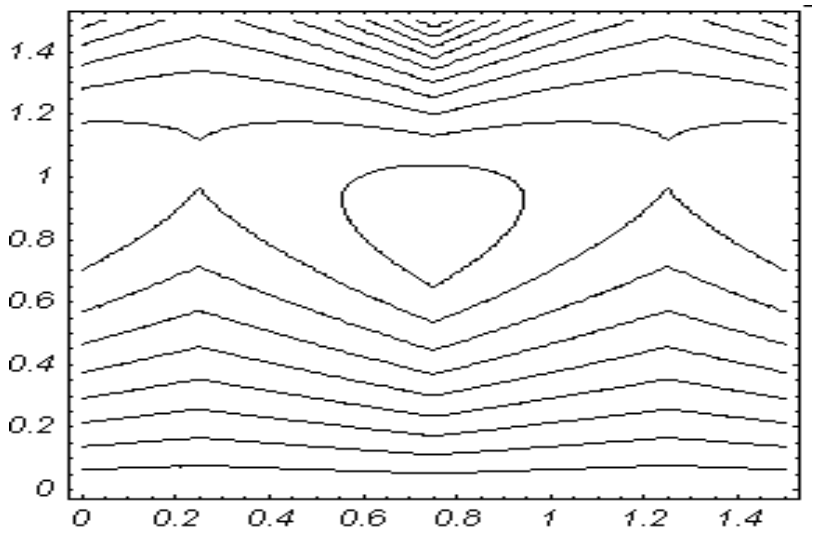

Figs.4.15 (d). Streamlines for triangular wave when $r_1 = 0.1$, $\epsilon = 0.1$, $Q = -2$, $N_t = 0.3$, $G_r = 0.3$, $B_r = 0.2$, $N_b = 0.3$.

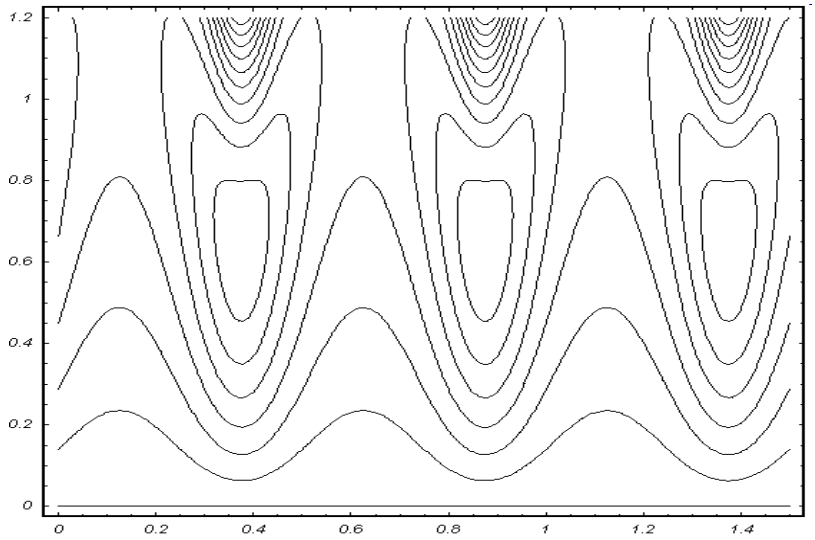

Figs.4.15 (e). Streamlines for multisinusoidal wave when $r_1 = 0.1$, $\epsilon = 0.1$, $Q = -2$, $N_t = 0.3$, $G_r = 0.3$, $B_r = 0.2$, $N_b = 0.3$.

4.5 Conclusion

This study examines the peristaltic flow of a nanofluid in an endoscope. Homotopy perturbation solutions have been evaluated for temperature and concentration profile, while exact solutions have been calculated for velocity profile. The main points of the performed analysis are as follows.

1. The pressure rise increases with the increase in ϕ (amplitude ratio) and N_t (thermophoresis parameter) while the pressure rise decreases with the increase in ϵ (radius ratio).

2. The frictional forces have an opposite behaviour as compared to the pressure rise.

3. It is seen that with the increase in the Brownian motion parameter N_b and the thermophoresis parameter N_t temperature profile increases.

4. Effects of Brownian motion parameter N_b and the thermophoresis parameter N_t on concentration profile are same.

5. Pressure gradient increases with an increase in ϕ for all considered waves.

6. The size of trapped bolus for triangular wave is small as compared to the other waves.

Appendix

$$
\begin{aligned}
A_1 &= 12(\log r_1 - \log r_2)^3,\ A_2 = -(N_b + N_t)(N_b + 2N_t),\ A_3 = N_t(N_b + N_t)(N_b + 2N_t),\\
A_4 &= \log r_1 - \log r_2,\ A_5 = 12N_b(\log r_1 - \log r_2)^3\ A_6 = 2\left(G_r N_b - B_r N_t\right)\left(N_b^2 + 3N_b N_t + 2N_t^2\right),\\
A_7 &= 2(N_b + 2N_t)\left(G_r N_b - B_r N_t\right) + \left(G_r N_b(-2 + N_b + 2N_t) - B_r N_t(N_b + 2N_t)\right)\log r_1\\
&\quad +\left(-B_r N_t(N_b + 2N_t) + G_r N_b\left(2 + N_b + 2N_t\right)\right)\log r_2,\\
A_8 &= 2(N_b + 2N_t)\left(G_r N_b - B_r N_t\right) + \left(-G_r N_b(2 - N_b - 2N_t) - B_r N_t(N_b + 2N_t)\right)\log r_1\\
&\quad +\left(-B_r N_t(N_b + 2N_t) - G_r N_b\left(2 - N_b - 2N_t\right)\right)\log r_2,\\
A_9 &= 2(3(N_b + N_t)(N_b + 2N_t)\left(G_r N_b - B_r N_t\right) - \left(-G_r N_b(N_b^2 + 3N_b\left(-2 + N_t\right) + 2(3(N_b + N_t)\right.\\
&\quad \left.(N_b + 2N_t)) + B_r(N_b^2 N_t + 2N_t^3 + 3N_b\left(4 + N_t^2\right))\right)\log r_1^2 + 3(N_b + N_t)(-B_r N_t(N_b + 2N_t)\\
&\quad \left(G_r N_b\left(2 + N_b + 2N_t\right)\right)\log r_2 + \left(-B_r(N_b^2 N_t + 2N_t^3 + 3N_b\left(4 + N_t^2\right)) + G_r N_b(N_b^2 + 3N_b\left(2 + N_t\right)\right.\\
&\quad \left.+2(-6 + N_t\left(3 + N_t\right))\right))\log r_2^2 + \log r_1(3(N_b + N_t)(G_r N_b(-2 + N_b + 2N_t) - B_r N_t(N_b + 2N_t)\\
&\quad +4(G_r N_b(6 + (N_b + N_t)(N_b + 2N_t) - B_r(N_b^2 N_t + 2N_t^3 + 3N_b\left(-2 + N_t^2\right)))\log r_2,\\
A_{10} &= -(N_b + N_t)(N_b + 2N_t)\left(G_r N_b - B_r N_t\right) + \log r_2(-3(N_b + N_t)(-B_r N_t(N_b + 2N_t) + G_r N_b(2\\
&\quad +N_b + 2N_t)) + \log r_2(B_r(N_b^2 N_t + 2N_t^3 + 3N_b\left(4 + N_t^2\right)) - G_r N_b(N_b^2 + 3N_b\left(2 + N_t\right) + 2(-6\\
&\quad +N_t\left(3 + N_t\right))) + 24\left(B_r + G_r\right)N_b\log r_2)),\\
A_{11} &= N_b^2 N_t + 2N_t^3 + 3N_b\left(4 + N_t^2\right) - G_r N_b(N_b^2 + 3N_b\left(-2 + N_t\right) + 2(-6 + N_t\left(-3 + N_t\right)),\\
A_{12} &= B_r(N_b^2 N_t + 2N_t^3 + 3N_b\left(4 + N_t^2\right)),\ A_{13} = G_r(N_b^2 + 3N_b\left(-2 + N_t\right) + 2\left(-6 - 3N_t + N_t^2\right)),\\
A_{14} &= G_r N_b(24 + 7N_b^2 + 2N_t\left(-3 + 7N_t\right) + 3N_b\left(-2 + 7N_t\right)) - B_r(7N_b^2 N_t + 14N_t^3 + 3N_b\left(-8 + N_t^2\right)),\\
A_{15} &= (N_b^2 N_t + 2N_t^3 + 3N_b\left(-8 + N_t^2\right)),\ A_{16} = \left(24 + 6N_b + N_b^2 + 6N_t + 3N_t N_b + 2N_t^2\right),\\
A_{17} &= 2(N_b + 2N_t)\left(G_r N_b - B_r N_t\right) + \left(G_r N_b(-2 + N_b - 2N_t) - B_r N_t(N_b + 2N_t)\right)\log r_1\\
&\quad -\left(-B_r N_t(N_b + 2N_t) + G_r N_b(2 + N_b + 2N_t)\right)\log r_2,\\
A_{18} &= -2(G_r N_b(6 - 2N_b^2 + N_b(3 - 6N_t) + (3 - 4N_t)N_t) + 2B_r(N_b^2 N_t + 2N_t^3 + 3N_b(1 + N_t^2))),
\end{aligned}
$$

$$
\begin{aligned}
A_{19} &= \log r_2(3(N_b+N_t)(-B_rN_t(N_b+2N_t)+G_rN_b(2+N_b+2N_t))+(-B_r(N_b^2N_t+2N_t^3+3N_b(4+N_t^2))\\
&\quad +G_rN_b(N_b^2+3N_b(2+N_t)+2(-6+N_t(3+N_t))))\log r_2,\\
A_{20} &= G_rN_b(24+7N_b^2+2N_t(-3+7N_t)+3N_b(-2+7N_t))-B_r(7N_b^2N_t+14N_t^3+3N_b(-8+7N_t^2)),\\
A_{21} &= \frac{1}{96A_4^3N_b\left(\log r_1-\log r_2\right)}(-(A_{10}-A_{19}-3A_{17}(N_b+N_t))\left(r_1^2-r_2^2\right)-2A_6r_1^2\log r_1^3+\log r_1^2((A_{18}\\
&\quad -A_{11}B_r)r_1^2+6A_7(N_b+N_t))r_1^2-\left(A_{18}-A_{11}B_r\right)r_2^2-2(A_{12}-A_{13}N_b)\left(r_1^2-r_2^2\right)\log r_1+r_2^2\log r_2\\
&\quad (A_9+6A_8(N_b+N_t)-6A_7(N_b+N_t)\log r_2+2A_6\log r_2^2)+\log r_1(-(A_9+6A_8(N_b+N_t))r_1^2\\
&\quad \left(r_1^2-r_2^2\right)\log r_2(A_{14}+A_{20}+(-2A_{15}B_r+2A_{16}G_rN_b)\log r_2))),\\
A_{22} &= \frac{\left(r_1^2-r_2^2\right)\left(\log r_1-\log r_2\right)^2}{4A_4^3},\\
A_{23} &= \frac{1}{96A_4^3N_b\left(\log r_1-\log r_2\right)}((96A_4^3N_b+(A_{10}-A_{19}-3A_{17}(N_b+N_t))r_1^2)\log r_2+\log r_1^2\log r_2\\
&\quad (-(A_{18}-A_{11}B_r+6A_7(N_b+N_t))r_1^2+\left(A_{14}+A_{20}\right)r_2^2+2((A_{12}-A_{13}N_b)r_1^2-A_{15}B_rr_2^2\\
&\quad +A_{16}N_bG_rr_2^2)\log r_2)+\log r_1^3((A_{18}-A_{11}B_r)r_2^2+2(A_6r_1^2+(-A_{12}+A_{13}N_b)r_2^2)\log r_2)\\
&\quad +\log r_1(-96A_4^3N_b+(-A_{10}+A_{19}+3A_{17}(N_b+N_t))r_2^2+\log r_2((A_9+6A_8(N_b+N_t))\\
&\quad \left(r_1^2-r_2^2\right)-\log r_2(A_{14}+A_{20})r_1^2-6A_7(N_b+N_t))r_2^2+2((-A_{15}B_r+A_{16}G_rN_b)r_1^2+A_6r_2^2)\log r_2))),\\
A_{24} &= -\frac{\left(r_2^2\log r_1-r_1^2\log r_2\right)\left(\log r_1-\log r_2\right)^2}{4A_4^3},\\
A_{25} &= -\frac{1}{6144}((r_1-r_2)^2\left(1536A_{21}A_4^3N_b-3072A_{23}A_4^3N_b-(16A_{10}-16A_{19}-3A_6-4(A_9+3\right.\\
&\quad \left.(4A_{17}+A_7+2A_8)(N_b+N_t))\right)(r_1-r_2)^2-3072A_{21}A_4^3N_b\log\left(r_1-r_2\right)+4\left(r_1-r_2\right)^2\\
&\quad (\log\left(r_1-r_2\right)(-3A_6-4(A_9+3(A_7+2A_8)(N_b+N_t))+6(A_6+4A_7(N_b+N_t))\log\left(r_1-r_2\right)\\
&\quad -8A_6\log\left(r_1-r_2\right)^2)+4\log r_1(\log r_1(A_{18}-A_{11}B_r-2(A_{12}-A_{13}N_b)\log r_2)+\log r_2\\
&\quad (A_{14}+A_{20}+(-2A_{15}B_r+2A_{16}G_rN_b\log r_2)))),\\
A_{26} &= \frac{\left(r_1-r_2\right)^2\left(4A_4^3(-A_{22}+2A_{24}+2A_{22}\log\left(r_1-r_2\right))+\left(r_1-r_2\right)^2\left(\log r_1-\log r_2\right)^3\right.}{16A_4^3}.
\end{aligned}
$$

Chapter 5

Influence of heat transfer on a peristaltic flow of Johnson Segalman fluid in a non uniform tube

5.1 Introduction

This chapter deals with the influence of heat transfer and magnetic field on a peristaltic flow of Johnson Segalman fluid in a non uniform tube. The governing equations of Johnson Segalman are simplified using the long wave length and low Reynolds number assumptions. In the wave frame of reference, an analytical solutions are computed with the help of two techniques namely (i) Perturbation technique (ii) HAM technique. The expressions for pressure rise, pressure gradient, velocity profile and temperature field have been calculated. The behavior of different physical parameters have been examined graphically. The pumping and trapping phenomena of various wave forms are also studied.

5.2 Mathematical Model

Johnson Segalman model is an integral type model which can also be described in rate type model. Consider an incompressible fluid for which continuity and momentum equation can be

written as follow

$$\operatorname{div} \mathbf{V} = \mathbf{0}, \tag{5.1}$$

$$\rho \frac{d\mathbf{V}}{dt} = \operatorname{div} \mathbf{S} + f. \tag{5.2}$$

The Cauchy stress $\bar{\mathbf{S}}$ for a Johnson-Segalman fluid [10] is defined as

$$\mathbf{S} = -P\mathbf{I} + 2\mu\mathbf{D} + \boldsymbol{\tau}, \tag{5.3}$$

$$\boldsymbol{\tau} + m\left(\frac{d\boldsymbol{\tau}}{dt} + \boldsymbol{\tau}\left(\mathbf{W_1} - a_3\mathbf{D}\right) + \left(\mathbf{W_1} - a_3\mathbf{D}\right)^T \boldsymbol{\tau}\right) = 2\eta\mathbf{D}. \tag{5.4}$$

In which f body force, μ and η are the viscosities, m is called the relaxation time and a_3 is called slip parameter $\mathbf{D}$ and $\mathbf{W_1}$ are the symmetric and skewsymmetric parts of the velocity gradient respectively and can be defined as

$$\mathbf{D} = \frac{1}{2}\left(\mathbf{L} + \mathbf{L}^T\right), \tag{5.5}$$

$$\mathbf{W_1} = \frac{1}{2}\left(\mathbf{L} - \mathbf{L}^T\right), \tag{5.6}$$

where $\mathbf{L} = \operatorname{grad} \mathbf{V}$.

In general, energy equation can be defined as

$$\rho \frac{de_1}{dt} = \boldsymbol{\tau}.\mathbf{L} - \operatorname{div} \hat{\mathbf{Q}} + \rho r_3, \tag{5.7}$$

where $\hat{Q}$ is the heat flux vector, $e_1 = \rho c_p$ is the specific internal energy, r_3 is the radiant heating and in the present problem we ignore the radiant heating.

According to Fourier law

$$\hat{Q} = -k \operatorname{grad} \bar{T},$$

where k is the constant of thermal conductivity and $\bar{T}$ is the temperature. Since we are dealing with the two dimensional flow, therefore,

$$\bar{T} = \bar{T}\left(\bar{R}, \bar{Z}\right).$$

5.3 Mathematical Formulation

Let us consider the peristaltic flow of an incompressible Johnson-Segalman fluid in a non uniform tube. The flow is generated by sinusoidal wave trains propagating with constant speed c along the walls. The geometry of the wall surface is defined as

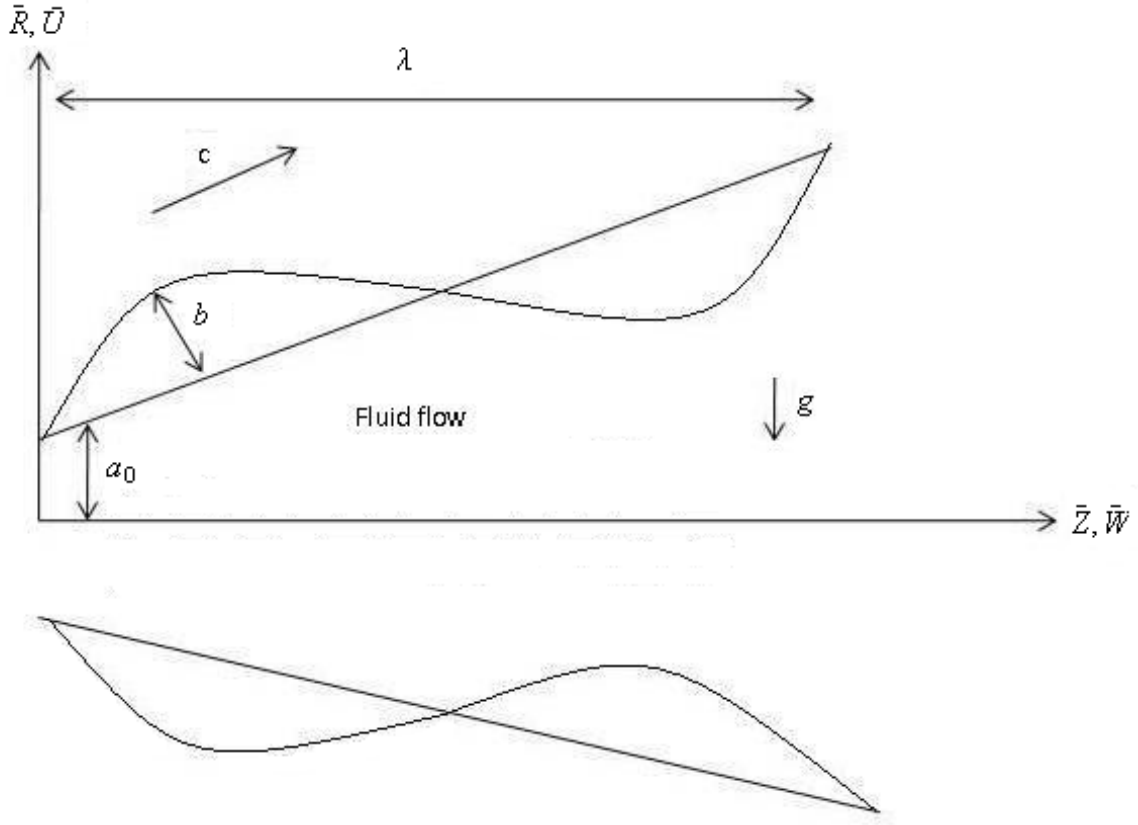

Fig.(5.a) . Geometry of the problem.

$$\bar{\mathbf{h}} = a\left(\bar{Z}\right) + b\sin\frac{2\pi}{\lambda}\left(\bar{Z} - c\bar{t}\right), \tag{5.8}$$

where $a\left(\bar{Z}\right) = a_0 + K\bar{Z}$, a_0 is the radius of the inlet, K is the constant whose magnitude depend on the length of the tube, b is the wave amplitude, λ is the wavelength, c is the propagation velocity and $\bar{t}$ is the time. We are considering the cylindrical coordinate system $(\bar{R}, \bar{Z})$, where $\bar{Z} - axis$ lies along the centerline of the tube and $\bar{R}$ is transverse to it.

The governing equations in the fixed frame for an incompressible flow are given as

$$\frac{\partial \bar{U}}{\partial \bar{R}} + \frac{\bar{U}}{\bar{R}} + \frac{\partial \bar{W}}{\partial \bar{Z}} = 0, \tag{5.9}$$

$$\begin{aligned} \rho\left(\frac{\partial}{\partial \bar{t}} + \bar{U}\frac{\partial}{\partial \bar{R}} + \bar{W}\frac{\partial}{\partial \bar{Z}}\right)\bar{U} &= -\frac{\partial \bar{P}}{\partial \bar{R}} + \frac{1}{\bar{R}}\frac{\partial}{\partial \bar{R}}\left(\bar{R}\boldsymbol{\tau}_{\bar{R}\bar{R}}\right) + \frac{\partial}{\partial \bar{Z}}\left(\boldsymbol{\tau}_{\bar{R}\bar{Z}}\right) - \frac{\boldsymbol{\tau}_{\bar{\theta}\bar{\theta}}}{\bar{R}} \\ &\quad +\mu\left(\frac{1}{\bar{R}}\frac{\partial}{\partial \bar{R}}\left(\bar{R}\frac{\partial \bar{U}}{\partial \bar{R}}\right) + \frac{\partial^2 \bar{U}}{\partial \bar{Z}^2}\right) + \rho g\cos\alpha, \end{aligned} \tag{5.10}$$

$$\begin{aligned} \rho\left(\frac{\partial}{\partial \bar{t}} + \bar{U}\frac{\partial}{\partial \bar{R}} + \bar{W}\frac{\partial}{\partial \bar{Z}}\right)\bar{W} &= -\frac{\partial \bar{P}}{\partial \bar{Z}} + \frac{1}{\bar{R}}\frac{\partial}{\partial \bar{R}}\left(\bar{R}\boldsymbol{\tau}_{\bar{R}\bar{Z}}\right) + \frac{\partial}{\partial \bar{Z}}\left(\boldsymbol{\tau}_{\bar{Z}\bar{Z}}\right) \\ &\quad +\mu\left(\frac{1}{\bar{R}}\frac{\partial}{\partial \bar{R}}\left(\bar{R}\frac{\partial \bar{W}}{\partial \bar{R}}\right) + \frac{\partial^2 \bar{W}}{\partial \bar{Z}^2}\right) + \rho g\sin\alpha, \end{aligned} \tag{5.11}$$

$$\begin{aligned} \rho c_p\left(\frac{\partial}{\partial \bar{t}} + \bar{U}\frac{\partial}{\partial \bar{R}} + \bar{W}\frac{\partial}{\partial \bar{Z}}\right)\bar{T} &= \boldsymbol{\tau}_{\bar{R}\bar{R}}\frac{\partial \bar{U}}{\partial \bar{R}} + \boldsymbol{\tau}_{\bar{R}\bar{Z}}\frac{\partial \bar{W}}{\partial \bar{R}} + \boldsymbol{\tau}_{\bar{Z}\bar{R}}\frac{\partial \bar{U}}{\partial \bar{Z}} + \boldsymbol{\tau}_{\bar{Z}\bar{Z}}\frac{\partial \bar{W}}{\partial \bar{Z}} \\ &\quad +k\left(\frac{\partial^2 \bar{T}}{\partial \bar{R}^2} + \frac{1}{\bar{R}}\frac{\partial \bar{T}}{\partial \bar{R}} + \frac{\partial^2 \bar{T}}{\partial \bar{Z}^2}\right), \end{aligned} \tag{5.12}$$

where k denotes the the thermal conductivity and c_p is the specific heat at constant pressure.

The corresponding boundary conditions are

$$\frac{\partial \bar{w}}{\partial \bar{r}} = 0, \qquad \text{at} \quad \bar{r} = 0, \tag{5.13a}$$

$$\bar{w} = 0, \quad at \quad \bar{r} = \bar{h} = a\left(\bar{z}\right) + b\sin\frac{2\pi}{\lambda}\left(\bar{z}\right), \tag{5.13b}$$

$$\frac{\partial \bar{T}}{\partial \bar{r}} = 0, \qquad \text{at} \quad \bar{r} = 0, \tag{5.13c}$$

$$\bar{T} = 0, \quad at \quad \bar{r} = \bar{h} = a\left(\bar{z}\right) + b\sin\frac{2\pi}{\lambda}\left(\bar{z}\right). \tag{5.13d}$$

We introduce the non-dimensional variables as

$$\begin{aligned}
R &= \frac{\bar{R}}{a_0},\ r=\frac{\bar{r}}{a_0},\quad Z=\frac{\bar{Z}}{\lambda},\quad z=\frac{\bar{z}}{\lambda},\ W=\frac{\bar{W}}{c},\ w=\frac{\bar{w}}{c},\\
U &= \frac{\lambda\bar{U}}{a_0 c},\ u=\frac{\lambda\bar{u}}{a_0 c},\ P=\frac{a_0^2\bar{P}}{c\lambda\left(\mu+\eta\right)},\ t=\frac{c\bar{t}}{\lambda},\quad \delta=\frac{a_0}{\lambda},\\
\mathrm{Re} &= \frac{\rho c a_0}{\mu},\ \tau=\frac{a_0\bar{\boldsymbol{\tau}}}{c\mu},\ E=\frac{\mu c}{\rho g a_0^2},\ E_c=\frac{c^2}{c_p\left(T_0-T_1\right)},\\
\mathrm{Pr} &= \frac{\mu c_p}{k},\ We=\frac{mc}{a_0},\ \theta\ =\frac{\left(\bar{T}-\bar{T}_1\right)}{\left(\bar{T}_0-\bar{T}_1\right)}.
\end{aligned} \tag{5.14}$$

Making use of Eqs. (2.12) and (5.14), Eqs. (5.9) to (5.12) along with boundary conditions (5.13a to 5.13d) under the assumptions of long wavelength $\delta << 1$ and low Reynolds number take the form

$$\left(\frac{\mu+\eta}{\mu}\right)\frac{\partial P}{\partial z}=\frac{1}{r}\frac{\partial}{\partial r}\left(r\boldsymbol{\tau}_{rz}\right)+\frac{1}{r}\frac{\partial}{\partial r}\left(r\frac{\partial w}{\partial r}\right)+\frac{\sin\alpha}{E}, \tag{5.15}$$

$$\frac{\partial P}{\partial r}=0, \tag{5.16}$$

$$\frac{1}{r}\frac{\partial}{\partial r}\left(r\frac{\partial\theta}{\partial r}\right)=-B_r\left(\frac{\partial w}{\partial r}S_{rz}\right), \tag{5.17}$$

where $B_r=E_c\,\mathrm{Pr}$ and

$$\tau_{rr}=W_e\left(1+a\right)\frac{\partial w}{\partial r}S_{rz}, \tag{5.18}$$

$$\tau_{zz}=-W_e\left(1-a\right)\frac{\partial w}{\partial r}S_{rz}, \tag{5.19}$$

$$\tau_{rz}=\frac{\frac{\eta}{\mu}\frac{\partial w}{\partial r}}{1+W_e^2\left(1-a^2\right)\left(\frac{\partial w}{\partial r}\right)^2}. \tag{5.20}$$

With the help of Eqs. (5.18) to (5.20), Eqs. (5.15) to (5.17) can be written as

$$\frac{1}{r}\frac{\partial}{\partial r}\left[r\left(\frac{\frac{\eta}{\mu}\frac{\partial w}{\partial r}}{1+W_e^2\left(1-a_3^2\right)\left(\frac{\partial w}{\partial r}\right)^2}\right)\right]+\frac{1}{r}\frac{\partial}{\partial r}\left(r\frac{\partial w}{\partial r}\right)+\frac{\sin\alpha}{E}\left(\frac{\mu}{\mu+\eta}\right)=\left(\frac{\mu+\eta}{\mu}\right)\frac{dP}{dz}, \tag{5.21}$$

$$\frac{dP}{dr}=0, \tag{5.22}$$

$$\frac{1}{r}\frac{\partial}{\partial r}\left(r\frac{\partial\theta}{\partial r}\right)=-B_r\left[\frac{\partial w}{\partial r}\left(\frac{\frac{\eta}{\mu}\frac{\partial w}{\partial r}}{1+W_e^2\left(1-a_3^2\right)\left(\frac{\partial w}{\partial r}\right)^2}\right)\right]. \tag{5.23}$$

in which δ, Re and We represent the wave, Reynolds and Weissenberg numbers, respectively.

The relevant boundary conditions are

$$\frac{\partial w}{\partial r} = 0, \quad \frac{\partial \theta}{\partial r} = 0 \quad \text{at} \quad r = 0, \tag{5.24a}$$

$$w = 0, \quad \theta = 0 \quad \text{at} \quad r = h = 1 + \frac{\lambda K z}{a_0} + \phi \sin 2\pi z. \tag{5.24b}$$

5.4 Perturbation Solution

Since, Eqs. (5.21) and (5.23) are non linear equations, we employ the regular perturbation to find the solution. For perturbation solution, we expand w, F and P as

$$w = w_0 + W_e^2 w_1 + O(We^4), \tag{5.25a}$$

$$\theta = \theta_0 + W_e^2 \theta_1 + O(We^4), \tag{5.25b}$$

$$F_1 = F_{10} + W_e^2 F_{11} + O(We^4), \tag{5.25c}$$

$$P = P_0 + W_e^2 P_1 + O(We^4). \tag{5.25d}$$

Substituting Eqs. (5.25a) to (5.25d) in Eqs. (5.21) to (5.24) and then find the solutions of all systems we arrive at the final solutions which are defined as

$$w = \left(\frac{r^2 - h^2}{4}\right)\left(\frac{\partial P}{\partial z} - b_1\right) + W_e^2 \left(\frac{G_4}{4}\left(r^4 - h^4\right)\right), \tag{5.26}$$

$$\theta = G_{10}\left(r^4 - h^4\right) + W_e^2 \left(G_{11}\left(r^8 - h^8\right) + G_{12}\left(r^6 - h^6\right) + G_{13}\left(r^4 - h^4\right)\right), \tag{5.27}$$

$$\frac{dP}{dz} = \frac{-8E\left(2F_1 + h^2\right) + h^4 b_1}{h^4} + W_e^2 \left(G_{14} h^2\right), \tag{5.28}$$

where

$$
\begin{aligned}
G_1 &= \left(\frac{\partial P_0}{\partial z} - b_1\right)\frac{1}{2}, \quad G_2 = -E_c \Pr \frac{\eta}{\mu} G_1^2, \quad G_3 = \frac{\partial P_1}{\partial z}\frac{1}{2}, \\
G_4 &= \left(1 - a_3^2\right)\left(\frac{\partial P_0}{\partial z} - b_1\right)^3 \frac{\eta}{\mu + \eta}\frac{1}{8}, \quad G_5 = -E_c \Pr \frac{\eta}{\mu} G_3^2, \\
G_6 &= -2E_c \Pr \frac{\eta}{\mu} G_3 G_2, \quad G_7 = -E_c \Pr \frac{\eta}{\mu} G_4^2, \quad G_8 = \left(1 - a_3^2\right) E_c \Pr \frac{\eta}{\mu} a_1^4, \\
G_9 &= G_6 + G_8, \quad G_{10} = \frac{G_2}{16}, \quad G_{11} = \frac{G_7}{64}, \quad G_{12} = \frac{G_9}{36}, \quad G_{13} = \frac{G_5}{16}, \\
G_{14} &= \left(a_3^2 - 1\right)\left(\frac{\partial P_0}{\partial z} - b_1\right)^3 \frac{\eta}{\mu + \eta}\frac{1}{6}, \quad b_1 = \frac{\sin\alpha}{E}\left(\frac{\mu}{\mu + \eta}\right), \\
b_2 &= We^2 \frac{\eta}{\mu + \eta}\left(a_3^2 - 1\right).
\end{aligned}
$$

The pressure rise ΔP and friction force F are given as

$$\Delta P = \int_0^1 \frac{dP}{dz} dz, \tag{5.29}$$

$$F = \int_0^1 h^2 \left(-\frac{dP}{dz}\right) dz, \tag{5.30}$$

where $\frac{dP}{dz}$ is defined in Eqs. (5.28).

The non-dimensional expressions for the five considered wave forms have been taken into account and are defined in chapter 1.

5.5 HAM Solution

In this section, we have found the HAM solution of Eqs. (5.21) to (5.24). For that we choose

$$w_0 = \left(\frac{r^2 - h^2}{4}\right)\left(\frac{\partial P}{\partial z} - b_1\right), \tag{5.31}$$

$$\theta_0 = \frac{a_2}{16}\left(r^2 - h^2\right), \tag{5.32}$$

as the initial guesses for both velocity and temperature profile. Further, the auxiliary linear operators for the Eqs. (5.26) and (5.28) are chosen as

$$\mathcal{L}_{wr}(w) = \frac{1}{r}\frac{\partial}{\partial r}\left(r\frac{\partial w_0}{\partial r}\right), \tag{5.33}$$

$$\mathcal{L}_{\theta r}(\theta) = \frac{1}{r}\frac{\partial}{\partial r}\left(r\frac{\partial \theta_0}{\partial r}\right). \tag{5.34}$$

The auxiliary linear operator has the property

$$\mathcal{L}_{wr}(C_1 r + C_2) = 0, \tag{5.35}$$

$$\mathcal{L}_{\theta r}(C_3 r + C_4) = 0. \tag{5.36}$$

We can define the following zeroth-order deformation problems

$$(1-q)\mathcal{L}_{wr}[\,\bar{w}\,(r,q) - \,w_0(r)] = q\hbar_w N_{wr}[\bar{w}\,(r,q)], \tag{5.37}$$

$$(1-q)\mathcal{L}_{\theta r}[\,\bar{\theta}\,(r,q) - \,\theta_0(r)] = q\hbar_\theta N_{\theta r}[\bar{\theta}\,(r,q)], \tag{5.38}$$

$$\frac{\partial \bar{w}}{\partial r}(r,q) = 0, \quad \frac{\partial \bar{\theta}}{\partial r}(r,q) = 0, \quad at\ r = 0, \tag{5.39}$$

$$\bar{w}\,(r,q) = 0, \quad \bar{\theta}\,(r,q) = 0, \quad at\ r = h. \tag{5.40}$$

In Eqs. (5.37) to (5.40), $\hbar_w$ and $\hbar_\theta$ denote the non-zero auxiliary parameter, $q\epsilon[0,1]$ is the embedding parameter and

$$N_{wr}[\bar{w}(r,q)] = \frac{\partial^2 w}{\partial r^2} + \frac{1}{r}\frac{\partial w}{\partial r} + \frac{b_2}{r}\left(\frac{\partial w}{\partial r}\right)^3 + 3b_2\frac{\partial^2 w}{\partial r^2}\left(\frac{\partial w}{\partial r}\right)^2 - \frac{dP}{dz} - b_1, \tag{5.41}$$

$$N_{\theta r}[\bar{\theta}(r,q)] = \frac{\partial^2 \theta}{\partial r^2} + \frac{1}{r}\frac{\partial \theta}{\partial r} + B_r\left(\frac{\partial w}{\partial r}\right)^2 - B_r We^2\frac{\eta}{\mu}\left(1-a^2\right)\left(\frac{\partial w}{\partial r}\right)^4. \tag{5.42}$$

Obviously

$$\frac{\partial \hat{w}\left(r,0\right)}{\partial r} = 0, \quad \hat{w}\left(r,1\right) = w\left(r\right), \tag{5.43}$$

$$\frac{\partial \hat{\theta}\left(r,0\right)}{\partial r} = 0, \quad \hat{\theta}\left(r,1\right) = \theta\left(r\right), \tag{5.44}$$

when q varies from 0 to 1, then $\hat{w}\left(r,q\right)$ and $\hat{\theta}\left(r,q\right)$ varies from initial guess to the solution $w\left(r\right)$ and $\hat{\theta}\left(r,q\right)$, varies from initial guess to the solution $\theta\left(r\right)$. Expanding $\hat{w}\left(r,q\right)$ and $\hat{\theta}\left(r,q\right)$ in Taylor's series with respect to an embedding parameter q, we have

$$\hat{w}\left(r,q\right) = w_0\left(r\right) + \sum_{n=1}^{\infty} w_m(r) q^m, \tag{5.45}$$

$$\hat{\theta}\left(r,q\right) = \theta_0\left(r\right) + \sum_{n=1}^{\infty} \theta_m(r) q^m, \tag{5.46}$$

$$w_m = \frac{1}{m!} \left.\frac{\partial^m \bar{w}\left(r,q\right)}{\partial q^m}\right|_{q=0}, \tag{5.47}$$

$$\theta_m = \frac{1}{m!} \left.\frac{\partial^m \bar{\theta}(r,q)}{\partial q^m}\right|_{q=0}. \tag{5.48}$$

Differentiating the zeroth order deformation m-times with respect to q and then dividing by $m!$ and finally setting $q = 0$, we get the following mth order deformation problem

$$\mathcal{L}_w[w_m(r) - \chi_m w_{m-1}(r)] = \hbar_w R_{wr}(r), \tag{5.49}$$

$$\mathcal{L}_\theta[\theta_m(r) - \chi_m \theta_{m-1}(r)] = \hbar_\theta R_{\theta r}(r), \tag{5.50}$$

where

$$R_{wr} = w''_{m-1} + \frac{1}{r}w'_{m-1} + \frac{b_2}{r}\sum_{i=0}^{m-1} w'_{m-1}w'_{m-1-i}w'_{m-k-1} + 3b_2\sum_{i=0}^{m-1} w'_{m-1}w'_{m-1-i}w''_{m-k-1} - \left(\frac{dP}{dz} - b_1\right)(1-\chi_m), \tag{5.51}$$

$$R_{\theta r} = \theta''_{m-1} + \frac{1}{r}\theta'_{m-1} + B_r\sum_{i=0}^{m-1} w'_{m-1}w'_{m-1-i} - B_rWe^2\frac{\eta}{\mu}\left(1-a^2\right)\sum_{k=0}^{m-1} w'_{m-1-k}\sum_{l=0}^{k} w'_{k-l}\sum_{j=0}^{l} w'_{l-j}\sum_{i=0}^{j} w'_{j-i}, \tag{5.52}$$

$$\chi_m = \begin{cases} 0, & m \le 1, \\ 1, & m > 1. \end{cases} \tag{5.53}$$

The solution of the above equations with the help of Mathematica can be calculated and presented as follow

$$w_m(r) = \lim_{M\to\infty}\left[\sum_{m=0}^{M} a^0_{m,0} + \sum_{n=1}^{2M+1}\left(\sum_{m=n-1}^{2M}\sum_{k=0}^{2m+1-n} a^k_{m,n}r^{2n+2}\right)\right], \tag{5.54}$$

$$\theta_m(r) = \lim_{M\to\infty}\left[\sum_{m=0}^{M} b^0_{m,0} + \sum_{n=1}^{2M+1}\left(\sum_{m=n-1}^{2M}\sum_{k=0}^{2m+1-n} b^k_{m,n}r^{4n+2}\right)\right], \tag{5.55}$$

where $a^0_{m,0}$, $b^0_{m,0}$, $a^k_{m,n}$ and $b^k_{m,n}$ are constants.

5.6 Numerical Results and Discussion

In this section we have presented the solution of the Johnson Segalman fluid model graphically. Figs. (5a) and (5b) are prepared for h-curves for velocity and temperature profile. Figs.5. c and 5.d show the comparison of perturbation and HAM solutions for velocity and temperature profile respectively. The expression for pressure rise ΔP is calculated numerically using mathematics software. The effects of various parameters on the pressure rise ΔP and frictional forces F are shown in Figs. 5.1 to 5.12 for various values of angle of inclination α, Weissenberg number We, amplitudes ratio ϕ, viscosities μ and η, relaxation time m and slip parameter a_3. It is observed

from Figs.5.1 to 5.6 that pressure rise increases with the increase in α, We, η and ϕ while decreases with the increase in μ and a_3. Moreover, the peristaltic pumping occurs in the region $0 \leq Q \leq 1.4$ for Figs. 5.2 to 5.5 and $0 \leq Q \leq 0.5$ for Fig. 5.6, other wise augmented pumping occurs. The variations of frictional forces are shown in Figs. 7 to 12. It can be seen that frictional forces have opposite behavior as compared to the pressure rise. Figs. 5.13 to 5.17 are prepared to see the behavior of pressure gradient for different wave shapes. It is seen that with increase in ϕ pressure gradient increases. Figs. 5.18 to 5.21 are prepared to see the behavior of temperature profile physically. It is analyzed that with the increase in μ temperature profile increases, moreover it is seen that temperature field decreases with the increase in η, B_r and We. The effects of different parameters on streamlines for the trapping phenomenon for five different wave forms can be seen through Fig. 5.22. It is observed that the size of trapping bolus in triangular wave is smaller as compared to the other waves.

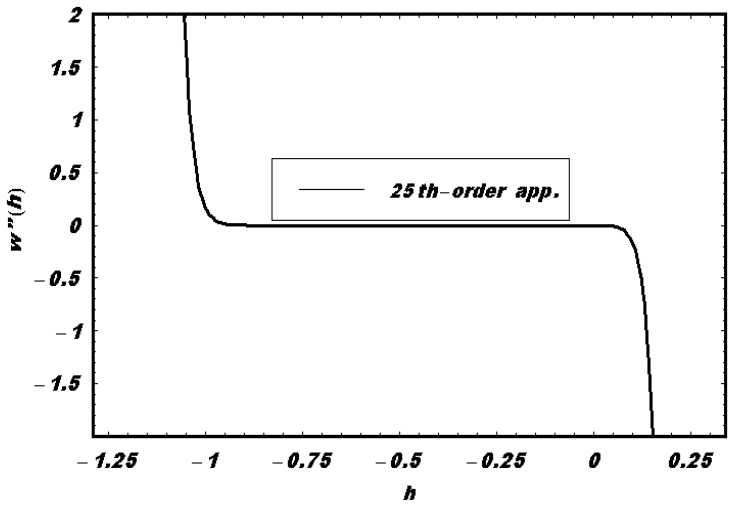

Fig. 5.*a*. $\hbar$ curve for velocity profile for $K = 0.04$, $\lambda = 0.01$, $a_0 = 0.01$, $\phi = 0.3$, $z = 0.1$, $We = 0.1$, $\mu = 0.02$, $\eta = 0.02$, $a = 0.5$, $E = 1.7$, $B_r = 0.4$.

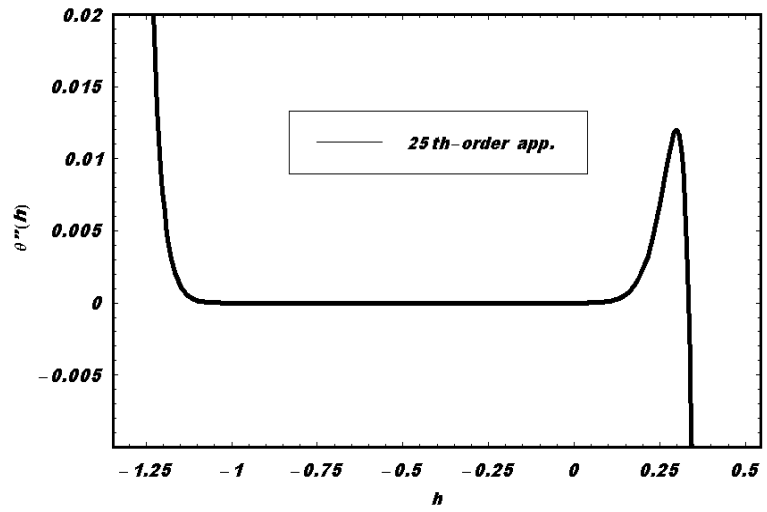

Fig. 5.*b*. $\hbar$ curve for temperature profile for $K = 0.04$, $\lambda = 0.01$, $a_0 = 0.01$, $\phi = 0.3$, $z = 0.1$, $We = 0.1$, $\mu = 0.02$, $\eta = 0.02$, $a = 0.5$, $E = 1.7$, $B_r = 0.4$.

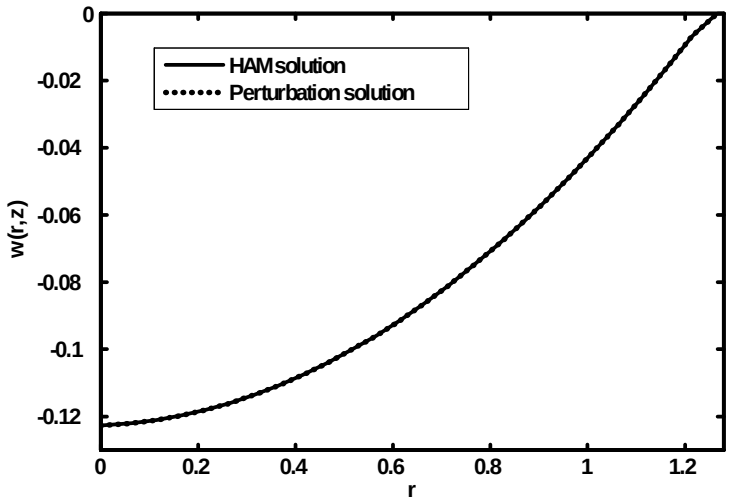

Fig. 5.*c*. Comparison of velocity profile for $K = 0.04$, $\lambda = 0.01$, $a_0 = 0.01$, $\phi = 0.3$, $z = 0.1$, $We = 0.1$, $\mu = 0.02$, $\eta = 0.02$, $a = 0.5$, $E = 1.7$, $B_r = 0.4$.

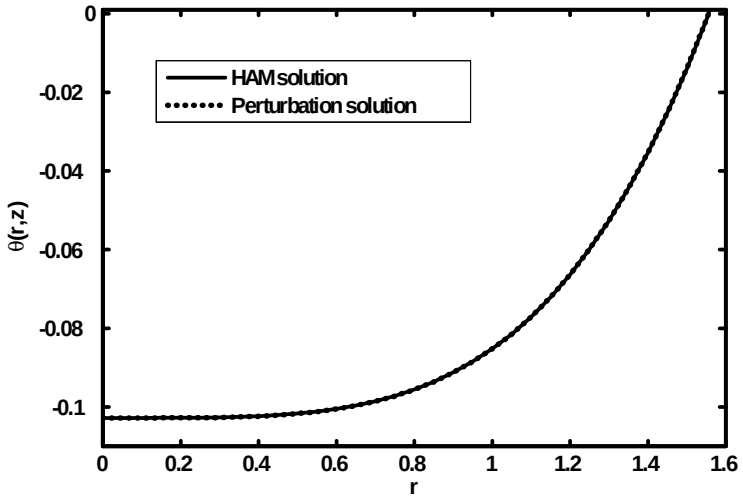

Fig. 5.*d*. Comparison of temperature profile for $K = 0.04$, $\lambda = 0.01$, $a_0 = 0.01$, $\phi = 0.3$, $z = 0.1$, $We = 0.1$, $\mu = 0.02$, $\eta = 0.02$, $a = 0.5$, $E = 1.7$, $B_r = 0.4$.

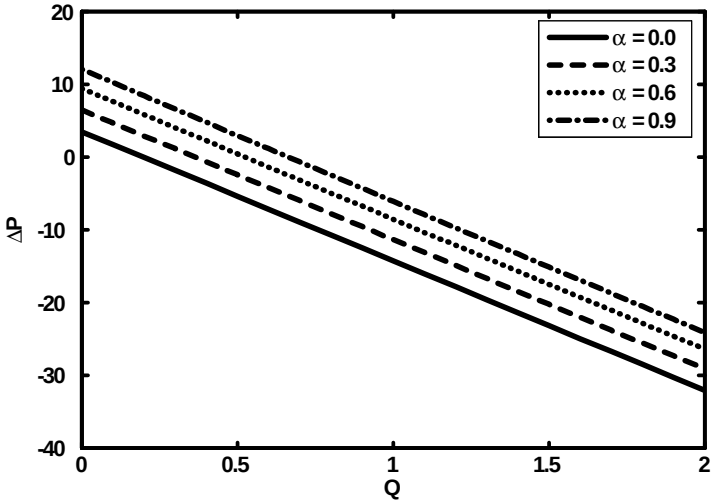

Fig.5.1. Pressure rise versus flow rate for $K = 0.4$, $\lambda = 0.1$, $a_0 = 0.1$, $\phi = 0.3$, $We = 0.1$, $\mu = 0.5$, $\eta = 0.5$, $a_3 = 0.3$, $E = 0.1$.

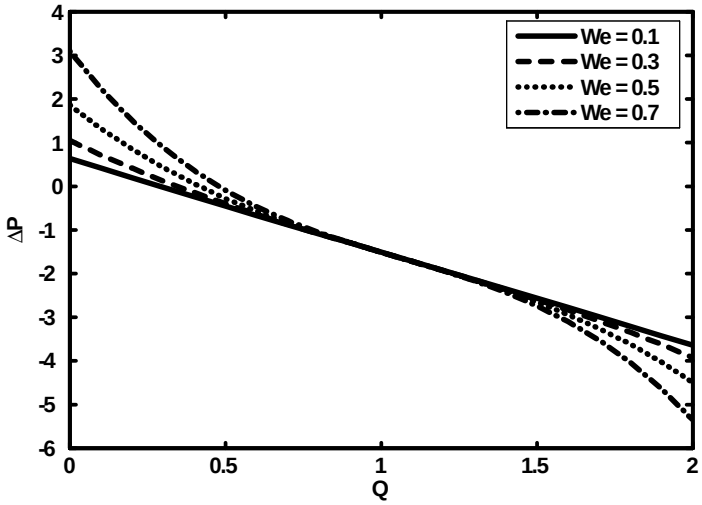

Fig.5.2. Pressure rise versus flow rate for $K = 0.9$, $\lambda = 0.7$, $a_0 = 0.2$, $\phi = 0.5$, $\alpha = 0.1$, $\mu = 0.5$, $\eta = 0.5$, $a_3 = 0.3$, $E = 0.1$.

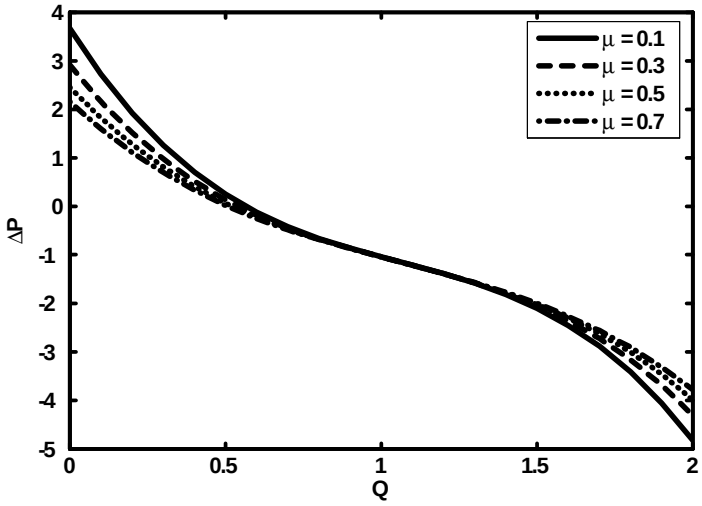

Fig.5.3. Pressure rise versus flow rate for $K = 0.9$, $\lambda = 0.7$, $a_0 = 0.2$, $\phi = 0.5$, $\alpha = 0.1$, $We = 0.5$, $\eta = 0.5$, $a_3 = 0.3$, $E = 0.1$.

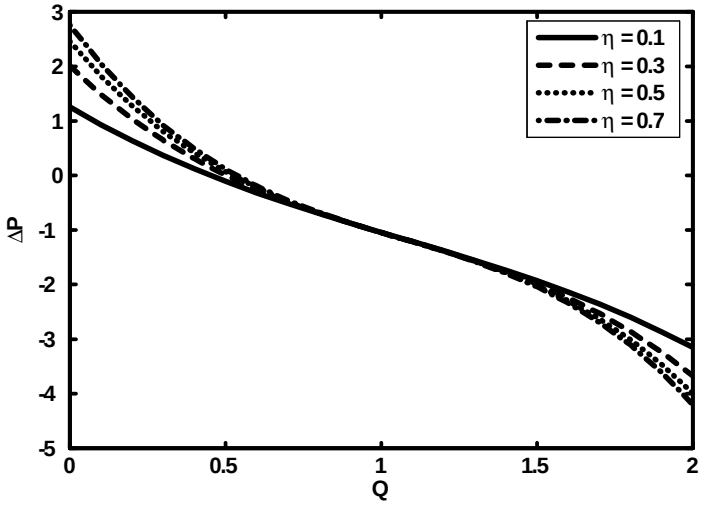

Fig.5.4. Pressure rise versus flow rate for $K = 0.9$, $\lambda = 0.7$, $a_0 = 0.2$, $\phi = 0.5$, $\alpha = 0.1$, $We = 0.5$, $\mu = 0.5$, $a_3 = 0.3$, $E = 0.1$.

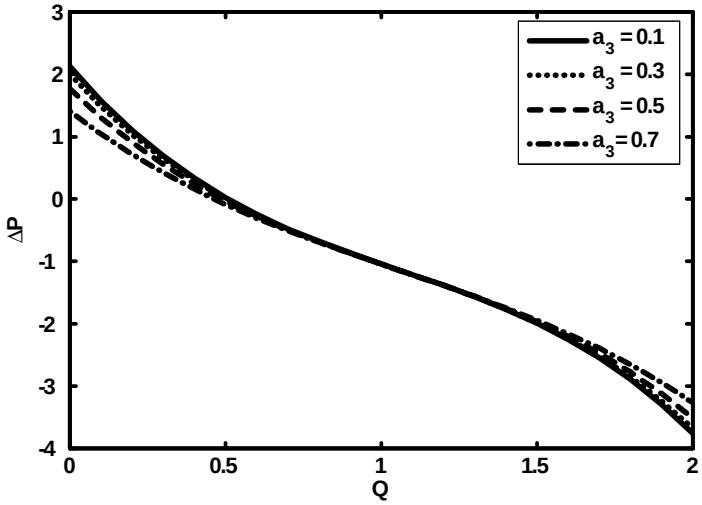

Fig.5.5. Pressure rise versus flow rate for $K = 0.9$, $\lambda = 0.7$, $a_0 = 0.2$, $\phi = 0.5$, $\alpha = 0.1$, $We = 0.5$, $\mu = 0.5$, $\eta = 0.5$, $E = 0.1$.

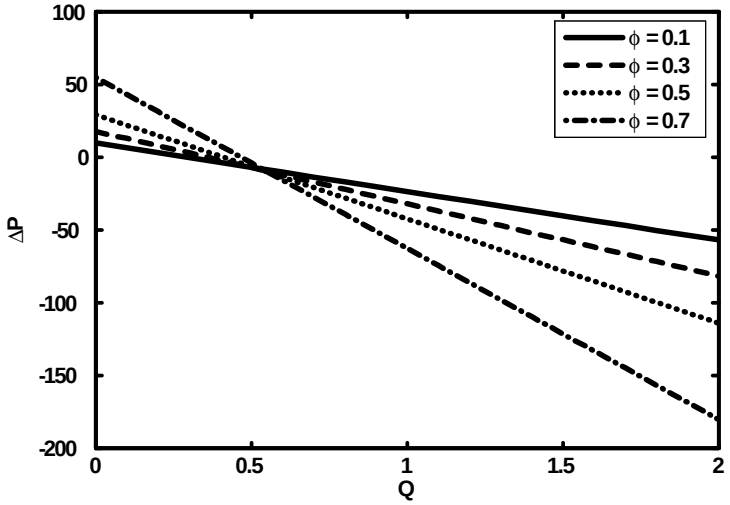

Fig.5.6. Pressure rise versus flow rate for $K = 0.01$, $\lambda = 0.01$, $a_0 = 0.02$, $a_3 = 0.5$, $\alpha = 0.1$, $We = 0.5$, $\mu = 0.5$, $\eta = 0.3$, $E = 0.1$.

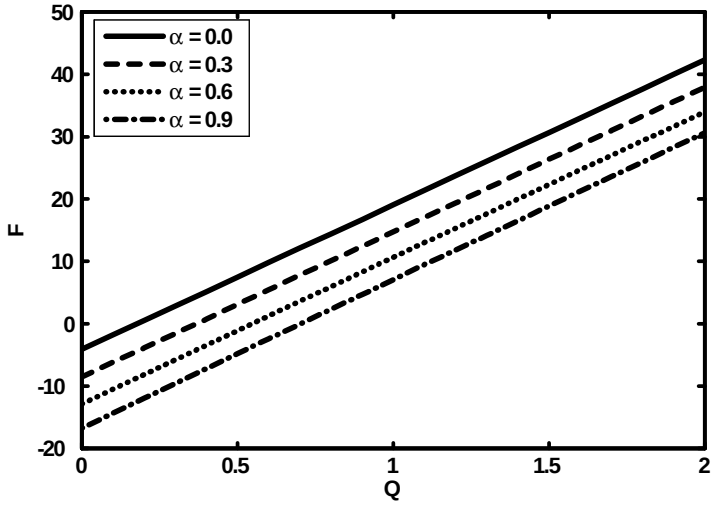

Fig.5.7. Frictional force versus flow rate for $K = 0.4$, $\lambda = 0.1$, $a_0 = 0.1$, $\phi = 0.3$, $We = 0.1$, $\mu = 0.5$, $\eta = 0.5$, $a_3 = 0.3$, $E = 0.1$.

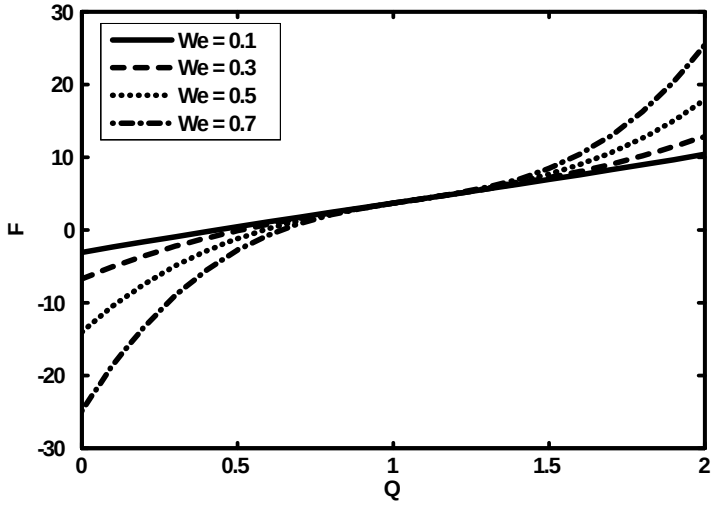

Fig.5.8. Frictional force versus flow rate for $K = 0.9$, $\lambda = 0.7$, $a_0 = 0.2$, $\phi = 0.5$, $\alpha = 0.1$, $\mu = 0.5$, $\eta = 0.5$, $a_3 = 0.3$, $E = 0.1$.

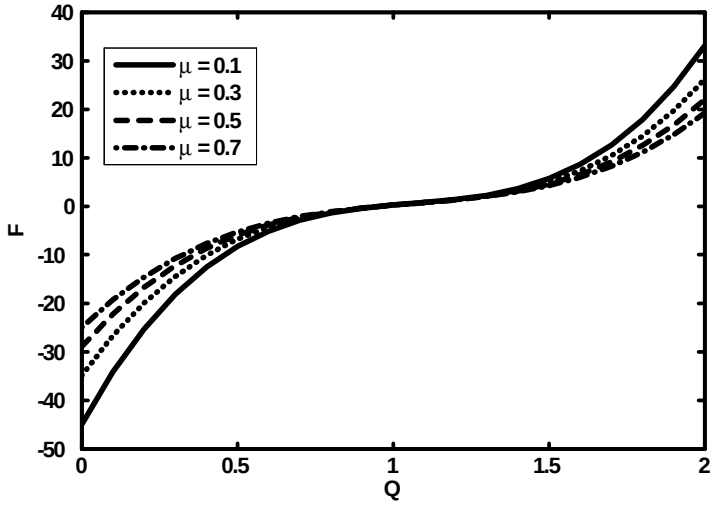

Fig.5.9. Frictional force versus flow rate for $K = 0.9$, $\lambda = 0.7$, $a_0 = 0.2$, $\phi = 0.5$, $\alpha = 0.1$, $We = 0.5$, $\eta = 0.5$, $a_3 = 0.3$, $E = 0.1$.

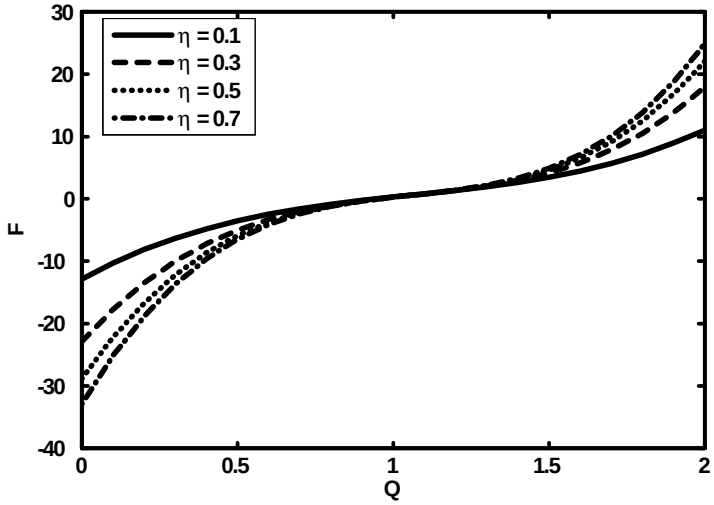

Fig.5.10. Frictional force versus flow rate for $K = 0.9$, $\lambda = 0.7$, $a_0 = 0.2$, $\phi = 0.5$, $\alpha = 0.1$, $We = 0.5$, $\mu = 0.5$, $a_3 = 0.3$, $E = 0.1$.

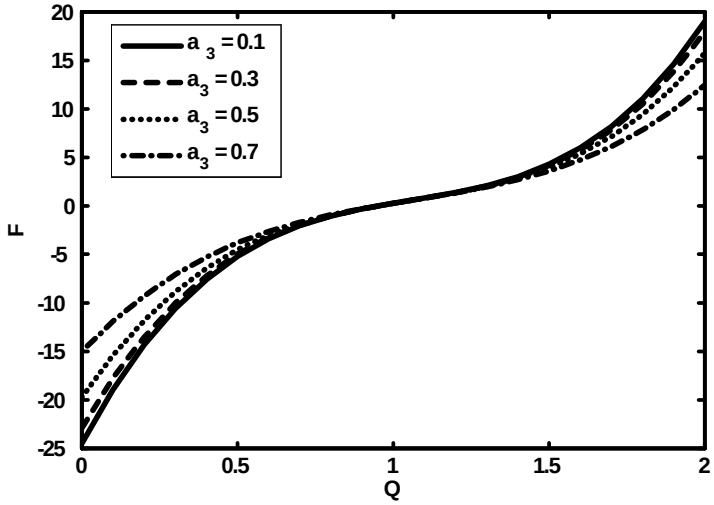

Fig.5.11. Frictional force versus flow rate for $K = 0.9$, $\lambda = 0.7$, $a_0 = 0.2$, $\phi = 0.5$, $\alpha = 0.1$, $We = 0.5$, $\mu = 0.5$, $\eta = 0.5$, $E = 0.1$.

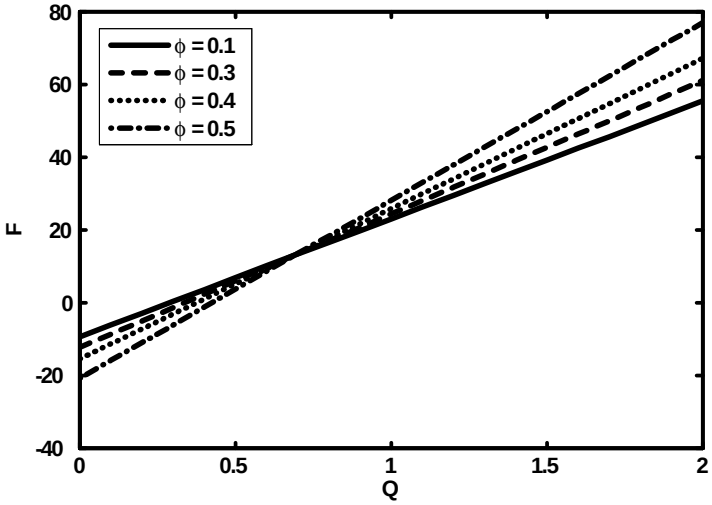

Fig.5.12. Frictional force versus flow rate for $K = 0.01$, $\lambda = 0.01$, $a_0 = 0.02$, $a_3 = 0.5$, $\alpha = 0.1$, $We = 0.5$, $\mu = 0.5$, $\eta = 0.3$, $E = 0.1$.

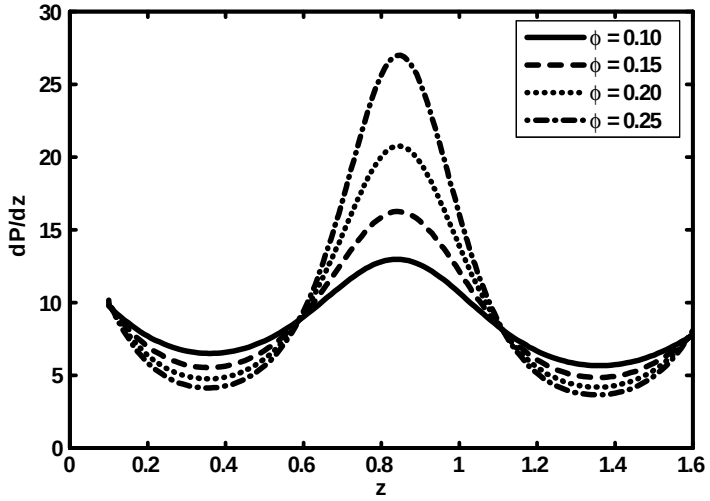

Fig.5.13. Pressure gradient versus z (Sinusoidal wave) for $K = 0.4$, $\lambda = 0.1$, $a_0 = 0.1$, $\alpha = 0.3$, $Q = -1.5$, $We = 0.1$, $\mu = 0.5$, $\eta = 0.5$, $a_3 = 0.3$, $E = 0.1$.

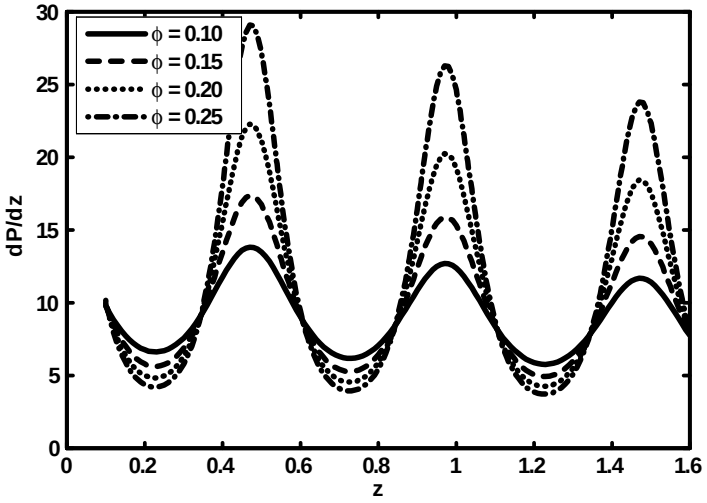

Fig.5.14. Pressure gradient versus z (Multi sinusoidal wave) for $K = 0.4$, $\lambda = 0.1$, $a_0 = 0.1$, $\alpha = 0.3$, $Q = -1.5$, $We = 0.1$, $\mu = 0.5$, $\eta = 0.5$, $a_3 = 0.3$, $E = 0.1$.

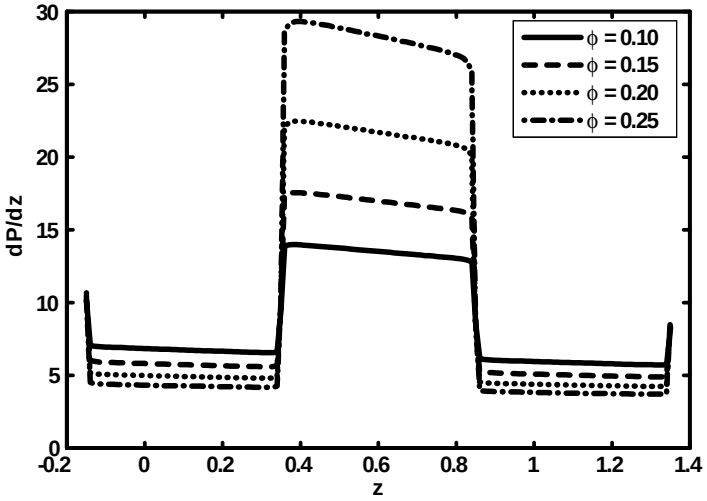

Fig.5.15. Pressure gradient versus z (Square wave) for $K = 0.4$, $\lambda = 0.1$, $a_0 = 0.1$, $\alpha = 0.3$, $Q = -1.5$, $We = 0.1$, $\mu = 0.5$, $\eta = 0.5$, $a_3 = 0.3$, $E = 0.1$.

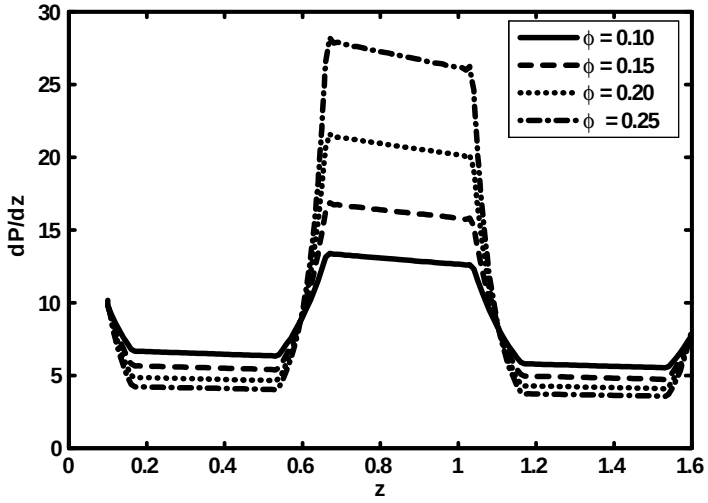

Fig.5.16. Pressure gradient versus z (Trapezoidal wave) for $K = 0.4$, $\lambda = 0.1$, $a_0 = 0.1$, $\alpha = 0.3$, $Q = -1.5$, $We = 0.1$, $\mu = 0.5$, $\eta = 0.5$, $a_3 = 0.3$, $E = 0.1$.

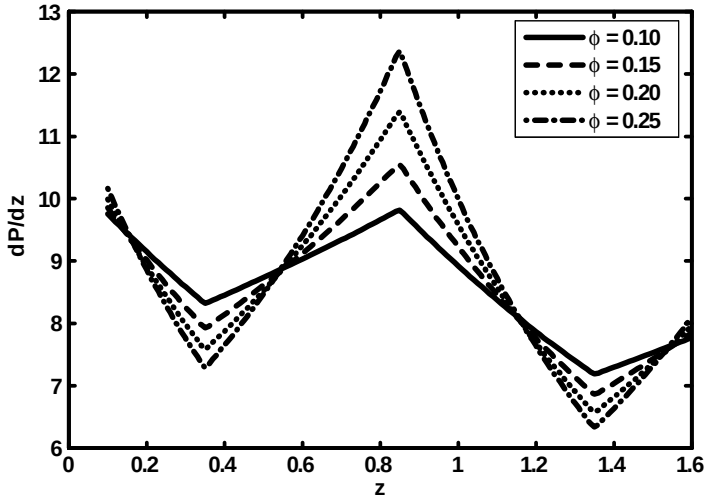

Fig.5.17. Pressure gradient versus z (Triangular wave) for $K = 0.4$, $\lambda = 0.1$, $a_0 = 0.1$, $\alpha = 0.3$, $Q = -1.5$, $We = 0.1$, $\mu = 0.5$, $\eta = 0.5$, $a_3 = 0.3$, $E = 0.1$.

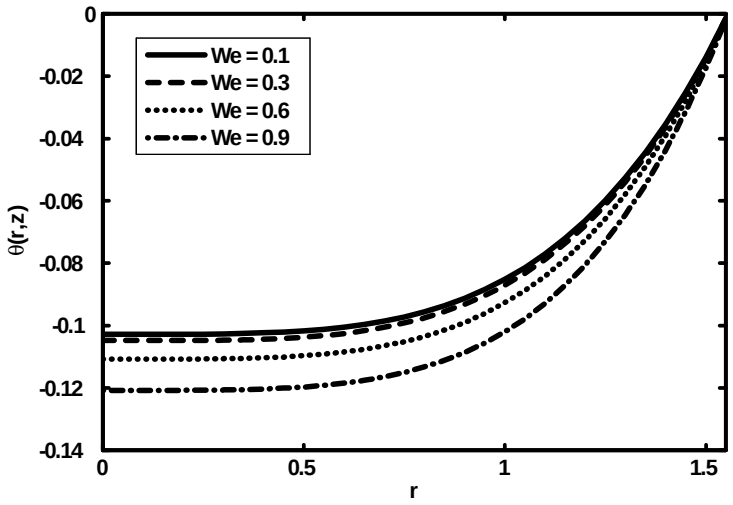

Fig.5.18. Temperature profile for $K = 0.4$, $\lambda = 0.1$, $Q = 0.5$, $z = 0.2$, $a_0 = 0.1$, $a_3 = 0.3$, $\alpha = 0.1$, $B_r = 0.5$, $\mu = 0.5$, $\eta = 0.5$, $E = 0.1$.

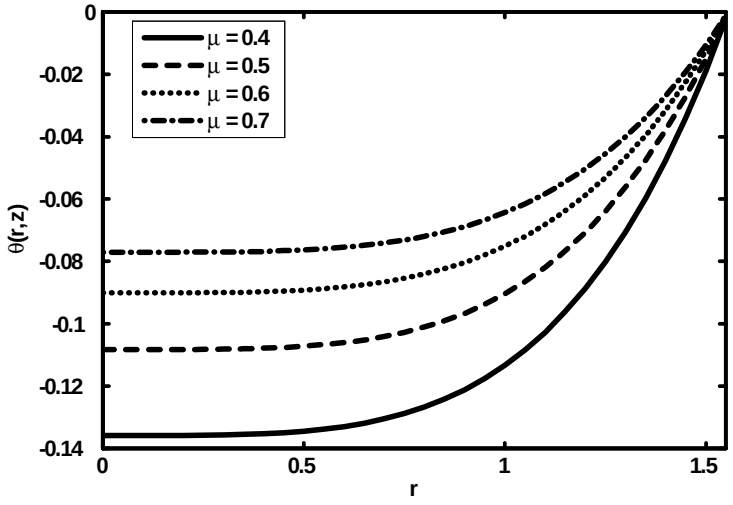

Fig.5.19. Temperature profile for $K = 0.4$, $\lambda = 0.1$, $Q = 0.5$, $z = 0.2$, $a_0 = 0.1$, $a_3 = 0.3$, $\alpha = 0.1$, $B_r = 0.5$, $We = 0.5$, $\eta = 0.5$, $E = 0.1$.

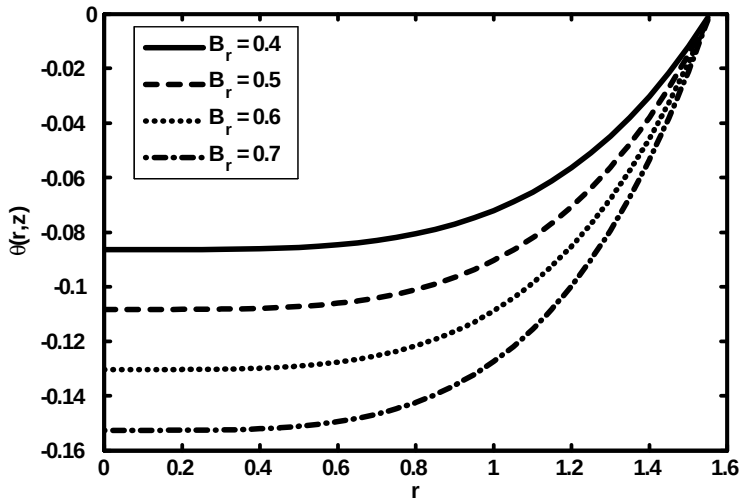

Fig.5.20. Temperature profile for $K = 0.4$, $\lambda = 0.1$, $Q = 0.5$, $z = 0.2$, $a_0 = 0.1$, $a_3 = 0.3$, $\alpha = 0.1$, $\eta = 0.5$, $\mu = 0.5$, $We = 0.5$, $E = 0.1$.

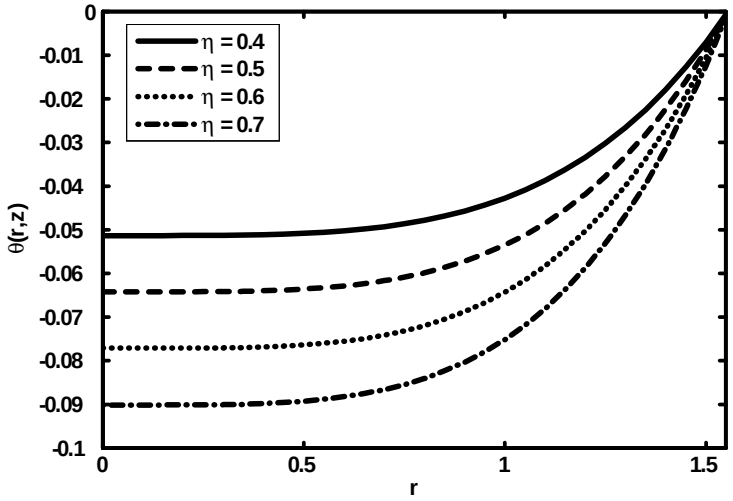

Fig.5.21. Temperature profile for $K = 0.4$, $\lambda = 0.1$, $Q = 0.5$, $z = 0.2$, $a_0 = 0.1$, $a_3 = 0.3$, $\alpha = 0.1$, $B_r = 0.5$, $\mu = 0.5$, $We = 0.5$, $E = 0.1$.

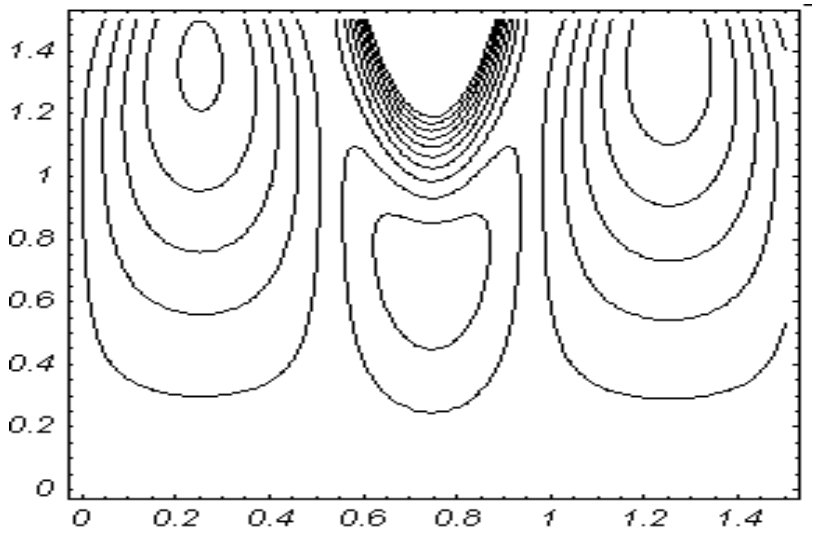

Fig. 5.22 (a) . Streamlines for sinusoidal wave when $K = 0.04$, $\lambda = 0.01$, $Q = 0.3$, $z = 0.2$, $a_0 = 0.01$, $a_3 = 0.3$, $\alpha = 0.1$, $\mu = 0.5$, $\eta = 0.5$, $E = 0.3$.

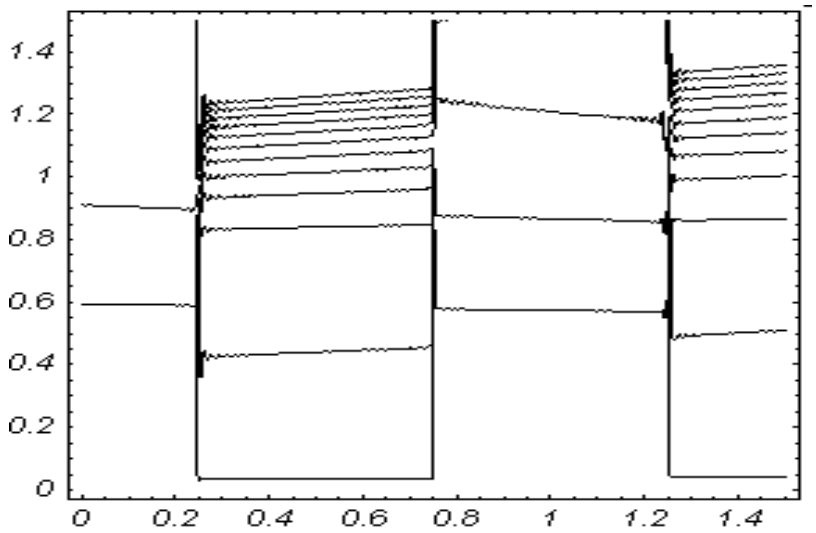

Fig. 5.22 (b) . Streamlines for square wave when $K = 0.04$, $\lambda = 0.01$, $Q = 0.3$, $z = 0.2$, $a_0 = 0.01$, $a_3 = 0.3$, $\alpha = 0.1$, $\mu = 0.5$, $\eta = 0.5$, $E = 0.3$.

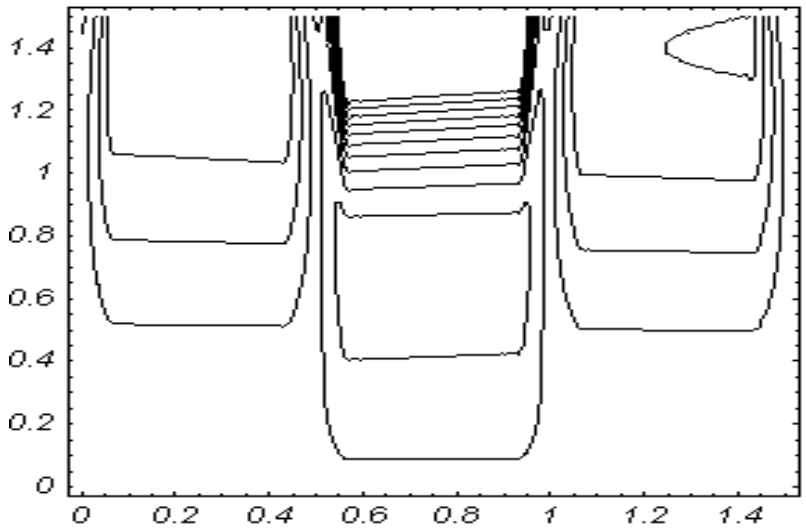

Fig. 5.22 (c) . Streamlines for trapezoidal wave when $K = 0.04$, $\lambda = 0.01$, $Q = 0.3$, $z = 0.2$, $a_0 = 0.01$, $a_3 = 0.3$, $\alpha = 0.1$, $\mu = 0.5$, $\eta = 0.5$, $E = 0.3$.

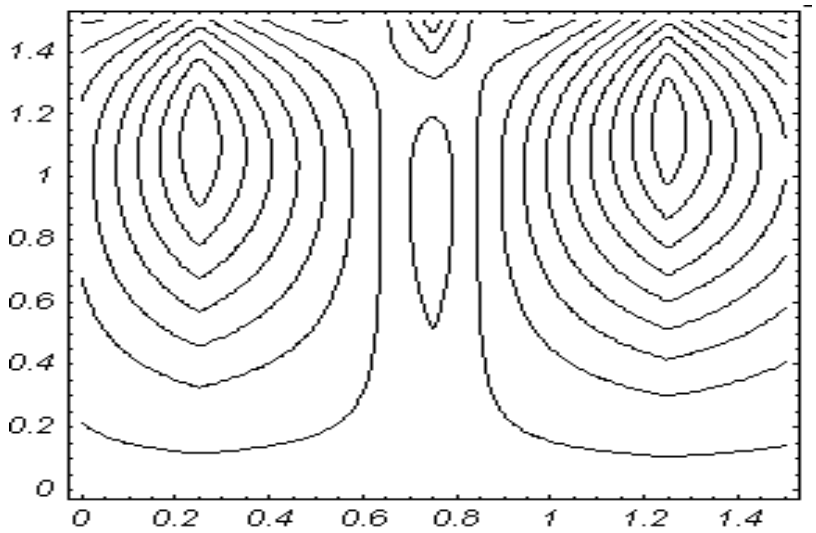

Fig. 5.22 (d) . Streamlines for triangular wave when $K = 0.04$, $\lambda = 0.01$, $Q = 0.3$, $z = 0.2$, $a_0 = 0.01$, $a_3 = 0.3$, $\alpha = 0.1$, $\mu = 0.5$, $\eta = 0.5$, $E = 0.3$.

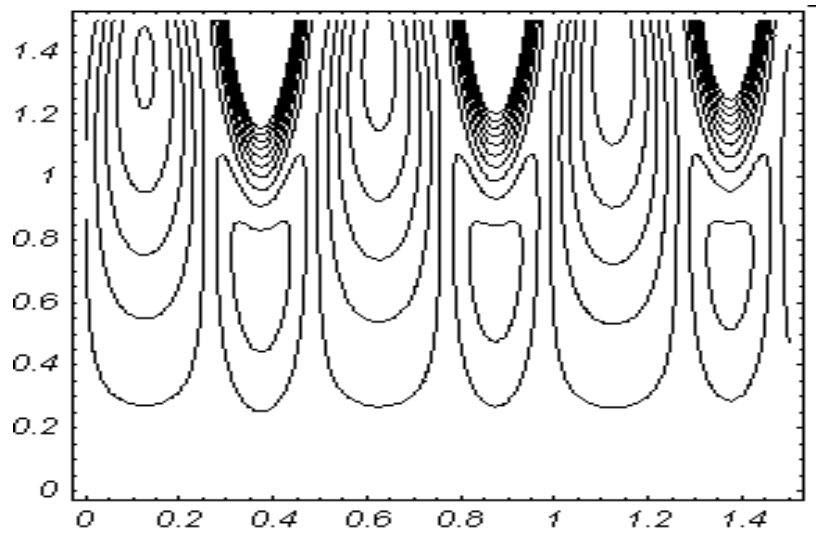

Fig. 5.22 (e) . Streamlines for multisinusoidal wave when
$K = 0.04$, $\lambda = 0.01$, $Q = 0.3$, $z = 0.2$, $a_0 = 0.01$, $a_3 = 0.3$,
$\alpha = 0.1$, $\mu = 0.5$, $\eta = 0.5$, $E = 0.3$.

5.7 Conclusion

The perturbation and HAM solutions of Eqs. (5.21) to (5.23) have been computed for velocity and temperature profile. The expressions for pressure rise frictional forces and pressure gradient have been discussed for five wave shapes. The following observations have been found

1. The pressure rise increases with the increase in α, We η and ϕ while decreases with increase in μ and a_3.

2. It is observed that frictional forces have an opposite behavior as compared to the pressure rise.

3. It is analyzed that with the increase in μ temperature profile increases, moreover it is seen that temperature field decreases with the increase in η, B_r and We.

4. The size of trapped bolus in triangular wave is smaller as compared to other waves

5. The pressure gradient increases with increase in ϕ for all five wave shapes.

Chapter 6

Analytical and numerical treatment for peristaltic transport of a tangent hyperbolic fluid in an endoscope

6.1 Introduction

This chapter deals with the study of peristaltic flow of a tangent hyperbolic fluid in an endoscope. The modelling of hyperbolic tangent fluid model for two dimensional flow in cylindrical coordinates are presented. Using the assumption of long wavelength and low Reynold number, the governing equations of hyperbolic tangent fluid for an endoscope have been solved using regular perturbation method and shooting method. The expression for pressure rise and frictional forces have been calculated using numerical integrations. At the end, various physical parameters have been shown pictorially.

6.2 Mathematical Model

For an incompressible fluid the continuity and momentum equations are defined in Eqs. (1.1) and (1.2). The basic equation for hyperbolic tangent fluid is given by [8]

$$\bar{\mathbf{S}} = -\bar{P}\mathbf{I} + \boldsymbol{\tau}, \tag{6.1}$$

$$\boldsymbol{\tau} = \left[\mu_\infty + (\mu_0 + \mu_\infty)\tanh\left(\Gamma\overline{\dot{\gamma}}\right)^n\right]\overline{\dot{\gamma}}, \tag{6.2}$$

in which μ_∞ is the infinite shear rate viscosity, μ_0 is the zero shear rate viscosity, Γ is the time constant, n is the power law index and $\overline{\dot{\gamma}}$ is defined as

$$\overline{\dot{\gamma}} = \sqrt{\frac{1}{2}\sum_i\sum_j \overline{\dot{\gamma}}_{ij}\overline{\dot{\gamma}}_{ji}} = \sqrt{\frac{1}{2}\Pi}, \tag{6.3}$$

where $\Pi = \frac{1}{2}trac\left(\text{grad}\, V + (\text{grad}\, V)^T\right)^2$. Here Π is the second invariant strain tensor. We consider the constitution Eq. (6.2), the case for which $\mu_\infty = 0$ and $\Gamma\overline{\dot{\gamma}} < 1$. The component of extra stress tensor therefore, take the form

$$\begin{aligned}\boldsymbol{\tau} &= \mu_0\left[(\Gamma\overline{\dot{\gamma}})^n\right]\overline{\dot{\gamma}} = \mu_0\left[(1+\Gamma\overline{\dot{\gamma}}-1)^n\right]\overline{\dot{\gamma}} \\ &= \mu_0\left[1+n(\Gamma\overline{\dot{\gamma}}-1)\right]\overline{\dot{\gamma}}.\end{aligned} \tag{6.4}$$

6.3 Mathematical Formulation

We have consider the peristaltic transport of an incompressible hyperbolic tangent fluid in an endoscope. The flow is generated by sinusoidal wave trains propagating with constant speed c along the walls of endoscope. The geometry of the wall surface is defined in Eqs. (2.13) and (2.14).

The governing equations in the fixed frame for an incompressible flow are

$$\frac{\partial \bar{U}}{\partial \bar{R}} + \frac{\bar{U}}{\bar{R}} + \frac{\partial \bar{W}}{\partial \bar{Z}} = 0, \tag{6.5}$$

$$\rho\left(\frac{\partial}{\partial \bar{t}} + \bar{U}\frac{\partial}{\partial \bar{R}} + \bar{W}\frac{\partial}{\partial \bar{Z}}\right)\bar{U} = -\frac{\partial \bar{P}}{\partial \bar{R}} + \frac{1}{\bar{R}}\frac{\partial}{\partial \bar{R}}\left(\bar{R}\boldsymbol{\tau}_{\bar{R}\bar{R}}\right) + \frac{\partial}{\partial \bar{Z}}\left(\boldsymbol{\tau}_{\bar{R}\bar{Z}}\right) - \frac{\boldsymbol{\tau}_{\bar{\theta}\bar{\theta}}}{\bar{R}}, \tag{6.6}$$

$$\rho\left(\frac{\partial}{\partial \bar{t}} + \bar{U}\frac{\partial}{\partial \bar{R}} + \bar{W}\frac{\partial}{\partial \bar{Z}}\right)\bar{W} = -\frac{\partial \bar{P}}{\partial \bar{Z}} + \frac{1}{\bar{R}}\frac{\partial}{\partial \bar{R}}\left(\bar{R}\boldsymbol{\tau}_{\bar{R}\bar{Z}}\right) + \frac{\partial}{\partial \bar{Z}}\left(\boldsymbol{\tau}_{\bar{Z}\bar{Z}}\right). \tag{6.7}$$

Introducing a wave frame $(\bar{r}, \bar{z})$ moving with velocity c away from the fixed frame $(\bar{R}, \bar{Z})$ by the transformations which are defined in Eqs. (1.11) and (1.12).

The corresponding boundary conditions are the symmetry at the center line and no-slip at the walls

$$\bar{w} = -c, \qquad \text{at} \quad \bar{r} = \bar{r}_1, \tag{6.8(a)}$$

$$\bar{w} = -c, \qquad \text{at } \bar{r} = \bar{r}_2 = a_2 + b\sin\frac{2\pi}{\lambda}(\bar{z}). \tag{6.8(b)}$$

Defining

$$\begin{aligned} R &= \frac{\bar{R}}{a_2}, \quad r = \frac{\bar{r}}{a_2}, \quad Z = \frac{\bar{Z}}{\lambda}, \quad z = \frac{\bar{z}}{\lambda}, \quad W = \frac{\bar{W}}{c}, \quad w = \frac{\bar{w}}{c}, \\ U &= \frac{\lambda\bar{U}}{a_2 c}, \quad u = \frac{\lambda\bar{u}}{a_2 c}, \quad p = \frac{a_2^2\bar{P}}{c\lambda\mu}, \quad t = \frac{c\bar{t}}{\lambda}, \quad \delta = \frac{a_2}{\lambda}, \mathrm{Re} = \frac{\rho c a_2}{\mu}, \\ r_2 &= \frac{\bar{r}_2}{a} = 1 + \phi\sin 2\pi z, \quad \dot{\gamma} = \frac{a_2}{c}\bar{\dot{\gamma}}, \ \tau = \boldsymbol{\tau}\frac{a_2}{\mu c}. \end{aligned} \tag{6.9}$$

Using the above non-dimensional quantities and the resulting equations can be written as

$$\frac{\partial u}{\partial r} + \frac{u}{r} + \frac{\partial w}{\partial z} = 0, \tag{6.10}$$

$$\mathrm{Re}\,\delta^3\left(u\frac{\partial}{\partial r} + w\frac{\partial}{\partial z}\right)u = -\frac{\partial P}{\partial r} + \frac{\delta}{r}\frac{\partial}{\partial r}(r\tau_{rr}) + \delta^2\frac{\partial}{\partial z}(\tau_{rz}), \tag{6.11}$$

$$\mathrm{Re}\,\delta\left(u\frac{\partial}{\partial r} + w\frac{\partial}{\partial z}\right)w = -\frac{\partial P}{\partial z} + \frac{1}{r}\frac{\partial}{\partial r}(r\tau_{rz}) + \delta\frac{\partial}{\partial z}(\tau_{zz}), \tag{6.12}$$

where

$$\begin{aligned} \tau_{rr} &= 2\left[1 + n(We\dot{\gamma} - 1)\right]\frac{\partial u}{\partial r}, \\ \tau_{rz} &= \left[1 + n(We\dot{\gamma} - 1)\right]\left(\frac{\partial u}{\partial z}\delta^2 + \frac{\partial w}{\partial r}\right), \\ \tau_{zz} &= 2\delta\left[1 + n(We\dot{\gamma} - 1)\right]\frac{\partial w}{\partial z}, \\ \dot{\gamma} &= \left[2\delta^2\left(\frac{\partial u}{\partial r}\right)^2 + \left(\frac{\partial w}{\partial r} + \frac{\partial u}{\partial z}\delta^2\right)^2 + 2\delta^2\left(\frac{\partial w}{\partial z}\right)^2\right]^{1/2}, \end{aligned}$$

in which δ, Re, We represent the wave, Reynolds and Weissenberg numbers, respectively. Under the assumptions of long wavelength $\delta << 1$ and low Reynolds number, neglecting the terms of order δ and higher, Eqs.(6.11) and (6.12) take the form

$$\frac{\partial P}{\partial r} = 0. \tag{6.13}$$

$$\frac{\partial P}{\partial z} = \frac{1}{r}\frac{\partial}{\partial r}\left[r\left(1+n(We\frac{\partial w}{\partial r}-1)\right)\frac{\partial w}{\partial r}\right], \tag{6.14}$$

$$w = -1, \quad \text{at} \quad r = r_1, \tag{6.15a}$$

$$w = -1, \text{ at } \quad r = r_2 = 1 + \phi \sin 2\pi z. \tag{6.15b}$$

6.4 Solution of the Problem

6.4.1 Perturbation Solution

For perturbation solution, we expand w, F_1 and P as

$$w = w_0 + We w_1 + O(We^2), \tag{6.16}$$

$$F_1 = F_{10} + We F_{11} + O(We^2), \tag{6.17}$$

$$P = P_0 + We P_1 + O(We^2). \tag{6.18}$$

Substituting above expressions in Eqs. (6.16) to (6.19), collecting the powers of We, we obtain the following systems

Zeroth Order System

$$\frac{\partial P_0}{\partial z} = \frac{1}{r}\frac{\partial}{\partial r}\left(r\,(1-n)\,\frac{\partial w_0}{\partial r}\right), \tag{6.19}$$

$$w_0 = -1, \quad \text{at} \quad r = r_1, \tag{6.20}$$

$$w_0 = -1, \text{ at } \quad r = r_2 = 1 + \phi \sin 2\pi z. \tag{6.21}$$

First Order System

$$\frac{\partial P_1}{\partial z} = \frac{1}{r}\frac{\partial}{\partial r}\left(r\left(1-n\right)\frac{\partial w_1}{\partial r}\right) + \frac{1}{r}\frac{\partial}{\partial r}\left(rn\left(\frac{\partial w_0}{\partial r}\right)^2\right), \tag{6.22}$$

$$w_1 = 0, \quad \text{at} \quad r = r_1, \tag{6.23}$$

$$w_1 = 0, \text{ at } \quad r = r_2 = 1 + \phi \sin 2\pi z. \tag{6.24}$$

Solution for Zeroth Order System

Solution of Eq.(6.19) satisfying the boundary conditions (6.20) and (6.21) can be written as

$$w_0 = -1 + \left(\frac{r^2}{4(1-n)} + \frac{H_3}{(1-n)}\ln r + H_4\right)\frac{\partial p_0}{\partial z}, \tag{6.25}$$

$$\frac{dP_0}{dz} = \frac{2F_0 + \left(r_2^2 - r_1^2\right)}{H_7}. \tag{6.26}$$

Solution for First Order System

Substituting the zeroth-order solution (6.25) into (6.22), the solution of the resulting problem satisfying the boundary conditions take the following form

$$\begin{aligned} w_1 = {} & \left(\frac{r^2}{4(1-n)} + \frac{H_3}{(1-n)}\ln r + H_4\right)\frac{\partial P_1}{\partial z} - \frac{n}{(1-n)^3}\left(\frac{r^3}{12} - \frac{H_3^2}{r}\right. \\ & \left. + H_3 r\right)\left(\frac{dP_0}{dz}\right)^2 + \frac{H_5}{(1-n)}\ln r + H_6\Bigg), \end{aligned} \tag{6.27}$$

$$\frac{dP_1}{dz} = \frac{2F_1 + H_8}{H_7}. \tag{6.28}$$

Summarizing the perturbation results for small parameter We, the expression for velocity field and pressure gradient can be written as

$$\begin{aligned} w = {} & -1 + \left(\frac{r^2}{4(1-n)} + \frac{H_3}{(1-n)}\ln r + H_4\right)\frac{\partial P}{\partial z} + We\left(\frac{n}{(1-n)^3}\left(\frac{r^3}{12} - \right.\right. \\ & \left.\left. \frac{H_3^2}{r} + H_3 r\right)\left(\frac{dP_0}{dz}\right)^2 + \frac{H_5}{(1-n)}\ln r + H_6\right), \end{aligned} \tag{6.29}$$

$$\frac{dP}{dz} = \frac{2F + \left(r_2^2 - r_1^2\right)}{H_7} + We\left(\frac{H_8}{H_7}\right), \tag{6.30}$$

where

$$\begin{aligned}
H_1 &= \frac{r_1^2 - r_2^2}{4(1-n)}, \quad H_2 = \frac{\ln r_1 - \ln r_2}{(1-n)}, \quad H_3 = -\frac{H_1}{H_2}, \\
H_4 &= -\left(\frac{r_1^2}{4(1-n)} + \frac{H_3}{(1-n)}\ln r_1\right), \\
H_5 &= -\frac{n}{H_2(1-n)^3}\left(\frac{r_1^3 - r_2^3}{12} - \left(\frac{1}{r_1} - \frac{1}{r_2}\right)H_3^2 + H_3(r_1 - r_2)\right)\left(\frac{dP_0}{dz}\right)^2, \\
H_6 &= \frac{n}{(1-n)^3}\left(\frac{r_1^3}{12} - \frac{1}{r_1}H_3^2 + H_3 r_1\right)\left(\frac{dP_0}{dz}\right)^2 - \frac{H_5}{(1-n)}\ln r_1, \\
H_7 &= \left(\frac{r_2^4 - r_1^4}{8(1-n)} + \frac{H_3}{(1-n)}\left(r_2^2\ln r_2 - r_1^2\ln r_1\right) - \frac{H_3}{2(1-n)}\left(r_2^2 - r_1^2\right) + H_4\frac{\left(r_2^2 - r_1^2\right)}{2}\right), \\
H_8 &= -\frac{n}{(1-n)^3}\left(\frac{r_2^5 - r_1^5}{30} - 2H_3^2\left(r_2 - r_1\right) + \frac{2H_3}{3}\left(r_2^3 - r_1^3\right)\right)\left(\frac{dP_0}{dz}\right)^2 \\
&\quad + \frac{H_5}{(1-n)}\left(r_2^2\ln r_2 - r_1^2\ln r_1 - \frac{\left(r_2^2 - r_1^2\right)}{2}\right).
\end{aligned}$$

The pressure rise ΔP and friction forces F on inner and outer tubes $F^{(0)}$, $F^{(i)}$, are given by

$$\Delta P = \int_0^1 \frac{dP}{dz} dz, \tag{6.31}$$

$$F^{(0)} = \int_0^1 r_1^2\left(-\frac{dP}{dz}\right) dz, \tag{6.32}$$

$$F^{(i)} = \int_0^1 r_2^2\left(-\frac{dP}{dz}\right) dz, \tag{6.33}$$

where $\frac{dP}{dz}$ is defined in Eqs. (6.30).

6.4.2 HAM Solution

In this section, we have found the HAM solution of Eqs. (6.13) to (6.15). For that we choose

$$w_0 = -1 + \left(\frac{r^2}{4(1-n)} + \frac{H_3}{(1-n)} \ln r + H_4 \right) \frac{\partial P}{\partial z}, \tag{6.34}$$

as the initial guess. Further, the auxiliary linear operator for the problem is taken as

$$\mathcal{L}_{wr} = \frac{1}{r} \frac{\partial}{\partial r} \left(r \frac{\partial}{\partial r} \right), \tag{6.35}$$

which satisfy

$$\mathcal{L}_{wr}(w_0) = 0. \tag{6.36}$$

We can define the following zeroth-order deformation problems

$$(1-q)\mathcal{L}_{wr}[\ \bar{w}\,(r,q) - \ w_0(r)] = q\hbar_w N_{wr}[\bar{w}\,(r,q)], \tag{6.37}$$

$$\begin{aligned} \bar{w}\,(r,q) &= -1, \ at\ r = r_1, \\ \bar{w}\,(r,q) &= -1, \ at\ r = r_2. \end{aligned} \tag{6.38}$$

In Eqs. (6.37) and (6.38), $\hbar_w$ denote the non-zero auxiliary parameter, $q\epsilon[0,1]$ is the embedding parameter and

$$N_{wr}[\bar{w}(r,q)] = (1-n)\frac{\partial^2 w}{\partial r^2} + \frac{1}{r}(1-n)\frac{\partial w}{\partial r} + \frac{nWe}{r}\left(\frac{\partial w}{\partial r}\right)^2 + 2nWe\frac{\partial^2 w}{\partial r^2}\frac{\partial w}{\partial r} - \frac{dP}{dz}. \tag{6.39}$$

Obviously

$$\hat{w}\,(r,0) = w_0, \quad \hat{w}\,(r,1) = w\,(r)\,, \tag{6.40}$$

when q varies from 0 to 1, then $\hat{w}\,(r,q)$ varies from initial guess to the solution $w\,(r)$. Expanding $\hat{w}\,(r,q)$ in Taylor's with respect to an embedding parameter q, we have

$$\hat{w}\,(r,q) = w_0\,(r) + \sum_{n=1}^{\infty} w_m(r) q^m, \tag{6.41}$$

$$w_m = \frac{1}{m!} \left. \frac{\partial^m \bar{w}\,(r,q)}{\partial q^m} \right|_{q=0}. \tag{6.42}$$

Differentiating the zeroth order deformation m-times with respect to q and then dividing by $m!$ and finally setting $q = 0$, we get the following mth order deformation problem

$$\mathcal{L}_w[w_m(r) - \chi_m w_{m-1}(r)] = \hbar_w R_{wr}(r), \tag{6.43}$$

where

$$\begin{aligned} R_{wr} &= (1-n)w''_{m-1} + \frac{1}{r}(1-n)w'_{m-1} + \frac{nWe}{r}\sum_{i=0}^{m-1} w'_{m-1-k}w'_k + 2nWe\sum_{k=0}^{m-1} w'_{m-1-k}w''_k \\ &\quad -\frac{dP}{dz}\,(1-\chi_m)\,, \end{aligned} \tag{6.44}$$

$$\chi_m = \begin{cases} 0, & m \le 1, \\ 1, & m > 1. \end{cases} \tag{6.45}$$

The solution of the above equation with the help of Mathematica can be calculated and presented as

$$\begin{aligned} w_m(r) &= \lim_{M->\infty}\left[\sum_{m=0}^{M} a^0_{m,0} + \sum_{n=1}^{2M+1}\left(\sum_{m=n-1}^{2M}\sum_{k=1}^{2m+1-n} a^k_{m,n} r^n \ln r\right)\right] \\ &\quad + \lim_{M->\infty}\left[\sum_{n=1}^{2M+1}\left(\sum_{m=n-1}^{2M}\sum_{k=0}^{2m+1-n} a^k_{m,n} r^{n+2}\right)\right]. \end{aligned} \tag{6.46}$$

6.5 Numerical Solution

The present problem consisting of Eqs (6.13) to (6.14) is also solved numerically by employing shooting method. The numerical results are also compared with the perturbation and HAM results and obtained a very good agreement between the three results.

r	Numerical sol	Perturbation sol	Error	HAM sol	Error
0.1	-1.00000	-1.00000	0.00000	-1.00000	0.00000
0.2	-1.02670	-1.02727	0.00005	-1.02727	0.00005
0.3	-1.04117	-1.04073	0.00004	-1.04074	0.00003
0.4	-1.04771	-1.04765	0.00005	-1.04765	0.00005
0.5	-1.05026	-1.05028	0.00001	-1.05028	0.00001
0.6	-1.05026	-1.04964	0.00004	-1.04963	0.00003
0.7	-1.04613	-1.04626	0.00001	-1.04626	0.00001
0.8	-1.04050	-1.04048	0.00001	-1.04047	0.00001
0.9	-1.03280	-1.03249	0.00004	-1.03249	0.00004
1.0	-1.02198	-1.02244	0.00004	-1.02244	0.00004
1.1	-1.01030	-1.01044	0.00001	-1.01043	0.00001
1.2	-1.00000	-1.00000	0.00000	-1.00000	0.00000

Table.6. Comparison of velocity field for $\varepsilon = 0.1$, $n = 0.02$, $We = 0.1$, $z = 0.1$, $\phi = 0.3$.

6.6 Results and Discussion

The analytical solution of the hyperbolic tangent model is discussed. The expression for pressure rise ΔP is calculated numerically using mathematics software. The effects of various parameters on the pressure rise ΔP are shown in Figs.6.1 to 6.12 for various values of Weissenberg number We, amplitude ratio ϕ, tangent hyperbolic power law index n and radius ratio ϕ. It is observed from Figs.6.1 to 6.4 that pressure rise increases for small values of Q $(-1 \leq Q \leq 0)$ with the increase in We, ε, n, and for ϕ pressure rise increases for small values of Q $(-1 \leq Q \leq 0.5)$ with increase in ϕ for large Q $(0.1 \leq Q \leq 1)$, the pressure rise decreases. We also observe that for different values of We, ε, n, and ϕ there is a linear relation between ΔP and $Q, i.e$, the pressure rise increases for small Q and decreases for large Q. The effects of frictional forces for inner and outer tube are illustrated in Figs. 6.5 to 6.12. It is observed that frictional forces have opposite behavior as compared to the pressure rise.

Figs. 6.13 to 6.16 show the pressure gradient for different values of ϕ, We, ε and Q. It is

observed that with increase in ϕ and ε pressure gradient increases while decreases with increase in We and Q.

6.7 Trapping

Another interesting phenomenon in peristaltic motion is trapping. It is basically the formation of an internally circulating bolus of fluid by closed streamlines. This trapped bolus pushed a head along with the peristaltic wave. Figs. (6.17) to (6.20) shows the trapping phenomenon for Q, n, ϕ and We. Figs. 6.17 illustrates the streamline graphs for different values of time mean flow rate Q. It is observed that when we increase Q the size of trapped bolus increases. Fig. 6.18 shows the streamlines for different values of (power law index) n. It is analyzed that with the increase in n size and number of trapping bolus decreases. Fig. 6.19 illustrate the streamline graphs for different values of ϕ. It is observed that with the increase in ϕ trapped bolus increases. The streamlines for different values We are shown in Fig. 6.20. It is evident from the figure that the size of the trapped bolus increases by increasing We.

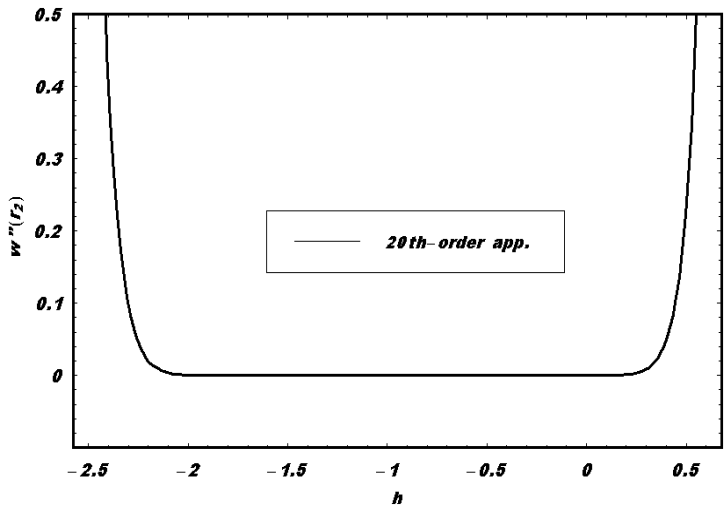

Fig. 6.a $\hbar$-curves are drawn at 20^{th}order of approximation for $\varepsilon = 0.1$, $n = 0.02$, $We = 0.1$, $z = 0.1$, $\phi = 0.3$.

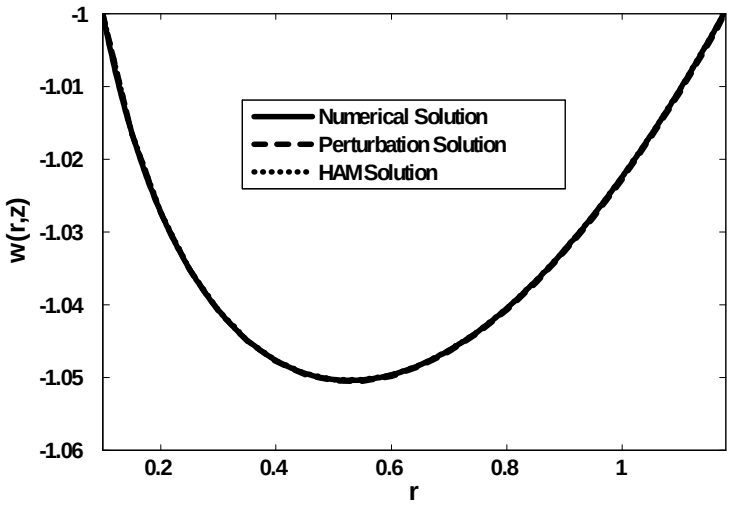

Fig.6.b. Comparison of velocity field for $\varepsilon = 0.1$, $n = 0.02$, $We = 0.1$, $z = 0.1$, $\phi = 0.3$.

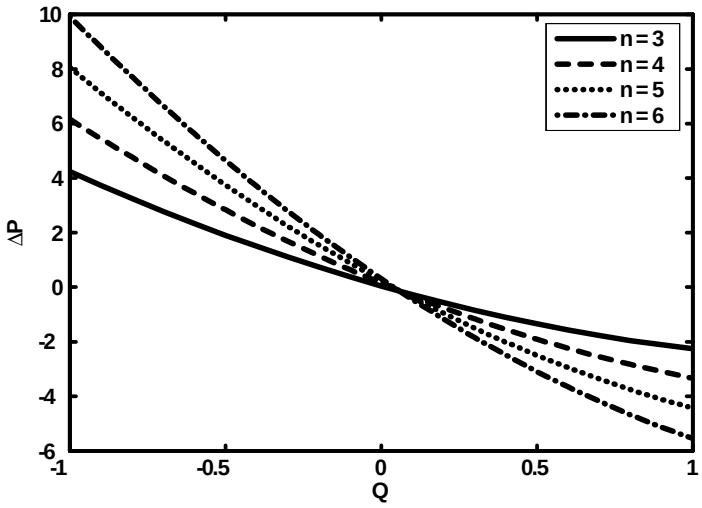

Fig.6.1. Pressure rise versus flow rate for $\varepsilon = 0.4$, $We = 0.01$, $\phi = 0.2$.

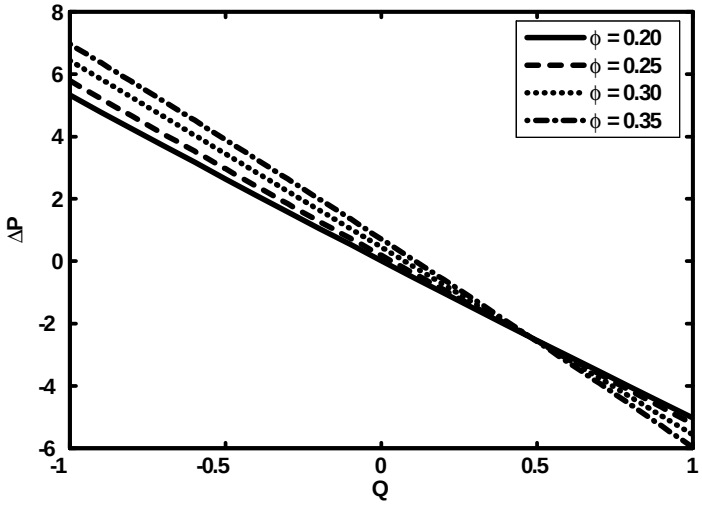

Fig.6.2. Pressure rise versus flow rate for $\varepsilon = 0.5$, $We = 0.001$, $n = 4$.

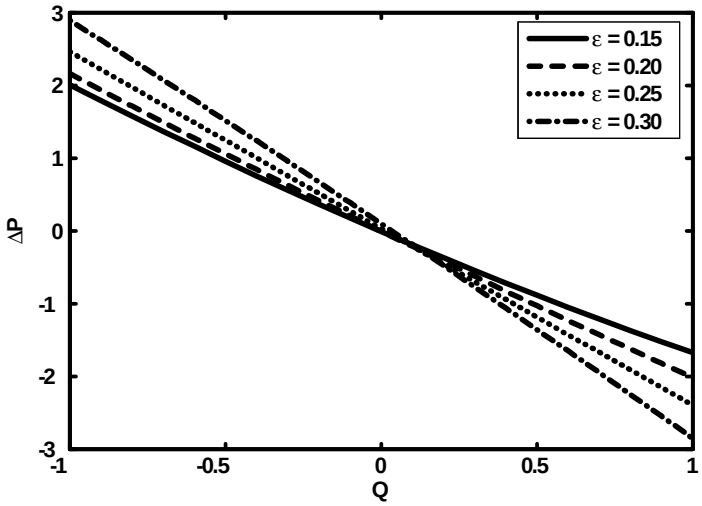

Fig.6.3. Pressure rise versus flow rate for $n = 4$, $We = 0.001$, $\phi = 0.5$.

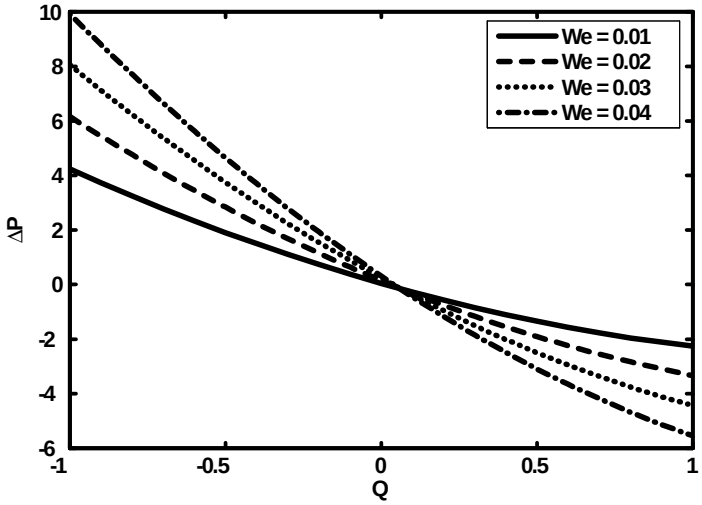

Fig.6.4. Pressure rise versus flow rate for $\varepsilon = 0.4$, $n = 2$, $\phi = 0.2$.

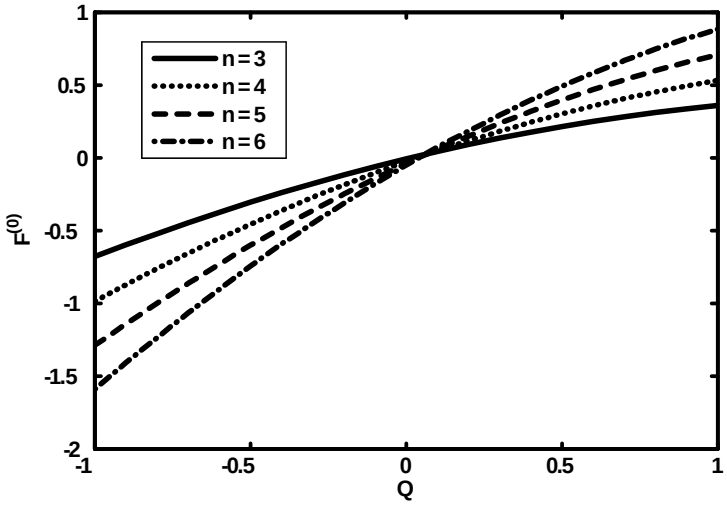

Fig.6.5. Frictional force(on inner tube) versus flow rate for $\varepsilon = 0.4$, $We = 0.01$, $\phi = 0.2$.

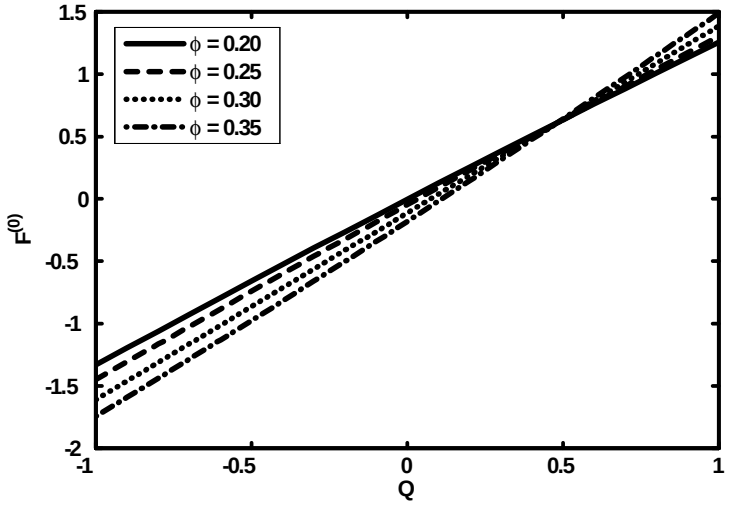

Fig.6.6. Frictional force (on inner tube) versus flow rate for $\varepsilon = 0.5$, $We = 0.001$, $n = 4$.

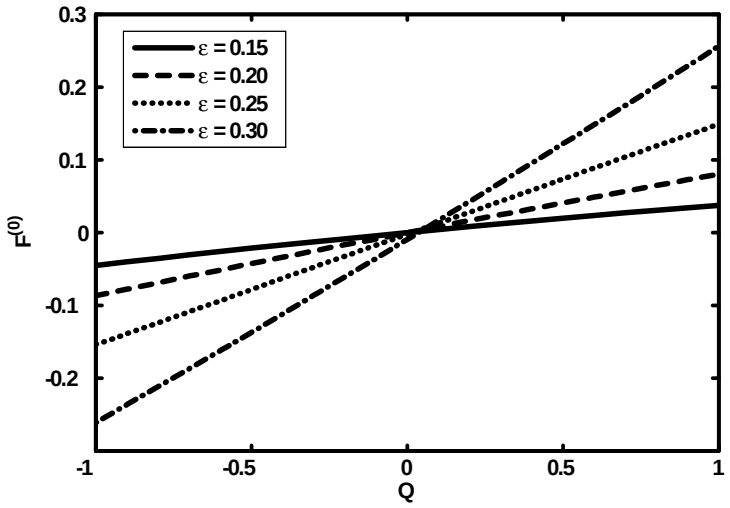

Fig.6.7. Frictional force(on inner tube) versus flow rate for $n = 4$, $We = 0.001$, $\phi = 0.5$.

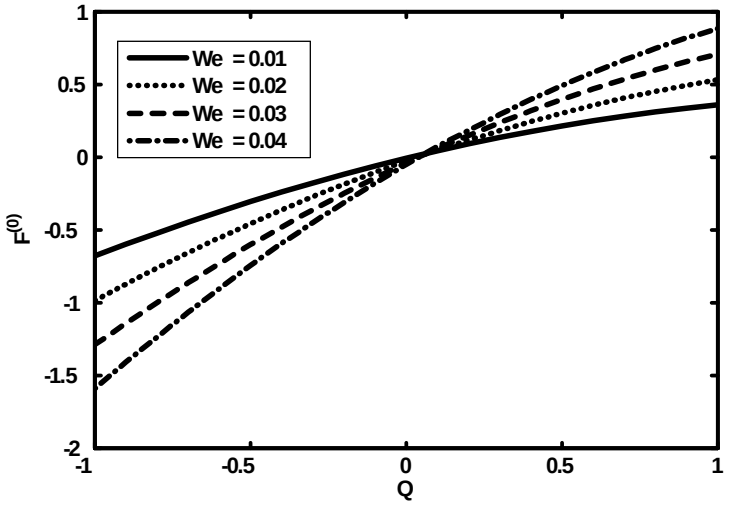

Fig.6.8. Frictional force(on inner tube) versus flow rate for $\varepsilon = 0.4$, $n = 2$, $\phi = 0.2$.

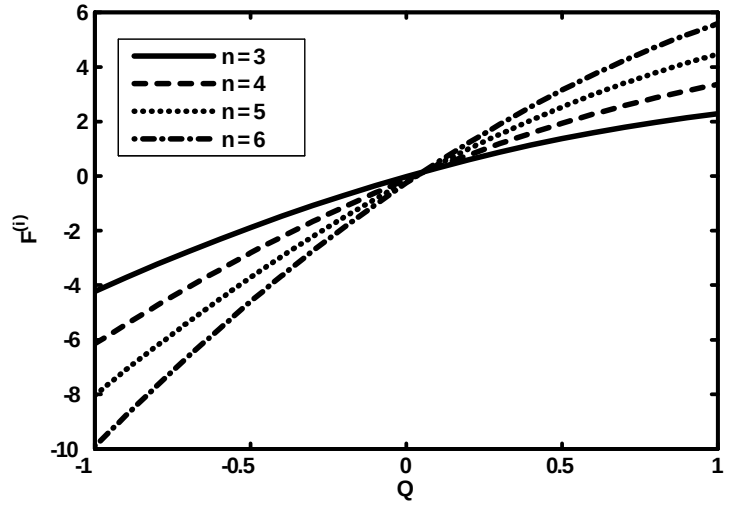

Fig.6.9. Frictional force(on outer tube) versus flow rate for $\varepsilon = 0.4$, $We = 0.01$, $\phi = 0.2$.

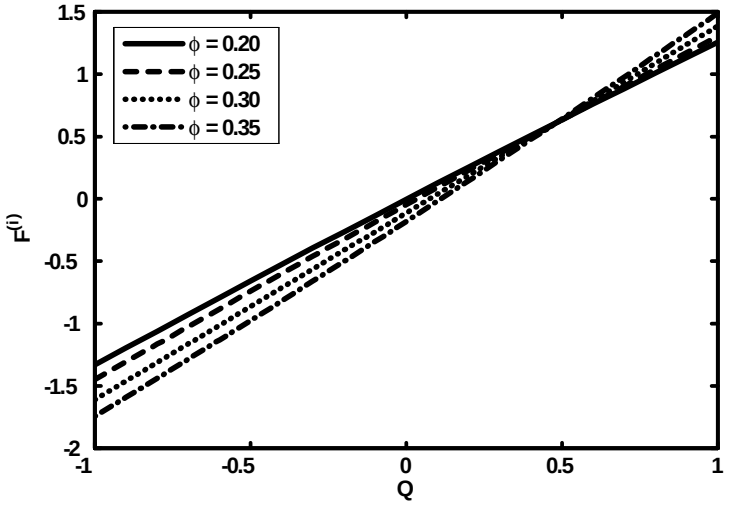

Fig.6.10. Frictional force (on outer tube) versus flow rate for $\varepsilon = 0.5$, $We = 0.001$, $n = 4$.

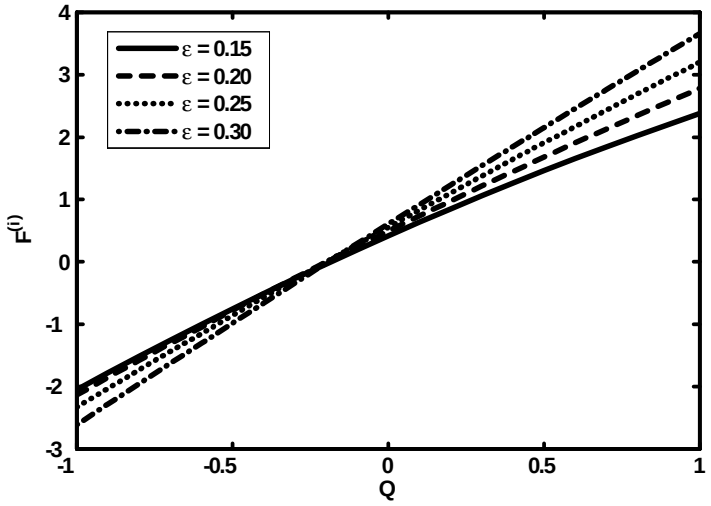

Fig.6.11. Frictional force(on outer tube) versus flow rate for $n = 4$, $We = 0.001$, $\phi = 0.5$.

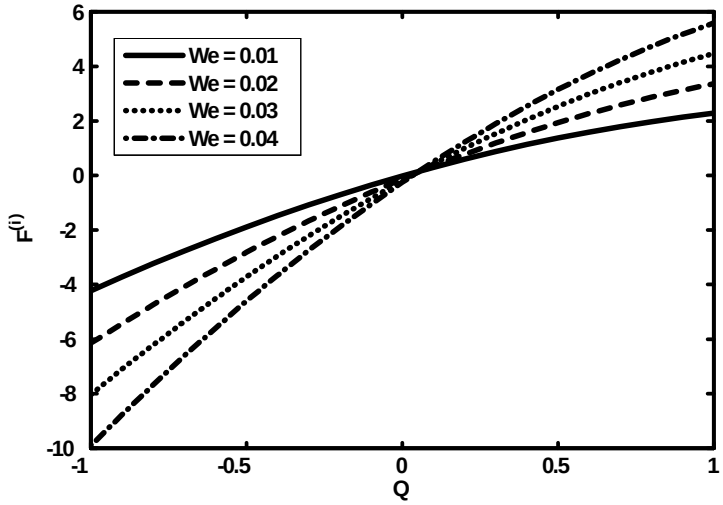

Fig.6.12. Frictional force(on outer tube) versus flow rate for $\varepsilon = 0.4$, $n = 2$, $\phi = 0.2$.

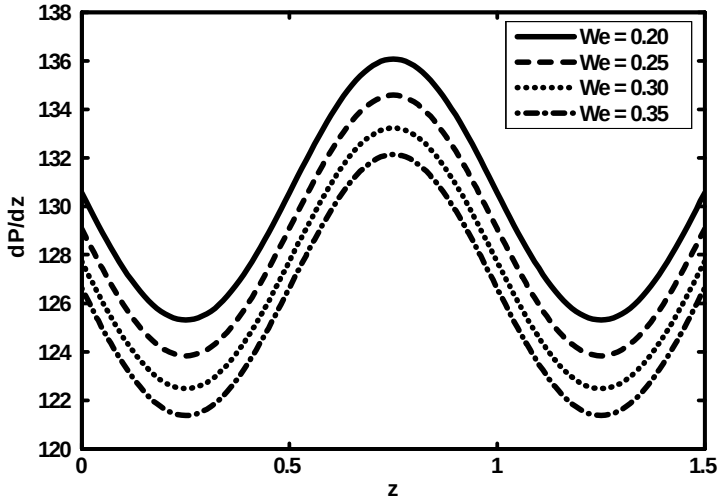

Fig.6.13. Pressure gradient versus z for $\varepsilon = 0.2$, $Q = -0.5$, $\phi = 0.1$, $n = 0.01$.

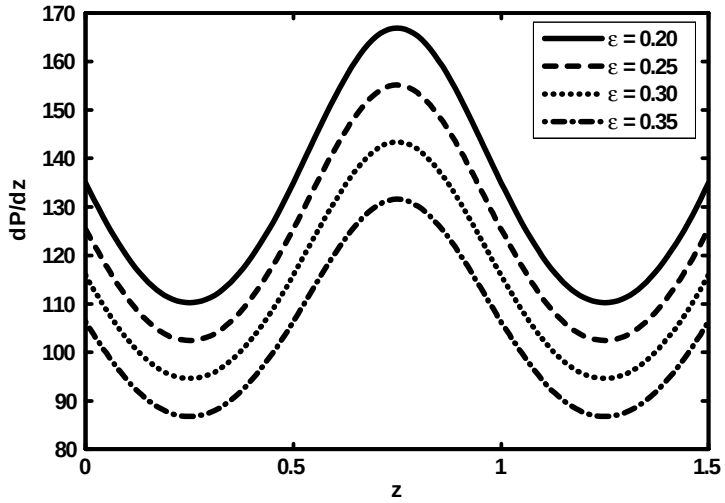

Fig.6.14. Pressure gradient versus z for $We = 0.1$, $Q = -0.5$, $\phi = 0.1$, $n = 0.02$.

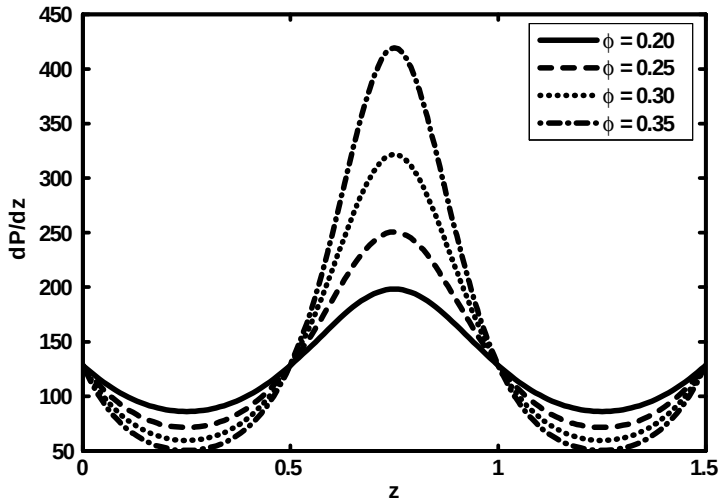

Fig.6.15. Pressure gradient versus z for $We = 0.1$, $Q = -0.5$, $\varepsilon = 0.01, n = 0.02$.

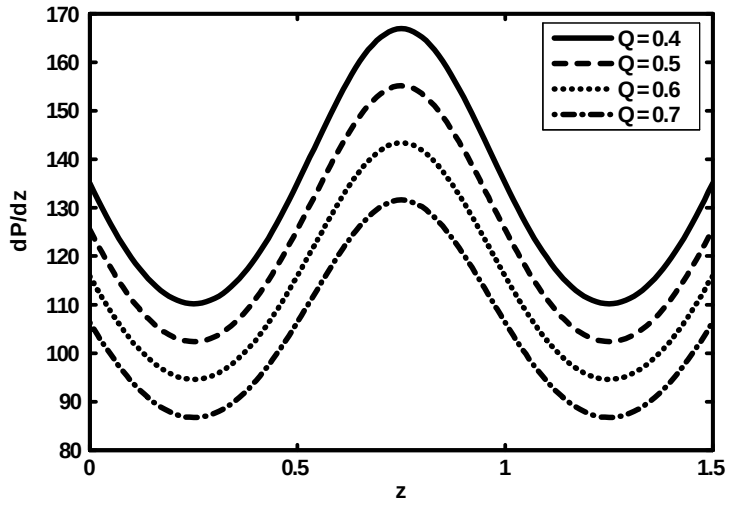

Fig.6.16. Pressure gradient versus z for $We = 0.1$, $\phi = 0.25$, $\varepsilon = 0.01$, $n = 0.02$.

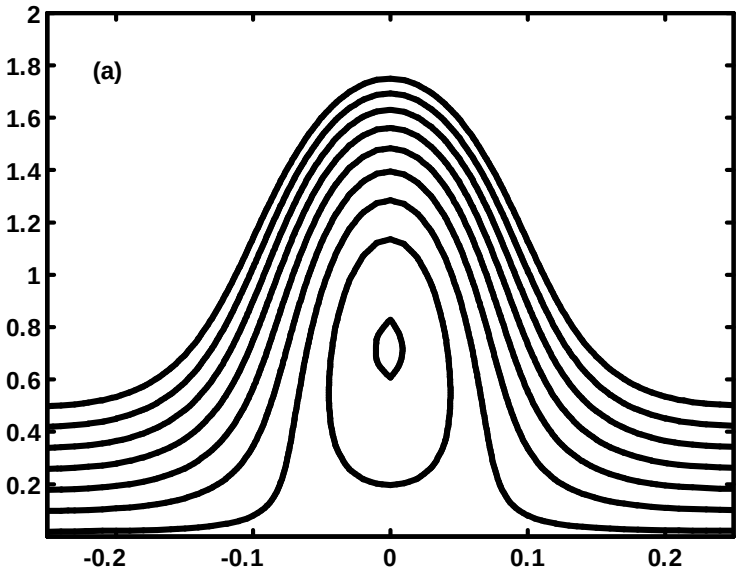
(a)
2
1.8
1.6
1.4
1.2
1
0.8
0.6
0.4
0.2
-0.2
-0.1
0
0.1
0.2

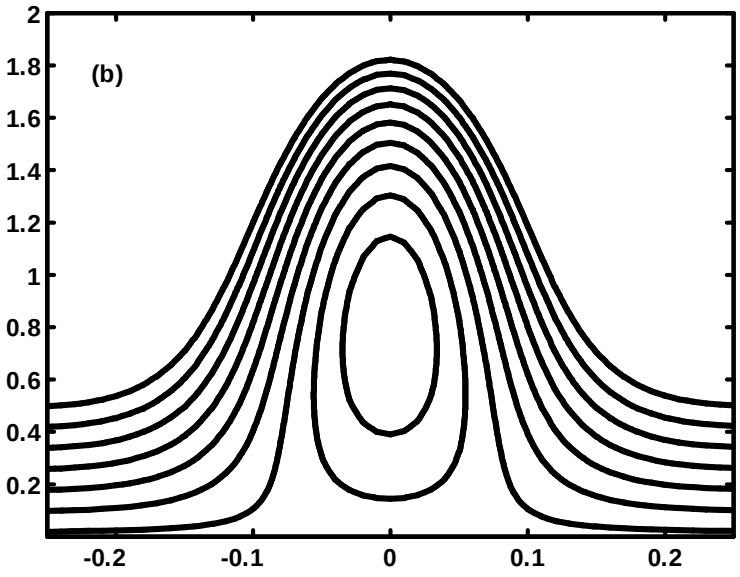
(b)
2
1.8
1.6
1.4
1.2
1
0.8
0.6
0.4
0.2
-0.2
-0.1
0
0.1
0.2

Fig. 6.17. Streamlines for different values of $\Theta = 0.1,\ 0.2$,(panels (a) to (b)) The other parameters are $We = 0.1$, $\varepsilon = 0.5$, $\phi = 0.1$, $n = 0.02$.

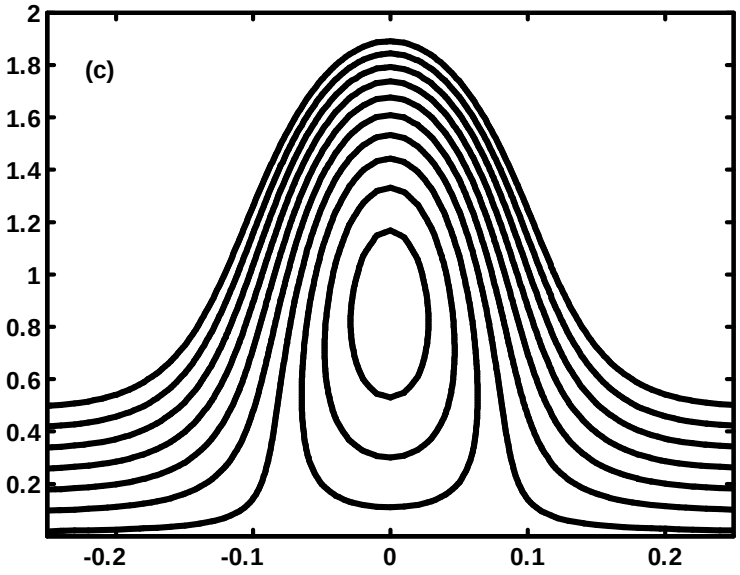

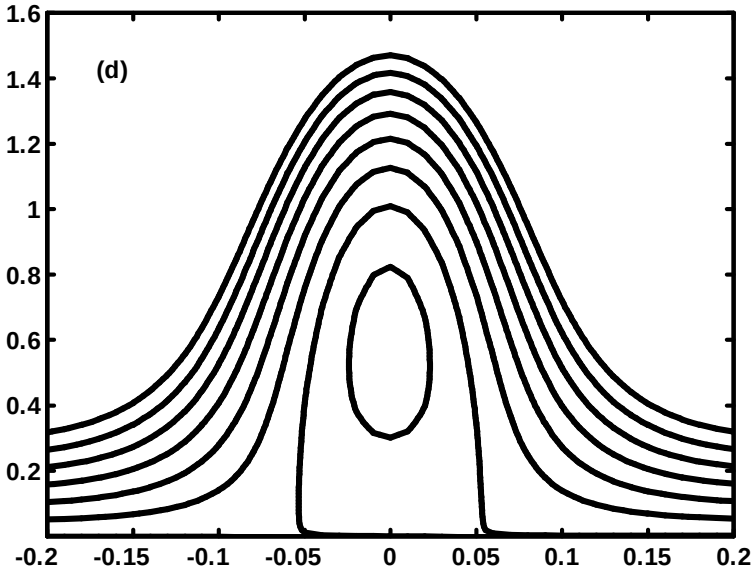

Fig. 6.18. Streamlines for different values of $n = 0.1$, 0.2,(panels (c) to (d)) The other parameters are $We = 0.1$, $\varepsilon = 0.5$, $\phi = 0.1$, $Q = 0.5$.

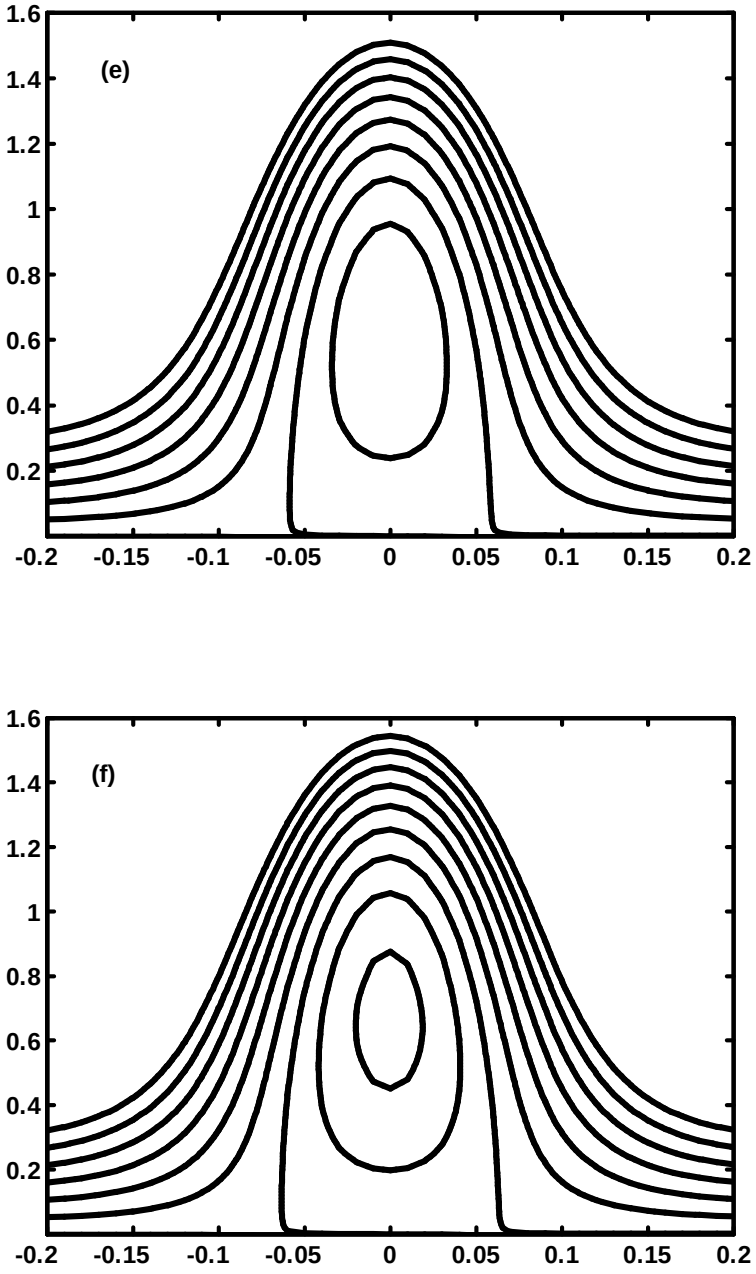

Fig. 6.19. Streamlines for different values of $\phi = 0.1$, 0.2,(panels (e) to (f)) The other parameters are $We = 0.1$, $\varepsilon = 0.5$, $n = 0.1$, $Q = 0.5$.

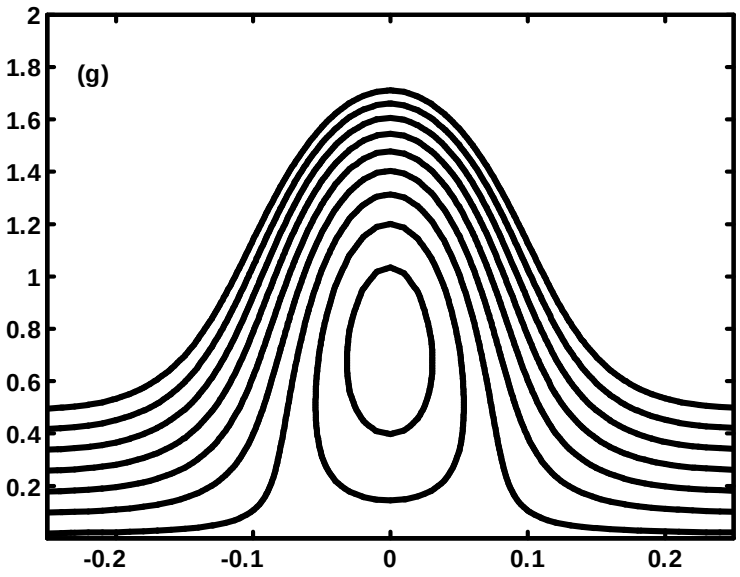

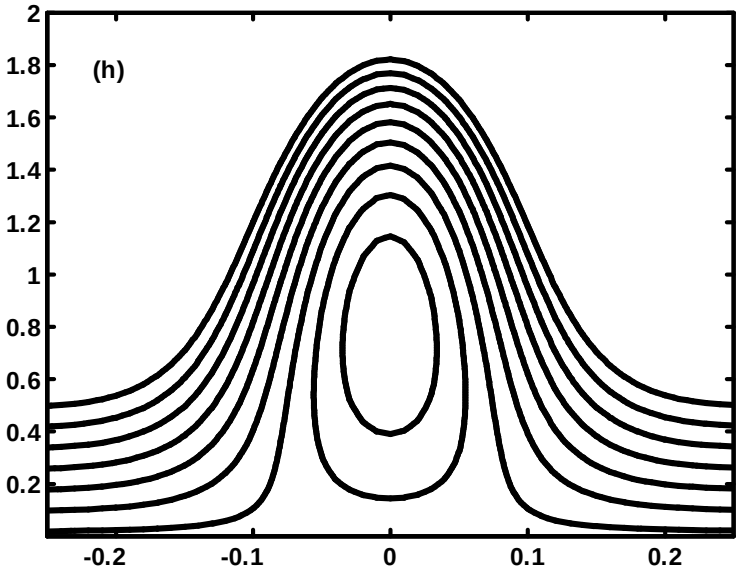

Fig. 6.20. Streamlines for different values of $We = 0.1$, 0.2,(panels (g) to (h)) The other parameters are $\phi = 0.1$, $\varepsilon = 0.5$, $n = 0.1$, $Q = 0.5$.

6.8 Conclusion

This chapter presents the numerical and analytical analysis of peristaltic transport of a tangent hyperbolic fluid in an endoscope. The governing two dimensional equations are modelled in cylindrical geometry and simplified using long wave length and low Reynolds number approximation. In the fixed frame of reference, three types of solutions named (i) Perturbation solution (ii) HAM solution and (iii) Numerical solutions are presented. The results are discussed through graphs. The main points can be summarized as follows:

1. It is observed that the pressure rise ΔP and volume flow rate Q has inversely linear relation between each other.

2. The pressure rise increases with the increase in Weissenberg number We, tangent hyperbolic power law index n and radius ratio ε, and decreases with an increase in amplitude ratio ϕ.

3. It is observed that with increase in ϕ and ε pressure gradient increases while decreases with increase in We and Q.

4. It is seen that frictional forces have an opposite behavior as compared to the pressure rise.

5. It is evident that the size of the trapped bolus increases by increasing We, ϕ, and Q while size of the trapped bolus decreases by increasing n.

Chapter 7

Combined effects of heat and chemical reactions on the peristaltic flow of Carreau fluid model in a diverging tube

7.1 Introduction

In the present chapter we have studied the peristaltic flow of a Carreau fluid in a non-uniform tube under the consideration of long wavelength in the presence of heat and mass transfer. The flow is investigated in a wave frame of reference moving with velocity of the wave c. Two types of analytical solutions have been evaluated (i) Perturbation method (ii) Homotopy analysis method for velocity, temperature and concentration field. Numerical integration have been used to obtain the graphical results for pressure rise and frictional forces. The effects of various emerging parameters are investigated for five different peristaltic waves.

7.2 Mathematical Model

For an incompressible fluid the balance of mass and momentum are defined in Eqs. (1.1) and (1.2). The constitutive equation for Carreau fluid is given by [35]

$$\frac{(\mu-\mu_\infty)}{(\mu_0-\mu_\infty)}=\left[1+\left(\Gamma\overline{\dot{\gamma}}\right)^2\right]^{\frac{(n-1)}{2}}, \tag{7.1}$$

$$\boldsymbol{\tau}=-\mu_0\left[1+\frac{(n-1)}{2}\left(\Gamma\overline{\dot{\gamma}}\right)^2\right]\overline{\dot{\gamma}}_{ij}, \tag{7.2}$$

in which $\boldsymbol{\tau}$ is the extra stress tensor, Γ is the time constant, n is the power law index and $\dot{\gamma}$ is defined as

$$\overline{\dot{\gamma}}=\sqrt{\frac{1}{2}\sum_i\sum_j\overline{\dot{\gamma}}_{ij}\overline{\dot{\gamma}}_{ji}}=\sqrt{\frac{1}{2}\Pi}. \tag{7.3}$$

Here Π is the second invariant strain tensor.

7.3 Mathematical Formulation

We have considered peristaltic flow of an incompressible Carreau fluid in a non uniform tube. The flow is generated by sinusoidal wave trains propagating with constant speed c along the walls of the tube. Heat and mass transfer phenomena has been taken into account. The walls of the tube is maintaining at temperature $\bar{T}_0$ and concentration $\bar{C}_0$ while at the centre we have used symmetry condition on both temperature and concentration. The geometry of the wall surface is defined in Eq. (5.8) . The governing equations in the fixed frame for an incompressible flow are given as

$$\frac{\partial\bar{U}}{\partial\bar{R}}+\frac{\bar{U}}{\bar{R}}+\frac{\partial\bar{W}}{\partial\bar{Z}}=0, \tag{7.4}$$

$$\rho\left(\frac{\partial}{\partial\bar{t}}+\bar{U}\frac{\partial}{\partial\bar{R}}+\bar{W}\frac{\partial}{\partial\bar{Z}}\right)\bar{U}=-\frac{\partial\bar{P}}{\partial\bar{R}}-\frac{1}{\bar{R}}\frac{\partial}{\partial\bar{R}}\left(\bar{R}\boldsymbol{\tau}_{\bar{R}\bar{R}}\right)-\frac{\partial}{\partial\bar{Z}}\left(\boldsymbol{\tau}_{\bar{R}\bar{Z}}\right)-\frac{\boldsymbol{\tau}_{\bar{\theta}\bar{\theta}}}{\bar{R}}, \tag{7.5}$$

$$\rho\left(\frac{\partial}{\partial\bar{t}}+\bar{U}\frac{\partial}{\partial\bar{R}}+\bar{W}\frac{\partial}{\partial\bar{Z}}\right)\bar{W}=-\frac{\partial\bar{P}}{\partial\bar{Z}}-\frac{1}{\bar{R}}\frac{\partial}{\partial\bar{R}}\left(\bar{R}\boldsymbol{\tau}_{\bar{R}\bar{Z}}\right)-\frac{\partial}{\partial\bar{Z}}\left(\boldsymbol{\tau}_{\bar{Z}\bar{Z}}\right), \tag{7.6}$$

$$\rho c_p\left(\frac{\partial}{\partial \bar{t}}+\bar{U}\frac{\partial}{\partial \bar{R}}+\bar{W}\frac{\partial}{\partial \bar{Z}}\right)\bar{T} = \boldsymbol{\tau}_{\bar{R}\bar{R}}\frac{\partial \bar{U}}{\partial \bar{R}}+\boldsymbol{\tau}_{\bar{R}\bar{Z}}\frac{\partial \bar{W}}{\partial \bar{R}}+\boldsymbol{\tau}_{\bar{Z}\bar{R}}\frac{\partial \bar{U}}{\partial \bar{Z}}+\boldsymbol{\tau}_{\bar{Z}\bar{Z}}\frac{\partial \bar{W}}{\partial \bar{Z}} + k\left(\frac{\partial^2 \bar{T}}{\partial \bar{R}^2}+\frac{1}{\bar{R}}\frac{\partial \bar{T}}{\partial \bar{R}}+\frac{\partial^2 \bar{T}}{\partial \bar{Z}^2}\right), \tag{7.7}$$

$$\left(\frac{\partial}{\partial \bar{t}}+\bar{U}\frac{\partial}{\partial \bar{R}}+\bar{W}\frac{\partial}{\partial \bar{Z}}\right)\bar{C} = D\left(\frac{\partial^2 \bar{C}}{\partial \bar{R}^2}+\frac{1}{\bar{R}}\frac{\partial \bar{C}}{\partial \bar{R}}+\frac{\partial^2 \bar{C}}{\partial \bar{Z}^2}\right) + \frac{DK_T}{T_m}\left(\frac{\partial^2 \bar{T}}{\partial \bar{R}^2}+\frac{1}{\bar{R}}\frac{\partial \bar{T}}{\partial \bar{R}}+\frac{\partial^2 \bar{T}}{\partial \bar{Z}^2}\right). \tag{7.8}$$

The corresponding boundary conditions in the wave frame are

$$\frac{\partial \bar{w}}{\partial \bar{r}}=0,\ \frac{\partial \bar{T}}{\partial \bar{r}}=0,\ \frac{\partial \bar{C}}{\partial \bar{r}}=0,\ \text{at } \bar{r}=0, \tag{7.9}$$

$$\bar{w}=0,\ \bar{T}=\bar{T}_0,\ \bar{C}=\bar{C}_0,\ at\ \bar{r}=\bar{h}=a\left(\bar{z}\right)+b\sin\frac{2\pi}{\lambda}\left(\bar{z}\right). \tag{7.10}$$

We introduce the non-dimensional variables

$$\begin{aligned}
R &= \frac{\bar{R}}{a},\ r=\frac{\bar{r}}{a},\quad Z=\frac{\bar{Z}}{\lambda},\quad z=\frac{\bar{z}}{\lambda},\ W=\frac{\bar{W}}{c},\ \ w=\frac{\bar{w}}{c},\ \dot{\gamma}=\frac{a}{c}\bar{\dot{\gamma}},\\
U &= \frac{\lambda \bar{U}}{ac},\ \ u=\frac{\lambda \bar{u}}{ac},\ \ P=\frac{a^2\bar{P}}{c\lambda\mu},\ \theta=\frac{\left(\bar{T}-\bar{T}_0\right)}{\bar{T}_0}, t=\frac{c\bar{t}}{\lambda},\quad \delta=\frac{a}{\lambda},\\
\mathrm{Re} &= \frac{\rho c a_2}{\mu},\ \tau_{11}=\frac{\lambda\boldsymbol{\tau}_{11}}{c\mu},\ \tau_{22}=\frac{\lambda\boldsymbol{\tau}_{22}}{c\mu},\ \tau_{33}=\frac{\lambda\boldsymbol{\tau}_{33}}{c\mu},\ S_r=\frac{\rho D K_T \bar{T}_0}{\mu T_m \bar{C}_0},\\
h &= \frac{\bar{h}}{a}=1+\frac{\lambda k z}{a_0}+\phi\sin 2\pi z,\ \boldsymbol{\tau}_{13}=\boldsymbol{\tau}_{31}=\frac{a\bar{\boldsymbol{\tau}}_{13}}{c\mu},\ We=\frac{c\Gamma}{a},\ S_c=\frac{\mu}{D\rho},\\
\sigma &= \frac{\left(\bar{C}-\bar{C}_0\right)}{\bar{C}_0},
\end{aligned} \tag{7.11}$$

in which R and Z are the dimensionless form of radial and transverse components respectively, S_r is the Soret number, S_c Schmidt number and We is the Weissenberg number.

With the help of Eqs. (1.11, 1.12) and (7.11), Eqs. (7.4) to (7.8) along with boundary conditions (7.9, 7.10) under the assumptions of long wavelength and low Reynolds number approximation take the form

$$\frac{\partial u}{\partial r}+\frac{u}{r}+\frac{\partial w}{\partial z}=0, \tag{7.12}$$

$$\frac{\partial P}{\partial r}=0, \tag{7.13}$$

$$\frac{\partial P}{\partial z} = \frac{1}{r}\frac{\partial}{\partial r}\left(r\left(\left(\frac{\partial w}{\partial r}\right) + \frac{(n-1)}{2}We^2\left(\frac{\partial w}{\partial r}\right)^3\right)\right), \tag{7.14}$$

$$\frac{\partial^2\theta}{\partial r^2} + \frac{1}{r}\frac{\partial\theta}{\partial r} = -B_r\left(\left(\frac{\partial w}{\partial r}\right)^2 + \frac{(n-1)}{2}We^2\left(\frac{\partial w}{\partial r}\right)^4\right), \tag{7.15}$$

$$0 = \frac{1}{S_c}\left(\frac{1}{r}\frac{\partial}{\partial r}\left(r\frac{\partial\sigma}{\partial r}\right)\right) + S_r\left(\frac{1}{r}\frac{\partial}{\partial r}\left(r\frac{\partial\theta}{\partial r}\right)\right). \tag{7.16}$$

In the above equations δ, Re represent the wave and Reynolds numbers, respectively. The corresponding boundary conditions are

$$\frac{\partial w}{\partial r} = 0, \quad \frac{\partial\theta}{\partial r} = 0, \quad \frac{\partial\sigma}{\partial r} = 0, \text{ at} \quad r = 0, \tag{7.17a}$$

$$w = 0, \quad \theta = 0, \quad \sigma = 0, \quad \text{at} \quad r = h = 1 + \frac{\lambda k z}{a_0} + \phi\sin 2\pi z. \tag{7.17b}$$

7.4 Solution of the Problem

7.4.1 Perturbation Solution

To get the solution of Eqs.(7.13) to (7.16), we employ the regular perturbation method to find the solution. For perturbation solution, we expand w, F_1, θ, σ and P as

$$w = w_0 + We^2 w_1 + O(We^4), \tag{7.18a}$$

$$F_1 = F_{10} + We^2 F_{11} + O(We^4), \tag{7.18b}$$

$$\theta = \theta_0 + We^2\theta_1 + O(We^4), \tag{7.18c}$$

$$\sigma = \sigma_0 + We^2\sigma_1 + O(We^4), \tag{7.18d}$$

$$P = P_0 + We^2 P_1 + O(We^4). \tag{7.18e}$$

The perturbation results for small parameter We^2, satisfying the conditions (7.17a) and (7.17b), for velocity temperature, concentration fields and pressure gradient can be written as

$$w(r,z) = \left(\frac{r^2-h^2}{4}\right)\frac{dP}{dz} - W_e^2\left(\frac{n-1}{64}\right)\left(-\frac{16F_1}{h^4}\right)^3\left(r^4-h^4\right), \tag{7.19}$$

$$\theta(r,z) = -B_r\left(\left(\frac{r^4-h^4}{64}\right)\left(\frac{dP}{dz}\right)^2 + W_e^2\left(\frac{1024(n-1)^2F_1^3\left(r^8-h^8\right)}{h^{24}} + \frac{(n-1)}{576}\left(\frac{dP}{dz}\right)^4\left(r^6-h^6\right)\right)\right), \tag{7.20}$$

$$\sigma(r,z) = S_rS_cB_r\left(\left(\frac{r^4-h^4}{64}\right)\left(\frac{dP}{dz}\right)^2 + W_e^2\left(\frac{1024(n-1)^2F_1^3\left(r^8-h^8\right)}{h^{24}} + \frac{(n-1)}{576}\left(\frac{dP}{dz}\right)^4\left(r^6-h^6\right)\right)\right), \tag{7.21}$$

$$\frac{dP}{dz} = -\frac{16F_1}{h^4} + W_e^2\left(-\frac{1024(n-1)F_1^3}{3h^{10}}\right). \tag{7.22}$$

The pressure rise ΔP and friction forces F are defined as follow

$$\Delta P = \int_0^1 \frac{dP}{dz}dz, \tag{7.23}$$

$$F^{(0)} = \int_0^1 r_1^2\left(-\frac{dP}{dz}\right)dz, \tag{7.24}$$

$$F^{(i)} = \int_0^1 r_2^2\left(-\frac{dP}{dz}\right)dz, \tag{7.25}$$

where $\frac{dP}{dz}$ is defined in Eq. (7.22).

For analysis, we have considered five waveforms namely sinusoidal, multi-sinusoidal, triangular, square and trapezoidal. The non-dimensional expressions for these wave forms are defined in chapter 1.

7.4.2 HAM Solution

HAM is an analytical technique to approximate the solution of highly non-linear equation. The solution by HAM is started by some initial guess. For that we choose

$$w_0 = \frac{dP}{dz}\left(\frac{r^2-h^2}{4}\right), \tag{7.26}$$

$$\theta_0 = -B_r\left(\frac{dP}{dz}\right)^2\left(\frac{r^2-h^2}{8}\right), \tag{7.27}$$

$$\sigma_0 = S_c S_r B_r\left(\frac{dP}{dz}\right)^2\left(\frac{r^2-h^2}{8}\right), \tag{7.28}$$

as the initial guesses of Eqs. (7.26) to (7.28). Further, the auxiliary linear operator for the problem are taken as

$$\mathcal{L}_{wr} = \frac{1}{r}\frac{\partial}{\partial r}\left(r\frac{\partial}{\partial r}\right), \tag{7.29}$$

$$\mathcal{L}_{\theta r} = \frac{1}{r}\frac{\partial}{\partial r}\left(r\frac{\partial}{\partial r}\right), \tag{7.30}$$

$$\mathcal{L}_{\sigma r} = \frac{1}{r}\frac{\partial}{\partial r}\left(r\frac{\partial}{\partial r}\right). \tag{7.31}$$

We can define the following zeroth-order deformation problems

$$(1-q)\mathcal{L}_{wr}[\ \bar{w}\,(r,q) - \ w_0(r)] = q\hbar_w N_{wr}[\bar{w}\,(r,q)], \tag{7.32}$$

$$(1-q)\mathcal{L}_{\theta r}[\ \bar{\theta}\,(r,q) - \ \theta_0(r)] = q\hbar_\theta N_{\theta r}[\bar{\theta}\,(r,q)], \tag{7.33}$$

$$(1-q)\mathcal{L}_{\sigma r}[\ \bar{\sigma}\,(r,q) - \ \sigma_0(r)] = q\hbar_\sigma N_{\sigma r}[\bar{\sigma}\,(r,q)], \tag{7.34}$$

$$\begin{aligned}
\frac{\partial \bar{w}\,(r,q)}{\partial r} &= 0,\ at\ r=0,\ \bar{w}\,(r,q)=0,\ at\ r=h=1+\frac{\lambda K z}{a_0}+\phi\sin 2\pi z, &(7.35)\\
\frac{\partial \bar{\theta}\,(r,q)}{\partial r} &= 0,\ at\ r=0,\ \bar{\theta}\,(r,q)=0,\ at\ r=h=1+\frac{\lambda K z}{a_0}+\phi\sin 2\pi z, &(7.36)\\
\frac{\partial \bar{\sigma}\,(r,q)}{\partial r} &= 0,\ at\ r=0,\ \bar{\sigma}\,(r,q)=0,\ at\ r=h=1+\frac{\lambda K z}{a_0}+\phi\sin 2\pi z. &(7.37)
\end{aligned}$$

In Eqs. (7.32) to (7.37), $\hbar_w$, $\hbar_\theta$ and $\hbar_\sigma$ denote the non-zero auxiliary parameter, $q\epsilon[0,1]$ is the embedding parameter and

$$N_{wr}[\bar{w}(r,q)] = \frac{1}{r}\frac{\partial w}{\partial r} + \frac{\partial^2 w}{\partial r^2} + \frac{W_e^2\,(n-1)}{2}\left(\frac{1}{r}\left(\frac{\partial w}{\partial r}\right)^3 + 3\left(\frac{\partial w}{\partial r}\right)^2\frac{\partial^2 w}{\partial r^2}\right) - \frac{dP}{dz}, \tag{7.38}$$

$$N_{\theta r}[\bar{\theta}(r,q)] = \frac{1}{r}\frac{\partial \theta}{\partial r} + \frac{\partial^2 \theta}{\partial r^2} + B_r\left(\left(\frac{\partial w}{\partial r}\right)^2 + \frac{W_e^2\,(n-1)}{2}\left(\frac{\partial w}{\partial r}\right)^4\right), \tag{7.39}$$

$$N_{\sigma r}[\bar{\sigma}(r,q)] = \frac{1}{r}\frac{\partial \sigma}{\partial r} + \frac{\partial^2 \sigma}{\partial r^2} + \frac{S_r S_c}{r}\frac{\partial \theta}{\partial r} + S_r S_c\frac{\partial^2 \theta}{\partial r^2}. \tag{7.40}$$

Obviously,

$$\frac{\partial \hat{w}\,(r,0)}{\partial r} = 0, \quad \hat{w}\,(r,1) = w\,(r)\,, \tag{7.41}$$

$$\frac{\partial \hat{\theta}\,(r,0)}{\partial r} = 0, \quad \hat{\theta}\,(r,1) = \theta\,(r)\,, \tag{7.42}$$

$$\frac{\partial \hat{\sigma}\,(r,0)}{\partial r} = 0, \quad \hat{\sigma}\,(r,1) = \sigma\,(r)\,, \tag{7.43}$$

when q varies from 0 to 1, then $\hat{w}\,(r,q)\,,\ \hat{\theta}\,(r,q)$ and $\hat{\sigma}\,(r,q)$ varies from initial guess to the solution $w\,(r)\,,\ \theta\,(r)$ and $\sigma\,(r)$ respectively. Expanding $\hat{w}\,(r,q)$, $\hat{\theta}\,(r,q)$ and $\hat{\sigma}\,(r,q)$ in Taylor's with respect to an embedding parameter q, we have

$$\hat{w}\,(r,q) = w_0\,(r) + \sum_{n=1}^{\infty} w_m(r) q^m, \tag{7.44}$$

$$\hat{\theta}\,(r,q) = \theta_0\,(r) + \sum_{n=1}^{\infty} \theta_m(r) q^m, \tag{7.45}$$

$$\hat{\sigma}\,(r,q) = \sigma_0\,(r) + \sum_{n=1}^{\infty} \sigma_m(r) q^m, \tag{7.46}$$

where

$$w_m = \frac{1}{m!}\left.\frac{\partial^m \bar{w}\,(r,q)}{\partial q^m}\right|_{q=0}, \tag{7.47}$$

$$\theta_m = \frac{1}{m!}\left.\frac{\partial^m \bar{\theta}\,(r,q)}{\partial q^m}\right|_{q=0}, \tag{7.48}$$

$$\sigma_m = \frac{1}{m!} \left. \frac{\partial^m \bar{\sigma}(r,q)}{\partial q^m} \right|_{q=0}. \tag{7.49}$$

Differentiating the zeroth order deformation m-times with respect to q and then dividing by $m!$ and finally setting $q = 0$, we get the following mth order deformation problem

$$\mathcal{L}_w[w_m(r) - \chi_m w_{m-1}(r)] = \hbar_w R_{wr}(r), \tag{7.50}$$

$$\mathcal{L}_\theta[\theta_m(r) - \chi_m \theta_{m-1}(r)] = \hbar_\theta R_{\theta r}(r), \tag{7.51}$$

$$\mathcal{L}_\sigma[\sigma_m(r) - \chi_m \sigma_{m-1}(r)] = \hbar_\sigma R_{\sigma r}(r), \tag{7.52}$$

where

$$\begin{aligned} R_{wr} &= w''_{m-1} + \frac{w'_{m-1}}{r} + \frac{W_e^2 (n-1)}{2} \left(\frac{1}{r} \sum_{k=0}^{m-1} w'_{m-1-k} \sum_{l=0}^{k} w'_{k-l} w_l{}' + 3 \sum_{k=0}^{m-1} w'_{m-1-k} \sum_{l=0}^{k} w'_{k-l} w_l{}'' \right) \\ &\quad - \frac{dP}{dz} (1 - \chi_m), \end{aligned} \tag{7.53}$$

$$R_{\theta r} = \theta''_{m-1} + \frac{1}{r} \theta'_{m-1} + B_r \left(\sum_{k=0}^{m-1} w'_{m-1-k} w_k{}' + \frac{(n-1)}{2} We^2 \sum_{k=0}^{m-1} w'_{m-1-k} \sum_{l=0}^{k} w'_{k-l} \sum_{j=0}^{l} w_{l-j}{}' w_j{}' \right), \tag{7.54}$$

$$R_{\sigma r} = \sigma''_{m-1} + \frac{1}{r} \sigma'_{m-1} + S_r S_c \theta''_{m-1} + \frac{S_r S_c}{r} \theta'_{m-1}, \tag{7.55}$$

$$\chi_m = \begin{cases} 0, & m \leq 1, \\ 1, & m > 1. \end{cases} \tag{7.56}$$

The solution of the above equations with the help of Mathematica can be calculated and presented as follow

$$w_m(r) = \lim_{M \to \infty} \left[\sum_{m=0}^{M} a_{m,0}^0 + \sum_{n=1}^{2M+1} \left(\sum_{m=n-1}^{2M} \sum_{k=0}^{2m+1-n} a_{m,n}^k r^{2n+2} \right) \right], \tag{7.57}$$

$$\theta_m(r) = \lim_{M \to \infty} \left[\sum_{m=0}^{M} b_{m,0}^0 + \sum_{n=1}^{2M+1} \left(\sum_{m=n-1}^{2M} \sum_{k=0}^{2m+1-n} b_{m,n}^k r^{2n+3} \right) \right], \tag{7.58}$$

$$\sigma_m(r) = \lim_{M \to \infty} \left[\sum_{m=0}^{M} c_{m,0}^0 + \sum_{n=1}^{2M+1} \left(\sum_{m=n-1}^{2M} \sum_{k=0}^{2m+1-n} c_{m,n}^k r^{2n+3} \right) \right], \tag{7.59}$$

where $a^0_{m,0}$, $a^k_{m,n}$, $b^0_{m,0}$, $b^k_{m,n}$, $c^0_{m,0}$ and $c^k_{m,n}$ are constants.

r	-1.60	-1.20	-0.80	-0.40	0.00	0.40	0.80	1.20	1.60
Perturb sol	0.0000	0.4026	0.7813	1.0093	1.0859	1.0098	0.7818	0.4026	0.0000
HAM sol	0.0000	0.3960	0.7692	0.0037	1.0686	0.9937	0.7692	0.3960	0.0000

Table.1. Comparison of velocity profile for $K = 0.4$, $z = 0.2$, $\lambda = 0.5$, $a_0 = 0.5$, $\phi = 0.4$, $We = 0.5$, $n = 0.3, \hbar = -0.7$, $\frac{dP}{dz} = 0.05$.

r	-1.60	-1.20	-0.80	-0.40	0.00	0.40	0.80	1.20	1.60
Perturb sol	0.0000	0.0141	0.0209	0.0225	0.0226	0.0225	0.0209	0.0141	0.0000
HAM sol	0.0000	0.0145	0.0215	0.0232	0.0233	0.0232	0.0215	0.0145	0.0000

Table.2. Comparison of temperature profile for $K = 0.4$, $z = 0.2$, $\lambda = 0.5$, $a_0 = 0.5$, $\phi = 0.4$, $B_r = 0.2$, $We = 0.5$, $n = 0.3, \hbar = -0.7$, $\frac{dP}{dz} = 0.05$.

r	-1.60	-1.20	-0.80	-0.40	0.00	0.40	0.80	1.20	1.60
Perturb sol	0.0000	-0.0035	-0.0052	-0.0056	-0.0057	-0.0056	-0.0052	-0.0035	0.0000
HAM sol	0.0000	-0.0036	-0.0054	-0.0058	-0.0057	-0.0058	-0.0054	-0.0036	0.0000

Table.3. Comparison of concentration profile for $K = 0.4$, $z = 0.2$, $\lambda = 0.5$, $a_0 = 0.5$, $\phi = 0.4$, $B_r = 0.2$, $We = 0.5$, $n = 0.3, \hbar = -0.7$, $\frac{dP}{dz} = 0.05$, $S_r = 0.5$, $S_c = 0.5$.

7.5 Numerical Results and Discussion

In this section we have presented the solution for the Carreau fluid model for diverging tube graphically. The expression for pressure rise ΔP is calculated numerically using mathematics software. The effects of various parameters on the pressure rise ΔP are shown in Figs. 7.3 to 7.7 for various values of Weissenberg number We, amplitude ratio ϕ, power law index n, wavelength λ and for different waveshapes. It is observed from Figs. 7.3 to 7.7 that pressure rise decreases with the increase in We, ϕ, λ, while the pressure rise increases with the increase in n. Peristaltic pumping region is $(0 \leq Q \leq 0.45)$ and augmented pumping region is $(0.46 \leq Q \leq 1)$ for Figs. 7.3 to 7.7. It is also analyzed through Fig. 7.7 that square wave has best peristaltic pumping characteristics, while trapezoidal wave has worst peristaltic pumping characteristics as compared to the other waves. Figs. 7.8 to 7.12 represents the behavior of frictional forces. It is depicted that frictional forces has an opposite behavior as compared to the pressure rise. Effects of temperature profile have been shown through Figs. 7.13 and 7.14. It is seen that

with the increase in B_r temperature profile increases, while decreases with an increase in n. The concentration field σ for different values of B_r and S_r are shown in Figs. 7.15 and 7.16. We observed that the concentration field decreases with the increase in B_r and S_r. Figs. 7.17 (a to e) are prepared to see the behavior of pressure gradient for different wave shapes. It is observed from the figures that for $z\epsilon\,[0, 0.5]$ and $[1.1, 1.5]$ the pressure gradient is small, and large pressure gradient occurs for $z\epsilon\,[0.51, 1]$, moreover, it is seen that with increase in ϕ pressure gradient increases. Figs. 7.18 shows the streamlines for different wave forms. It is observed that the size of the trapped bolus in triangular wave is small as compared to the other waves.

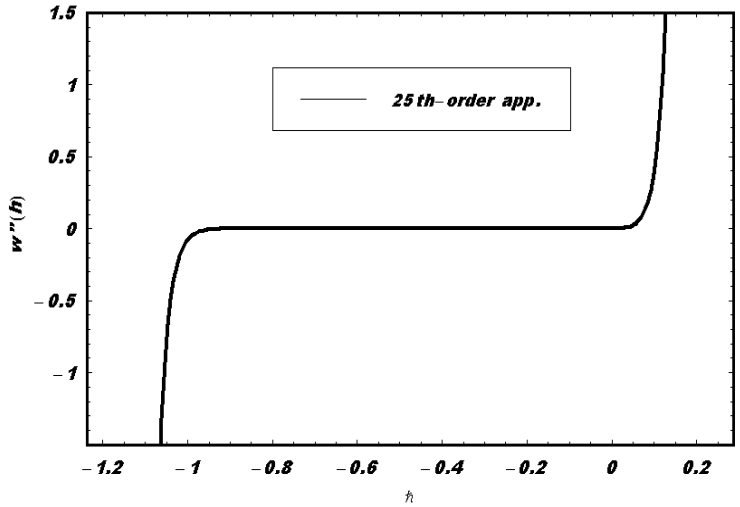

Figs.7.1. (a) $\hbar$-curve for velocity profile for $K = 0.4$, $z = 0.2$,
$\lambda = 0.5$, $a_0 = 0.5$, $\phi = 0.4$, $We = 0.5$, $n = 0.3$, $B_r = 0.2$,
$S_r = 0.5$, $S_c = 0.5$, $\frac{dP}{dz} = 0.05$.

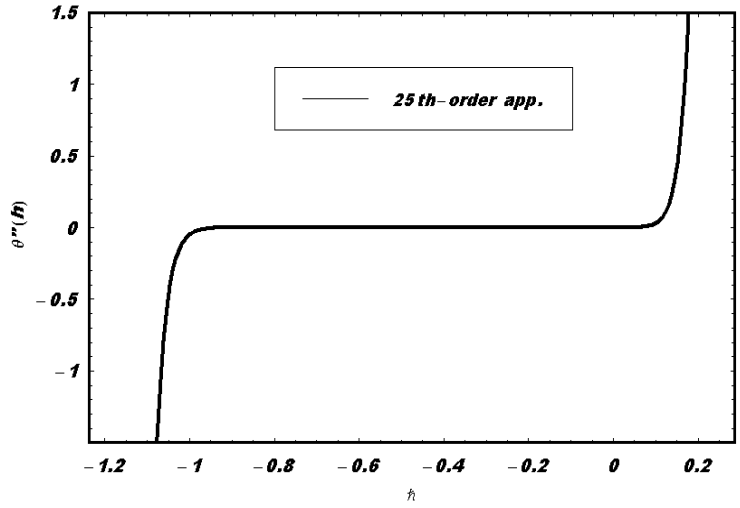

Figs.7.1. (b) $\hbar$-curve for temperature profile for $K = 0.4$, $z = 0.2$, $\lambda = 0.5$, $a_0 = 0.5$, $\phi = 0.4$, $We = 0.5$, $n = 0.3$, $B_r = 0.2$, $S_r = 0.5$, $S_c = 0.5$, $\frac{dP}{dz} = 0.05$.

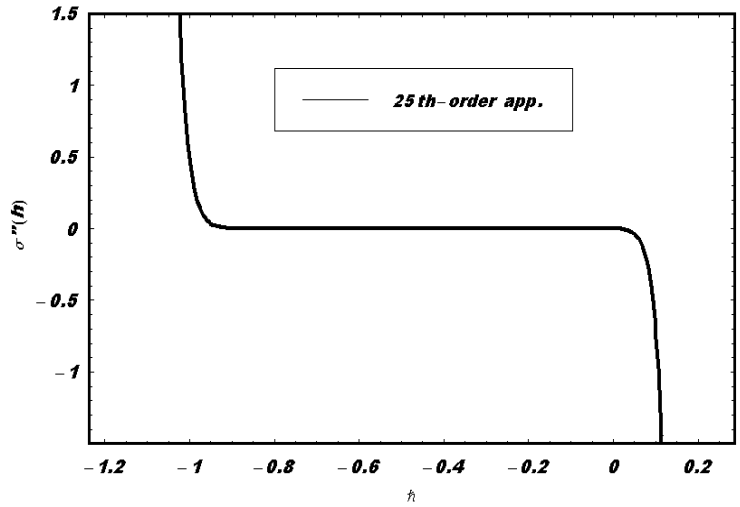

Figs.7.1. (c) $\hbar$-curve for concentration profile for $K = 0.4$, $z = 0.2$, $\lambda = 0.5$, $a_0 = 0.5$, $\phi = 0.4$, $We = 0.5$, $n = 0.3$, $B_r = 0.2$, $S_r = 0.5$, $S_c = 0.5$, $\frac{dP}{dz} = 0.05$.

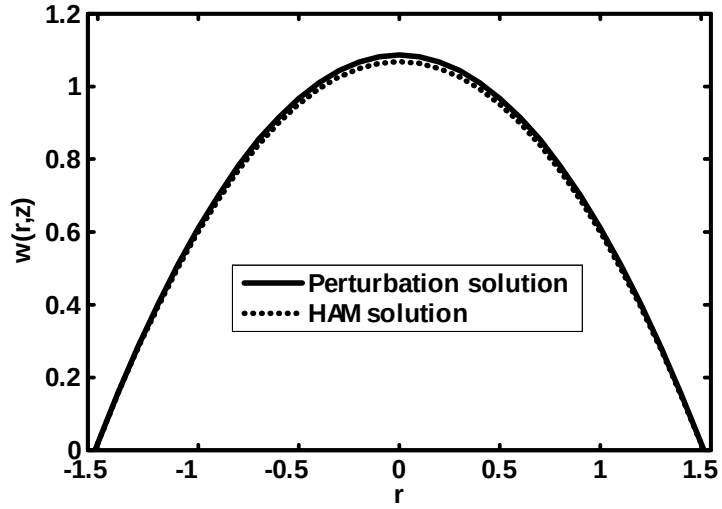

Figs.7.2 (a) . Comparison of velocity profile for $K = 0.4$, $z = 0.2$, $\lambda = 0.5$, $a_0 = 0.5$, $\phi = 0.4$, $We = 0.5$, $n = 0.3$, $B_r = 0.2$, $S_r = 0.5$, $S_c = 0.5, \hbar = -0.7$, $\frac{dP}{dz} = 0.05$.

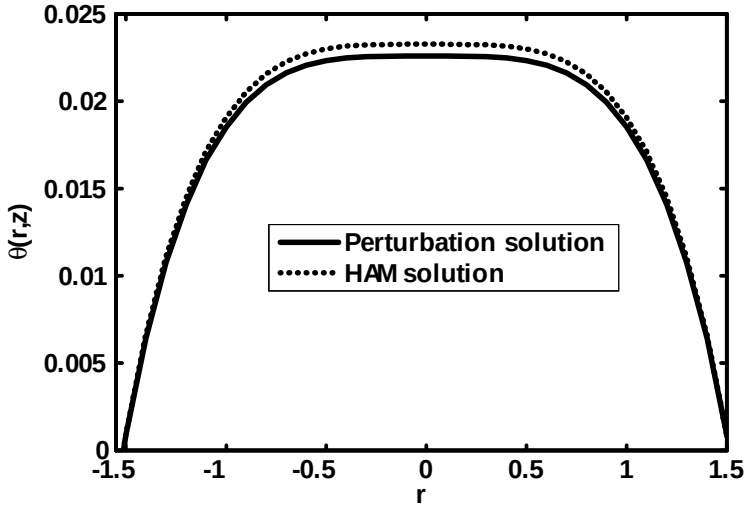

Figs.7.2 (b) . Comparison of temperature profile for $K = 0.4$, $z = 0.2$, $\lambda = 0.5$, $a_0 = 0.5$, $\phi = 0.4$, $We = 0.5$, $n = 0.3$, $B_r = 0.2$, $S_r = 0.5$, $S_c = 0.5, \hbar = -0.7$, $\frac{dP}{dz} = 0.05$.

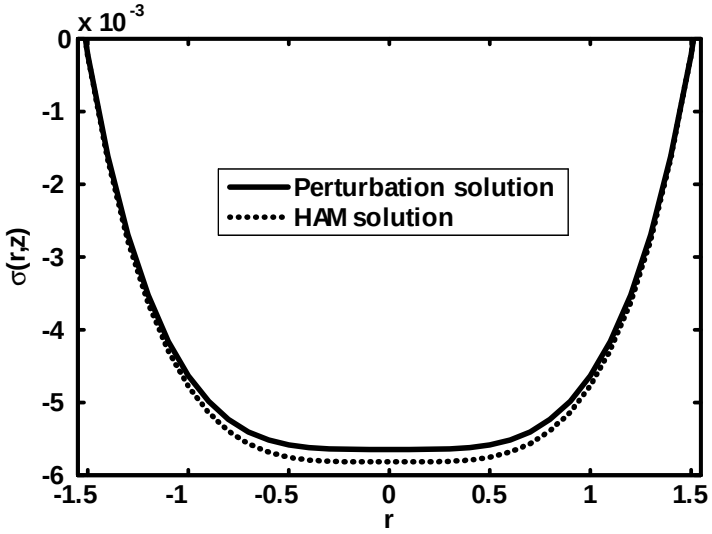

Figs.7.2 (c) . Comparison of concentration profile, for $K = 0.4$, $z = 0.2$, $\lambda = 0.5$, $a_0 = 0.5$, $\phi = 0.4$, $We = 0.5$, $n = 0.3$, $B_r = 0.2$, $S_r = 0.5$, $S_c = 0.5, \hbar = -0.7$, $\frac{dP}{dz} = 0.05$.

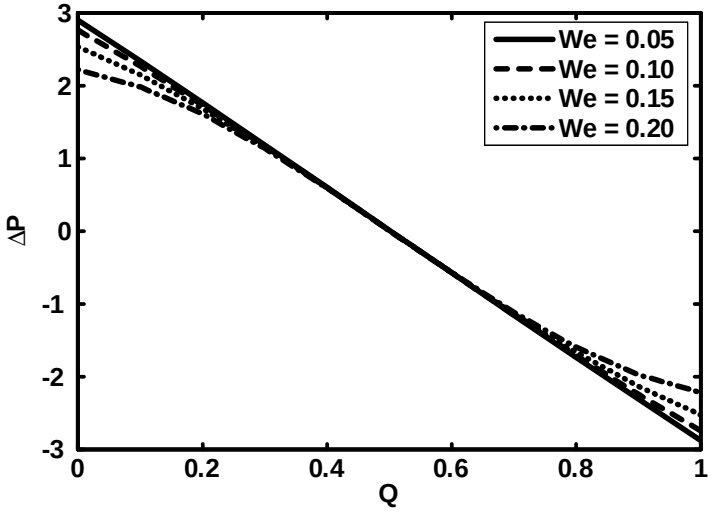

Figs.7.3. Pressure rise versus flow rate for $K = 0.5$, $\lambda = 1.5$, $a_0 = 0.5$, $\phi = 0.1$, $n = 0.05$.

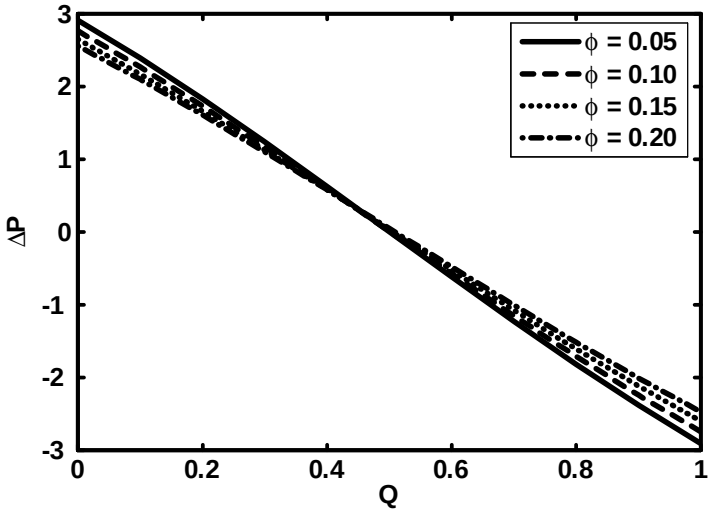

Figs.7.4. Pressure rise versus flow rate for $K = 0.5$, $\lambda = 1.5$, $a_0 = 0.5$, $We = 0.1$, $n = 0.05$.

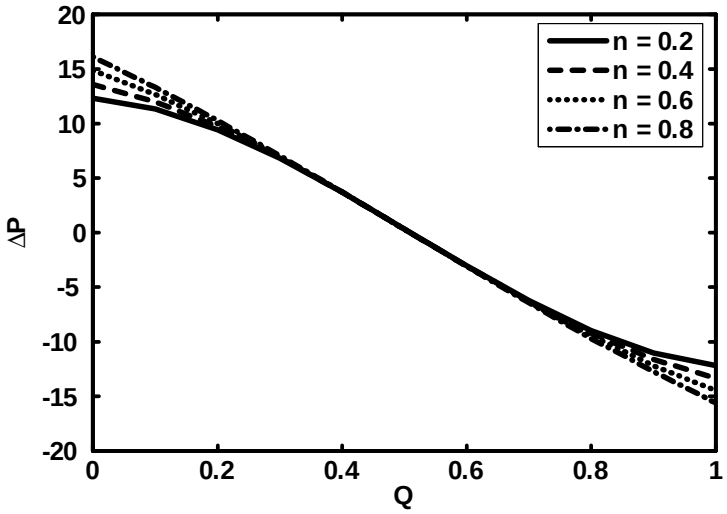

Figs.7.5. Pressure rise versus flow rate for $K = 0.5$, $\lambda = 1.5$, $a_0 = 0.5$, $\phi = 0.2$, $We = 0.1$.

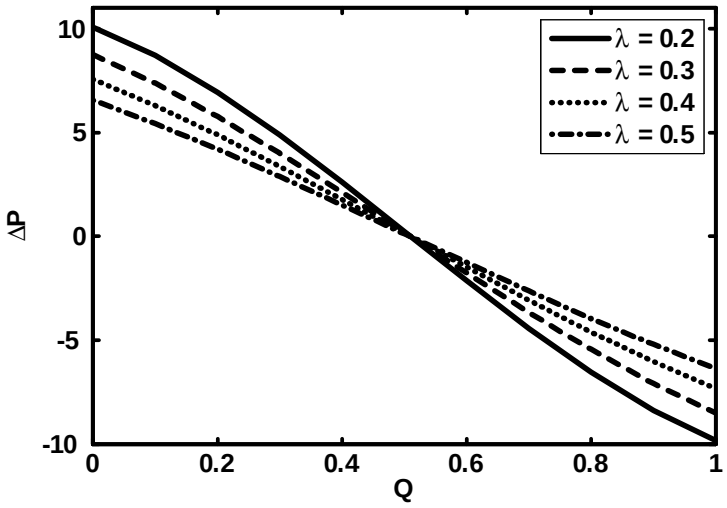

Figs.7.6. Pressure rise versus flow rate for $K = 0.5$, $n = 0.05$, $a_0 = 0.5$, $\phi = 0.1$, $n = 0.05$.

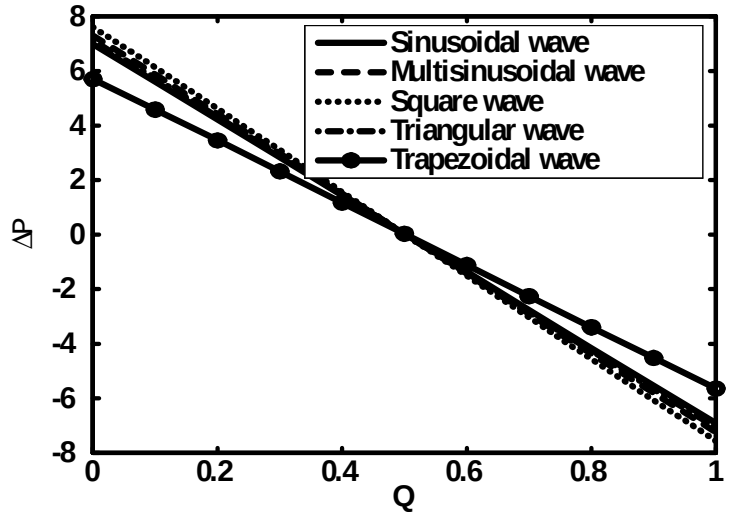

Figs.7.7. Pressure rise versus flow rate for $K = 0.5$, $\lambda = 0.05$, $a_0 = 0.05$, $\phi = 0.1$, $n = 0.5$, $We = 0.05$.

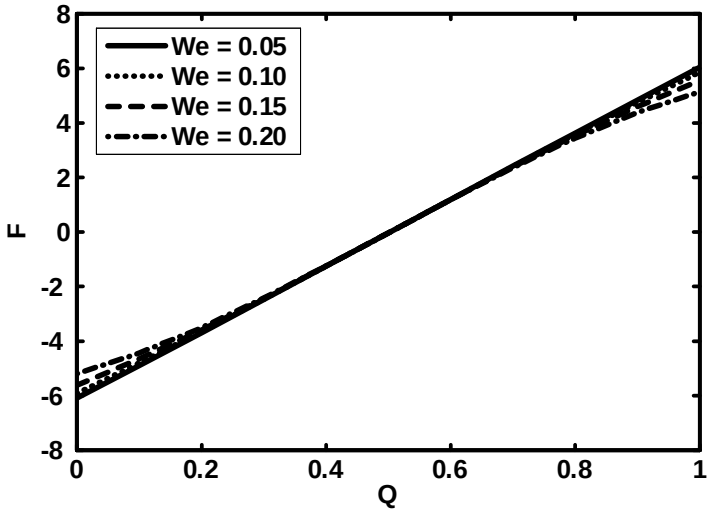

Figs.7.8. Frictional force versus flow rate for $K = 0.5$, $\lambda = 1.5$, $a_0 = 0.5$, $\phi = 0.1$, $n = 0.05$.

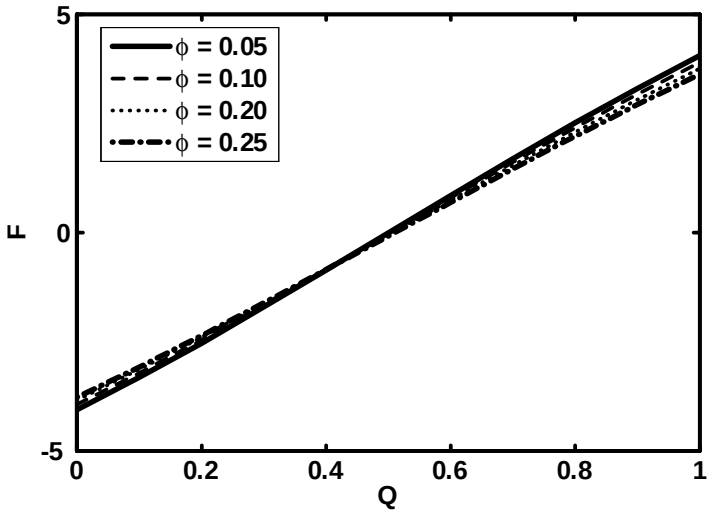

Fig.7.9. Frictional force versus flow rate for $K = 0.5$, $\lambda = 1.5$, $a_0 = 0.5$, $We = 0.1$, $n = 0.05$.

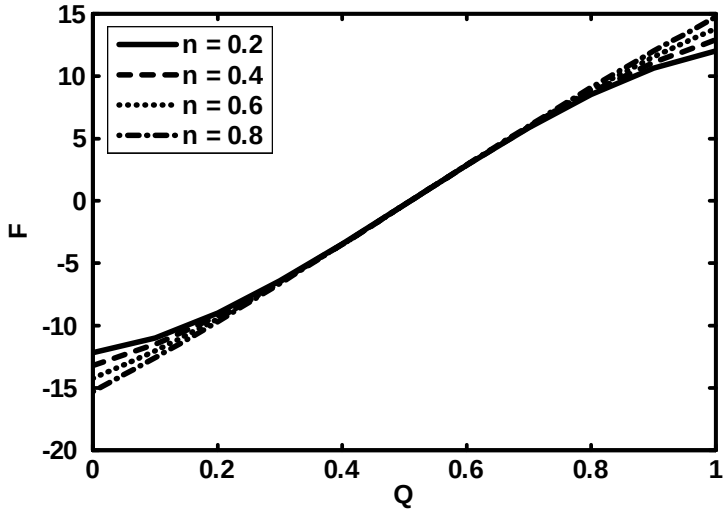

Figs.7.10. Frictional force versus flow rate for $K = 0.5$, $\lambda = 1.5$, $a_0 = 0.5$, $\phi = 0.2$, $We = 0.1$.

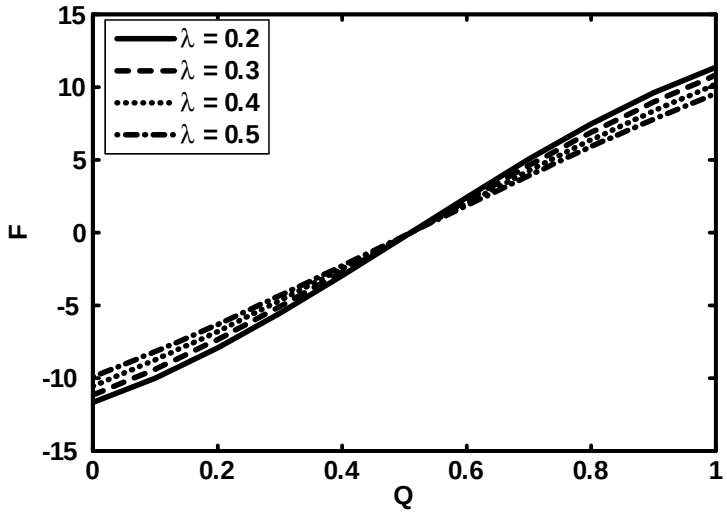

Figs.7.11. Frictional force versus flow rate for $K = 0.5$, $n = 0.05$, $a_0 = 0.5$, $\phi = 0.1$, $n = 0.05$.

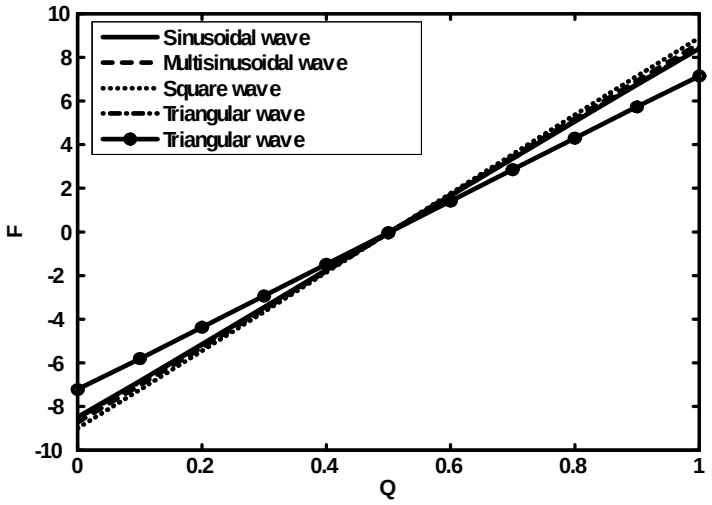

Figs.7.12. Frictional force versus flow rate for $K = 0.5$, $\lambda = 0.05$, $a_0 = 0.05$, $\phi = 0.1$, $n = 0.5$, $We = 0.05$.

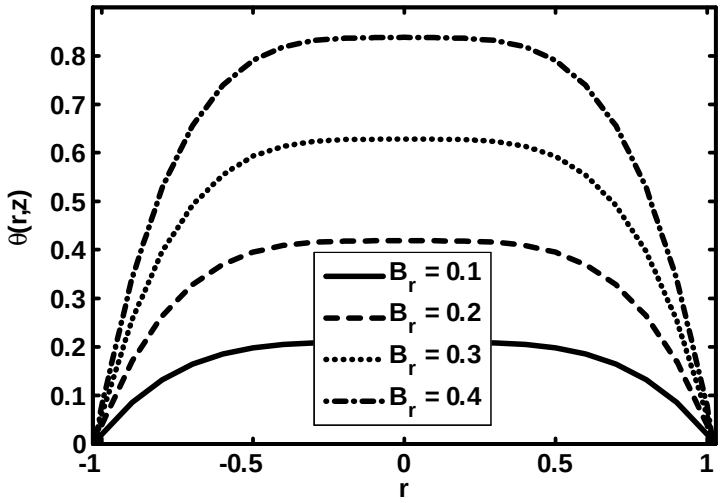

Figs.7.13. Temperature profile for $n = 0.5$ $K = 0.05$, $\lambda = 0.05$, $a_0 = 0.05$, $\phi = 0.1$, $We = 0.05$.

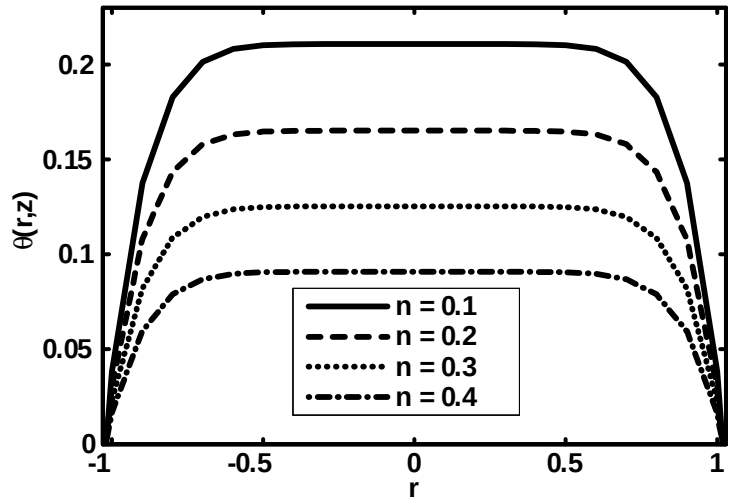

Figs.7.14. Temperature profile for $B_r = 0.2$, $K = 0.05$, $\lambda = 0.05$, $a_0 = 0.05$, $\phi = 0.1$, $We = 0.05$.

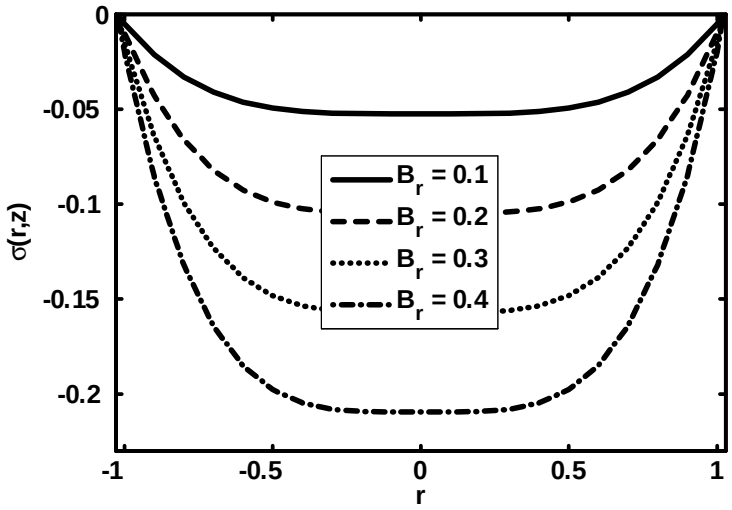

Figs.7.15. Temperature profile for $S_r = 0.5$, $K = 0.05$, $\lambda = 0.05$, $a_0 = 0.05$, $\phi = 0.1$, $n = 0.5$, $We = 0.05$, $S_c = 0.5$.

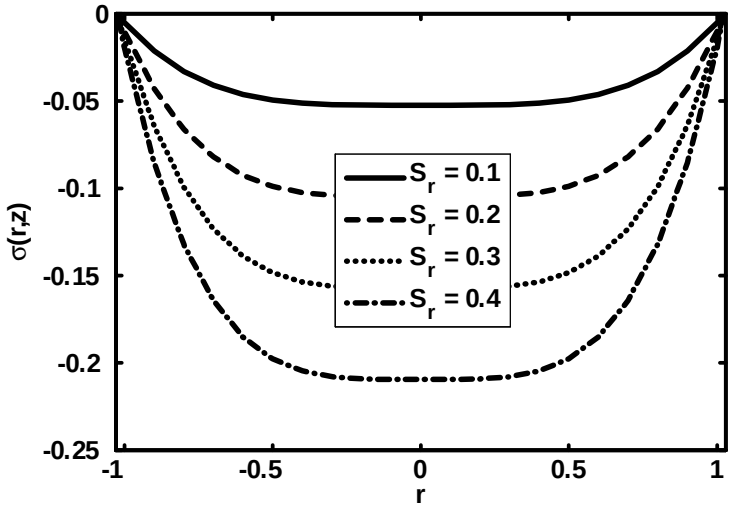

Figs.7.16. Temperature profile for $B_r = 0.2$, $K = 0.05$, $\lambda = 0.05$, $a_0 = 0.05$, $\phi = 0.1$, $n = 0.5$, $We = 0.05$, $S_c = 0.5$.

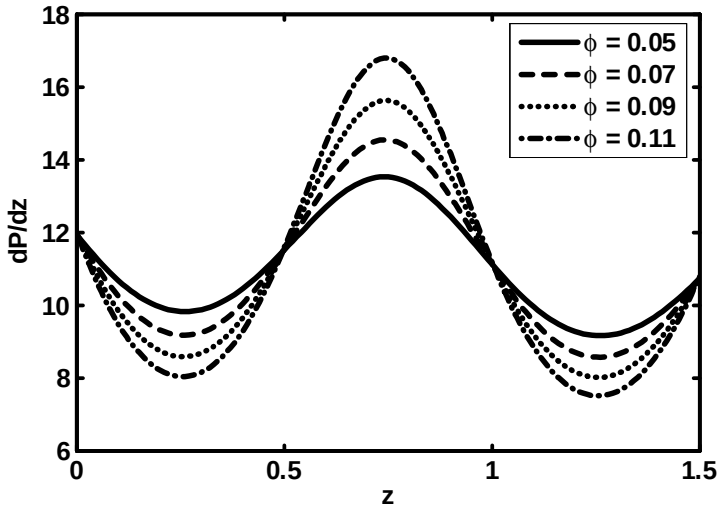

Fig.7.17. (a) . Pressure gradient versuz z for (Sinusoidal wave) $K = 0.02$, $Q = 0.1$, $We = 0.1$, $\lambda = 0.02$, $a_0 = 0.02$, $n = 0.5$.

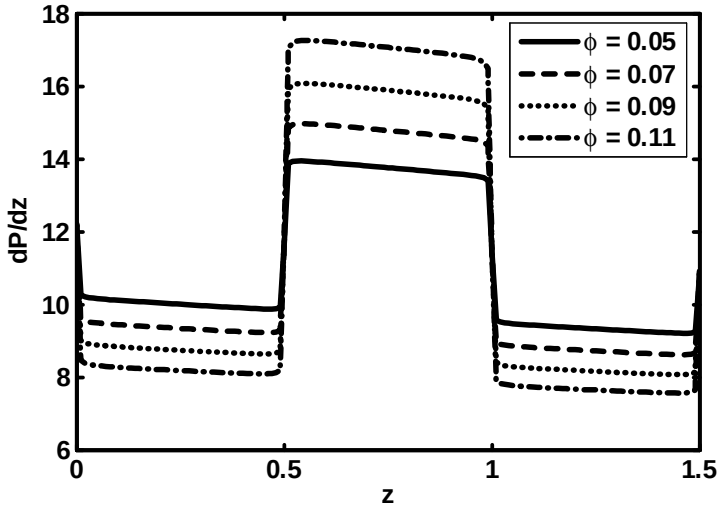

Fig.7.17. (b) . Pressure gradient versuz z for (Square wave) $K = 0.02$, $Q = 0.1$, $We = 0.1$, $\lambda = 0.02$, $a_0 = 0.02$, $n = 0.5$.

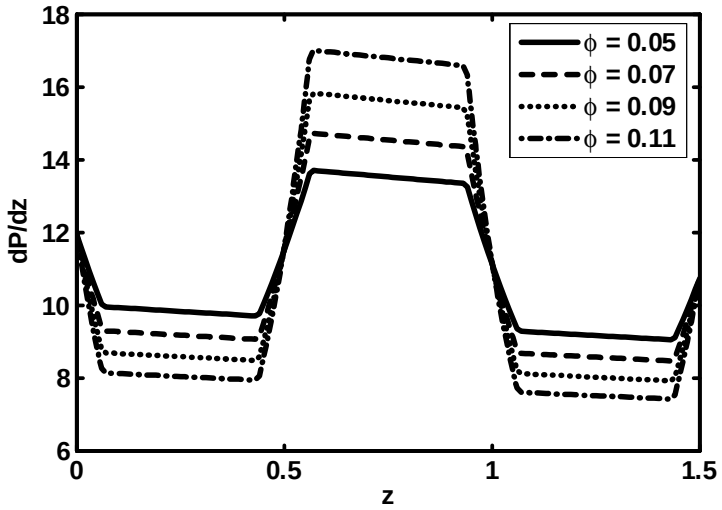

Fig.7.17. (c) . Pressure gradient versuz z for (Trapezoidal wave) $K = 0.02$, $Q = 0.1$, $We = 0.1$, $\lambda = 0.02$, $a_0 = 0.02$, $n = 0.5$.

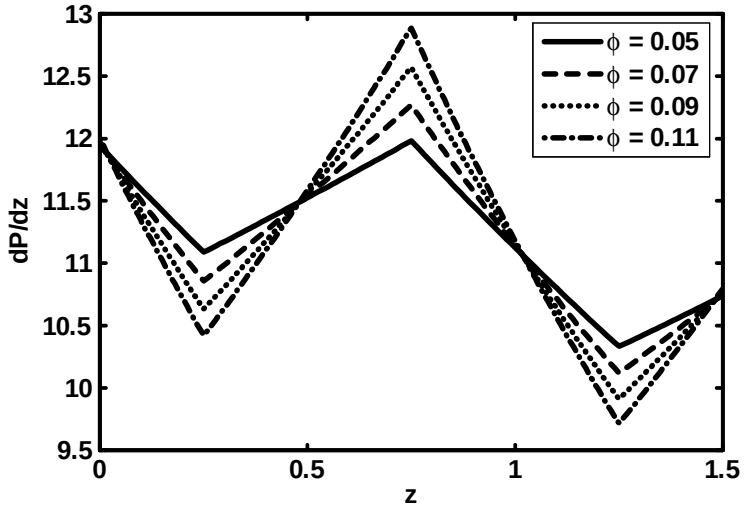

Fig.7.17. (d) . Pressure gradient versuz z for (Triangular wave) $K = 0.02$, $Q = 0.1$, $We = 0.1$, $\lambda = 0.02$, $a_0 = 0.02$, $n = 0.5$.

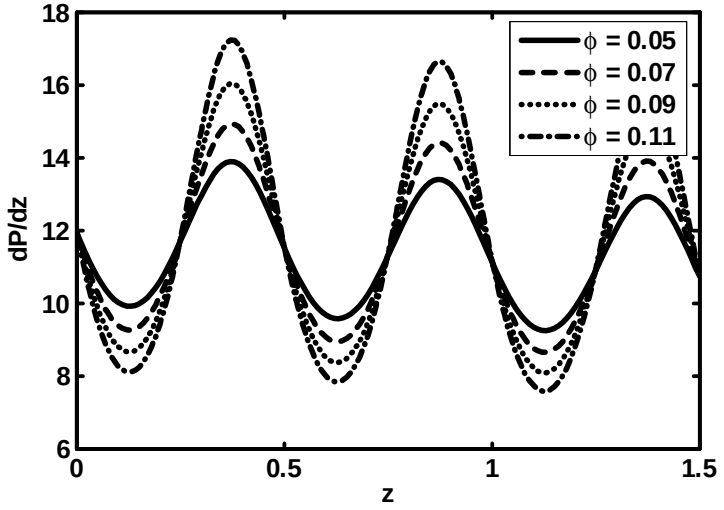

Fig.7.17. (e) . Pressure gradient versuz z for (Multisinusoidal wave) $K = 0.02$, $Q = 0.1$, $We = 0.1$, $\lambda = 0.02$, $a_0 = 0.02$, $n = 0.5$.

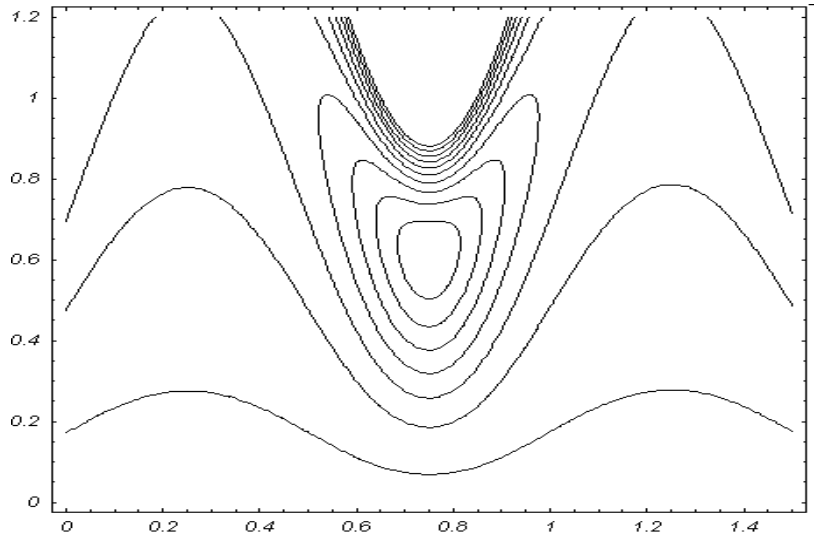

Fig.7.18 (a). Pressure gradient versuz z for sinusoidal wave when $K = 0.02$, $Q = 0.1$, $We = 0.1$, $\lambda = 0.02$, $a_0 = 0.02$, $n = 0.5$, $\phi = 0.2$.

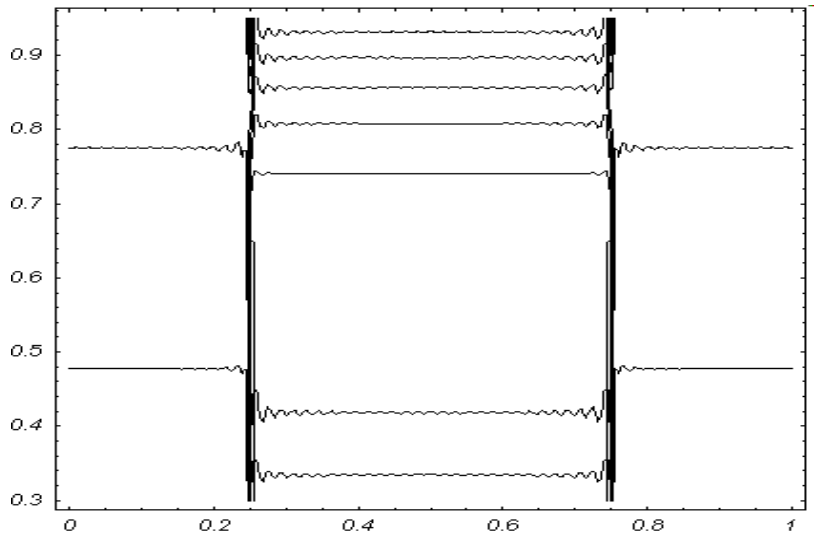

Fig.7.18 (b). Pressure gradient versuz z for square wave when $K = 0.02$, $Q = 0.1$, $We = 0.1$, $\lambda = 0.02$, $a_0 = 0.02$, $n = 0.5$, $\phi = 0.2$.

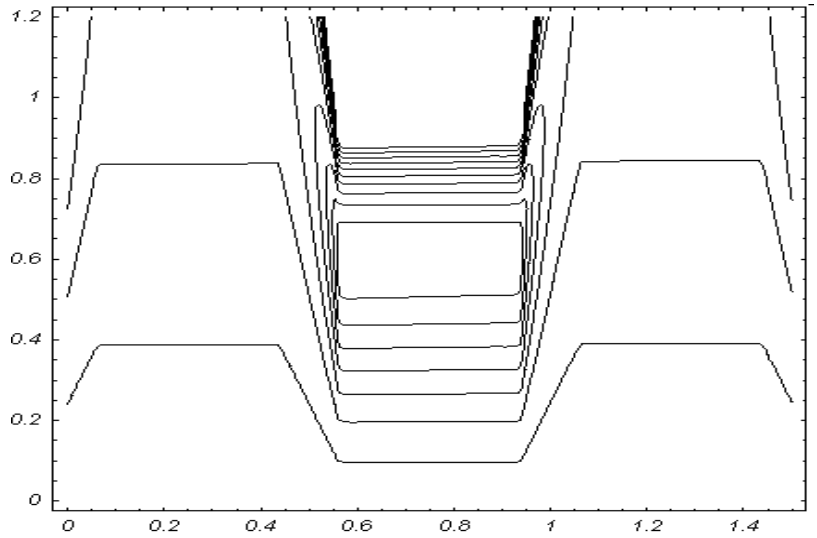

Fig.7.18 (c). Pressure gradient versuz z for trapezoidal wave when $K = 0.02$, $Q = 0.1$, $We = 0.1$, $\lambda = 0.02$, $a_0 = 0.02$, $n = 0.5$, $\phi = 0.2$.

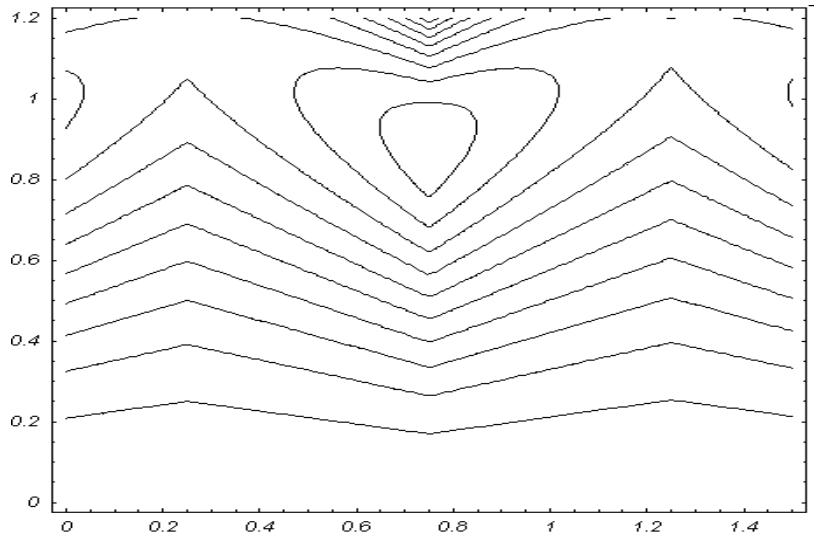

Fig.7.18 (d). Pressure gradient versuz z for triangular wave when $K = 0.02$, $Q = 0.1$, $We = 0.1$, $\lambda = 0.02$, $a_0 = 0.02$, $n = 0.5$, $\phi = 0.2$.

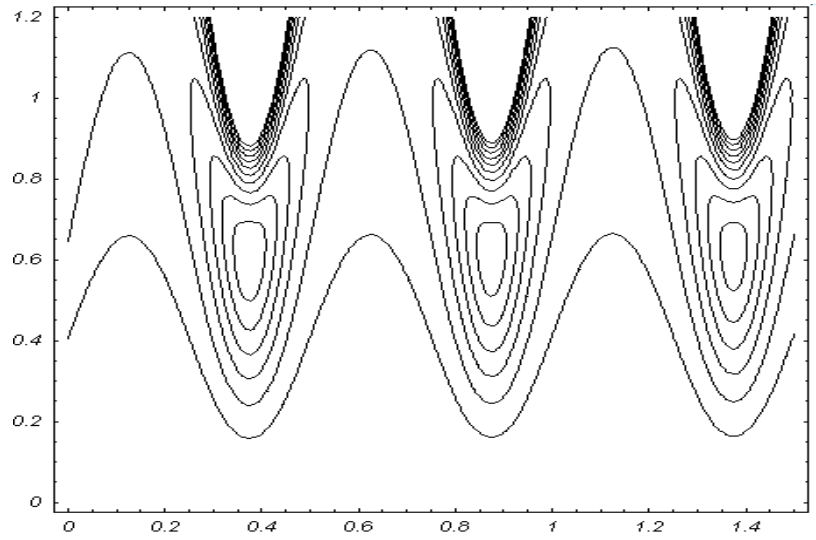

Fig.7.18 (e). Pressure gradient versuz z for multisinusoidal wave when $K = 0.02$, $Q = 0.1$, $We = 0.1$, $\lambda = 0.02$, $a_0 = 0.02$, $n = 0.5$, $\phi = 0.2$.

7.6 Conclusion

This study examines the influence of heat and mass transfer on the peristaltic flow of a Carreau fluid in a diverging tube. Two types of solution have been evaluated. The main points of the performed analysis are as follow

1. The perturbation solution and homotopy solutions are identical upto four digits.
2. The effects of We, λ and ϕ on the pressure rise are same.
3. The frictional forces have an opposite behaviour as compared to the pressure rise.
4. Effects of B_r and n on temperature profile are opposite.
5. Concentration profile has an opposite behaviour as compared to the temperature profile.
6. Pressure gradient increases with an increase in ϕ.
7. The size of trapped bolus for triangular wave is small as compared to the other waves.

Chapter 8

Analytical and numerical analysis of Vogel's model of viscosity on the peristaltic flow of Jeffrey fluid

8.1 Introduction

In the present chapter, we have analyzed the effects of temperature dependent viscosity on the peristaltic flow of Jeffrey fluid through the gap between two coaxial horizontal tubes. The inner tube is maintained at a temperature T_0 and the outer tube has sinusoidal wave travelling down its wall and it is exposed to temperature T_1. The governing problem is simplified using longwave length and low Reynolds number approximations. Regular perturbation in terms of small viscosity parameter is used to get the expressions for the temperature and velocity for Vogel's models of viscosity. The numerical solution of the problem has also been computed by shooting method and an agreement of numerical solutions and analytical solutions had been presented. The expressions for pressure rise and friction force are calculated numerically. Graphical results and trapping phenomenon is presented at the end of the chapter to see the physical behavior of different parameter.

8.2 Formulation of the Problem

Consider the flow of a Jeffrey fluid through the gap between two coaxial horizontal tubes. The inner tube is maintained at a temperature $\bar{T}_0$ and the outer tube has a sinusoidal wave travelling down its wall and it is exposed to temperature $\bar{T}_1$. We select cylindrical coordinates with $\bar{R}$ along the radial direction and the $\bar{Z}$ along the centre line of the inner and outer tubes. The shape of the two walls are defined in Eqs. (2.7) and (2.8) . The governing equations in the fixed frame for an incompressible flow are given as

$$\frac{\partial \bar{U}}{\partial \bar{R}} + \frac{\bar{U}}{\bar{R}} + \frac{\partial \bar{W}}{\partial \bar{Z}} = 0, \tag{8.1}$$

$$\rho\left(\frac{\partial}{\partial \bar{t}} + \bar{U}\frac{\partial}{\partial \bar{R}} + \bar{W}\frac{\partial}{\partial \bar{Z}}\right)\bar{U} = -\frac{\partial \bar{P}}{\partial \bar{R}} + \frac{1}{\bar{R}}\frac{\partial}{\partial \bar{R}}\left(\bar{R}\boldsymbol{\tau}_{\bar{R}\bar{R}}\right) + \frac{\partial}{\partial \bar{Z}}\left(\boldsymbol{\tau}_{\bar{R}\bar{Z}}\right) - \frac{\boldsymbol{\tau}_{\bar{\theta}\bar{\theta}}}{\bar{R}}, \tag{8.2}$$

$$\rho\left(\frac{\partial}{\partial \bar{t}} + \bar{U}\frac{\partial}{\partial \bar{R}} + \bar{W}\frac{\partial}{\partial \bar{Z}}\right)\bar{W} = -\frac{\partial \bar{P}}{\partial \bar{Z}} + \frac{1}{\bar{R}}\frac{\partial}{\partial \bar{R}}\left(\bar{R}\boldsymbol{\tau}_{\bar{R}\bar{Z}}\right) + \frac{\partial}{\partial \bar{Z}}\left(\boldsymbol{\tau}_{\bar{Z}\bar{Z}}\right), \tag{8.3}$$

$$\begin{aligned}\rho c_p\left(\frac{\partial}{\partial \bar{t}} + \bar{U}\frac{\partial}{\partial \bar{R}} + \bar{W}\frac{\partial}{\partial \bar{Z}}\right)\bar{T} &= \boldsymbol{\tau}_{\bar{R}\bar{R}}\frac{\partial \bar{U}}{\partial \bar{R}} + \boldsymbol{\tau}_{\bar{R}\bar{Z}}\frac{\partial \bar{W}}{\partial \bar{R}} + \boldsymbol{\tau}_{\bar{Z}\bar{R}}\frac{\partial \bar{U}}{\partial \bar{Z}} + \boldsymbol{\tau}_{\bar{Z}\bar{Z}}\frac{\partial \bar{W}}{\partial \bar{Z}} \\ &\quad + k\left(\frac{\partial^2 \bar{T}}{\partial \bar{R}^2} + \frac{1}{\bar{R}}\frac{\partial \bar{T}}{\partial \bar{R}} + \frac{\partial^2 \bar{T}}{\partial \bar{Z}^2}\right).\end{aligned} \tag{8.4}$$

The constitutive equation for the extra stress tensor $\bar{\boldsymbol{\tau}}$ in Jeffrey fluid is defined by [7]

$$\boldsymbol{\tau} = \frac{\mu\left(\bar{T}\right)}{1+\lambda_1}\left(\dot{\boldsymbol{\gamma}} + \lambda_2 \ddot{\boldsymbol{\gamma}}\right). \tag{8.5}$$

In the above equation, $\mu\left(\bar{T}\right)$ is temperature dependent viscosity, λ_1 is the ratio of relaxation to retardation times, $\dot{\boldsymbol{\gamma}}$ (vector quantity) the shear rate, λ_2 the retardation time $\left(\tilde{\lambda}_1 = \lambda_1 c/R,\ \tilde{\lambda}_2 = c\lambda_2/R\right)$ and dots denote the differentiation with respect to time.

We introduce the non-dimensional variables

$$\begin{aligned}
R &= \frac{\bar{R}}{a},\quad r=\frac{\bar{r}}{a_2},\quad Z=\frac{\bar{Z}}{\lambda},\quad z=\frac{\bar{z}}{\lambda},\quad W=\frac{\bar{W}}{c},\quad w=\frac{\bar{w}}{c},\\
U &= \frac{\lambda\bar{U}}{a_2 c},\quad u=\frac{\lambda\bar{u}}{a_2 c},\quad P=\frac{a_2^2\bar{P}}{c\lambda\mu_0},\ \theta=\frac{\left(\bar{T}-\bar{T}_1\right)}{\left(\bar{T}_0-\bar{T}_1\right)},\quad \mathrm{Pr}=\frac{\mu_0 c_p}{k},\\
\mu(\theta) &= \frac{\bar{\mu}\left(\bar{T}\right)}{\mu_0},\ t=\frac{c\bar{t}}{\lambda},\quad \delta=\frac{a_2}{\lambda},\ \mathrm{Re}=\frac{\rho c a_2}{\mu_0},\ \tau=\frac{a_2\boldsymbol{\tau}}{c\mu_0},\\
r_1 &= \frac{\bar{r}_1}{a_2}=\epsilon,\ r_2=\frac{\bar{r}_2}{a_2}=1+\phi\sin\left(2\pi z\right),\ E_c=\frac{c^2}{c_p\left(T_0-T_1\right)}.
\end{aligned}\tag{8.6}$$

Making use of Eqs. (1.11, 1.12, 8.5) and (8.6), Eqs. (8.1) to (8.4) take the form

$$\frac{\partial u}{\partial r}+\frac{u}{r}+\frac{\partial w}{\partial z}=0,\tag{8.7}$$

$$\mathrm{Re}\,\delta^3\left(u\frac{\partial}{\partial r}+w\frac{\partial}{\partial z}\right)u=-\frac{\partial P}{\partial r}+\frac{\delta}{r}\frac{\partial}{\partial r}\left(r\tau_{rr}\right)+\delta^2\frac{\partial}{\partial z}\left(\tau_{rz}\right)-\frac{\delta\tau_{\theta\theta}}{r},\tag{8.8}$$

$$\mathrm{Re}\,\delta\left(u\frac{\partial}{\partial r}+w\frac{\partial}{\partial z}\right)w=-\frac{\partial P}{\partial z}+\frac{1}{r}\frac{\partial}{\partial r}\left(r\tau_{rz}\right)+\delta\frac{\partial}{\partial z}\left(\tau_{zz}\right),\tag{8.9}$$

$$\begin{aligned}
\mathrm{Re}\,\delta\,\mathrm{Pr}\left(u\frac{\partial}{\partial r}+w\frac{\partial}{\partial z}\right)\theta &= E_c\,\mathrm{Pr}\left(\delta\frac{\partial u}{\partial r}\tau_{rr}+\frac{\partial w}{\partial r}\tau_{rz}+\delta^2\frac{\partial u}{\partial z}\tau_{zr}+\tau_{zz}\frac{\partial w}{\partial z}\delta\right)\\
&\quad+\frac{\partial^2\theta}{\partial r^2}+\frac{1}{r}\frac{\partial\theta}{\partial r}+\delta^2\frac{\partial^2\theta}{\partial z^2},
\end{aligned}\tag{8.10}$$

$$w = -1,\quad u=0\ \text{ at } r=r_1=\varepsilon,\tag{8.11a}$$

$$w = -1,\quad \text{at } r=r_2=1+\phi\sin\left(2\pi z\right),\tag{8.11b}$$

$$\theta = 1,\qquad \text{at } r=r_1,\tag{8.11c}$$

$$\theta = 0,\qquad \text{at } r=r_2,\tag{8.11d}$$

where ε is the radius ratio, ϕ is the wave amplitude and

$$\tau_{rr}=\frac{2\delta\mu\left(\theta\right)}{1+\lambda_1}\left[1+\frac{\lambda_2 c\delta}{a_2}\left(u\frac{\partial}{\partial r}+w\frac{\partial}{\partial z}\right)\right]\frac{\partial u}{\partial r},\tag{8.12a}$$

$$\tau_{rz} = \frac{\mu(\theta)}{1+\lambda_1}\left[1+\frac{\lambda_2 c}{\lambda}\left(u\frac{\partial}{\partial r}+w\frac{\partial}{\partial z}\right)\right]\left(\delta^2\frac{\partial u}{\partial z}+\frac{\partial w}{\partial r}\right), \tag{8.12b}$$

$$\tau_{zz} = \frac{2\delta\mu(\theta)}{1+\lambda_1}\left[1+\frac{\lambda_2 c\delta}{a_2}\left(u\frac{\partial}{\partial r}+w\frac{\partial}{\partial z}\right)\right]\frac{\partial w}{\partial z}. \tag{8.12c}$$

Making use of Eq. (8.12a) to (8.12c) and using the assumptions of long wavelength and low Reynolds number R_e, Eqs. (8.8) to (8.10) take the form

$$0 = \frac{\partial P}{\partial r}, \tag{8.13}$$

$$0 = -\frac{\partial P}{\partial z}+\frac{1}{r}\frac{\partial}{\partial r}\left(\frac{r\mu(\theta)}{1+\lambda_1}\left(\frac{\partial w}{\partial r}\right)\right), \tag{8.14}$$

$$0 = E_c \Pr\left(\frac{\mu(\theta)}{1+\lambda_1}\left(\frac{\partial w}{\partial r}\right)^2\right)+\frac{\partial^2\theta}{\partial r^2}+\frac{1}{r}\frac{\partial\theta}{\partial r}. \tag{8.15}$$

In typical situations, the viscosity of the real fluid varies with temperature. Therefore in the proceeding paragraphs we consider well known Vogel's viscosity model.

8.3 Vogel's Viscosity Model

Vogel's model of viscosity is defined as [41]

$$\mu(\theta) = \mu_0 \exp\left[\frac{A}{B+\theta}-T_0\right]. \tag{8.16}$$

The Maclaurin's series expansion of above equation in simplified form can be written as

$$\mu(\theta) = n_2 - \Gamma_1\theta + O(\Gamma_1)^2, \tag{8.17}$$

where

$$n_2 = n_1+\Gamma_2, \quad \Gamma_2 = \frac{\mu_0 A}{B}, \quad n_1 = \mu_0(1-T_0), \quad C = \frac{1}{B}, \Gamma_1 = \Gamma_2 C.$$

Using Eq. (8.17) in Eqs. (8.14) and (8.15), we have

$$0 = -\frac{\partial P}{\partial z}+\frac{1}{r}\frac{\partial}{\partial r}\left[\frac{(n_2-\Gamma_1\theta)\,r}{1+\lambda_1}\left(\frac{\partial w}{\partial r}\right)\right], \tag{8.18}$$

$$\frac{1}{r}\frac{\partial}{\partial r}\left(r\frac{\partial\theta}{\partial r}\right) = -E_c P_r\left[\left(a_1-\Gamma_1\theta\right)\left(\frac{\partial w}{\partial r}\right)^2\right]. \tag{8.19}$$

8.4 Solution of the Problem

Using regular perturbation method by considering Γ_1 as perturbation parameter, The solutions of the Eqs. (8.18) and (8.19) can be directly written as

$$\begin{aligned} w &= \frac{\partial P}{\partial z}\left(\frac{r^2}{4S_2}+B_1\ln r-\frac{r_1^2}{4S_2}-B_1\ln r_1\right)-1 \\ &+\Gamma_1\left(\frac{1}{\left(1+\lambda_1\right)a_2}\left[S_1\frac{r^6}{6}+S_2\frac{r^4}{4}+S_3\frac{r^2}{2}+S_4\left(\frac{r^2\left(\ln r\right)^2}{2}-\frac{r^2\ln r}{2}+\frac{r^2}{4}\right)\right.\right. \\ &\left.\left.+S_5\frac{\left(\ln r\right)^3}{3}+S_6\left(\frac{r^2\ln r}{2}-\frac{r^2}{4}\right)+S_7\frac{\left(\ln r\right)^2}{2}+S_8\ln r\right]+S_{11}\ln r+S_{12}\right), \end{aligned} \tag{8.20}$$

$$\begin{aligned} \theta &= S_2\left(\frac{1}{S_2^2}\frac{r^4}{64}+S_1^2\frac{\left(\ln r\right)^2}{2}+\frac{B_1}{S_2}\frac{r^2}{4}\right)+S_3\ln r+S_4+\Gamma_1\left(\left(S_{25}r^2+S_{26}r^4\right.\right. \\ &+S_{27}r^6+S_{28}r^8+S_{29}r^{10}+S_{30}r^{12}+S_{31}r^2\ln r+S_{32}r^4\ln r+S_{33}r^6\ln r+S_{34}r^8\ln r \\ &S_{35}r^2\left(\ln r\right)^2+S_{36}r^4\left(\ln r\right)^2+S_{37}r^6\left(\ln r\right)^2+S_{44}\left(\ln r\right)^5+S_{45}\left(\ln r\right)^6+S_{46}r^2\left(\ln r\right)^4 \\ &\left.\left.+\ S_{47}r^4\left(\ln r\right)^4\right)+S_7\ln r+S_8\right), \end{aligned} \tag{8.21}$$

$$\begin{aligned} \frac{dP}{dz} &= \frac{8S_{22}\left[2F+\left(r_2^2-r_1^2\right)\right]}{\left(r_2^4-r_1^4\right)+8S_2S_{11}\left[r_2^2\ln r_2-r_1^2\ln r_1-\left(r_2^2-r_1^2\right)/2\right]-2r_1^2\left(r_2^2-r_1^2\right)-\beta_1} \\ &+\frac{\Gamma_1 8a_2\left(-M_3\right)}{\left(r_2^4-r_1^4\right)+8S_2S_{11}\left[r_2^2\ln r_2-r_1^2\ln r_1-\left(r_2^2-r_1^2\right)/2\right]-2r_1^2\left(r_2^2-r_1^2\right)-\beta_1} \end{aligned} \tag{8.22}$$

The corresponding stream function $\left(u=-\frac{1}{r}\frac{\partial\Psi}{\partial z}\ \text{ and }\ w=\frac{1}{r}\frac{\partial\Psi}{\partial r}\right)$ can be written as

$$\begin{aligned} \Psi &= \gamma_1 r^2+\gamma_2 r^4+\gamma_3 r^6+\gamma_4 r^8+\gamma_5 r^2\ln r+\gamma_6 r^4\ln r \\ &+\gamma_7 r^2\left(\ln r\right)^2+\gamma_8 r^4\left(\ln r\right)^2+\gamma_9 r^2\left(\ln r\right)^3. \end{aligned} \tag{8.23}$$

All the appearing constants can be evaluated by simple algebraic algorithm.

The pressure rise ΔP and friction forces F on inner and outer tubes $F^{(i)}$, $F^{(o)}$, are given by

$$\Delta P = \int_0^1 \frac{dP}{dz} dz, \tag{8.24}$$

$$F^{(i)} = \int_0^1 r_1^2 \left(-\frac{dP}{dz}\right) dz, \tag{8.25}$$

$$F^{(o)} = \int_0^1 r_2^2 \left(-\frac{dP}{dz}\right) dz, \tag{8.26}$$

where $\frac{dP}{dz}$ is defined in Eqs. (8.22).

8.5 Comparison Between Numerical and Perturbation Solutions

Here the problem consisting of equations (8.22) and (8.23) is also solved numerically by employing shooting method. A comparison of the numerical solution and the perturbation solution has been presented through table and graphs and are shown below. The error between the two solutions is also presented.

r	Numerical Solution	Perturbation Solution	Error
0.10	-1.000000	-1.000000	0.000000
0.20	-1.013794	-1.013630	0.013794
0.30	-1.021658	-1.025596	0.021658
0.40	-1.024916	-1.029419	0.024916
0.50	-1.024579	-1.029579	0.024579
0.60	-1.021612	-1.025542	0.021612
0.70	-1.017000	-1.020091	0.017000
0.80	-1.011452	-1.013534	0.011452
0.90	-1.005817	-1.006817	0.005817
1.00	-1.000000	-1.000000	0.000000

Table.8.1. Comparison of axial velocity for perturbation and numerical solutions when $\lambda_1 = 0.1, B = 0.2,\ A = 0.3, \phi = 0.6, \epsilon = 0.1, \frac{dP}{dz} = 0.4, z = 0.5,\ P_r = 0.1, E_c = 0.2, T_0 = 0.5,\ \mu_0 = 0.4.$

8.6 Numerical Results and Discussion

In order to analyze the quantitative effects of the various physical parameter involved in the present analysis we use the symbolic software Mathematical and the results are displayed graphically. Figs 8.1 and 8.2 show the comparison of numerical solution and perturbation solution for velocity and temperature profile. The average pressure rise ΔP versus time averaged mean flow rate Q is plotted (for Vogel's viscosity model) for different values of viscosity parameter Γ_1, Jeffrey parameter λ_1, in Figs 8.3 and 8.4. Figs. 8.3 and 8.4 shows that the maximum pressure rise occurs at zero flow rate for different values of Γ_1 and λ_1. It can also be analyzed that increasing Γ_1 and λ_1, pressure rise decreases in the region $Q\epsilon\,[0, 0.45]$ and in the region $Q\epsilon\,[0.46, 1.5]$ the pressure rise increases with the increase in Γ_1 and λ_1. Peristaltic pumping occurs in the region $0 \leq Q < 0.45$, otherwise augmented pumping occurs. It is also observed that in Vogel's viscosity model, the range of pressure rise is much smaller than in the Reynold's viscosity model.

The frictionless force F for inner and outer tube denoted by $F^{(i)}$ and $F^{(o)}$ respectively, are plotted in Figs. 8.5 to 8.8. The region in which both $F^{(i)}$ and $F^{(o)}$ are positive, denotes the region where reflux phenomenon occurs and the region where $F^{(i)}$ and $F^{(o)}$ are negative designate to peristaltic pumping. We observed that the frictionless force has the opposite behavior as compared to pressure rise. It is observed that $F^{(i)}$ and $F^{(o)}$ increases with increases in Γ_1 and λ_1.

Figs. 8.9 and 8.10 represents the physical behavior of the temperature field. It is found that with increasing β and λ_1 the temperature field increases.

8.7 Trapping

Another interesting phenomenon in peristaltic motion is trapping. It is basically the formation of an internally circulating bolus of fluid by closed streamlines. This trapped bolus pushed a head along with the peristaltic wave. Figs. 8.11 and 8.12 are prepared for Vogel's model

streamlines. The effects of time averaged flow rate Q on trapping can be seen through Figs. 8.11 (v to y) . It is observed that the size of the trapped bolus increases as we increase flow rate Q. Figs. 8.12 (h_1 to i_1) are plotted to see the effects of λ_1, it is seen that trapped bolus decreases with the increase of λ_1.

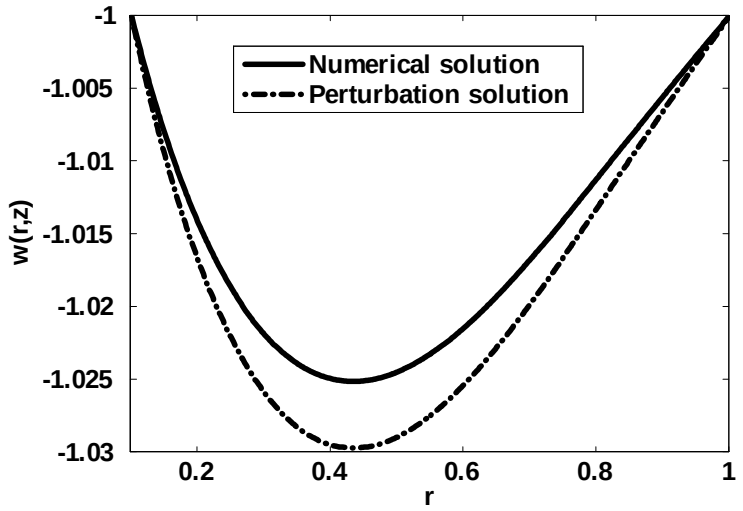

Fig.8.1. Comparison of axial velocity for $\lambda_1 = 0.1$, $B = 0.2$, $A = 0.3$, $\phi = 0.6$, $\epsilon = 0.1$, $z = 0.5$, $P_r = 0.1$, $E_c = 0.2$, $T_0 = 0.5$, $\mu_0 = 0.4$.

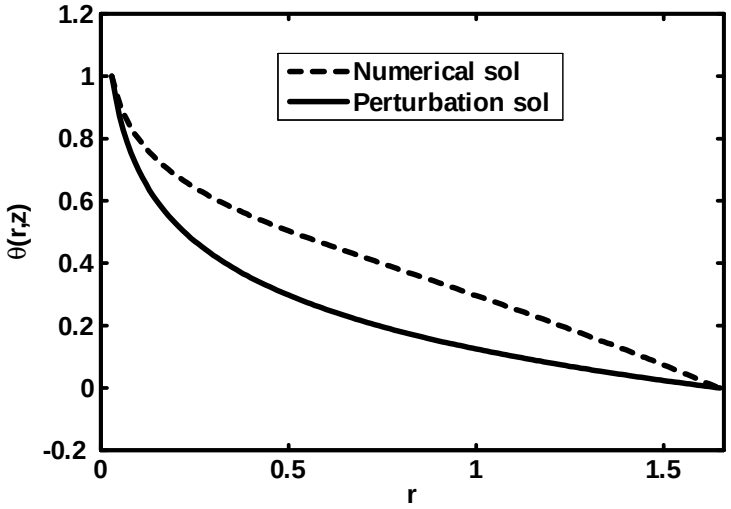

Fig.8.2. Comparison of temperature profile for
$\lambda_1 = 0.1, B = 0.2,\ A = 0.3, \phi = 0.6, \epsilon = 0.1, \frac{dP}{dz} = 0.4, z = 0.5,$
$P_r = 0.1, E_c = 0.2, T_0 = 0.5, \mu_0 = 0.4.$

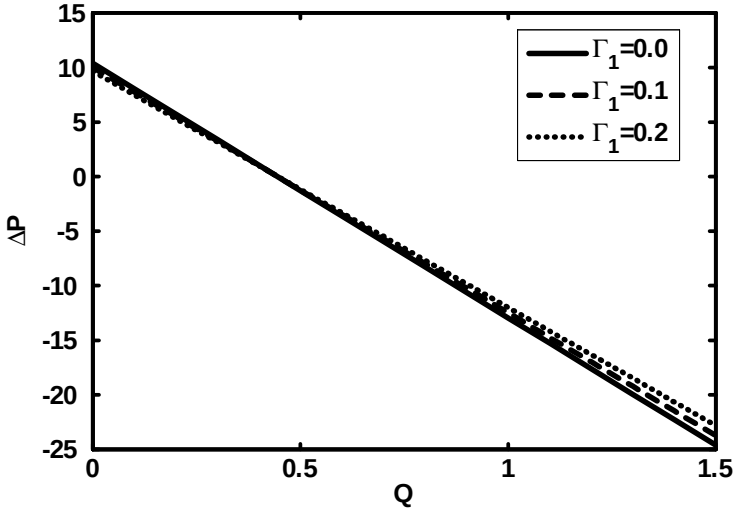

Fig.8.3. Pressure rise versus flow rate for $\varepsilon = 0.03$, $\phi = 0.6$,
$E_c = 0$, Pr $= 0$, $\lambda_1 = 0.2$, $\mu_0 = 0.5$, $A = 1$, $B = 1$, $a = 0.1$.

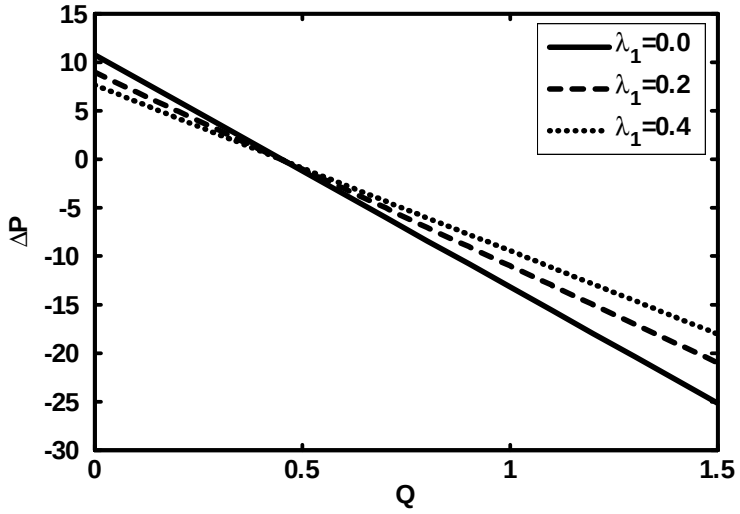

Fig.8.4. Pressure rise versus flow rate for
$\varepsilon = 0.03, \phi = 0.6, E_c = 0, \mathrm{Pr} = 0,$
$\beta = 0.2, \mu_0 = 0.5, A = 1, B = 1, a = 0.1.$

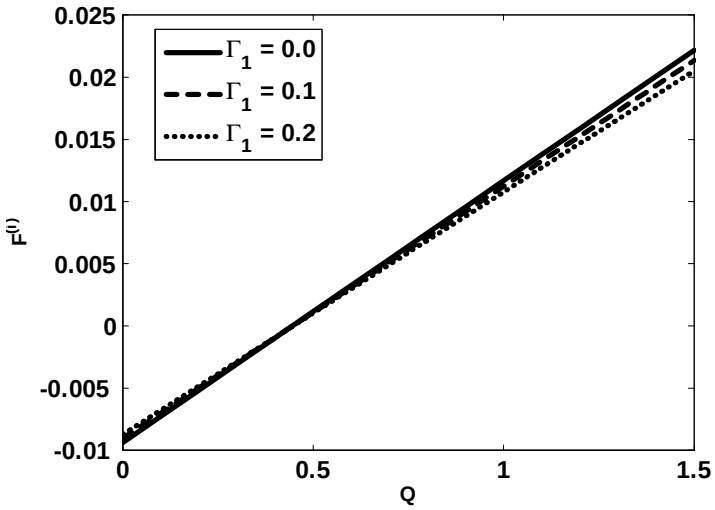

Fig.8.5. Frictional force on inner tube ($\mathrm{F}_{\lambda}^{(i)}$) versus flow rate
for $\varepsilon = 0.03, \phi = 0.6, E_c = 0, \mathrm{Pr} = 0, \lambda_1 = 0.2,$
$\mu_0 = 0.5, A = 1, B = 1, a = 0.1.$

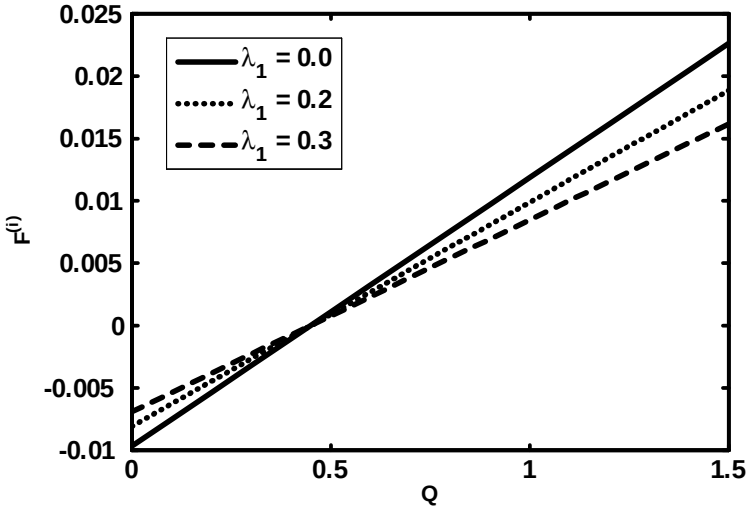

Fig.8.6. Frictional force on inner tube ($\mathrm{F}_{\lambda}^{(i)}$) versus flow rate for $\varepsilon = 0.03, \phi = 0.6, E_c = 0, \mathrm{Pr} = 0, \beta = 0.2,$ $\mu_0 = 0.5, A = 1, B = 1, a = 0.1.$

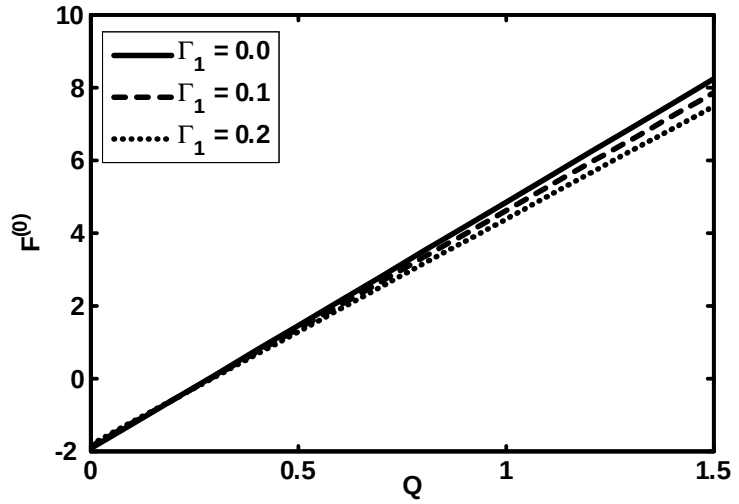

Fig.8.7. Frictional force on outer tube ($\mathrm{F}_{\lambda}^{(0)}$) versus flow rate for $\varepsilon = 0.03, \phi = 0.6, E_c = 0, \mathrm{Pr} = 0, \lambda_1 = 0.2,$ $\mu_0 = 0.5, A = 1, B = 1, a = 0.1.$

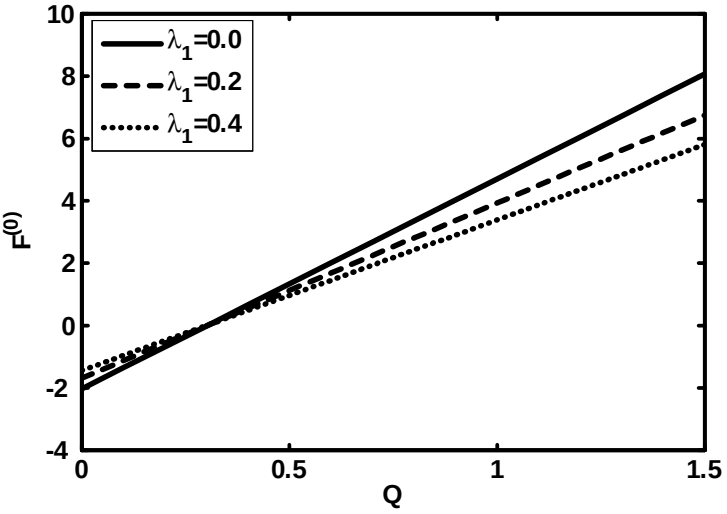

Fig.8.8. Frictional force on outer tube ($\mathrm{F}_{\lambda}^{(0)}$) versus flow rate for $\varepsilon = 0.03, \phi = 0.6, E_c = 0, \mathrm{Pr} = 0, \beta = 0.2,$ $\mu_0 = 0.5, A = 1, B = 1, a = 0.1.$

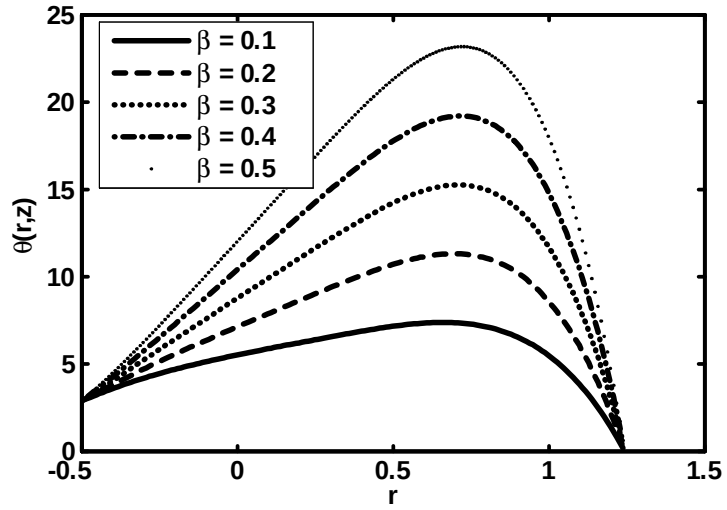

Fig.8.9. Temperature field for $\lambda_1 = 0.01, \phi = 0.6, E_c = -0.15, \mathrm{Pr} = 0.25,$ $Q = 0.5, z = 0.1, \mu_0 = 0.5, A = 1, B = 1, a = 0.1.$

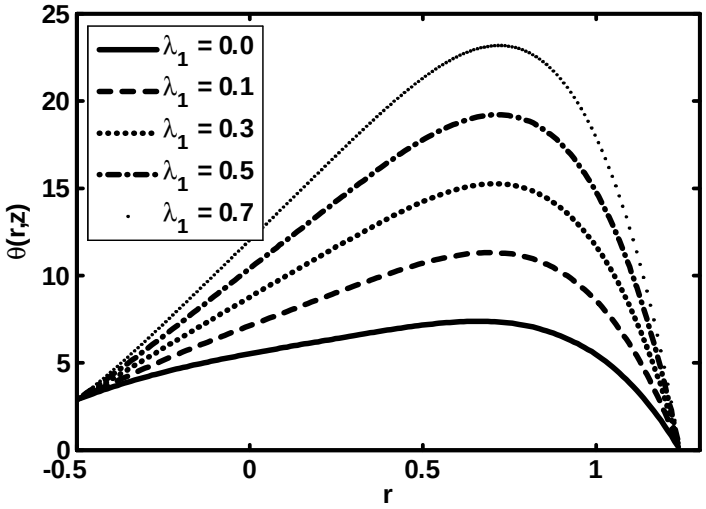

Fig. 8.10. Temperature field for

$\beta = 0.01, \phi = 0.6, E_c = -0.15, \mathrm{Pr} = 0.25,$

$Q = 0.5, z = 0.1, \mu_0 = 0.5, A = 1, B = 1, a = 0.1.$

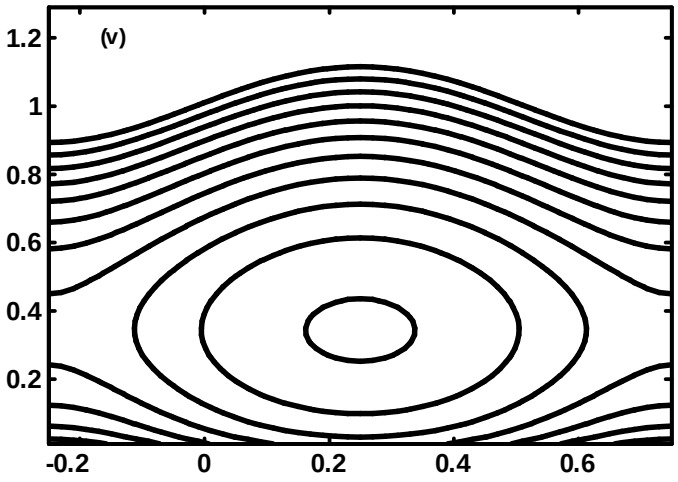

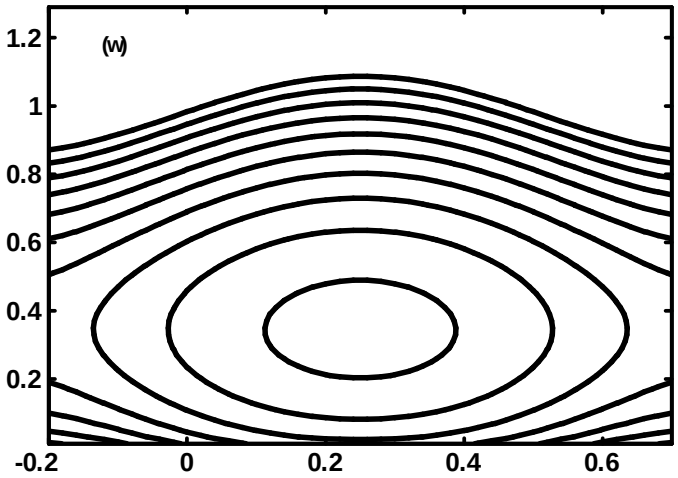

Figs. 8.11. Streamlines for different values of $Q = .92, .94$,(panels (v) to (w)) The other parameters are $\phi = 0.1$, $E_c = 0.9$, $\mathrm{Pr} = 0.1$, $\lambda_1 = 0.5$, $\Gamma_1 = 0.09$, $\varepsilon = 0.3$, $\mu_0 = 0.5, A = 1, B = 1, a = 0.1$.

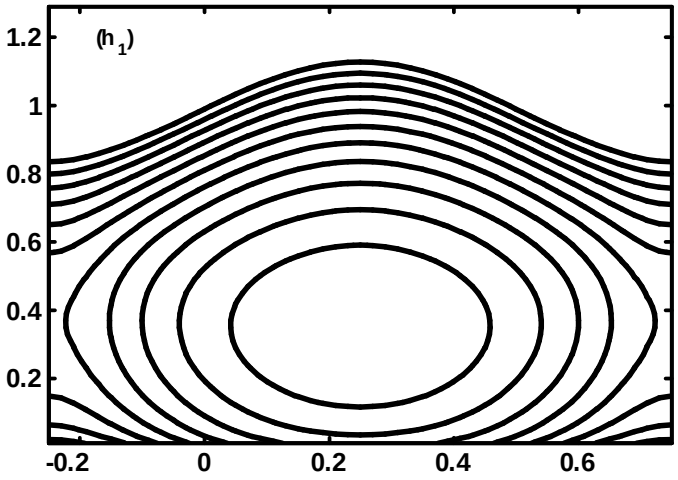

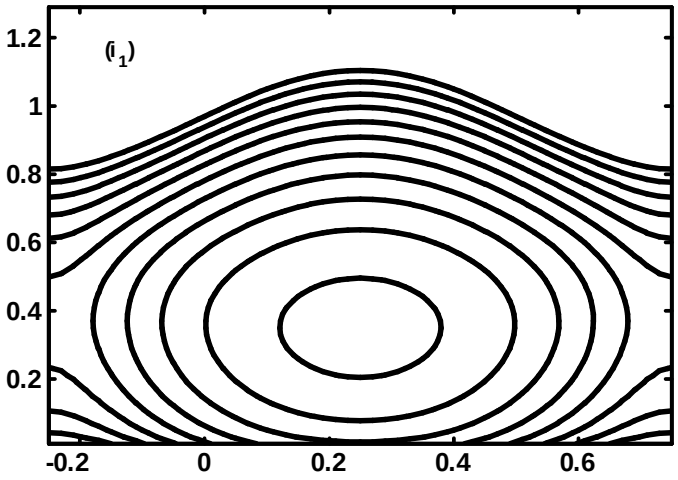

Figs. 8.12. Streamlines for different values of $\lambda_1 = 0.1,\ 0.2$,(panels (h_1) to (i_1)) The other parameters are $Q = 0.95$, $\phi = .15$, $E_c = 2$, $\Pr = 0.3$, $\Gamma_1 = 0.09$, $\varepsilon = 0.3$, $\mu_0 = 0.5, A = 1, B = 1, a = 0.1$.

8.8 Conclusion

Here we have analyzed the peristaltic flow of a Jeffrey fluid in an endoscope. The analytical and numerical solutions have been calculated for Vogel's viscosity models. A comparison of the analytical and numerical solution have also been given. The graphical results are presented to discuss the physical behavior of the problem. We have found the following observations:

1. The pressure rise decreases in peristaltic pumping region with an increase in λ_1 and Γ_1.

2. The frictions forces have an opposite results as compared to the pressure rise.

3. The temperature field increases with the increase in β and λ_1.

4. It is observed that the volume and size of the trapped bolus increases with increase in flow rate.

5. The volume and size of the trapped bolus decreases with the increase in Jeffrey parameter.

Chapter 9

Characteristics of heating scheme and mass transfer on the peristaltic flow for an Eyring-Powell fluid in an endoscope

9.1 Introduction

In this chapter Eyring-Powell peristaltic fluid flow with heat and mass transfer analysis have been investigated. New fluid model have been presented in peristaltic literature. The governing equations for proposed Eyring-Powell fluid model are derived in cylindrical coordinates both in fixed and moving frame of reference. Complex system of equations have been simplified using long wavelength and low Reynolds number approximation. The momentum and heat/mass transfer balance equations are solved analytically and numerically by employing perturbation method and shooting technique. Graphical results have been discussed for pressure rise, frictional forces, temperature and concentration profile. Comparison of perturbation and numerical solutions have been presented through table and figures. Five different waves forms have been considered for analysis. Trapping phenomena have been presented for different wave forms.

9.2 Mathematical Model

The constitutive equation for Eyring-Powell fluid model is given by [37]

$$\boldsymbol{\tau} = \mu\nabla\mathbf{V} + \frac{1}{\beta_1}\sinh^{-1}\left(\frac{1}{c_1}\nabla\mathbf{V}\right), \tag{9.1}$$

and

$$\sinh^{-1}\left(\frac{1}{c_1}\nabla\mathbf{V}\right) \approx \frac{1}{c_1}\nabla\mathbf{V} - \frac{1}{6}\left(\frac{1}{c_1}\nabla\mathbf{V}\right)^3, \qquad \left|\frac{1}{c_1}\nabla\mathbf{V}\right| \ll 1, \tag{9.2}$$

where μ is the coefficient of shear viscosity, β_1 and c_1 are the material constants of Eyring-Powell fluid model.

9.3 Mathematical Formulation

We have considered peristaltic flow of an incompressible Eyring-Powell fluid in an endoscope. The flow is generated by sinusoidal wave trains propagating with constant speed c along the wall of the upper tube. Heat and mass transfer phenomena have been consider giving temperature $\bar{T}_0$, $\bar{T}_1$ and concentration $\bar{C}_0$ and $\bar{C}_1$ to the inner and outer tube respectively. The geometry of the wall surfaces is defined in chapter two. The governing equations in the fixed frame for an incompressible flow are given as

$$\frac{\partial\bar{U}}{\partial\bar{R}} + \frac{\bar{U}}{\bar{R}} + \frac{\partial\bar{W}}{\partial\bar{Z}} = 0, \tag{9.3}$$

$$\rho\left(\frac{\partial}{\partial\bar{t}} + \bar{U}\frac{\partial}{\partial\bar{R}} + \bar{W}\frac{\partial}{\partial\bar{Z}}\right)\bar{U} = -\frac{\partial\bar{P}}{\partial\bar{R}} - \frac{1}{\bar{R}}\frac{\partial}{\partial\bar{R}}\left(\bar{R}\boldsymbol{\tau}_{\bar{R}\bar{R}}\right) - \frac{\partial}{\partial\bar{Z}}\left(\boldsymbol{\tau}_{\bar{R}\bar{Z}}\right) - \frac{\boldsymbol{\tau}_{\bar{\theta}\bar{\theta}}}{\bar{R}}, \tag{9.4}$$

$$\rho\left(\frac{\partial}{\partial\bar{t}} + \bar{U}\frac{\partial}{\partial\bar{R}} + \bar{W}\frac{\partial}{\partial\bar{Z}}\right)\bar{W} = -\frac{\partial\bar{P}}{\partial\bar{Z}} - \frac{1}{\bar{R}}\frac{\partial}{\partial\bar{R}}\left(\bar{R}\boldsymbol{\tau}_{\bar{R}\bar{Z}}\right) - \frac{\partial}{\partial\bar{Z}}\left(\boldsymbol{\tau}_{\bar{Z}\bar{Z}}\right), \tag{9.5}$$

$$\begin{aligned}\rho c_p\left(\frac{\partial}{\partial\bar{t}} + \bar{U}\frac{\partial}{\partial\bar{R}} + \bar{W}\frac{\partial}{\partial\bar{Z}}\right)\bar{T} &= \boldsymbol{\tau}_{\bar{R}\bar{R}}\frac{\partial\bar{U}}{\partial\bar{R}} + \boldsymbol{\tau}_{\bar{R}\bar{Z}}\frac{\partial\bar{W}}{\partial\bar{R}} + \boldsymbol{\tau}_{\bar{Z}\bar{R}}\frac{\partial\bar{U}}{\partial\bar{Z}} + \boldsymbol{\tau}_{\bar{Z}\bar{Z}}\frac{\partial\bar{W}}{\partial\bar{Z}} \\ &\quad + k\left(\frac{\partial^2\bar{T}}{\partial\bar{R}^2} + \frac{1}{\bar{R}}\frac{\partial\bar{T}}{\partial\bar{R}} + \frac{\partial^2\bar{T}}{\partial\bar{Z}^2}\right),\end{aligned} \tag{9.6}$$

$$\left(\frac{\partial}{\partial \bar{t}}+\bar{U}\frac{\partial}{\partial \bar{R}}+\bar{W}\frac{\partial}{\partial \bar{Z}}\right)\bar{C} = D\left(\frac{\partial^2 \bar{C}}{\partial \bar{R}^2}+\frac{1}{\bar{R}}\frac{\partial \bar{C}}{\partial \bar{R}}+\frac{\partial^2 \bar{C}}{\partial \bar{Z}^2}\right) + \frac{DK_T}{T_m}\left(\frac{\partial^2 \bar{T}}{\partial \bar{R}^2}+\frac{1}{\bar{R}}\frac{\partial \bar{T}}{\partial \bar{R}}+\frac{\partial^2 \bar{T}}{\partial \bar{Z}^2}\right). \tag{9.7}$$

We introduce the non-dimensional variables as follow

$$\begin{aligned}
R &= \frac{\bar{R}}{a_2},\ r=\frac{\bar{r}}{a_2},\ Z=\frac{\bar{Z}}{\lambda},\ z=\frac{\bar{z}}{\lambda},\ W=\frac{\bar{W}}{c},\ w=\frac{\bar{w}}{c},\ U=\frac{\lambda \bar{U}}{a_2 c},\\
u &= \frac{\lambda \bar{u}}{a_2 c}, P=\frac{a_2^2 \bar{P}}{c\lambda\mu},\ t=\frac{c_1 \bar{t}}{\lambda},\ \delta=\frac{a_2}{\lambda},\ \mathrm{Re}=\frac{\rho c_1 a_2}{\mu},\ \tau=\frac{a_2 \boldsymbol{\tau}}{\mu c},\\
S_c &= \frac{\mu}{D\rho},\ \theta=\frac{\left(\bar{T}-\bar{T}_1\right)}{\left(\bar{T}_0-\bar{T}_1\right)},\ S_r=\frac{\rho D K_T\left(\bar{T}_0-\bar{T}_1\right)}{\mu T_m\left(\bar{C}_0-\bar{C}_1\right)},\ P_r=\frac{\rho v c_p}{k},\\
E_c &= \frac{c^2}{c_p\left(\bar{T}_0-\bar{T}_1\right)},\ \sigma=\frac{\left(\bar{C}-\bar{C}_1\right)}{\left(\bar{C}_0-\bar{C}_1\right)},\ r_1=\frac{\bar{r}_1}{a_2}=\epsilon,\ r_2=\frac{\bar{r}_2}{a_2}.
\end{aligned} \tag{9.8}$$

With the help of Eqs. (1.11, 1.12) and (9.8), Eqs. (9.3) to (9.7) under the assumptions of long wavelength and low Reynolds number approximation take the form

$$\frac{\partial u}{\partial r}+\frac{u}{r}+\frac{\partial w}{\partial z}=0, \tag{9.9}$$

$$\frac{\partial P}{\partial r}=0, \tag{9.10}$$

$$\frac{\partial P}{\partial z}=\frac{1}{r}\frac{\partial}{\partial r}\left[r\left((1+M)\left(\frac{\partial w}{\partial r}\right)-K\left(\frac{\partial w}{\partial r}\right)^3\right)\right], \tag{9.11}$$

$$\frac{\partial^2 \theta}{\partial r^2}+\frac{1}{r}\frac{\partial \theta}{\partial r}=-B_r\left(\left((1+M)\left(\frac{\partial w}{\partial r}\right)^2-K\left(\frac{\partial w}{\partial r}\right)^4\right)\right), \tag{9.12}$$

$$0=\frac{1}{S_c}\left(\frac{1}{r}\frac{\partial}{\partial r}\left(r\frac{\partial \sigma}{\partial r}\right)\right)+S_r\left(\frac{1}{r}\frac{\partial}{\partial r}\left(r\frac{\partial \theta}{\partial r}\right)\right). \tag{9.13}$$

In the above equations δ and Re represent the wave and Reynolds numbers, respectively and

$$M=1/\mu_1\beta c_1 \text{ and } N=Mc_1^2/6a^2c_1^2,$$

where M and N are the dimensionless parameter of Eyring-Powell fluid model.

The corresponding boundary conditions are

$$w = -1,\ \theta = 1,\ \sigma = 1 \text{ at } r = r_1 = \varepsilon, \tag{9.14a}$$

$$w = -1,\ \theta = 0,\ \sigma = 0,\ \text{at } r = r_2 = 1 + \phi \sin(2\pi z). \tag{9.14b}$$

9.4 Solution of the Problem

9.4.1 Perturbation Solution

Since Eqs. (9.11) to (9.13) are non-linear equation therefore we are interested in analytical solutions with the help of perturbation method. For perturbation solution, we expand w, F, θ and P by taking N as perturbation parameter

$$w = w_0 + Nw_1 + O(N^2), \tag{9.15a}$$

$$P = P_0 + NP_1 + O(N^2), \tag{9.15b}$$

$$F_1 = F_{10} + NF_{11} + O(N^2), \tag{9.15c}$$

$$\theta = \theta_0 + N\theta_1 + O(N^2). \tag{9.15d}$$

The perturbation results for small parameter N, satisfying the conditions (9.14a) and (9.14b), the expression for velocity, temperature, concentration field and pressure gradient can be written as

$$\begin{aligned} w(r,z) = {} & -1 + \left(\frac{r^2}{4(1+M)} + \frac{E_1 \ln r}{(1+M)} + E_2\right)\frac{dP}{dz} + N\left(\frac{1}{(1+M)^4}\left(\frac{r^4}{32} - \frac{E_1^3}{2r^2}\right.\right. \\ & \left.\left. + \frac{3E_1 r^2}{8} + \frac{3E_1 \ln r}{2}\right) + \frac{E_3 \ln r}{(1+M)} + E_4\right), \end{aligned} \tag{9.16}$$

$$\frac{dP}{dz} = \frac{F_1 + (r_2^2 - r_1^2) + N(-E_6)}{E_5}, \tag{9.17}$$

$$\begin{aligned}\theta(r,z) &= -B_r\left(\frac{1}{(1+M)}\left(\frac{r^4}{64}+E_1^2\left(\frac{r^2\ln r}{2}-\frac{r^2}{4}\right)+\frac{E_1 r^2}{4}\right)\left(\frac{dP}{dz}\right)^2+E_7\ln r+E_8\right)\\ &+N\left(\frac{1}{36864(1+M)^7 r^4}\left(-B_r(2304E_1^6-9216E_1^3(-2E_3(1+M)^3+E_1(-2\right.\right.\\ &+M(3+M)))))r^2+2304E_1(E_1^2+6E_3(1+M)^3-3E_1(-1+2M(3+M+\\ &(3+M))))r^6+144(9E_1^2+4E_3 1+M)^3-2E_1(1+4M(3+M(3+M))))r^8\\ &+64(3E_1-(1+M)^3)r^{10}+9r^{12}+4608(9E_1^2+6E_1^4-8E_1^3(1+M)^3\\ &\left.\left.+12E_1E_3(1+M)^3+8E_3^2(1+M)^6)\frac{r^4(\ln r)^2}{2})+E_9\ln r+E_{10}\right)\right), \qquad (9.18)\end{aligned}$$

$$\begin{aligned}\sigma(r,z) &= S_r S_c\left(B_r\left(\frac{1}{(1+M)}\left(\frac{r^4}{64}+E_1^2\left(\frac{r^2\ln r}{2}-\frac{r^2}{4}\right)+\frac{E_1 r^2}{4}\right)\left(\frac{dP}{dz}\right)^2+E_7\ln r+E_8\right)\right.\\ &+N\left(\frac{1}{36864(1+M)^7 r^4}\left(-B_r(2304E_1^6-9216E_1^3(-2E_3(1+M)^3+E_1(-2\right.\right.\\ &+M(3+M)))))r^2+2304E_1(E_1^2+6E_3(1+M)^3-3E_1(-1+2M(3+M+\\ &(3+M))))r^6+144(9E_1^2+4E_3 1+M)^3-2E_1(1+4M(3+M(3+M))))r^8\\ &+64(3E_1-(1+M)^3)r^{10}+9r^{12}+4608(9E_1^2+6E_1^4-8E_1^3(1+M)^3\\ &\left.\left.\left.+12E_1E_3(1+M)^3+8E_3^2(1+M)^6)\frac{r^4(\ln r)^2}{2})+E_9\ln r+E_{10}\right)\right)\right), \qquad (9.20)\end{aligned}$$

where the involved constants (E_1 to E_{10}) have been evaluated using Mathematica.

The corresponding stream function can be defined as

$$\left(u=-\frac{1}{r}\frac{\partial\Psi}{\partial z}\quad\text{and}\quad w=\frac{1}{r}\frac{\partial\Psi}{\partial r}\right). \qquad (9.21)$$

The pressure rise ΔP and friction forces F on inner and outer tubes $F^{(0)}$, $F^{(i)}$, are given by

$$\Delta P=\int_0^1\frac{dP}{dz}dz, \qquad (9.22)$$

$$F^{(0)}=\int_0^1 r_1^2\left(-\frac{dP}{dz}\right)dz, \qquad (9.23)$$

$$F^{(i)} = \int_0^1 r_2^2 \left(-\frac{dP}{dz}\right) dz. \tag{9.24}$$

where $\frac{dP}{dz}$ is defined in Eq. (9.21).

For analysis, we have considered five waveforms namely sinusoidal, multi-sinusoidal, triangular, square and trapezoidal. The non-dimensional expressions for these wave forms are defined in chapter 1.

1. Sinusoidal wave:

$$r_2(z) = 1 + \phi \sin(2\pi z)$$

2. Triangular wave:

$$r_2(z) = 1 + \phi \left\{ \frac{8}{\pi^3} \sum_{n=1}^{\infty} \frac{(-1)^{n+1}}{(2n-1)} \sin(2\pi (2n-1) z) \right\}$$

3. Square wave:

$$r_2(z) = 1 + \phi \left\{ \frac{4}{\pi} \sum_{n=1}^{\infty} \frac{(-1)^{n+1}}{(2n-1)} \cos(2\pi (2n-1) z) \right\}$$

4. Trapezoidal wave:

$$r_2(z) = 1 + \phi \left\{ \frac{32}{\pi^2} \sum_{n=1}^{\infty} \frac{\sin\frac{\pi}{8}(2n-1)}{(2n-1)^2} \sin(2\pi (2n-1) z) \right\}$$

5. Multi sinusoidal wave:

$$r_2(z) = 1 + \phi \sin(2m\pi z).$$

9.4.2 Numerical Solution

Here we have presented the numerical solutions for velocity profile. To get the numerical solution shooting method have been taken into account. The numerical solution is also compared with the perturbation solution. The difference between the values of two solutions are shown through Figs. $9.1(a)$, $9.1(b)$ and table 9.1. It is noticed here that there is a small difference between perturbation and numerical solution. This happens because the perturbation solutions are computed here only small values of N. If one take the value of N very very small both the

solutions are 100% same which are shown in tabel 1. However, for large N, the solutions are not identical, because the perturbation solutions are valid for small values of N.

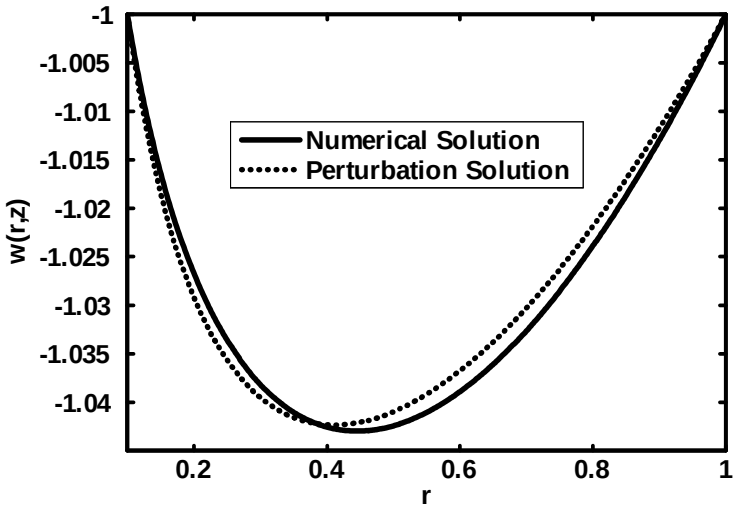

Fig.9.1 (a). Comparison of axial velocity for $N = 0.1$, $\phi = 0.4, \epsilon = 0.1, z = 0.5,\ M = 0.5$.

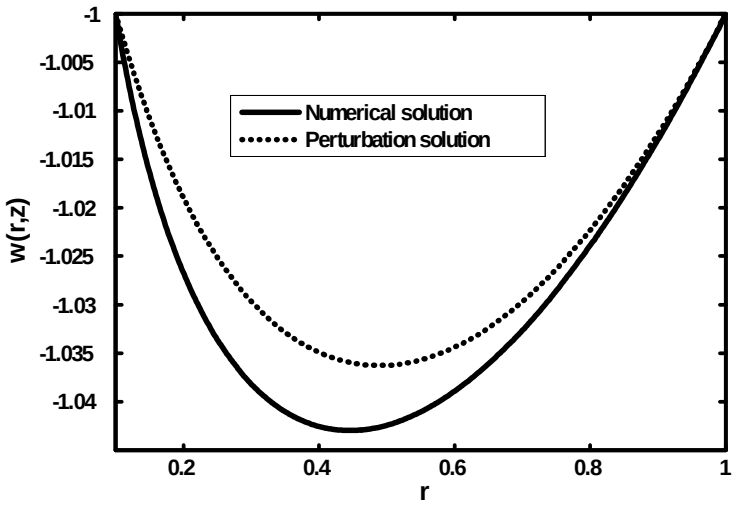

Fig.9.1 (b). Comparison of axial velocity when $N = 0.5$, $\phi = 0.4, \epsilon = 0.1, \frac{dp}{dz} = 0.4, z = 0.5,\ M = 0.5$.

r	Numerical Sol when ($N = 0.1$)	Perturb Sol	Numerical Sol when ($N = 0.5$)	Perturb Sol
0.10	−1.000000	−1.000000	−1.000000	−1.000000
0.15	−1.013079	−1.014210	−1.016465	−1.010710
0.20	−1.020100	−1.021160	−1.029170	−1.018960
0.25	−1.026625	−1.030789	−1.037464	−1.025111
0.30	−1.030679	−1.031621	−1.042150	−1.031621
0.35	−1.045808	−1.038601	−1.045808	−1.035891
0.40	−1.036289	−1.040463	−1.047766	−1.038451
0.45	−1.037758	−1.041561	−1.048315	−1.039621
0.50	−1.038221	−1.041632	−1.048003	−1.037822
0.55	−1.037908	−1.040785	−1.046604	−1.038521
0.60	−1.036671	−1.037642	−1.044183	−1.037642
0.65	−1.034967	−1.036805	−1.041439	−1.029661
0.70	−1.032094	−1.033389	−1.037320	−1.028631
0.75	−1.029015	−1.029900	−1.033230	−1.025292
0.80	−1.024494	−1.024958	−1.027559	−1.022292
0.85	−1.020031	−1.020021	−1.022216	−1.018654
0.90	−1.013829	−1.014380	−1.015081	−1.014380
0.95	−1.007942	−1.007858	−1.007172	−1.006592
1.00	−1.000000	−1.000000	−1.000000	−1.000000

Table.9.1. Comparison of axial velocity for perturbation and numerical solutions when (a) $N = 0.1$, (b) $N = 0.5$, other parameters are $\phi = 0.4, \epsilon = 0.1,\ z = 0.5,\ M = 0.5$.

9.5 Graphical Discussion

To see the variations in pressure rise, frictional force, pressure gradient and streamlines caused by the amplitude ratio ϕ, Eyring-Powell fluid parameters N and M, we have prepared Figs. (9.2 to 9.7). Figs. 9.2 to 9.5 show the variation of pressure versus flow rate for different parameters of interest. We observed that the increase in the values of ϕ and M causes the increase in pressure rise while with the increase in N causes the decrease in pressure rise. It is also analyzed through

Fig. 9.5 (a) that triangular wave has best peristaltic pumping characteristics, while square wave has worst peristaltic pumping characteristics as compared to the other waves. Moreover, the peristaltic pumping occurs in the region $-2 \leq Q \leq 0.5$, and augmented pumping occurs in the region $0.51 \leq Q \leq 2$. The variations of frictional forces are plotted in Figs. 9.6 to 9.10. It can be seen that frictional forces have opposite behavior as compared to the pressure rise. Figs. 9.11 (a) to 9.11 (e) are prepared to see the variation of pressure gradient for different wave shapes. It is observed from the figures that for $z\epsilon\,[0, 0.5]$ and $[1.1, 1.5]$, the pressure gradient is small and large pressure gradient occurs for $z\epsilon\,[0.51, 1]$. Moreover, it is seen that with increase in ϕ pressure gradient increases. The effects of different parameters on streamlines for the trapping phenomenon for five different wave forms can be seen through Figs. 9.12 (a) to 9.12 (e). It is observed that the size of trapping bolus in triangular wave is smaller as compared to the other waves. Temperature profile have been plotted in Figs. 9.13 (a) and 9.13 (b). It have been analyzed through figures that temperature profile decreases with an increase in N, while increases with an increase in B_r. Figs. 9.14 (a) and 9.14 (b) are display for concentration profile. It is analyzed that with an increase in B_r and S_r concentration profile decreases.

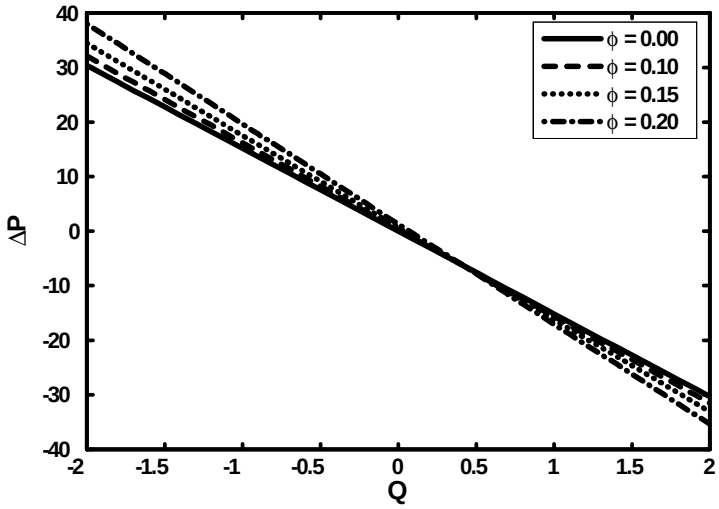

Figs.9.2. Pressure rise versus flow rate for $\epsilon = 0.05$, $r_1 = 0.05$, $N = 0.1$, $M = 5$.

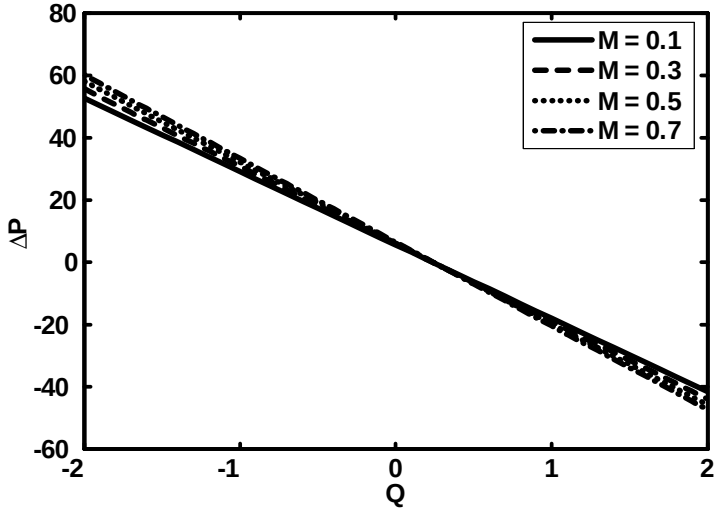

Figs.9.3. Pressure rise versus flow rate for $\epsilon = 0.05$, $r_1 = 0.05$, $N = 0.1$, $\phi = 0.4$.

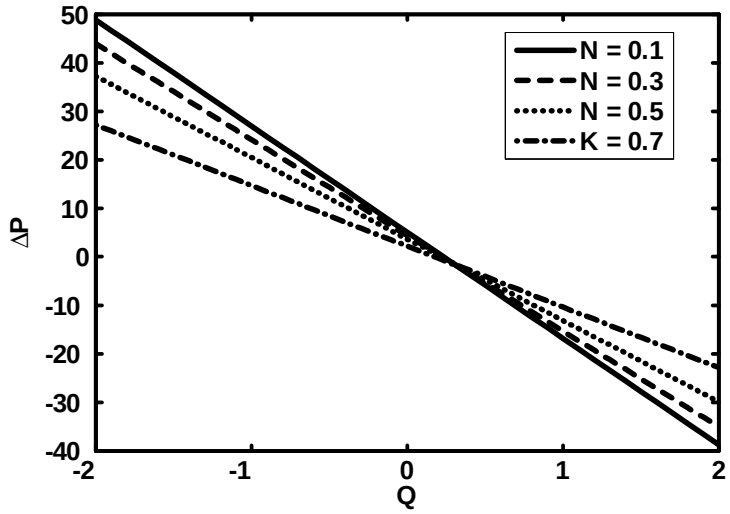

Figs.9.4. Pressure rise versus flow rate for $\epsilon = 0.05$, $r_1 = 0.05$, $M = 5$, $\phi = 0.4$.

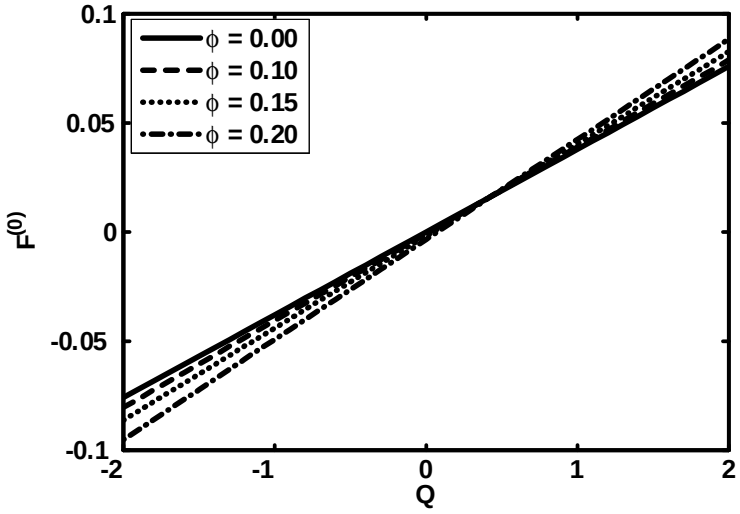

Figs.9.5. Frictional force for inner tube versus flow rate for $\epsilon = 0.05$, $r_1 = 0.05$, $N = 0.1$, $M = 5$.

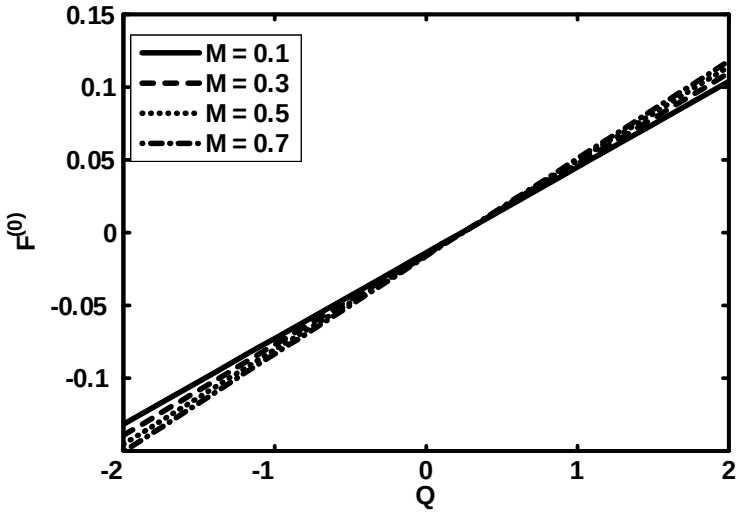

Figs.9.6. Frictional force for inner tube versus flow rate for $\epsilon = 0.05$, $r_1 = 0.05$, $N = 0.1$, $\phi = 0.4$.

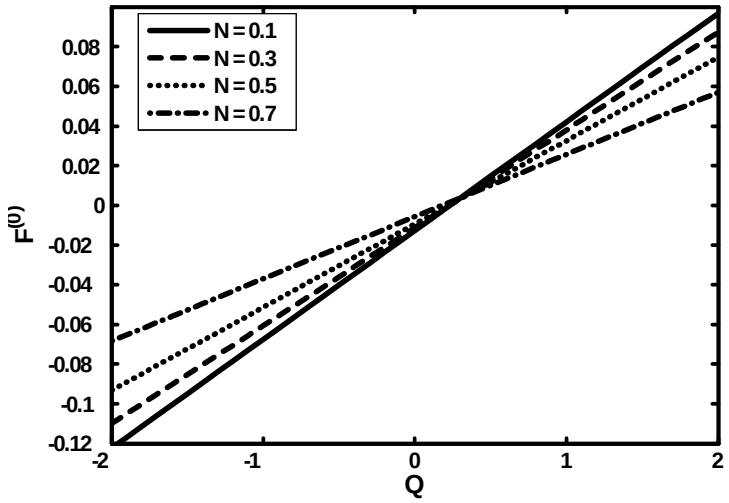

Figs.9.7. Frictional force for inner tube versus flow rate for $\epsilon = 0.05$, $r_1 = 0.05$, $M = 5$, $\phi = 0.4$.

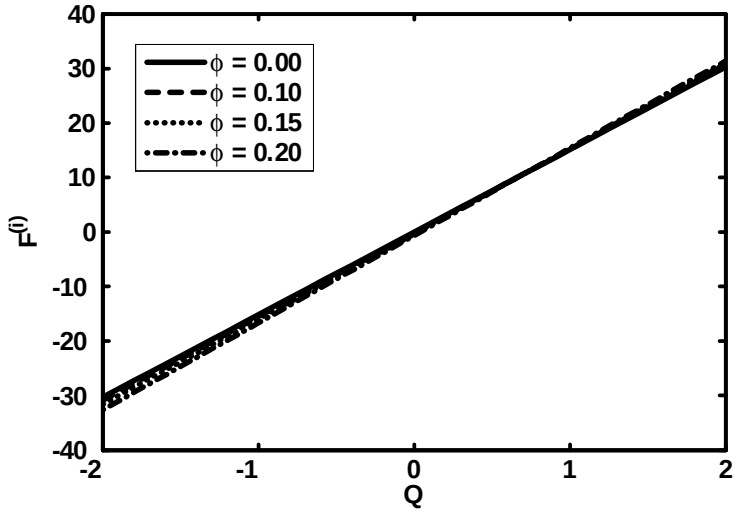

Figs.9.8. Frictional force for outer tube versus flow rate for $\epsilon = 0.05$, $r_1 = 0.05$, $N = 0.1$, $M = 5$.

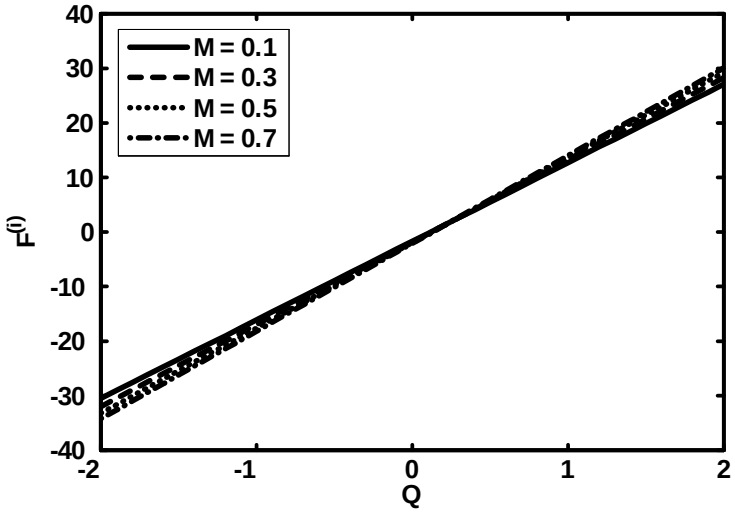

Figs.9.9. Frictional force for outer tube versus flow rate for $\epsilon = 0.05$, $r_1 = 0.05$, $N = 0.1$, $\phi = 0.4$.

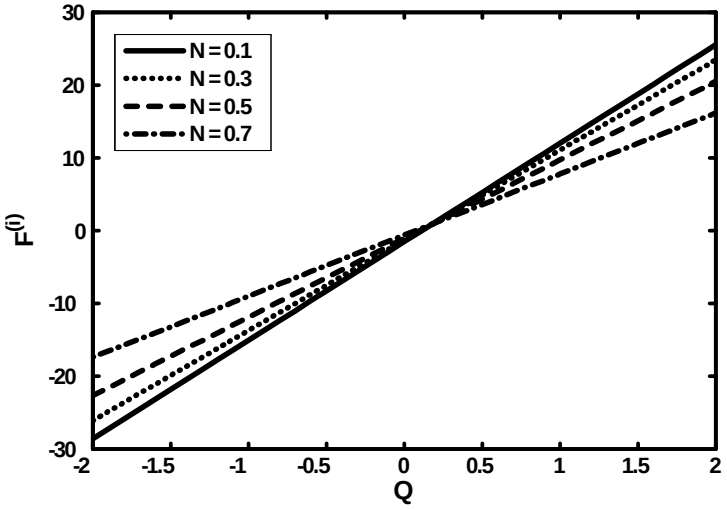

Figs.9.10. Frictional force for outer tube versus flow rate for $\epsilon = 0.05$, $r_1 = 0.05$, $M = 5$, $\phi = 0.4$.

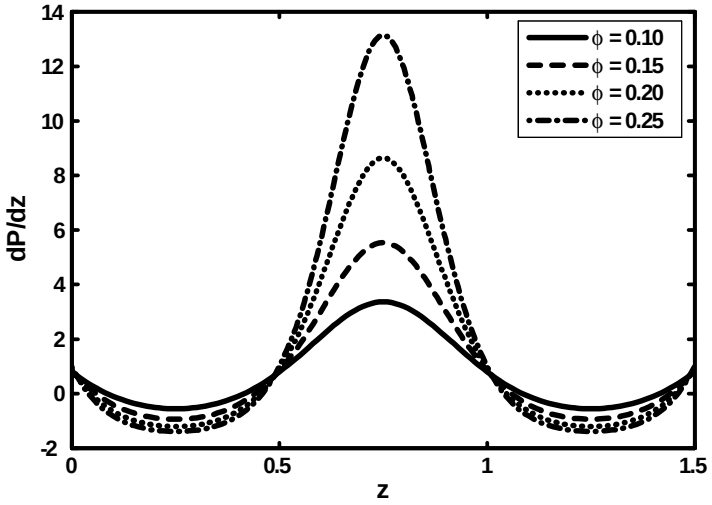

Fig.9.11 (a). Pressure gradient versus z for Sinusoidal wave for $\epsilon = 0.05$, $r_1 = 0.05$, $M = 5$, $Q = -0.05$, $N = 0.1$.

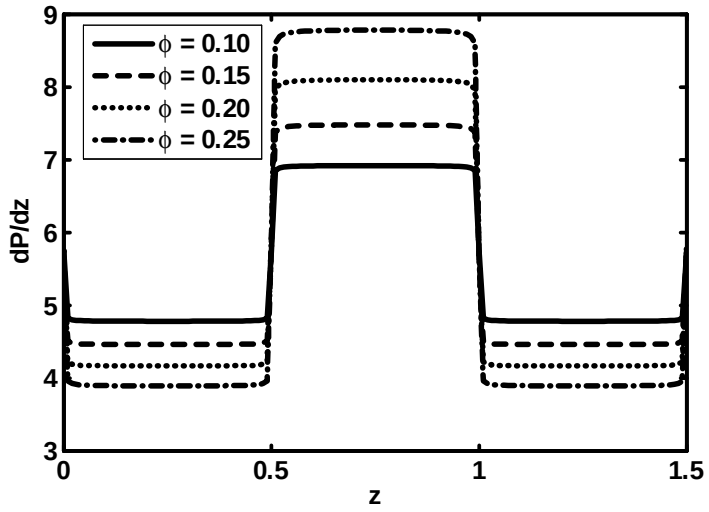

Fig.9.11 (b). Pressure gradient versus z for Square wave for $\epsilon = 0.05$, $r_1 = 0.05$, $M = 5$, $Q = -0.05$, $N = 0.1$.

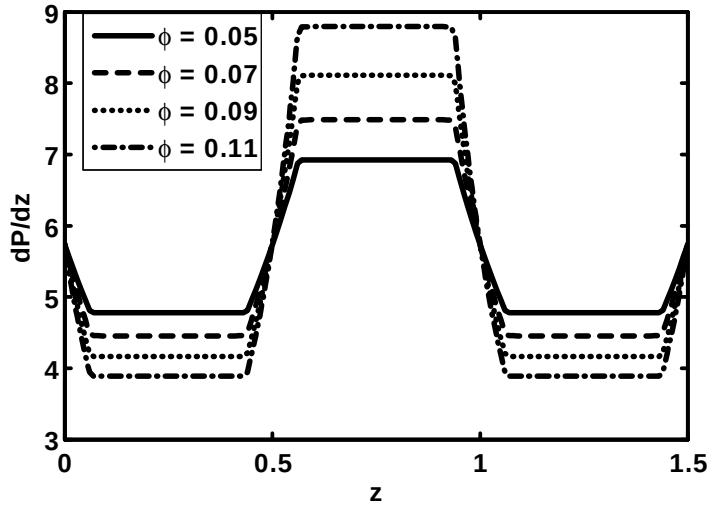

Fig.9.11 (c). Pressure gradient versus z for trapezoidal wave for $\epsilon = 0.05$, $r_1 = 0.05$, $M = 5$, $Q = -0.05$, $N = 0.1$.

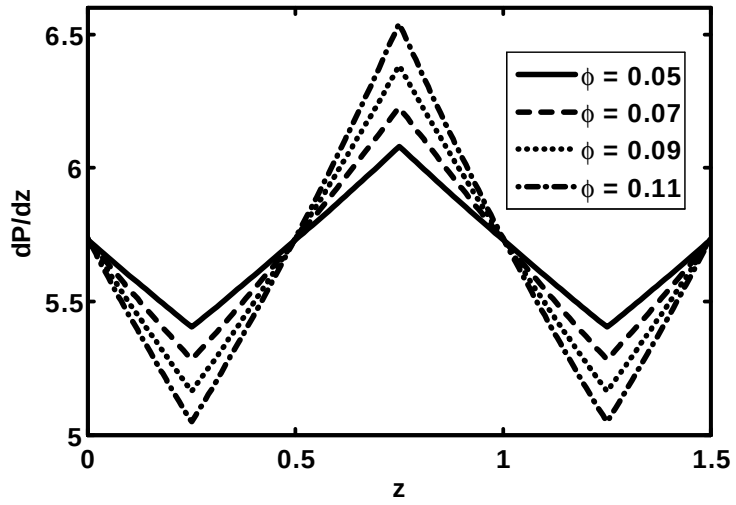

Fig.9.11 (d). Pressure gradient versus z for Triangular wave for $\epsilon = 0.05$, $r_1 = 0.05$, $M = 5$, $Q = -0.05$, $N = 0.1$.

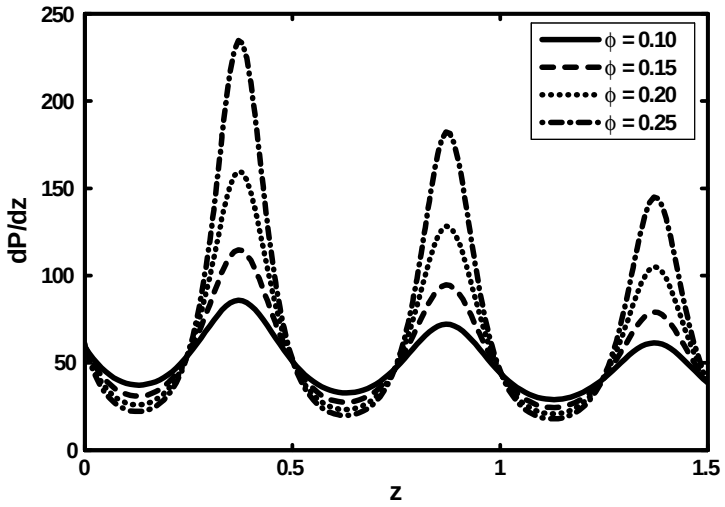

Fig.9.11 (e). Pressure gradient versus z for Multsinusoidal wave for $\epsilon = 0.05$, $r_1 = 0.05$, $M = 5$, $Q = -0.05$, $N = 0.1$.

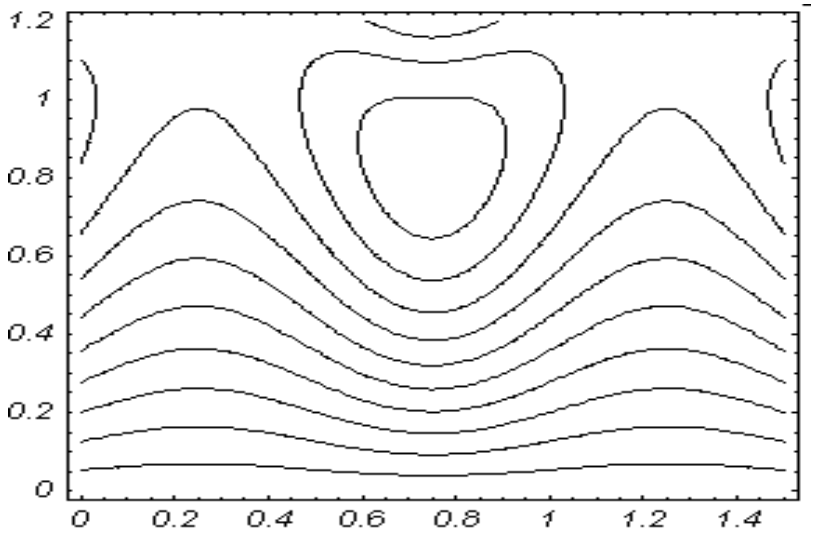

Fig.9.12 (a). Streamlines for sinusoidal wave when $\epsilon = 0.05$, $r_1 = 0.05$, $M = 5$, $Q = -0.05$, $N = 0.1$.

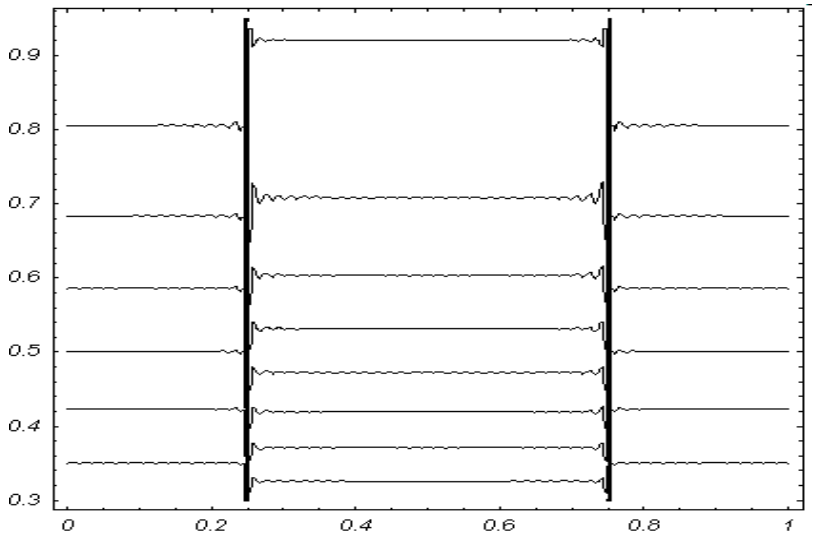

Fig.9.12 (b). Streamlines for square wave when $\epsilon = 0.05$, $r_1 = 0.05$, $M = 5$, $Q = -0.05$, $N = 0.1$.

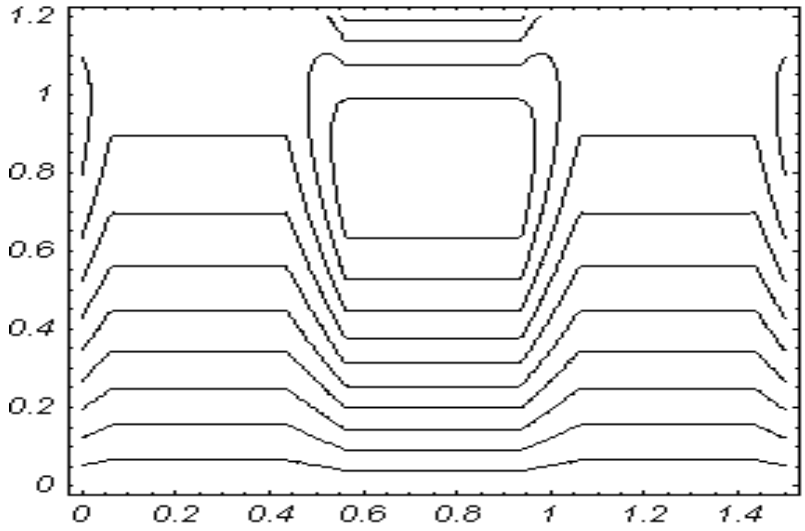

Fig.9.12 (c). Streamlines for trapezoidal wave when $\epsilon = 0.05$, $r_1 = 0.05$, $M = 5$, $Q = -0.05$, $N = 0.1$.

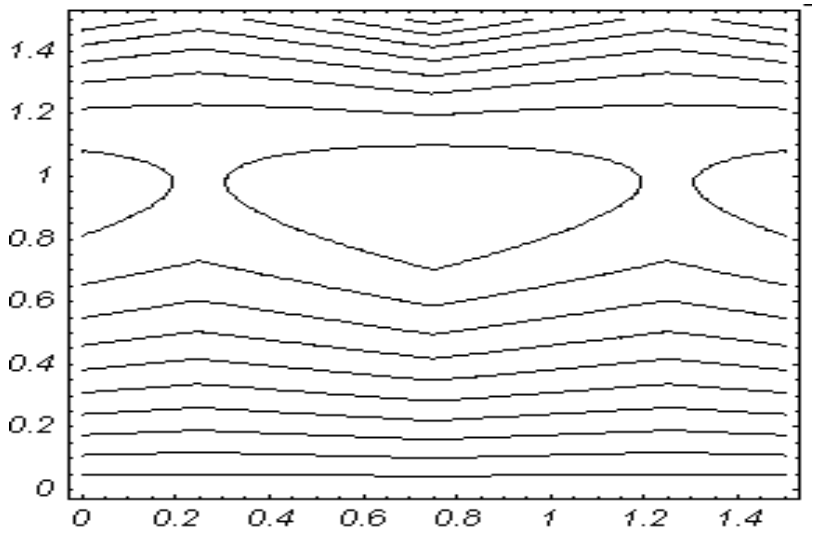

Fig.9.12 (d). Streamlines for triangular wave when $\epsilon = 0.05$, $r_1 = 0.05$, $M = 5$, $Q = -0.05$, $N = 0.1$.

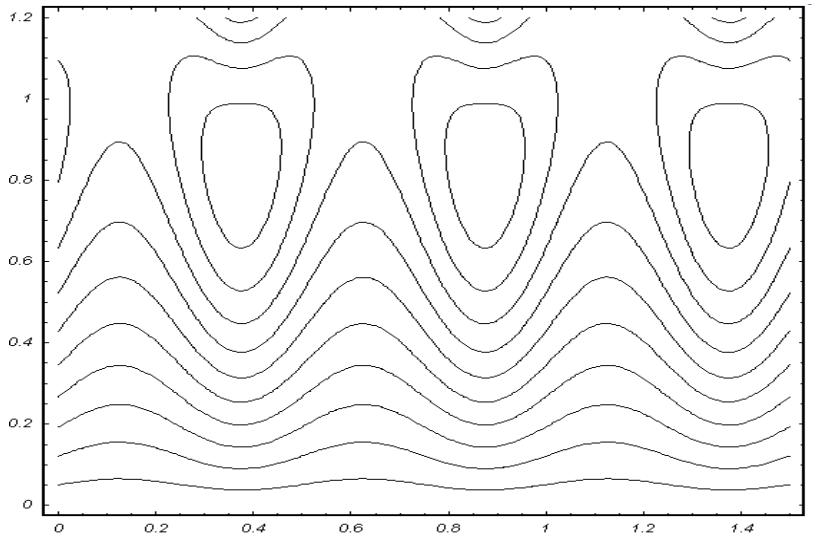

Fig.9.12 (e). Streamlines for multisinusoidal wave when $\epsilon = 0.05$, $r_1 = 0.05$, $M = 5$, $Q = -0.05$, $N = 0.1$.

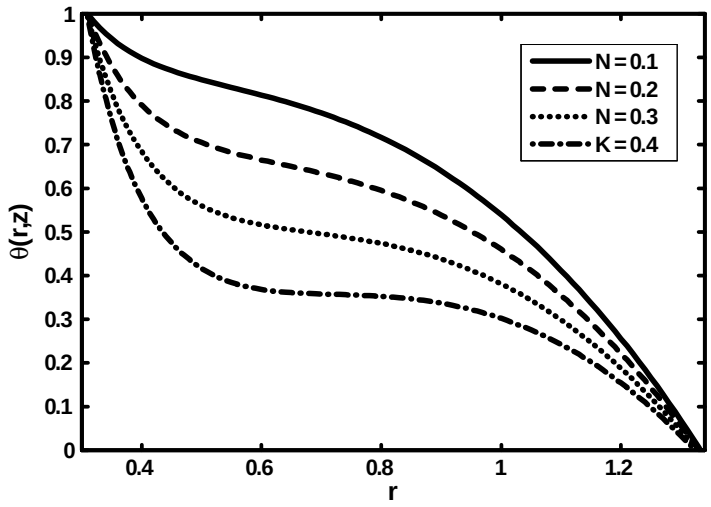

Fig.9.13 (a). Temperature profile for $B_r = 0.5$, $\epsilon = 0.3$, $r_1 = 0.3$, $M = 5$, $Q = 1$, $\phi = 0.9$, $z = 0.1$, $N = 0.1$.

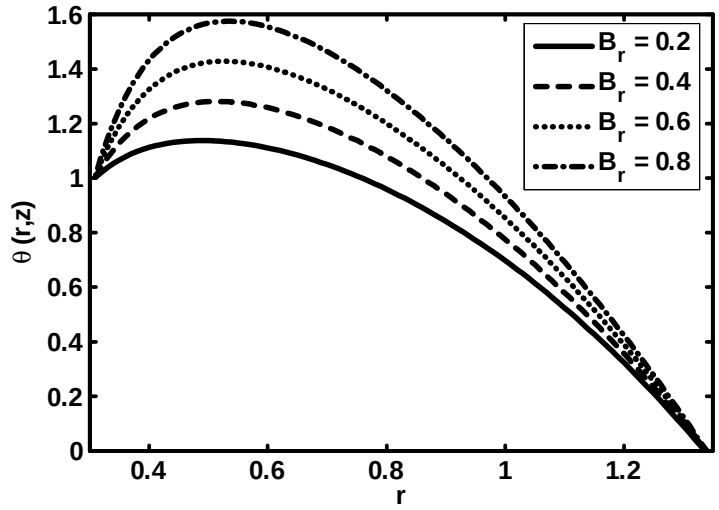

Fig.9.13 (b). Temperature profile for $N = 0.3$, $\epsilon = 0.3$, $r_1 = 0.3$, $M = 5$, $Q = 1$, $\phi = 0.9$, $z = 0.1$.

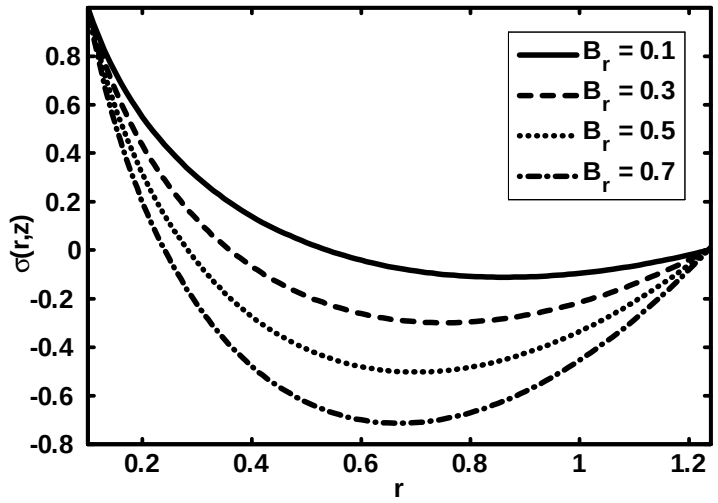

Fig.9.14 (a). Concentration profile for $S_r = 0.5$, $\epsilon = 0.1$, $r_1 = 0.1$, $N = 0.4$, $M = 5$, $Q = 1$, $\phi = 0.9$, $z = 0.1$, $N = 0.1$.

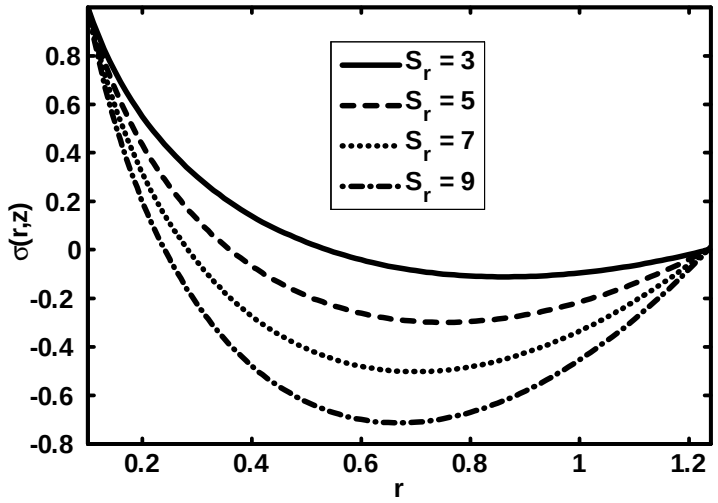

Fig.9.14 (b). Concentration profile for $B_r = 0.3$, $\epsilon = 0.1$, $r_1 = 0.1$, $M = 5$, $Q = 1$, $\phi = 0.9$, $z = 0.1$, $N = 0.1$.

9.6 Conclusions

This study examines the influence of heat and mass transfer on the peristaltic flow of a Eyring-Powell fluid in an endoscope. Analytical and numerical solutions have been evaluated using regular perturbation and shooting technique. The main points of the performed analysis are as follows.

1. Perturbation and numerical solutions are in good agreement for small N.
2. The effects of ϕ and M on the pressure rise are same.
3. Pressure rise decreases with an increase in N.
4. The frictional forces have an opposite behaviour as compared to the pressure rise.
5. The triangular wave has best peristaltic pumping characteristics, while square wave has worst peristaltic pumping characteristics as compared to the other waves.
6. Pressure gradient increases with an increase in ϕ. It is also observed that for $z\epsilon\,[0, 0.5]$ and $[1.1, 1.5]$ the pressure gradient is small and large pressure gradient occurs for $z\epsilon\,[0.51, 1]$.
7. The size of trapped bolus for triangular wave is small as compared to the other waves.
8. Temperature profile has opposite behaviour for B_r and N.
9. Concentration profile decreases with an increase in B_r and S_r.

Chapter 10

Simulation of heat transfer on the peristaltic flow of a Jeffrey-six constant fluid in a diverging tube

10.1 Introduction

Here peristaltic flow of a Jeffrey-six constant fluid in a non uniform tube is investigated under the assumption of longwavelength and low Reynolds number approximations. The dimensionless quantities are used to simplify momentum and energy equations assuming that fluid physical/rheological properties remain constant. Regular perturbation method is invoked to find an analytical solution for the velocity and temperature field. The variation of pressure rise and frictional forces with the different parameter are also examined numerically. Results are also presented graphically at the end of the chapter.

10.2 Mathematical Model

The constitutive equation for a six-constant Jeffreys fluid model is given by [31]

$$\begin{aligned} &\bar{\tau}+\bar{\lambda}_{\mathbf{1}}\left[\frac{d\bar{\boldsymbol{\tau}}}{dt}-\bar{W}_1.\bar{\tau}+\bar{\tau}.\bar{W}_1+d\left(\bar{\tau}.\bar{D}+\bar{D}.\bar{\boldsymbol{\tau}}\right)+b_1\left(\bar{\boldsymbol{\tau}}.\bar{D}\right)\mathbf{I}+c_2\bar{D}tr\bar{\tau}\right] \\ = \;& 2\mu\left[D+\bar{\lambda}_{\mathbf{2}}\left(\frac{d\bar{D}}{dt}-\bar{W}_1.\bar{D}+\bar{D}.\bar{W}_1+2d\bar{D}.\bar{D}+b_1\left(\bar{D}.\bar{D}\right)\mathbf{I}\right)\right] \end{aligned} \tag{10.1}$$

where

$$\bar{D}\,(\text{symmetric part of velocity gradient}) = \frac{\nabla\bar{V}+(\nabla\bar{V})^T}{2},$$

$$\bar{W}_1\,(\text{antisymmetric part of velocity gradient}) = \frac{\nabla\bar{V}-(\nabla\bar{V})^T}{2},$$

d, b_1, c_2 are material constant of a six-constant Jeffreys fluid model, $\bar{\lambda}_{\mathbf{1}}$ is the relaxation time $\bar{\lambda}_{\mathbf{2}}$ is the delay time.

10.3 Mathematical Formulation

We have considered peristaltic flow of an incompressible Jeffrey-six constant fluid in a non uniform tube. The flow is generated by sinusoidal wave trains propagating with constant speed c along the walls of the tube. The upper wall of the tube is maintaining at temperature $\bar{T}_0$ and at the centre we have used symmetry condition on temperature. The geometry of the wall surface is defined in Eq. (5.8)

The governing equations in the fixed frame for an incompressible flow are given as

$$\frac{\partial\bar{U}}{\partial\bar{R}}+\frac{\bar{U}}{\bar{R}}+\frac{\partial\bar{W}}{\partial\bar{Z}}=0, \tag{10.1}$$

$$\rho\left(\frac{\partial}{\partial\bar{t}}+\bar{U}\frac{\partial}{\partial\bar{R}}+\bar{W}\frac{\partial}{\partial\bar{Z}}\right)\bar{U}=-\frac{\partial\bar{P}}{\partial\bar{R}}+\frac{1}{\bar{R}}\frac{\partial}{\partial\bar{R}}\left(\bar{R}\boldsymbol{\tau}_{\bar{R}\bar{R}}\right)+\frac{\partial}{\partial\bar{Z}}\left(\boldsymbol{\tau}_{\bar{R}\bar{Z}}\right)+\frac{\boldsymbol{\tau}_{\bar{\theta}\bar{\theta}}}{\bar{R}}, \tag{10.2}$$

$$\rho\left(\frac{\partial}{\partial\bar{t}}+\bar{U}\frac{\partial}{\partial\bar{R}}+\bar{W}\frac{\partial}{\partial\bar{Z}}\right)\bar{W}=-\frac{\partial\bar{P}}{\partial\bar{Z}}+\frac{1}{\bar{R}}\frac{\partial}{\partial\bar{R}}\left(\bar{R}\boldsymbol{\tau}_{\bar{R}\bar{Z}}\right)+\frac{\partial}{\partial\bar{Z}}\left(\boldsymbol{\tau}_{\bar{Z}\bar{Z}}\right), \tag{10.3}$$

$$\rho c_p\left(\frac{\partial}{\partial \bar{t}}+\bar{U}\frac{\partial}{\partial \bar{R}}+\bar{W}\frac{\partial}{\partial \bar{Z}}\right)\bar{T} = \boldsymbol{\tau}_{\bar{R}\bar{R}}\frac{\partial \bar{U}}{\partial \bar{R}}+\boldsymbol{\tau}_{\bar{R}\bar{Z}}\frac{\partial \bar{W}}{\partial \bar{R}}+\boldsymbol{\tau}_{\bar{Z}\bar{R}}\frac{\partial \bar{U}}{\partial \bar{Z}}+\boldsymbol{\tau}_{\bar{Z}\bar{Z}}\frac{\partial \bar{W}}{\partial \bar{Z}} + k\left(\frac{\partial^2 \bar{\boldsymbol{\tau}}}{\partial \bar{R}^2}+\frac{1}{\bar{R}}\frac{\partial \bar{\boldsymbol{\tau}}}{\partial \bar{R}}+\frac{\partial^2 \bar{\boldsymbol{\tau}}}{\partial \bar{Z}^2}\right). \tag{10.4}$$

We introduce the non-dimensional variables as follow

$$\begin{aligned} R &= \frac{\bar{R}}{a},\ r=\frac{\bar{r}}{a},\quad Z=\frac{\bar{Z}}{\lambda},\quad z=\frac{\bar{z}}{\lambda},\ W=\frac{\bar{W}}{c},\ w=\frac{\bar{w}}{c},\ \tau=\frac{a\boldsymbol{\tau}}{c\mu} \\ U &= \frac{\lambda \bar{U}}{ac},\ u=\frac{\lambda \bar{u}}{ac},\ P=\frac{a^2\bar{P}}{c\lambda\mu},\ t=\frac{c\bar{t}}{\lambda},\quad \delta=\frac{a}{\lambda}, \mathrm{Re}=\frac{\rho c a}{\mu}, \\ h &= \frac{\bar{h}}{a}=1+\frac{\lambda K z}{a_0}+\phi\sin 2\pi z,\ \lambda_1=\frac{\lambda_1 c}{a},\ \lambda_2=\frac{\bar{\lambda}_2 c}{a}, \\ E_c &= \frac{c^2}{c_p\bar{T}_0},\ \theta=\frac{\left(\bar{T}-\bar{T}_0\right)}{\bar{T}_0},\quad \mathrm{Pr}=\frac{\mu c_p}{k}. \end{aligned} \tag{10.5}$$

Making use of Eqs. (1.11, 1.12) and (10.5), Eqs. (10.1) to (10.4) under the assumptions of long wavelength $\delta << 1$ and low Reynolds number take the form

$$0=-\frac{\partial P}{\partial z}+\frac{1}{r}\frac{\partial}{\partial r}\left(r\tau_{rz}\right), \tag{10.6}$$

$$\frac{\partial P}{\partial r}=0, \tag{10.7}$$

$$\frac{1}{r}\frac{\partial}{\partial r}\left(r\frac{\partial \theta}{\partial r}\right)=-B_r\left(\frac{\partial w}{\partial r}\tau_{rz}\right), \tag{10.8}$$

$$\frac{\partial w}{\partial r} = 0,\ \frac{\partial \theta}{\partial r}=0 \ \text{ at } \quad r=0, \tag{10.9a}$$

$$w = 0,\ \theta=0 \ \text{ at } \quad r=h=1+\frac{\lambda K z}{a_0}+\phi\sin 2\pi z. \tag{10.9b}$$

where

$$\begin{aligned}
\tau_{rz} &= \frac{\frac{\partial w}{\partial r}\left[1+\lambda_1\lambda_2\left(1-d\left(d+b_2\right)-\frac{c_2}{2}\left(2d+3b_2\right)\right)\left(\frac{\partial w}{\partial r}\right)^2\right]}{\left[1+\lambda_1^2\left(1-d\left(d+b_2\right)-\frac{c_2}{2}\left(2d+3b_2\right)\right)\left(\frac{\partial w}{\partial r}\right)^2\right]},\\
\tau_{rr} &= \lambda_2\left(\frac{\partial w}{\partial r}\right)^2\left(1+d+b_2\right)-\lambda_1\left(\frac{\partial w}{\partial r}\right)\left(1+d+b_2\right)\tau_{rz},\\
\tau_{zz} &= \lambda_2\left(\frac{\partial w}{\partial r}\right)^2\left(-1+d+b_2\right)-\lambda_1\left(\frac{\partial w}{\partial r}\right)\left(-1+d+b_2\right)\tau_{rz},\\
\tau_{\theta\theta} &= \lambda_2\left(\frac{\partial w}{\partial r}\right)^2 b_2-\lambda_1\left(\frac{\partial w}{\partial r}\right)b\tau_{rz},\\
B_r &= E_c\,\mathrm{Pr}\,.
\end{aligned}$$

Finally, in simplified form Eqs. (10.6) to (10.9b) can be written as

$$\frac{\partial P}{\partial r}=0, \tag{10.10}$$

$$\frac{\partial P}{\partial z}=\frac{1}{r}\frac{\partial}{\partial r}\left(r\left(\frac{\partial w}{\partial r}+\alpha_2\alpha_3\left(\frac{\partial w}{\partial r}\right)^3+\alpha_4\alpha_2^2\left(\frac{\partial w}{\partial r}\right)^5\right)\right), \tag{10.11}$$

$$\frac{1}{r}\frac{\partial}{\partial r}\left(r\frac{\partial\theta}{\partial r}\right)=-B_r\left(\left(\frac{\partial w}{\partial r}\right)^2+\alpha_2\alpha_3\left(\frac{\partial w}{\partial r}\right)^4+\alpha_4\alpha_2^2\left(\frac{\partial w}{\partial r}\right)^6\right), \tag{10.12}$$

$$\frac{\partial w}{\partial r} = 0,\quad \frac{\partial\theta}{\partial r}=0 \quad \text{at} \quad r=0, \tag{10.13a}$$

$$w = 0,\quad \theta=0 \quad \text{at} \quad r=h=1+\frac{\lambda K z}{a_0}+\phi\sin 2\pi z. \tag{10.13b}$$

in which

$$\alpha_2=1-d\left(d+b\right)-\frac{c}{2}\left(2d+3b\right),\quad \alpha_3=\lambda_1\lambda_2-\lambda_1,\quad \alpha_4=-\lambda_1^3\lambda_2.$$

10.4 Solution of the Problem

We have used perturbation method to find analytical solution of Eqs. (10.11) and (10.12). For perturbation solution, we expand w, F, P and θ by taking α as perturbation parameter

$$w = w_0 + \alpha_2 w_1 + \alpha_2^2 w_2 + O(\alpha_2^3), \tag{10.14}$$

$$P = P_0 + \alpha_2 P_1 + \alpha_2^2 P_2 + O(\alpha_2^3), \tag{10.15}$$

$$F_1 = F_{10} + \alpha_2 F_{11} + \alpha_2^2 F_{12} + O(\alpha_2^3), \tag{10.16}$$

$$\theta = \theta_0 + \alpha_2 \theta_1 + \alpha_2^2 \theta_2 + O(\alpha_2^3). \tag{10.17}$$

The perturbation results for small parameter α, satisfying the conditions (10.13a) and (10.13b) can be written as

$$\begin{aligned} w = & \left(\frac{r^2 - h^2}{4}\right)\frac{\partial P}{\partial z} + \alpha_2\left(J_1\left(\frac{r^4 - h^4}{4}\right)\right) \\ & +\alpha_2^2\left(J_{11}\left(r^{10} - h^{10}\right) + J_{12}\left(r^8 - h^8\right) + J_{13}\left(r^6 - h^6\right) + \right. \\ & \left. J_{14}\left(r^4 - h^4\right)\right), \end{aligned} \tag{10.18}$$

$$\begin{aligned} \theta = & J_{16}\left(r^4 - h^4\right) + \alpha_2\left(J_{22}\left(r^8 - h^8\right) + J_{23}\left(r^6 - h^6\right) + J_{24}\left(r^4 - h^4\right)\right) \\ & +\alpha_2^2\left(J_{36}\left(r^{20} - h^{20}\right) + J_{37}\left(r^{18} - h^{18}\right) + J_{38}\left(r^{16} - h^{16}\right) + \right. \\ & \left(J_{39}\left(r^{14} - h^{14}\right) + J_{40}\left(r^{12} - h^{12}\right) + J_{41}\left(r^{10} - h^{10}\right) + J_{42}\left(r^8 - h^8\right)\right. \\ & \left. +J_{43}\left(r^6 - h^6\right) + J_{44}\left(r^4 - h^4\right)\right), \end{aligned} \tag{10.19}$$

$$\frac{dP}{dz} = \frac{-16F}{h^4} + \alpha_2\left(-\frac{4J_1 h^2}{3}\right) + \alpha_2^2\left(-\frac{2}{3}J_2 h^8 - \frac{4}{5}J_3 h^6 - J_9 h^4\right), \tag{10.20}$$

where

$$
\begin{aligned}
J_1 &= -\alpha_2\left(\frac{dP_0}{dz}\right)^3\frac{1}{8},\quad J_2=-\alpha_3 J_1^3,\quad J_3=-3\alpha_3\left(\frac{dP_1}{dz}\right)\frac{J_1^2}{2},\quad J_4=-3\alpha_3\left(\frac{dP_1}{dz}\right)^2\frac{J_1}{4},\\
J_5 &= \alpha_3\left(\frac{dP_1}{dz}\right)^3\frac{1}{8},\quad J_6=-\alpha_3\left(\frac{dP_0}{dz}\right)^5\frac{1}{32},\quad J_7=-3\alpha_3\left(\frac{dP_0}{dz}\right)^2\frac{J_1}{4},\\
J_8 &= -3\alpha_3\left(\frac{dP_0}{dz}\right)^2\left(\frac{dP_1}{dz}\right)\frac{1}{8},\quad J_9=J_4+J_6+J_7,\quad J_{10}=J_5+J_8,\quad J_{11}=\frac{J_2}{10},\\
J_{12} &= \frac{J_3}{8},\quad J_{13}=\frac{J_9}{6},\quad J_{14}=\frac{J_{10}}{4},\quad J_{15}=-\frac{B_r}{4}\left(\frac{dP_0}{dz}\right)^2,\quad J_{16}=\frac{J_{15}}{16},\\
J_{17} &= -\frac{B_r\alpha_1}{16}\left(\frac{dP_0}{dz}\right)^2,\quad J_{18}=-B_rJ_1^2,\quad J_{19}=-B_rJ_1\left(\frac{dP_1}{dz}\right),\quad J_{20}=-\frac{B_r}{4}\left(\frac{dP_1}{dz}\right)^2,\\
J_{21} &= J_{19}+J_{17},\quad J_{22}=\frac{J_{18}}{64},\quad J_{23}=\frac{J_{21}}{36},\quad J_{24}=\frac{J_{20}}{16},\quad J_{25}=-100B_rJ_1^2,\\
J_{26} &= -160B_rJ_{11}J_{12},\quad J_{27}=-120B_rJ_{11}J_{13}-64B_rJ_{12}^2,\quad J_{28}=-80B_rJ_{11}J_{14}-84B_rJ_{12}J_{13},\\
J_{29} &= -\left(\frac{dP_2}{dz}\right)10B_rJ_{11}-B_r64J_{12}J_{14}-36B_rJ_{13}^2,\quad J_{30}=-\left(\frac{dP_2}{dz}\right)8B_rJ_{12}-B_r48J_{13}J_{14},\\
J_{31} &= -\left(\frac{dP_2}{dz}\right)6B_rJ_{13}-16B_rJ_{14}^2,\quad J_{32}=-\left(\frac{dP_2}{dz}\right)4B_rJ_{14},\quad J_{33}=-\left(\frac{dP_2}{dz}\right)^2\frac{1}{4}B_r,\\
J_{34} &= -\alpha_2B_r\left(\frac{dP_2}{dz}\frac{1}{2}\right)^6,\quad J_{35}=J_{34}+J_{31},\quad J_{36}=\frac{J_{25}}{400},\quad J_{37}=\frac{J_{26}}{324},\quad J_{38}=\frac{J_{27}}{256},\\
J_{39} &= \frac{J_{28}}{296},\quad J_{40}=\frac{J_{29}}{144},\quad J_{41}=\frac{J_{30}}{100},\quad J_{42}=\frac{J_{35}}{64},\quad J_{43}=\frac{J_{32}}{36},\quad J_{44}=\frac{J_{33}}{16}.
\end{aligned}
$$

The corresponding stream function can be calculated as follow

$$u=-\frac{1}{r}\frac{\partial\Psi}{\partial z}\quad\text{and}\quad w=\frac{1}{r}\frac{\partial\Psi}{\partial r}. \tag{10.21}$$

The pressure rise ΔP and friction forces F are defined as follow

$$\Delta P=\int_0^1\frac{dP}{dz}dz, \tag{10.22}$$

$$F=\int_0^1 h^2\left(-\frac{dP}{dz}\right)dz, \tag{10.23}$$

where $\frac{dP}{dz}$ is defined in Eqs. (10.20).

The non-dimensional expressions for the five considered wave forms are defined in chapter 1.

10.5 Graphical Discussion

To see the variations in pressure rise, frictional force and pressure gradient caused by the amplitude ratio ϕ, Jeffrey-six constant fluid parameter α, relaxation time λ_1, retardation time λ_2, we have prepared Figs. (10.2 to 10.15). Figs. 10.2 to 10.5 show the variation of pressure versus flow rate for different physical parameters of the problem. We observed that the increase in the values of α_2, ϕ and λ_1, causes the increase in pressure rise while the increase λ_2 causes decrease in pressure rise. The peristaltic pumping region for Figs. 10.2 and 10.4 is $0 \leq Q \leq 0.5$, peristaltic pumping region for Fig. 10.3 is $0 \leq Q \leq 1.1$, while peristaltic pumping for Fig. 10.5 is $-0.5 \leq Q \leq 0.4$, other wise augmented pumping occurs. The variations of frictional forces are plotted in Figs. 10.6 to 10.9. It can be seen that frictional forces have opposite behavior as compared to the pressure rise. Figs. 10.10 to 10.14 are prepared to see the variation of pressure gradient for different wave shapes. It is observed from these figures that for $z\epsilon\,[0, 0.5]$ and $[1.1, 1.5]$ the pressure gradient is small and large pressure gradient occurs for $z\epsilon\,[0.51, 1]$. Moreover, it is seen that with increase in ϕ pressure gradient increases. The effects of different parameters on streamlines for the trapping phenomenon for five different wave forms can be seen through Fig. 10.15. It is observed that the size of trapping bolus in triangular wave is

smaller as compared to the other waves.

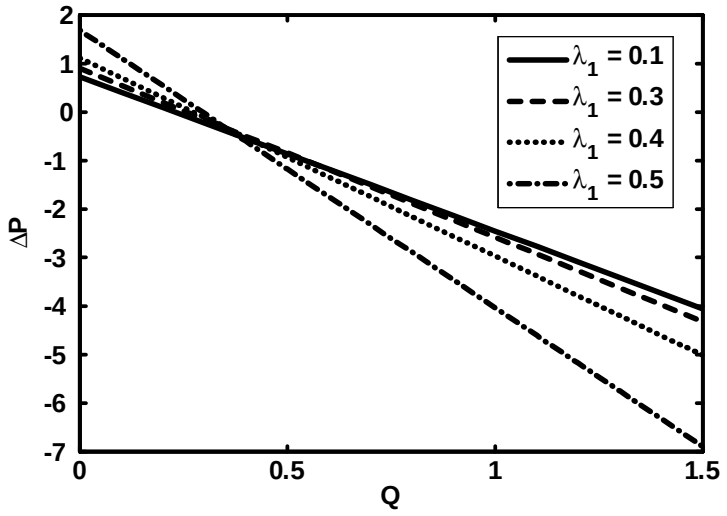

Fig.10.2. Pressure rise versus flow rate for $\alpha_2 = 0.4$, $\lambda_2 = 0.3, K = 0.4$, $\lambda = 0.1$, $a_0 = 0.1$.

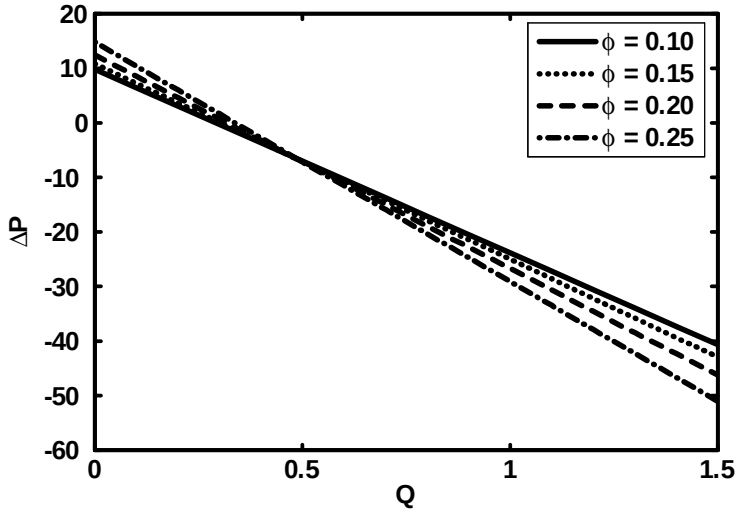

Fig.10.3. Pressure rise versus flow rate for $\alpha_2 = 0.4$, $K = 0.4$, $\lambda = 0.1$, $a_0 = 0.1$, $\lambda_1 = 0.4$, $\lambda_2 = 0.3$.

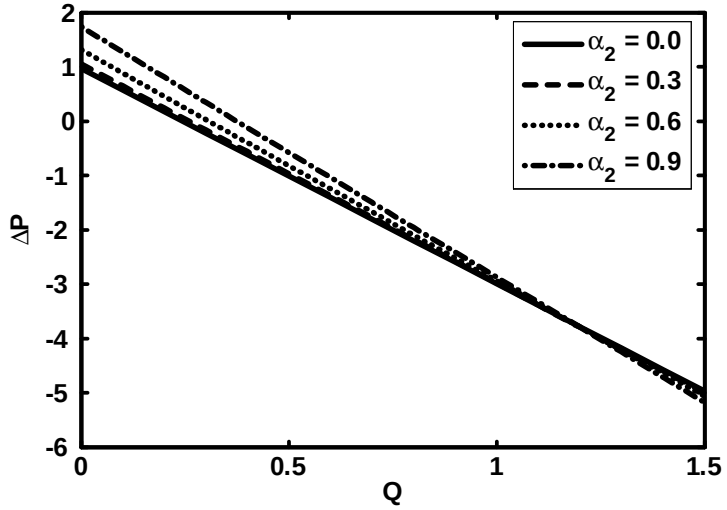

Fig.10.4. Pressure rise versus flow rate for $\phi = 0.4$, $K = 0.4$, $\lambda = 0.1$, $a_0 = 0.1$, $\lambda_1 = 0.4$, $\lambda_2 = 0.3$.

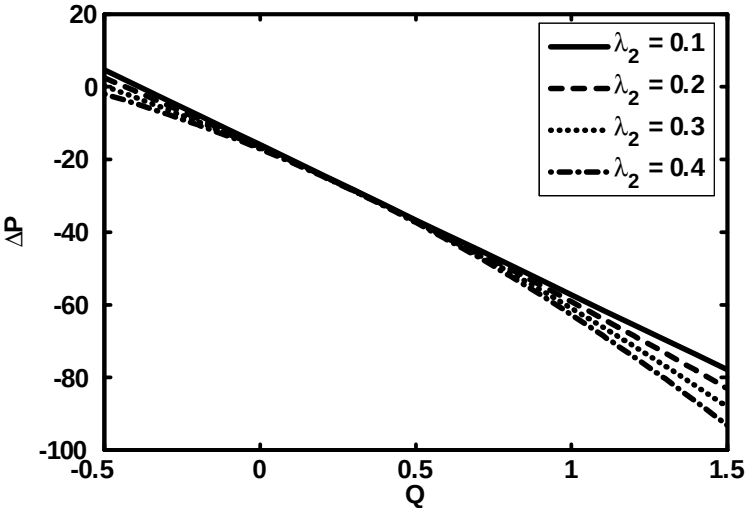

Fig.10.5. Pressure rise versus flow rate for $\phi = 0.4$, $K = 0.4$, $\lambda = 0.1$, $a_0 = 0.1$, $\alpha_2 = 0.4$, $\lambda_1 = 0.3$.

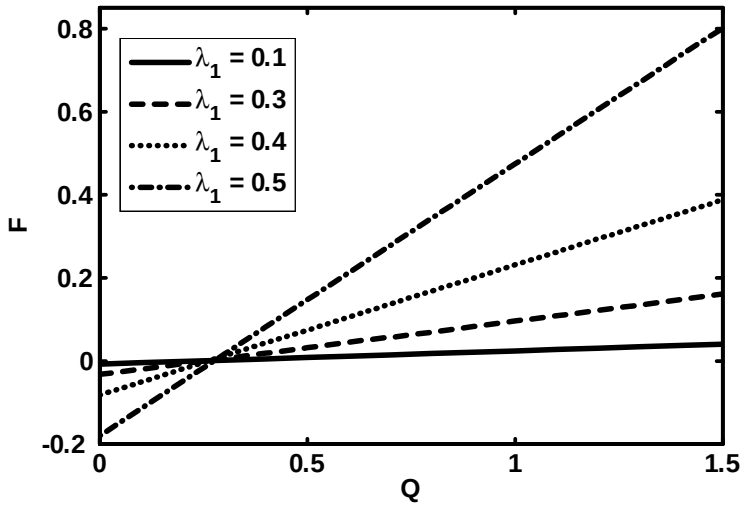

Fig.10.6. Frictional forces versus flow rate for $\alpha_2 = 0.4$, $K = 0.4$, $\lambda = 0.1$, $a_0 = 0.1$, $\lambda_2 = 0.3$.

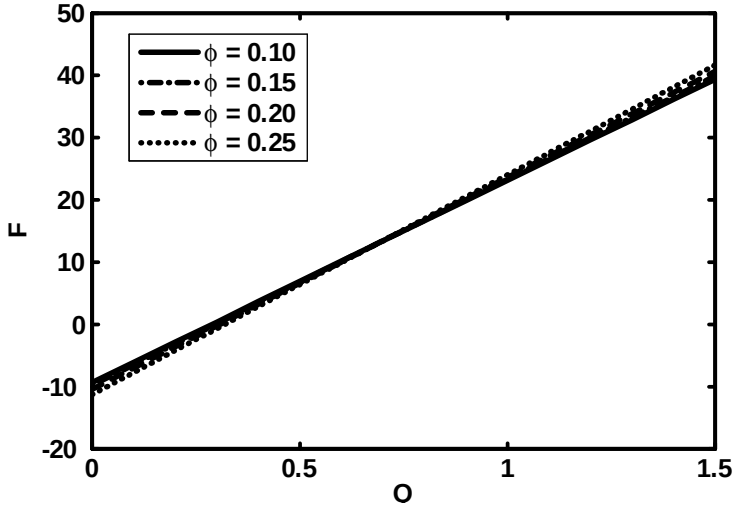

Fig.10.7. Frictional forces versus flow rate for $K = 0.4$, $\lambda = 0.1$, $a_0 = 0.1$, $\lambda_1 = 0.4$, $\lambda_2 = 0.3$.

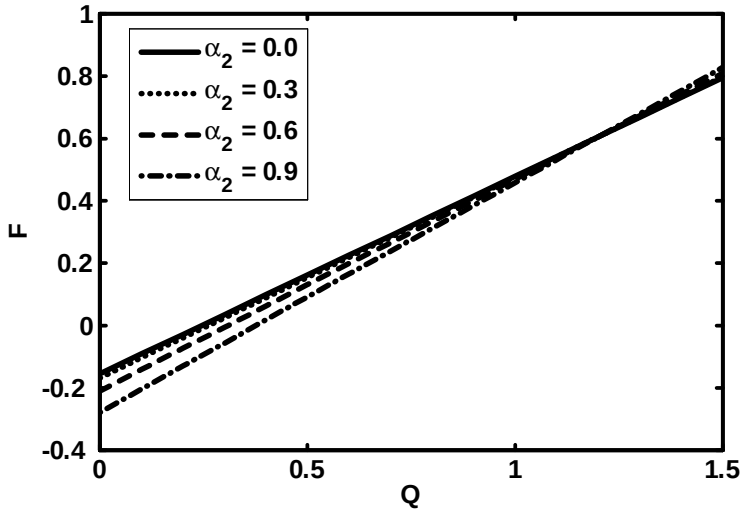

Fig.10.8. Frictional forces versus flow rate for $\phi = 0.4$, $K = 0.4$, $\lambda = 0.1$, $a_0 = 0.1$, $\lambda_1 = 0.4$, $\lambda_2 = 0.3$.

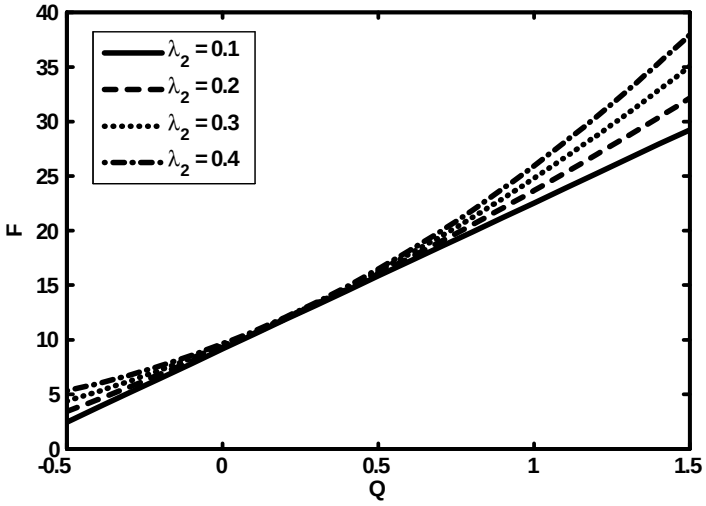

Fig.10.9. Frictional forces versus flow rate for $\phi = 0.4, K = 0.4$, $\lambda = 0.1$, $a_0 = 0.1$, $\alpha_2 = 0.4$, $\lambda_1 = 0.3$.

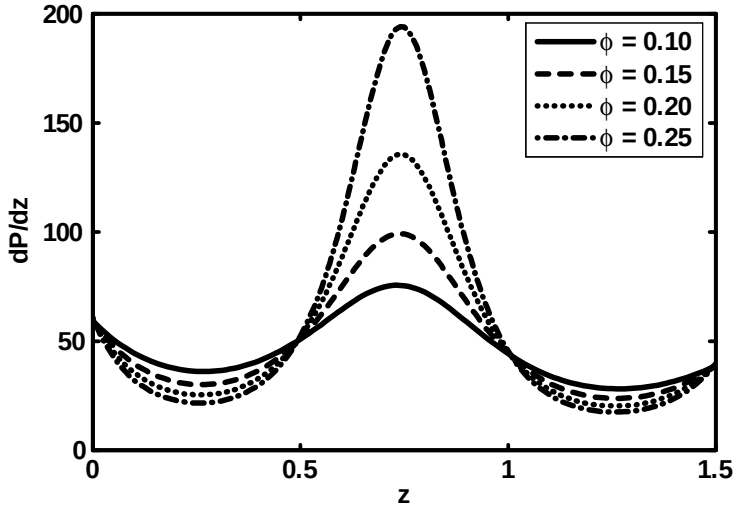

Fig.10.10. Pressure gradient versus z for (Sinusoidal wave) $Q = -2$, $K = 0.4$, $\lambda = 0.1$, $a_0 = 0.1$, $\alpha_2 = 0.1$, $\lambda_1 = 0.4$, $\lambda_2 = 0.3$.

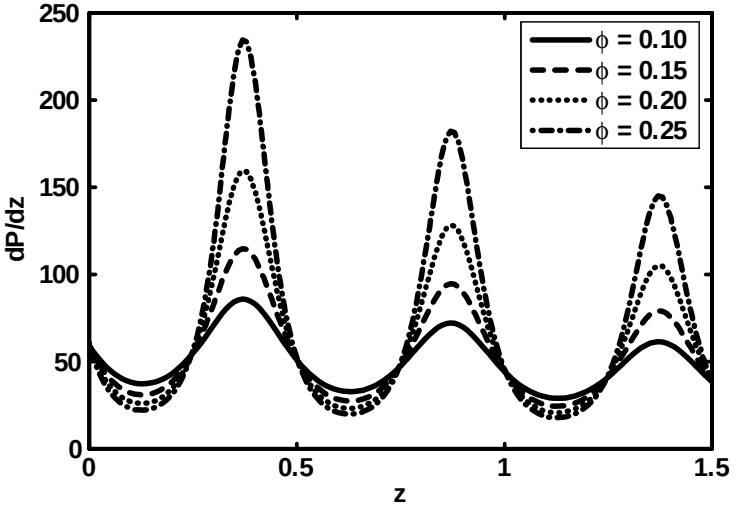

Fig.10.11. Pressure gradient versus z for (MultiSinusoidal wave) $Q = -2$, $K = 0.4$, $\lambda = 0.1$, $a_0 = 0.1$, $\alpha_2 = 0.1$, $\lambda_1 = 0.4$, $\lambda_2 = 0.3$.

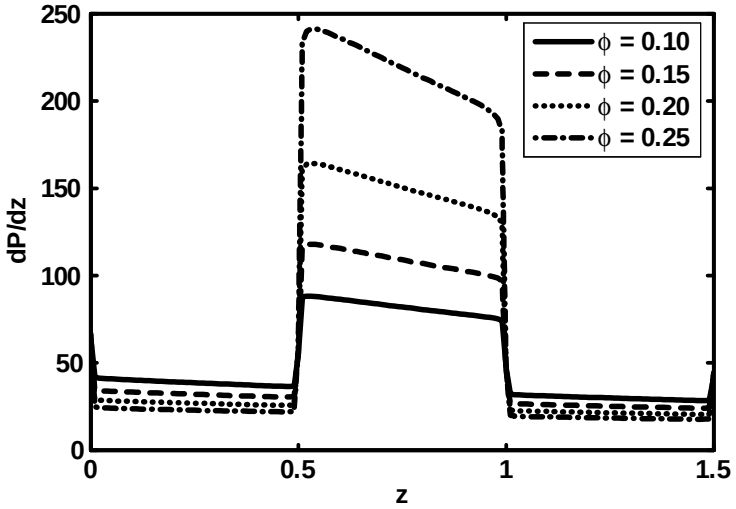

Fig.10.12. Pressure gradient versus z for (Square wave)
$Q = -2$, $K = 0.4$, $\lambda = 0.1$, $a_0 = 0.1$, $\alpha_2 = 0.1$, $\lambda_1 = 0.4$,
$\lambda_2 = 0.3$.

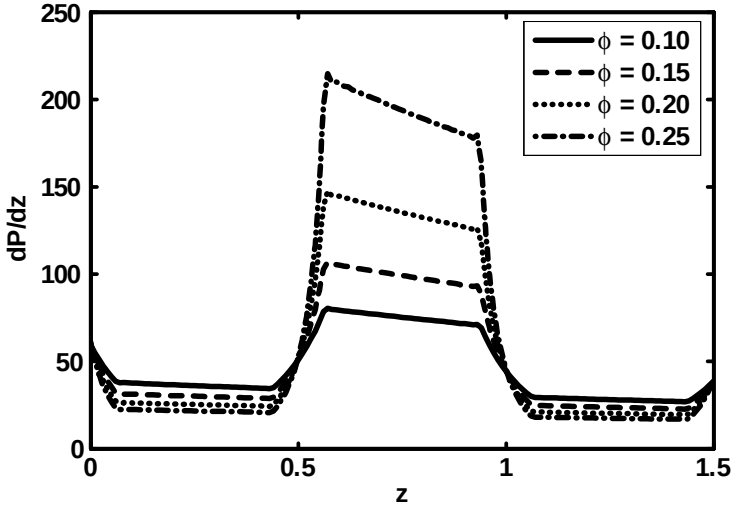

Fig.10.13. Pressure gradient versus z for (Trapezoidal wave)
$Q = -2$, $K = 0.4$, $\lambda = 0.1$, $a_0 = 0.1$, $\alpha_2 = 0.1$, $\lambda_1 = 0.4$,
$\lambda_2 = 0.3$.

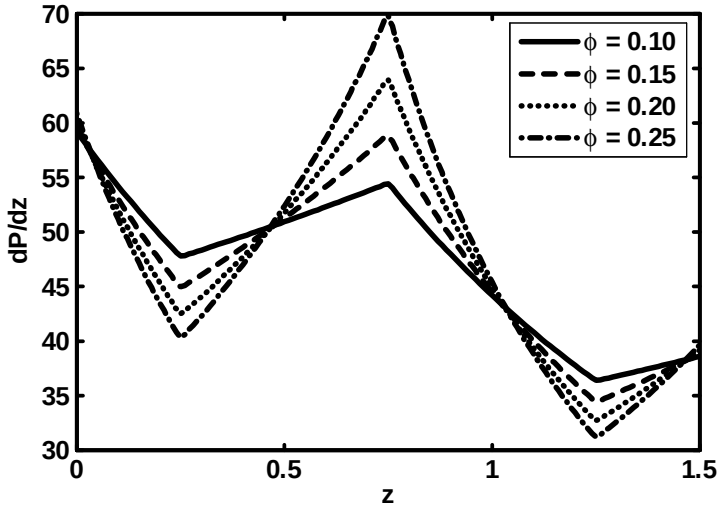

Fig.10.14. Pressure gradient versus z for (Triangular wave) $Q = -2$, $K = 0.4$, $\lambda = 0.1$, $a_0 = 0.1$, $\alpha_2 = 0.1$, $\lambda_1 = 0.4$, $\lambda_2 = 0.3$.

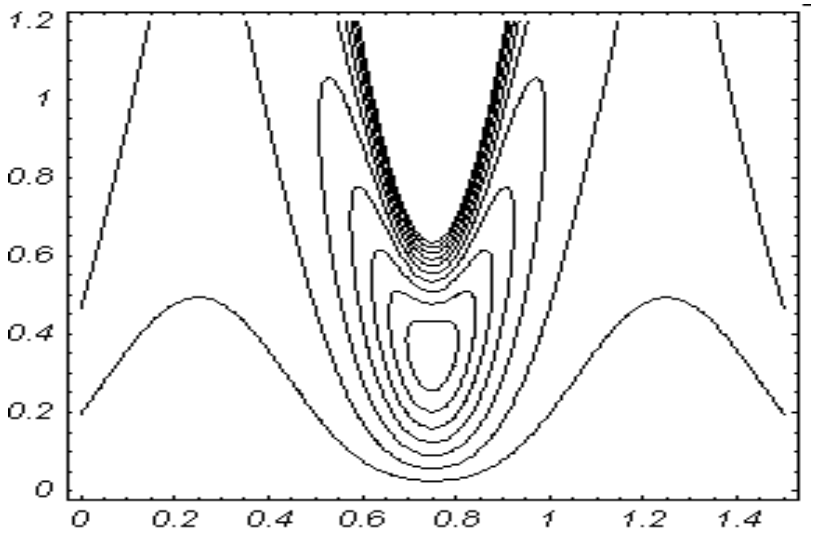

Fig. (10.15) (a) . Streamlines for sinusoidal wave when $Q = -2$, $K = 0.4$, $\lambda = 0.1$, $a_0 = 0.1$, $\alpha_2 = 0.1$, $\lambda_1 = 0.4$, $\lambda_2 = 0.3$, $\phi = 0.4$.

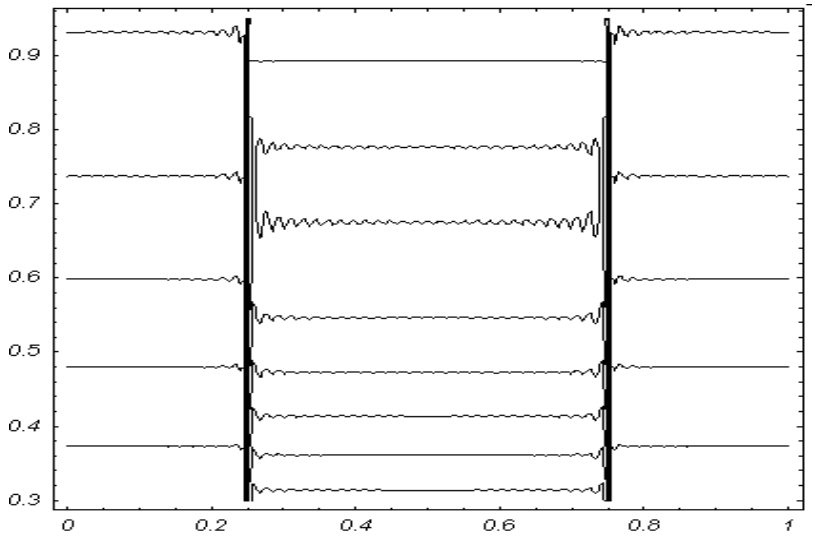

Fig. (10.15) (b) . Streamlines for square wave when $Q = -2$, $K = 0.4$, $\lambda = 0.1$, $a_0 = 0.1$, $\alpha_2 = 0.1$, $\lambda_1 = 0.4$, $\lambda_2 = 0.3$, $\phi = 0.4$.

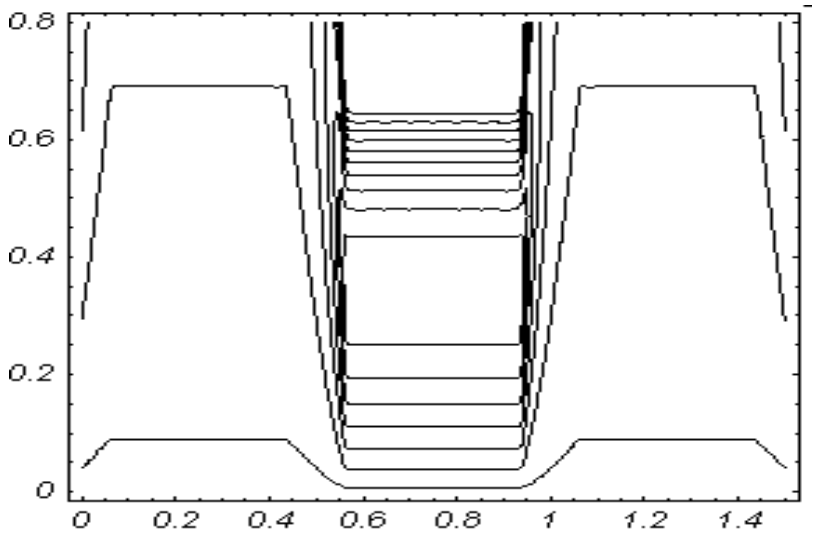

Fig. (10.15) (c) . Streamlines for trapezoidal wave when $Q = -2$, $K = 0.4$, $\lambda = 0.1$, $a_0 = 0.1$, $\alpha_2 = 0.1$, $\lambda_1 = 0.4$, $\lambda_2 = 0.3$, $\phi = 0.4$.

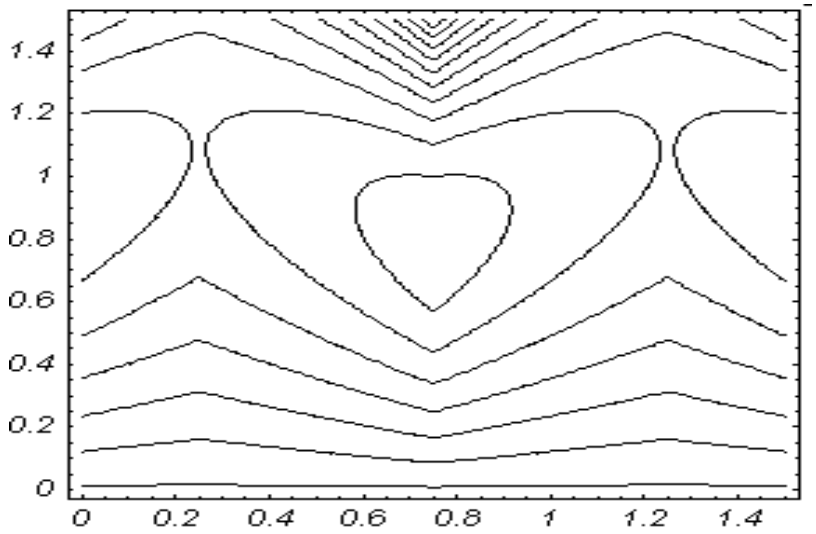

Fig. (10.15) (d) . Streamlines for triangular wave when $Q = -2$, $K = 0.4$, $\lambda = 0.1$, $a_0 = 0.1$, $\alpha_2 = 0.1$, $\lambda_1 = 0.4$, $\lambda_2 = 0.3$, $\phi = 0.4$.

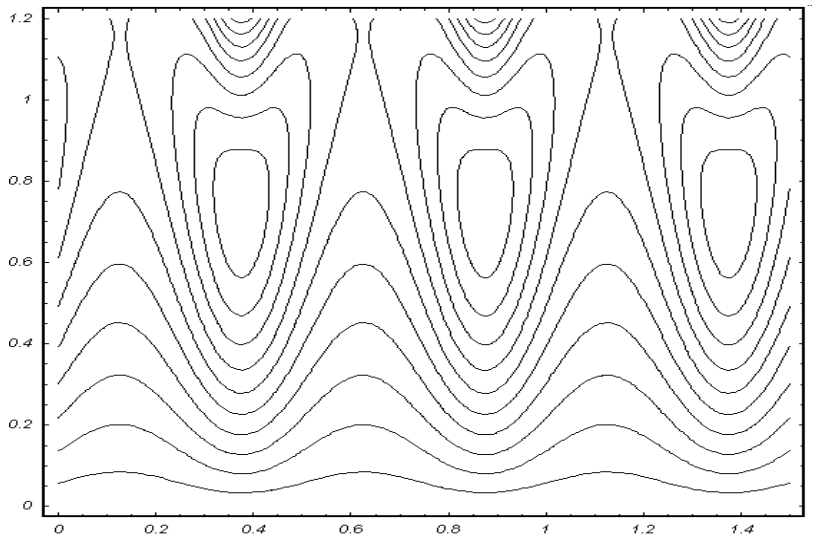

Fig. (10.15) (e) . Streamlines for multisinusoidal wave when $Q = -2$, $K = 0.4$, $\lambda = 0.1$, $a_0 = 0.1$, $\alpha_2 = 0.1$, $\lambda_1 = 0.4$, $\lambda_2 = 0.3$, $\phi = 0.4$.

10.6 Conclusion

This chapter presents the simulation of heat transfer on the peristaltic flow of a Jeffrey-six constant fluid in a diverging tube. The governing two dimensional equations have been modeled and then simplified using long wave length approximation. The simplified equations are solved analytically using regular perturbation method. The results are discussed through graphs. The main ponts of the performed analysis are as follows:

1. It is observed that the increase in the values of α_2, ϕ and λ_1, causes the increase in pressure rise while the increase λ_2 causes decrease in pressure rise..
2. The frictional forces have an opposite behaviour as compared to the pressure rise.
3. It is seen that with increase in ϕ pressure gradient increases.
4. It is observed that the size of trapping bolus in triangular wave is smaller as compared to the other waves.

Chapter 11

Conclusions

The main points of thesis can be summarized as follows

1. It is observed that the relation between pressure rise and volume flow rate are inversely proportional to each other.

2. In the peristaltic pumping region the pressure rise increases with the increase in angle of inclination, amplitude ratio, wave length and decreases with an increase in Walter,s B fluid parameter.

3. It is seen that frictional forces have opposite behavior as compared to the pressure rise.

4. It is seen that pressure gradient increases with increase in amplitude.

5. It is observed that the size of trapping bolus in triangular wave is smaller as compared to the trapezoidal and sinusoidal waves.

6. It is observed that in the peristaltic pumping region, pressure rise increases with the increase in Weissenberg number while the pressure rise decreases with increase in radius ratio.

7. It is depicted that with increase in Weissenberg number and flow rate pressure gradient decreases while pressure gradient increases with increase in amplitude ratio.

8. The pressure rise increases with the increase Sisko fluid parameter.

9. The pressure rise increases with the increase in amplitude ratio and thermophoresis parameter.

10. It is seen that with the increase in the Brownian motion parameter and the thermophoresis parameter temperature profile increases.

11. Effects of Brownian motion parameter and the thermophoresis parameter on concentration profile are same.

12. It is analyzed that with the increase in viscosity parameter temperature profile increases. Moreover it is seen that temperature field decreases with the increase in Brinkman number and Weissenberg number.

13. Effects of Brinkman and power law index on temperature profile are opposite.

14. Concentration profile has an opposite behaviour as compared to the temperature profile.

15. The pressure rise decreases in peristaltic pumping region with an increase in ratio of relaxation to retardation time and viscosity parameter.

16. The temperature field increases with the increase in ratio of relaxation to retardation.

17. It is observed that the volume and size of the trapped bolus increases with increase in flow rate.

18. The volume and size of the trapped bolus decreases with the increase in ratio of relaxation to retardation time.

19. Perturbation and numerical solutions are in good agreement for small Eyring Powel fluid parameter.

20. Pressure rise decreases with an increase in Eyring Powel fluid parameter.

21. Temperature profile has opposite behaviour for Brinkman and in Eyring Powell fluid.

22. Concentration profile decreases with an increase in Brinkman and Soret number.

References

1. A. H. Shapiro, M. Y. Jaffrin, S. L. Weinberg, Peristaltic pumping with long wave length at low Reynolds number, J. of Fluid Mech. **37**, 799(1969).

2. T. W. Latham, Fluid motion in a peristaltic pump, M. Sc, Thesis, Massachusetts Institute of technology, Cambridge, 1966.

3. J. C. Burns, T. Parkes, Peristaltic motion, J. of Fluid Mech. **29**, 731(1967).

4. C. Barton, S. Raynor, Peristaltic flow in tubes, Bull. Math. Biophys. **30**, 663(1968).

5. M. Y. Jaffrin, A. H. Shapiro, Peristaltic puming, Ann. Rev. Fluid Mech. **3**, 13(1971).

6. E. F. Elshehawey, N. T. Eladabe, E. M. Elghazy, A. Ebaid, Peristaltic transport in an asymmetric channel through a porous medium. Appl. Math. Comput. **182**, 140(2006)

7. M. Kothandapani, S. Srinivas, Peristaltic Transport of a Jeffrey fluid under the effect of magnetic field in an asymmetric channel, Int. J. Non-linear Mechanics. **43**, 915 (2008).

8. S. Nadeem, Safia Akram, Peristaltic transport of a Hyperbolic tangent fluid model in an asymmetric channel, Zeitschrift fur Naturforschung A. **64a**, 559 (2009).

9. Md. Asif Iqbal, Visva-Bharati, An unsteady peristaltic transport phenomena of non-Newtonian-A Generalised Approach. Appl. Math. and Comput. **76**, 1 (2008) .

10. M. Ealshahed and M. H. Haroun, Peristaltic transport of Johnson-Segalman fluid under effect of a magnetic field, Math.Prob. in Eng. **6**, 663 (2005).

11. M. H. Haroun, Effect of Deborah number and phase difference on peristaltic transport of a third order fluid in an asymmetric channel, Commun Nonlinear Sci Numer Simulat. **4**, 463 (2007).

12. T. Hayat, N. Ali, S. Asghar, A mathematical description of peristaltic hydromagnetic flow in a tube, Appl. Math. Comput. **188**, 1491 (**2**007).

13. V. Seshadri, Z. Hasan, And B.B Gupta,Peristaltic pumping in non-uniform distensible tubes with different wave forms. J. Biophys Et Med. Nucl. **8**, 9 (1984) .

14. S. Nadeem, Noreen Sher Akbar, Influence of heat transfer on a peristaltic transport of Herschel Bulkley fluid in a non-uniform inclined tube, Commun. in Nonlinear Sci. Numer. Simul. **14**, 4100(2009).

15. K. Vajravelu, S. Sreenadh, V. Ramesh Babu, Peristaltic Transport of a Herschel-Bulkley fluid in a an inclined tube, Int J of Non-linear Mech. **40**, 83 (2005) .

16. T.Hayat, M.U. Qureshi, Q. Hussain, Effect of heat transfer on the peristaltic flow of an electrically conducting fluid in a porous space, Appl. Math. Modelling. **33**, (2009) 1862.

17. G. Radhakrishnamacharya, Ch. Srinivasulu, Influence of wall properties on peristaltic transport with heat transfer. C. R. Mecanique. **335**, 369 (2007) .

18. K. Vajravelu , G. Radhakrishnamacharya and V. Radhakrishnamurty, Peristaltic flow and heat transfer in a vertical porous annulus with long wave approximation. Int J Non linear Mech. **42**, (2007) 754.

19. Kh.S Mekheimer and Y. Abd Elmaboud, The influence of heat transfer and magnetic field on peristaltic transport of a Newtonian fluid in a vertical annulus: Application of an endoscope. Phys Lett A. **37**, 1657 (2007) .

20. R. C. Eberhart and A. Shitzer, Heat Transfer in Medicine and Biology, Springer; 1 edition. 1985.

21. Srinivas, S., Gayathri, R, Kothandapani, M. The influence of slip conditions, wall properties and heat transfer on MHD peristaltic transport, Comput. Phys. Commun. **180**, 2115 (2009) .

22. Kothandapani, M., Srinivas, S. On the influence of wall properties in the MHD peristaltic transport with heat transfer and porous medium, Phys. Lett A. **372**, 4586(2008).

23. T. Hayat, N. Ali, Q. Hussain, S. Asghar, Slip effects on the peristaltic transport of MHD fluid with variable viscosity, Phys. Lett. A. **372**, 1477 (2008) .

24. S. Nadeem, Noreen Sher Akbar, Effects of heat transfer on the peristaltic transport of MHD Newtonian fluid with variable viscosity: application of Adomian decomposition method, Commun. in Nonlinear Sci. Numer. Simul. **14**, 3844(2009).

25. S. Nadeem, Noreen Sher Akbar and M. Hameed, Peristaltic transport and heat transfer of a MHD Newtonian fluid with variable viscosity, Int J of numer meths in fluids. **63**, 1375(2010).

26. A. El. Hakeem, A.EI Naby , A.E.M El. Misery and I.I.El Shamy, Hydromagnetic flow of fluid with variable viscosity in a uniform tube with peristalsis, J.Phys A. **368**, 535 (2003) .

27. N. T. M. Eldabe, M. F. El-Sayed, A. Y. Ghaly and H. M. Sayed, Mixed convective heat and mass transfer in a non-Newtonian fluid at a peristaltic surface with temperature-dependent viscosity, Archi. of Appl. Mech. **78**, 599 (2007) .

28. S. Srinivas, M. Kothandapani, The influence of heat and mass transfer on MHD peristaltic flow through a porous space with compliant walls, Appl. Math and Comput. **213**, 197 (2009) .

29. S. Nadeem, Noreen Sher Akbar, Naheeda Bibi and Sadaf Ashiq, Influence of heat and mass transfer on peristaltic flow of a third order fluid in a diverging tube. Commun Nonlinear Sci Numer Simulat. **15**, 2916(2010).

30. S. Nadeem and Noreen Sher Akbar, Influence of radially varying MHD on the peristaltic flow in an annulus with heat and mass transfer, Taiwan institute of chem. Eng. **41,** 286(2010).

31. S. Nadeem, Noreen Sher Akbar, Influence of heat and mass transfer on a peristaltic motion of a Jeffrey-six constant fluid in an annulus, Heat and Mass Transfer. **46**, 485(2010).

32. S. Nadeem, Noreen Sher Akbar, Influence of heat and chemical reactions on Walter's B fluid model for blood flow through a tapered artery, Taiwan institute of chem. Eng. **42**, 67(2011).

33. S. Nadeem, Noreen Sher Akbar and K. Vajravelue, Peristaltic flow of a Sisko fluid in an endoscope: analytical and numerical solutions, Int. J. of Comput. Math. **88**, 1013(2011).

34. S. Nadeem and Noreen Sher Akbar, Numerical solutions of peristaltic flow of Williamson fluid with radially varying MHD in an endoscope, Int. J. for Numer. Meth. in Fluids. **66**, 212(2011).

35. A. El. Hakeem, A.EI Naby , A.E.M El. Misery and I.I.El Shamy, Separation in the flow through peristaltic motion of a carreau fluid in uniform tube, Physica A. **343**, 1 (2004) .

36. W.A. Khan, and I. Pop, Boundary-layer flow of a nanofluid past a stretching sheet, Int. J. Heat and Mass transfer. **53**, 2477 (2010) .

37. R. E. Powell and H. Eyring, Mechanism for the relaxation theory of viscosity. Nature. **154**, 427(1944).

38. J.H. He, Approximate analytical solution for seepage flow with fractional derivatives in porous media, Comput. Methods Appl. Mech. Eng. **167**, 57(1998).

39. J.H. He, Application of homotopy perturbation method to nonlinear wave equations, Chaos, Solitons & Fractals. **26**, 695(2005).

40. S. Liao, On the homotopy analysis method for nonlinear problems, Appl. Math. Comp. **147**, 499(2004).

41. S. Nadeem and M. Ali. Analytical solutions for pipe flow of a fourth grade fluid with Reynold and Vogel's models of viscosities. Commun Nonlinear Sci Numer Simulat. **14**, 2073(2009).

42. A. W. Sisko. The Flow of Lubricating Greases, Indust. and Eng. Chem. **50**, 1789(1958).